Role of Sulfur in the Preservation of Organic Molecules in Hydrocarbon Source Rocks of Contrasting Compositions

A thesis submitted to the University of Manchester for the degree of Doctor of Philosophy in the Faculty of Science and Engineering

2021

Yusuf Abubakar, FHEA

Department of Earth and Environmental Sciences

Contents

Figures

Tables

Abbreviation

1,2DMB – 1,2-Dimethylbenze

2ET – 2-Ethylthiophene

2MT/T – 2-Methylthiophene over Toluene

2,3DMT – 2,3-Dimethylthiophene

2,4DMT – 2,4-Dimethylthiophene

2,5DMT – 2,5-Dimethylthiophene

ATR-FTIR – Attenuated Total Reflectance-Fourier Transform Infrared Spectroscopy

BT/T – Benzothiophenes over Toluene

$CaCO_3$ – Calcium Carbonate

CHNS – Organic Elemental Carbon, Hydrogen, Nitrogen and Sulfur Analyses

CO_2 – Carbon Dioxide

DLS – Diamond Light Source

EDS – Energy Dispersive X-ray Spectroscopy

EMPA – Electron Microprobe Analysis

ESEM – Environmental Scanning Electron Microscopy

FeS_2 – Pyrite

GS – Grey Shale Member of the Whitby Mudstone Formation

H_2S – Hydrogen Sulfide

HBI – Highly Branched Isoprenoid

H/C – Hydrogen over Carbon Atomic Ratio

HS – Hand Specimen

IC – Inorganic Carbon

ICDD – International Centre for Diffraction Data

ICP-AES – Inductively Coupled Plasma-Atomic Emission Spectroscopy

JR – Jet Rock Member of the Whitby Mudstone Formation

KCF – Kimmeridge Clay Formation

MF – Monterey Formation

MF-XRF – Micro-Focus–X-ray Fluorescence

OC – Organic Carbon

OM – Organic Matter

OSCs – Organic Sulfur Compounds

ppm – Parts Per Million

Py-GC-MS – Pyrolysis-Gas Chromatography-Mass Spectrometry

S/C – Sulfur over Carbon Atomic Ratio

SRS-XRF – Synchrotron Rapid Scanning–X-ray Fluorescence

SSRL – Stanford Synchrotron Radiation Lightsource

TIC – Total Inorganic Carbon

TOC – Total Organic Carbon

TS – Thin Section

WMF – Whitby Mudstone Formation

wt. % – Weight Percent

XANES – X-ray Absorption Near Edge Structure

XAS – X-ray Absorption Spectroscopy

XRD – X-ray Powder Diffraction

XRF – X-ray Fluorescence

Thesis Abstract

Abundance of carbon dioxide (CO_2) in the atmosphere is known to escalate greenhouse conditions/climate warming. The only way to naturally mitigate this devastating phenomenon is by massive sequestration of CO_2 in sediments as either carbonate rocks or organic matter (OM). Preservation through sulfurisation is considered one of the important pathways through which OM can be stored in the geosphere for millions of years. However, the formation of iron sulfides, primarily pyrite (FeS_2), is suggested to be a competitor to this process. Therefore, it remains unclear what factors are critical in the preservation of OM through sulfurisation and the stability of the sulfurised OM in the sedimentary record. There is a dearth of, particularly, spatial information on sulfur (S) and iron (Fe) inventories (oxidation states) at high resolution that could improve our understanding of sulfurisation and FeS_2 formation processes as well as the environmental conditions during time of deposition. In this project samples from model organic and S-rich basins, e.g. the Kimmeridge Clay (KCF), Monterey (MF) and Whitby Mudstones Formations (WMF), as well as laboratory synthesised materials, products of sulfurised glucose reacted with Fe (II) chloride, were robustly analysed using a wide range of organic/inorganic geochemical, petrographic and probe analyses as well as state-of-the-art synchrotron-based techniques (X-ray fluorescence imaging and X-ray absorption near edge structure). For the first time, S and Fe oxidations states were spatially-resolved both at low and high resolutions. Results indicate widespread presence of sulfurised OM in the KCF, in line with relatively low influx of reactive Fe and the presence of stable euxinic conditions in the water column over a relatively long period of time, promoting the preservation of substantial amounts of OM through sulfurisation. In contrast, the presence of sulfurised OM was transitional in the MF, in line with fluctuating redox conditions in the water column over time likely due to profuse biological production, and less significant in the WMF likely due to the abundance of reactive Fe outcompeting the formation of sulfurised OM.

The reaction of sulfurised glucose with Fe indicate, for the first time, that some S in the sulfurised glucose were utilised by Fe to form metastable FeS materials which were subsequently converted to minerals with co-ordination of S and Fe that is similar to the co-ordination environment and oxidation state of S and Fe in S^{-2} Fe sulfide minerals (likely pyrrhotite or troilite). Some of these S^{-2} minerals further converted to form traces of a more stable S^{-1} iron sulfides likely FeS_2. However, there was still sulfurised glucose present at the end of the experiment, suggesting that potentially specific parts of the S originally bound to the glucose were lost during the experiments. The metastable FeS materials were either formed

from breaking of weak S-S bonds while strong C-S bonds were stable and could be preserved for millions of years. It can currently not be excluded that if the experiments were run for a longer period of time more/all S in the sulfurised glucose would be stripped off to form iron sulfides. Therefore, reaction between OM and S could be said to be partially reversible in the presence of reactive Fe species but further experiments are required to arrive at full bound conclusions. This project for the first time introduced the use of novel synchrotron technologies that could be potentially used to study the oxidation states of S, Fe, and other elements from other depositional settings such as ancient and recent oxic and dysoxic milieus and other laboratory synthesised material such as sulfurised humic and fulvic type OMs.

Declaration

I declare no portion of the work referred to in the thesis has been submitted in support of an application for another degree or qualification of this or any other university or other institute of learning.

Yusuf Abubakar, FHEA

Copyright Statement

The author of this thesis (including any appendices and/or schedules to this thesis) owns the copyright/related rights in it (the "Copyright") and he has given The University of Manchester certain rights to use such Copyright, including for administrative purposes.

Copies of this thesis, either in full or in extracts and whether in hard or electronic copy, may be made only in accordance with the Copyright, Designs and Patents Act 1988 (as amended) and regulations issued under it or, where appropriate, in accordance with licensing agreements which the University has from time to time. This page must form part of any such copies made.

The ownership of certain Copyright, patents, designs, trademarks and other intellectual property (the "Intellectual Property") and any reproductions of copyright works in the thesis, for example graphs and tables ("Reproductions"), which may be described in this thesis, may not be owned by the author and may be owned by third parties. Such Intellectual Property and Reproductions cannot and must not be made available for use without the prior written permission of the owner(s) of the relevant Intellectual Property and/or Reproductions.

Further information on the conditions under which disclosure, publication and commercialisation of this thesis, the Copyright and any Intellectual Property and/or Reproductions described in it may take place is available in the University IP Policy (see http://documents.manchester.ac.uk/DocuInfo.aspx?DocID=24420), in any relevant Thesis restriction declarations deposited in the University Library, The University Library's regulations (see http://www.library.manchester.ac.uk/about/regulations/) and in The University's policy on Presentation of Theses.

The Author

Yusuf Abubakar holds a BSc. (Hons.) degree in Geology and an MSc degree in Petroleum Geochemistry from the University of Maiduguri (2012; Nigeria) and Newcastle University (2015; UK) respectively. He worked as a Research Fellow – Geologist/Geochemist at Desert Research, Monitoring and Control Centre (Nigeria), researching renewable energy and climate change before joining the Department of Earth and Environmental Sciences at the University of Manchester (UK) in late 2016, where the work reported in this thesis was carried out. During this time, he has given talks at International Meeting on Organic Geochemistry and the British Organic Geochemistry Society, where he was awarded the best presentation prize. He has also won several research, travel, and conference grants from various funding and research institutes. Yusuf Abubakar is a fellow of the UK Higher Education Academy (FHEA) and the founder and chief executive officer of FlanXus, an integrated low-carbon energy company.

Acknowledgements

Special thanks to my supervisors; Prof Bart E. van Dongen (principal), Dr Victoria Coker, Prof Kevin G. Taylor, and Prof Roy A. Wogelius, for their consistent support, brilliant guidance, and encouragement without whom this project would not have been possible.

Sincere gratitude to my parent and siblings; sisters – Zainab, Fatima, Kalthum, and Khadijah, and brother – Qasim, for their love, firm support, and keeping the faith.

My utmost appreciation to Petroleum Technology Development Fund (Nigeria) for funding this project. I also extend my appreciation to Diamond Light Source (DLS, UK), for additional funding which supported the high-profile synchrotron-based analyses presented in this project.

I am grateful to the following colleagues; Dr Heath Bagshaw, for training on FTIR and ESEM-EDS; Dr John Waters, for training on XRD; Dr John Fellowes, for training on optical microscopy and EMPA; Mr Paul Lythgoe and Mr Alastair Bewsher, for training on the many geochemical facilities in Williamson Research Center; Dr Tina Geraki, for training on X-ray imaging and XANES at DLS, UK and Dr Nick Edwards for help with X-ray imaging and XANES at Stanford Synchrotron Radiation Lightsource (SSRL, US).

Many thanks to my friends and colleagues in Nigeria, UK, and around the world for the support, moments shared will forever be memorable.

Dedication

To my beloved parent.

Chapter 1

1 Introduction and Review

1.1 The Carbon Cycle and its Importance to Climate Change

Mean atmospheric temperature is rapidly increasing due to enormous anthropogenic emissions of greenhouse gases, primarily carbon dioxide (CO_2; Dufresne and Bony, 2008; Heald et al., 2008; Ramanathan and Feng, 2009). Global warming, from increases in CO_2 levels, is known to intensify geologic and hydrologic processes such as glacial melting, rise in sea levels, erratic rainfall, and volcanic activity which contribute to unpredictable seasons, floods, droughts, and agricultural failures that bedevils sustenance of life on earth at present (Mirza, 2003; Kundzewicz et al., 2014; Liu et al., 2014; Anderegg et al., 2020; Greenspan et al., 2020; Lannuzel et al., 2020; Schwarzwald et al., 2020).

On a wide-ranging series of geologically pertinent and resolvable time scales, from 10^3 to > 10^6 years, climate variability is believed to be fundamentally coerced by imbalance in atmospheric CO_2, itself regulated by an active equilibrium between differing CO_2 contributions from volcanic activities and rock metamorphism, and the purging of CO_2 from the atmosphere-ocean-land reservoirs through erosion and weathering and burial of carbon (C) in marine sediments (Berner, 1991; Berner and Caldeira, 1997; Kump et al., 2000; Ridgwell and Zeebe, 2005). To understand this concept lucidly, climatic conditions such as greenhouse events and rapid global cooling and their driving forces through earth's history need better understanding (for a review, see Larson, 1991; Larson and Erba, 1999; Ruddiman, 2001; Leckie et al., 2002; Wagner et al., 2003). CO_2 is considered the most important C fraction on earth where, in pre-industrial times, if sufficient in the atmosphere, trapped heat radiated from the earth's surface to neutralize the cooled earth (- 33 ºC) and maintain a favourable temperature for the sustenance of life (Lorius et al., 1990). However, with the emergence of industrialization, the release of CO_2 to the atmosphere has doubled through contribution from anthropogenic sources (Archer et al., 2009; Keeling and Shertz, 1992; Steinberg, 1999; Sundquist et al., 2009). This affects the climate by distorting the equilibrium between inbound solar radiation and outbound heat released by the earth, thus leading to greenhouse conditions (Lorius et al., 1990). The only way to naturally avert this devastating phenomenon is by massive sequestration of CO_2 in sedimentary rocks as either carbonates or organic matter (OM) in sediments as black shales (Ruddiman, 2001). Therefore, the C cycle is critical, as it is the main driver of these important processes.

The global C cycle encompasses reactions within, and exchange among, the key global pools of the land, atmosphere and ocean (Emerson and Hedges, 2008; Houghton, 2003). The vital reactions are production and obliteration of calcium carbonate ($CaCO_3$) and OM through precipitation/dissolution and photosynthesis/respiration, respectively (Ducklow and McCallister, 2004; Field and Raupach, 2004; Schlesinger, 1997). The swap among the pools is largely through CO_2 gas exchange, burial of $CaCO_3$ rocks and flow of dissolved inorganic C in rivers (Emerson and Hedges, 2008). Generally, the C cycle is divided into two sections; a larger sub-cycle involving sediment diagenesis and organic C preservation over million years otherwise known as the geochemical cycle and a smaller sub-cycle which takes place on timescales of hundred years and relates to C exchange between the atmosphere, biosphere and the hydrosphere, mainly through photosynthesis (Rullkötter, 2006). Rullkötter (2006) further noted that these two sub-cycles are knitted together by a small reciprocal flux and primarily from biochemical to geochemical sub-cycles this flux is through the burial of C as either OM or carbonate rocks, whilst from geochemical to biochemical the flux of CO_2 is through weathering and erosion of sedimentary rocks. Figure 1.1 shows a simplified C cycle knitting the biological and the geochemical sub-cycles.

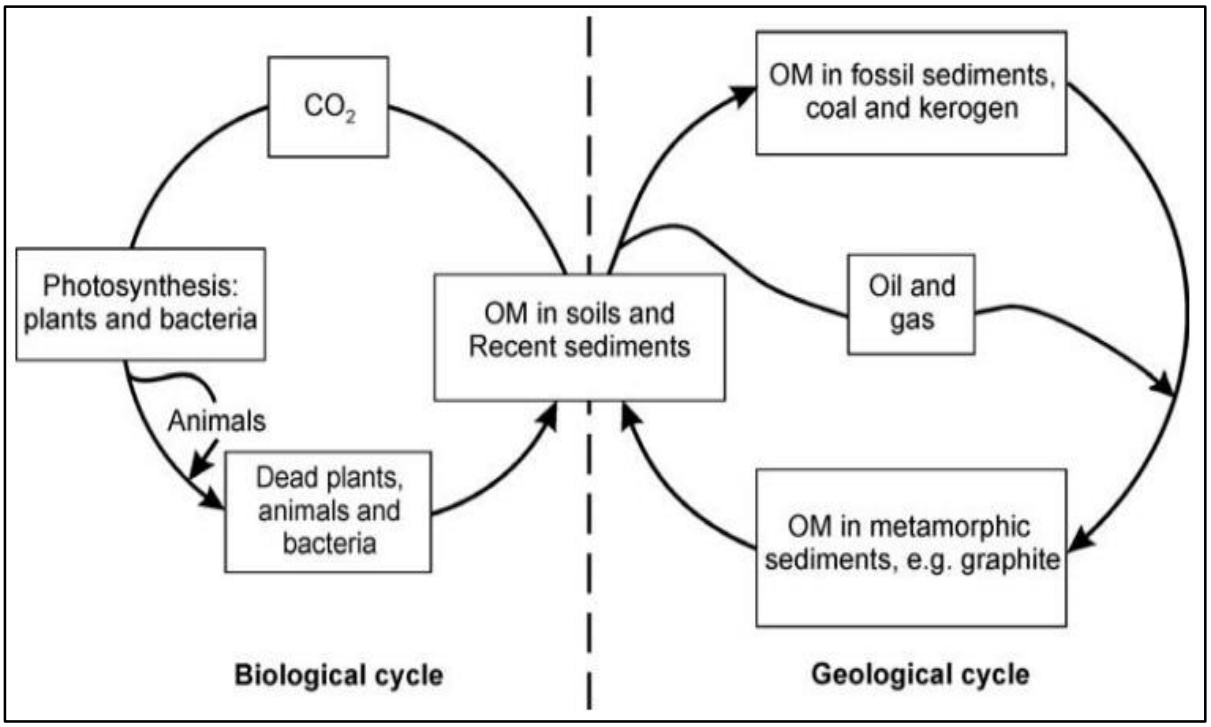

Figure 1.1: Schematic diagram of the global carbon cycle showing the link between the biological and geochemical sub-cycles (adapted from Tissot and Welte, 1984; Rullkötter, 2006).

Focusing solely on the marine part of the biochemical sub-cycle, CO_2 from the atmosphere is fixed to the ocean by marine phytoplankton (Arrigo, 2007; Schlesinger, 1997; Schlesinger and

Bernhardt, 2013). However, in shallow marine settings where sunlight sufficiently reaches the ocean bottom, phytobenthos are the key primary producers of organic C. Bacteria metabolising dead organisms in the water column and terrestrial plant debris transported to the ocean by agents of transportation also represent another major C source. The combined C fixed by marine plants/organisms and terrestrial plants debris is collectively referred to as the primary production (Krumbein and Swart, 1983; Tissot and Welte, 1984; Peters et al., 2005). C fixed by marine plants/organisms is labile thus readily remineralised whereas C from terrestrial plants is refractory, hence better preserved (Hedges et al., 1997; van Dongen et al., 2000; Blair and Aller, 2012).

On a global scale, the contribution of multicellular marine plants (e.g. seaweeds) to primary production in the marine environments is minute. Marine phytoplankton are the key players in the marine part of the biochemical C cycle (Arrigo, 2007). These unicellular organisms account for about 50 % of global CO_2 uptake at the atmosphere-ocean interface (Field et al., 1998; Field and Raupach, 2004). They transform CO_2 to OM through photosynthesis to build their cellular structures and for their cellular respiration (Riebesell et al., 2007). Some of the organic molecules that escape utilisation eventually sink down to the seafloor where most is either remineralised or sequestered in the sediments as sedimentary OM (Demaison and Moore, 1980; Pedersen and Calvert, 1990; Tyson, 2005). Faecal pellets and the organic remains of phytoplankton and zooplankton represent the particulate organic C (Mopper and Degens, 1979; Watanabe and Kuwae, 2015), which can be transformed to dissolved organic C or respired wholly to CO_2 (Burdige, 2007; Hülse et al., 2017). A small fraction of the particulate OM reaches the ocean bottom where it is mostly recycled by benthonic macro-organisms, although preservation of a minute portion cannot be discounted (Hedges et al., 2001). This process of effectively removing CO_2 from the atmosphere and locking it in the sediments for hundreds to millions years is termed the biological pump (Arrigo, 2007; Emerson and Hedges, 2008).

The process of long term preservation of OM and the precipitation of carbonates represent the geochemical sub-cycle (Rullkötter, 2006). Schimel et al. (1995) noted that about 40×10^{18} g C is stockpiled in the reservoirs of the geochemical sub-cycle. It is estimated that about 0.6% of the OM produced by marine biomass is preserved in the sediments (Hunt, 1996). This preserved fraction eventually transforms into fossil fuels where it can be exploited, utilised and C released back to the atmosphere in the form of CO_2 (Speirs et al., 2015), where if released in abundance, the balance between the mechanisms that control the earth's climate is distorted, ultimately leading to global warming.

1.2 Accumulation of Organic Carbon in Marine Sediments

The amount of organic C preserved in marine sediments is, as mentioned above, primarily controlled by; (1) the primary production in the water column and/or influx of terrestrial OM (Calvert, 1987; Calvert and Pedersen, 1992; Pedersen and Calvert, 1990) and (2) the (microbial) degradation during transport through the water column and in the (surface) sediments (Demaison and Moore, 1980; Rullkötter, 2006). Primary production is generally highest in areas with substantial input of nutrients such as upwelling regions and continental margins, which explains the relatively high amounts of OM preserved in these regions (Kolonic et al., 2002; Wagner et al., 2013).

Much of primary production is degraded in the water column by marine biota (Ouverney and Fuhrman, 2000; McCarren et al., 2010; Herndl and Reinthaler, 2013; Landa et al., 2015; Li et al., 2015; 2016). This degradation depends largely on the size of the OM, its tendency to form fluffy aggregates (marine snows), ocean depth and oxygen exposure time (Suess, 1980). Of the afforementioned factors, ocean depth and oxygen exposure time are considered the most critical in OM preservation as OM is largely degraded in deep oceans compared to shelf seas (Suess, 1980).

Degradation of primary production by marine microbes is a continual process and occurs even in sediments (Sinninghe Damsté et al., 2002; Horner-Devine et al., 2003; Naeher et al., 2012; Mann and Lazier, 2013; Oni et al., 2015). As microbes degrade OM, they tend to also consume dissolved oxygen in the water column and sediments. With time, ocean anoxia dominates and the size of microbial communities shrink, hence remnant unremineralised OM reach the seafloor (Demaison and Moore, 1980; Demaison, 1991; Peters et al., 2005; Rullkötter, 2006) and subsequently gets preserved (Demaison, 1991; Sinninghe Damsté, et al., 2002). Some studies suggest that sulfurisation of OM also known as ‘‘*preservation through sulfurisation*’’ or ‘‘*natural vulcanisation*’’ (Fig. 1.2) can also be an important process for the preservation of OM in sediments (Sinninghe Damsté et al., 1987, 1988, 1989; Kohnen et al., 1989; Tegelaar et al., 1989; Orr and Sinninghe Damste, 1990; Sinninghe Damsté and de Leeuw, 1990; Schouten et al., 1995; Koopmans et al., 1996; van Kaam-Peters et al., 1997, 1998, Werne et al., 2000, 2004, 2008; van Dongen et al., 2003a; 2003b; 2006). Sulfurisation commences with the reduction of sulfate in the ocean to sulfide by anaerobic microbes whilst concurrently oxidising OM (Canfield et al., 1986; Filley et al., 2002; Luckge et al., 2002; Werne et al., 2003; Schunck et al., 2013; Turchyn et al., 2015; Bradley et al., 2016; Antler et al., 2017). The reduced inorganic sulfur (S) can react with, and sulfurise, unremineralised OM that reaches the seafloor

making it less prone to utilisation, even by robust anaerobic microbes, hence, ultimately the OM is preserved forming an S-rich kerogen (type IIS; Tegelaar et al., 1989; Sinninghe Damsté and de Leeuw, 1990; van Kaam-Peters et al., 1998; Werne et al., 2003; Amrani and Aizenshtat, 2004; van Dongen et al., 2006).

Sulfidic/euxinic conditions can extend up to the photic zone and down to the sediments and pore water, which can further decrease OM remineralisation in the water column and sediments, resulting in more OM being preserved (Peters et al., 2005; Bowden et al., 2006; van Dongen et al., 2006). Previous studies showed that through sulfurisation, even labile organic C, such as carbohydrates, can be preserved (Sinninghe Damsté et al., 1998; van Kaam-Peters et al., 1998; Kok et al., 2000; van Dongen et al., 2003). van Dongen et al. (2006), for instance, showed the presence of sulfurised carbohydrates in the kerogen of the Blackstone band of the Jurassic Kimmeridge Clay Formation. This could explain the unusually high amounts of organic C (up to 60 wt. %) preserved in this setting. Sulfurised organic compounds were also reported in other organic-rich source rocks such as, the Miocene Monterey Formation (Orr, 1986; Zaback and Pratt, 1992; Nelson et al., 1995), in many exploited petroleum source rocks (Orr, 1978; 1986; Waldo et al., 1991) and recently in a well preserved frog from the late Miocene Libros biota (McNamara et al., 2016).

Organic sulfur compounds (OSCs) formed through sulfurisation are the second most abundant reduced S pool in sedimentary rocks (Amrani, 2014; Anderson & Pratt, 1995; Werne et al., 2003), often attaining values of 35 %, and sometimes higher (Werne et al., 2004). In some potential source rocks like, for example the Upper Cretaceous Ghareb Formation and the Monterey Formation, OSCs are the dominant reduced S fraction (Werne et al., 2004). OSCs are vital in the formation (Macquaker et al., 2014; Tissot and Welte, 1984), preservation (Kohnen et al., 1989; Sinninghe Damsté and de Leeuw, 1990; Wakeham et al., 1995; van Kaam-Peters et al., 1997, 1998; Sinninghe Damsté et al., 1998; Kok et al., 2000; Werne et al., 2000, 2008; van Dongen et al., 2003, 2006), thermal maturity (Tissot and Welte, 1984) and mechanical properties of organic-rich mudstones (Laubach et al., 2009; Macquaker et al., 2014).

The discovery of a clear link between OSCs and biological markers (biomarkers) provided evidence for the sulfurisation of OM at molecular levels (Valisolalao et al., 1984; Sinninghe Damsté et al., 1986; Schmid et al., 1987). The S atoms in these molecules are situated at certain locations, where they substitute functional groups such as carbonyl and/or hydroxyl groups

(van Dongen et al., 2003a; 2003b). Amrani (2014) noted that these compounds are structurally distinct from biosynthetic S compounds. There are two major pathways of sulfurisation, intramolecular and intermolecular additions (Sinninghe Damsté et al., 1989). In intermolecular addition, reduced inorganic S incorporates into OM to form macromolecules through polysulfide linkages (Adam et al., 1993; Kohnen et al., 1991; Riboulleau et al., 2000) whereas in intramolecular addition, S species bind with an organic molecule that has at least two functional groups, where after a series of rearrangements, thermodynamically stable ring compounds such as thiolanes are formed (Schaeffer et al., 2006; Werne et al., 2003).

S can be incorporated into organic C via nucleophilic, electrophilic or radical mechanisms depending on conditions of reaction such as pH, temperature and the medium (e.g. water or organic) within which the reaction occurs (Krein, 1993). According to Aizenshtat et al. (1995), nucleophilic substitution takes place under neutral to basic pH, hence considered the most prevalent mechanism in marine milieus, whereas, Smith and March (2001) reported that in acidic environments, where protons are readily present, electrophilic mechanism is dominant. The radical mechanism is predominant at higher temperatures (Hebting et al., 2003). However, a study has suggested that radical substitution is a possibility even at relatively low temperatures (Perlinger et al., 2002). The mechanism of sulfurisation is very sensitive to the conditions of reaction. The distribution of products and reactants can change even at temperatures considered mild (50 - 100 ºC; (Amrani et al., 2006). Highly acidic or basic situations can trigger aromatization and formation of thiophenes otherwise known to occur at high temperatures to take place at ambient temperatures (Lalonde et al., 1987; Fukushima et al., 1992; Krein and Aizenshtat, 1993).

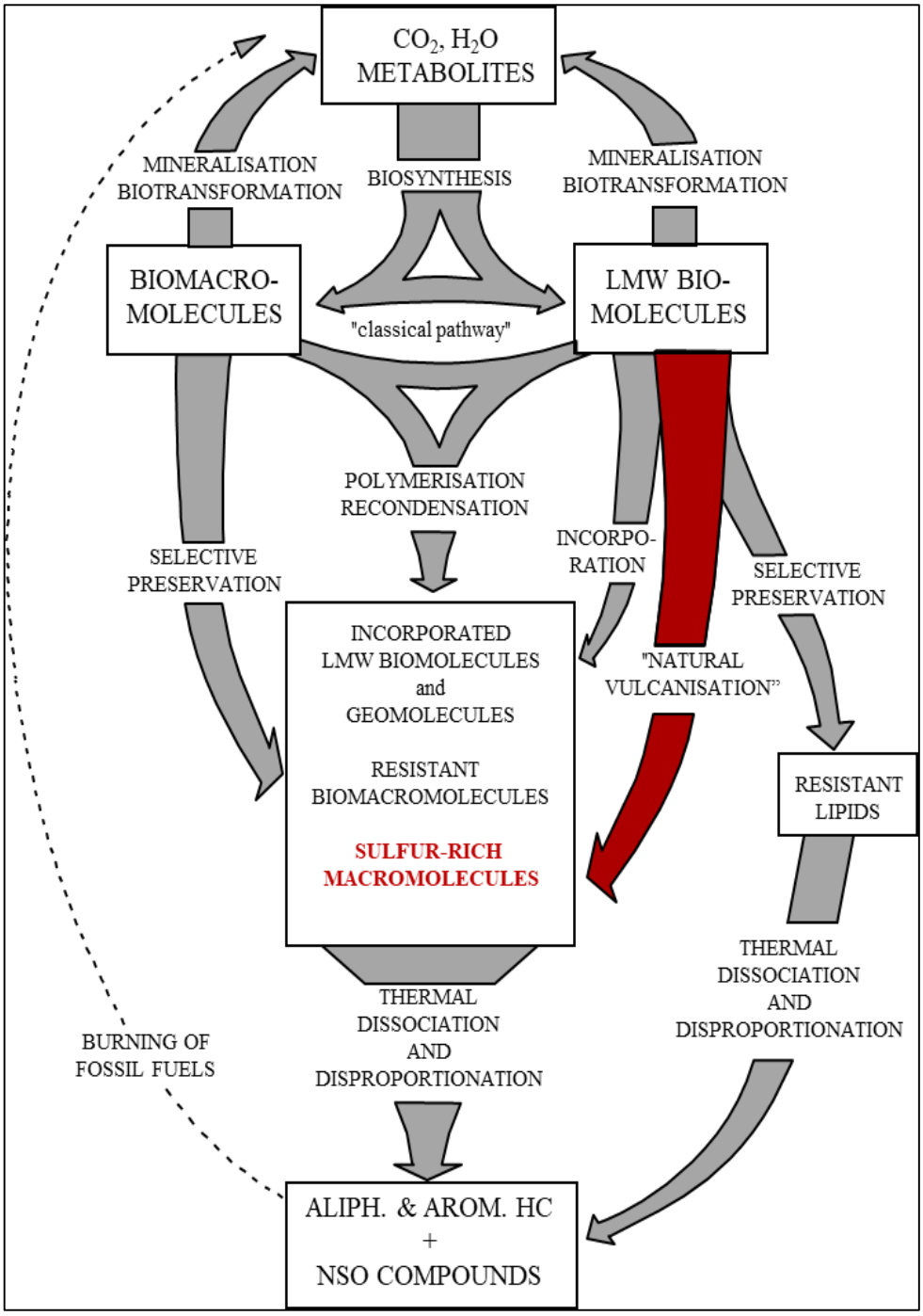

Figure 1.2: Mechanism of kerogen formation (adapted from Tegelaar et al., 1989).

1.3 Formation and Fate of Organic Sulfur Compounds

According to Tissot and Welte (1984), biosynthetic OSCs are chemically labile, hence, the amount of S in OM is supposed to decrease during compaction (diagenesis). However, interestingly, studies show that the percentage of S in OM increases with compaction and is often higher than the initial biomass S content (0.5 - 1 wt. %; Orr, 1986; Orr and Sinninghe Damsté, 1990). This phenomenon was, for example, observed in sediments from the Peru Margin, where S to C atomic/weight ratio increased with burial (Fig. 1.3; Mossmann et al.,

1991). Additionally, similar $\delta^{34}S$ values were seen between OM and pore water S in mature and immature sediments, implying a common source (Francois, 1987; Passier et al., 1999; Werne et al., 2003). As ^{34}S-depleted pore water S originates from microbial reduction of sulfate (Kaplan and Rittenberg, 1964), there is no doubt that the secondary enrichment of S in kerogen is through abiotic diagenetic processes (Amrani, 2014; Werne et al., 2003), indicating that sulfurisation is a sedimentary process. However, recent studies indicate rapid sulfurisation of OM in anoxic water columns (Raven et al., 2016; 2020). For instance, S isotope studies in the Cariaco basin revealed that rapid sulfurisation of OM occured in the water column where proto-kerogen is sulfurised, taking the isotopic signatures (as low as - 76 ‰) of the immediate products of sulfate reduction by microbes (Raven et al., 2016). Additionally, Raven et al. (2020) reported rapid reaction between microbially reduced S and sinking OM in the Eastern Tropical North Pacific oxygen minimum zone. However, these are currently the only studies to date documenting sulfurisation in the water column. To summarise, sulfurisation is primarily a sedimentary process (Sinninghe Damsté and de Leeuw, 1990; Werne et al., 2004; Amrani, 2014; Macquaker et al., 2014) but it remains unclear where exactly sulfurisation starts.

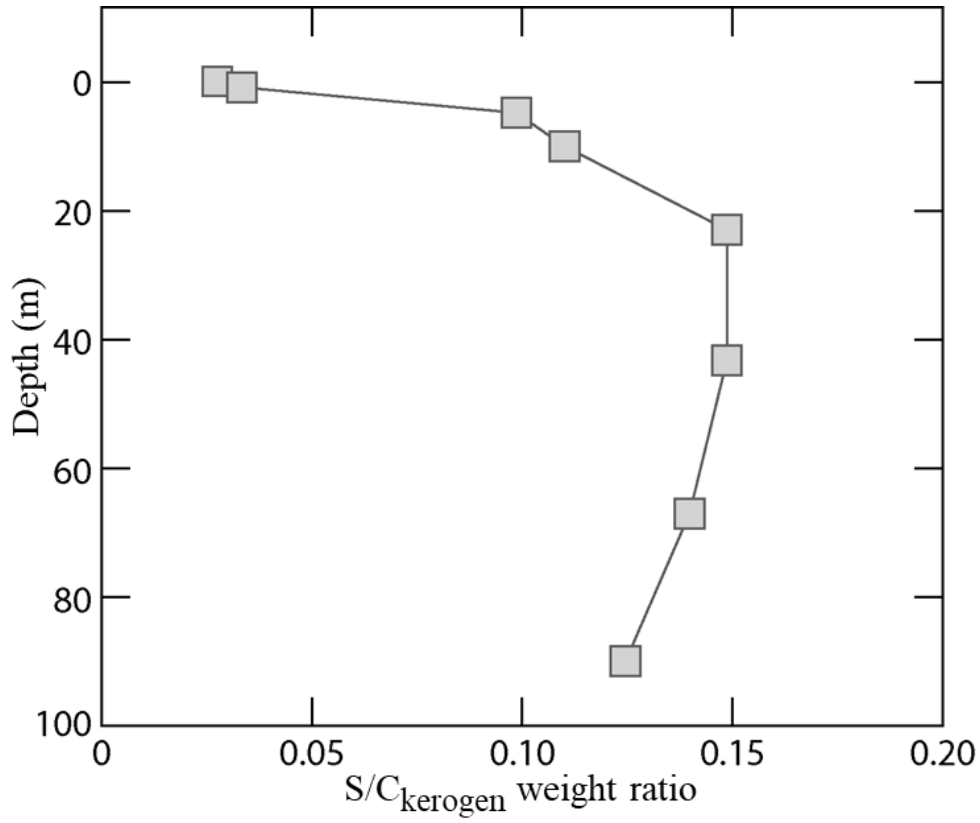

Figure 1.3: The plot of sulfur to carbon weight ratios of organic matter in Peru Margin sediments versus depth (adapted from Mossmann et al., 1991).

1.4 Timing of sulfurisation

Although timing of sulfurisation is still not fully construed due to the intricacies involved in the incorporation of reduced S into OM (Amrani, 2014), analyses indicate that sulfurisation starts on a timescale of days to 10 k.years (Werne et al., 2004; Raven et al., 2016, 2020). Radiocarbon studies on sediments from Cariaco basin, indicated that highly branched isoprenoids (HBI) compounds and malabaricatriene are sulfurised on time scales of 100 years and 10 k.years, respectively (Werne et al., 2000). Work done by Wakeham et al. (1995) and Sinninghe Damsté et al. (2007) on other HBI compound also showed sulfurisation on timescales of 100 years. Sulfurisation in lacustrine sediments younger than 100 years is also documented (Urban et al., 1999). Steroids in Ace lake (Antartica) sediments were sulfurised on time scales of a 1000 to 3000 years (Kok et al., 2000). Schouten et al. (1994) and Amrani and Aizenshtat (2004a) attributed the large variations seen in sulfurisation rates of different organic compounds to their respective reactivities. For example, laboratory investigation on phytenal and phytadiene showed that the former is sulfurised on a timescale of hours to days whereas the later takes weeks to be sulfurised (Amrani and Aizenshtat, 2004a; 2004b). Amrani (2014) noted that differences in reactivities and timing of formation of OSCs can have a significant influence on their isotopic composition owing to the fact that reduced inorganic S becomes isotopically enriched with depth as a consequence of sulfate utilisation by sulfate reducers (Fig. 1.4a). Therefore, OSCs formed at different depth will have contrasting isotopic compositions with those forming in the near surface sediment being isotopically light and those deep down the sedimentary column being isotopically heavy (Fig 1.4b; Anderson and Pratt, 1995).

Equilibrium fractionation and bacterial oxidation may affect certain type of S species. For example, Mossmann et al., (1991) suggested that elemental S and S_x^{2-} are ^{34}S enriched compared to pyrite (FeS_2) because both are formed by the oxidation of hydrogen sulfide (H_2S) diffusing across the sediment-water interface, whereas FeS_2 is precipitated directly from porewater sulfide. Other, oxic S species, for example polythionates can be isotopically enriched by 19 % relative to bisulfide (Kaplan and Rittenberg, 1964). However, Anderson and Pratt (1995) noted that their role as a sulfurisation agent is doubtful. The existence and stable isotopic relationships of OSCs and reduced inorganic S species in sedimentary rocks have aided in understanding the pathways and timing of S incorporation into OM in variety of environments, including modern (e.g. Cariaco basin; Raven et al., 2015; 2016; Li et al., 2011; Werne et al., 2000; 2003; 2008) and ancient systems (e.g. Monterey Formation; Zaback and Pratt, 1992).

However, the timing and pathway of S incorporation into OM is still poorly understood due to complexity of the processes involved and documented studies so far are suggesting a need for high resolution studies for proper understanding.

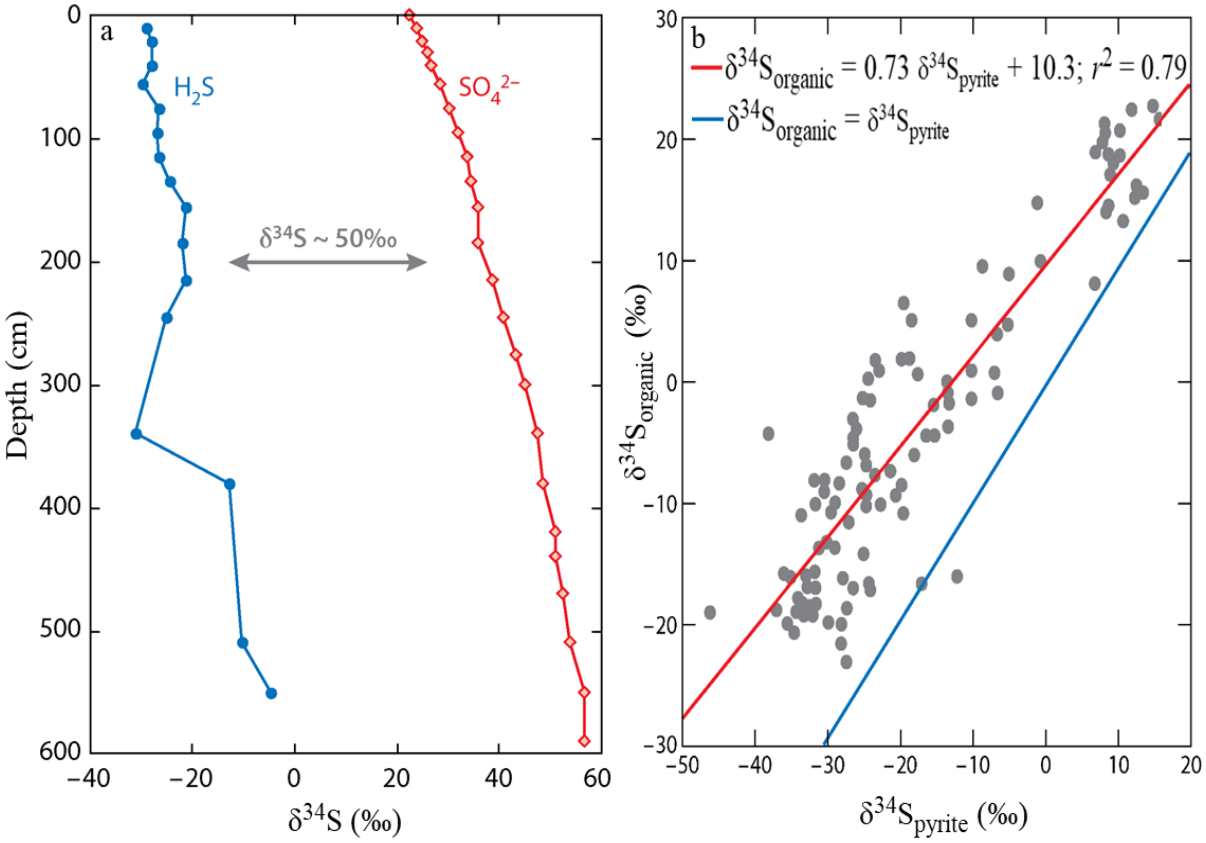

Figure 1.4: (a) Plot of hydrogen sulfide and pore water sulfate indicating large fractionation and gradual isotopic (^{34}S) enrichment of both sulfate and sulfide (adapted from Werne et al., 2003). (b) $\delta^{34}S$ relationship between organic sulfur compounds and coexisting pyrite in sulfur dominated milieus around the world. Despite their common sulfur source, organic sulfur compounds are isotopically enriched compared to associated pyrite (adapted from Anderson and Pratt, 1995).

1.5 Sulfurization and the Crucial Role of Iron Oxides

The incorporation of S into sedimentary OM is governed by a number of different factors including the relative composition of pore water buffering rock materials like silicates (Michalopoulos and Aller, 2004) and carbonates (Moore et al., 2004), the composition of reductants [the equilibrium between OM type inputs (marine against terrestrial) and biogenic methane] present in the water column and at the sediment-water interface used to enhanced microbial activity (Coleman et al., 1985), the composition of oxidants in pore waters (Curtis et al., 1977), the relative abundance of reduced S (Coleman et al., 1985) and the bioavailability of iron (Fe) oxides (Adams et al., 2006). The interplay between these factors during early diagenesis determine the fate of OM (Macquaker et al., 2014). During early mudstone diagenesis, the presence of reactive clay minerals can trigger silicate- and carbonate-buffering

reactions to occur efficiently. These reactions can reduce Fe (III) oxide, enriching pore water with Fe (II) oxide, thus naturally sequestrate reduced S species as iron sulfides (mainly FeS_2) and ultimately leading to S depleted OM being preserved (Raiswell et al., 1994; Macquaker et al., 2014). On the other hand, the absence of bioavailable Fe and reactive clay minerals during early diagenesis leads to pore water being acidic with high concentrations of reduced S hence, resulting in the effective preservation of sulfurised OM (Berner and Raiswell, 1983; Luckge et al., 2002; Macquaker et al., 2014; Tegelaar et al., 1989). This is a widely accepted concept although the stability of sulfurised OM especially during fresh influx of bioavailable Fe species from eolian dust, glacial melts and/or continental run offs into sediments and S-rich pore-water where sulfurisation has or is taking place is unclear. In addition, in instances of change of ocean redox from reducing to oxidising, oxic conditions can extend to the sediments and pore-water. In such situations, the fate of already sulfurised OM is unknown especially if pore-water become enriched in bioavailable Fe species. The lack of clarity on the competition between sulfurisation of OM and FeS_2 formation and stability of sulfurised OM in the presence of excess bioavailable Fe is largely due to the multiple network of metabolic and abiotic chemical reactions that operate concurrently to form sulfurised OM and FeS_2 (Sinninghe Damsté et al., 1990; Wakeham et al., 1995; Raiswell and Anderson, 2005; Raven et al., 2016; Shawar et al., 2018). Bulk, molecular, isotopic and imaging analyses provide us with invaluable information about S and Fe in mudstones/sediments (Sinninghe Damsté et al., 1987; Orr and Sinninghe Damsté, 1990; Sinninghe Damsté and de Leeuw, 1990; Kohnen et al., 1991; Bertrand et al., 1995; Boussafir et al., 1995; Hartgers et al., 1996; Koopmans et al., 1996; van Kaam-Peters et al., 1998; Riboulleau et al., 2000; Taylor and Macquaker, 2000, 2011; Grice et al., 2003; Werne et al., 2003, 2004, 2008; van Dongen et al., 2006; Heitmann and Blodau, 2006; Amrani et al., 2009; Macquaker et al., 2014; Raven et al., 2016; 2019; Meshoulam and Amrani, 2017; Smith et al., 2017; Grotheer et al., 2017; Shawar et al., 2018; Mahoney et al., 2019; Qin et al., 2019; Zheng et al., 2019). However, there is a dearth of information as regards S and Fe inventories (oxidation states) and their micron scale spatial distribution in sediments/mudstones which is necessary to fully comprehend OM sulfurization and FeS_2 formation processes in the sedimentary record.

Recently, studies have employed state-of-the-art synchrotron-based techniques such as X-ray imaging and X-ray absorption near edge structure (XANES) to non-destructively map and study the oxidation states of S, Fe and other elements in fossils, their extant equivalents and human organ (Castillo-Michel et al., 2016; Anné et al., 2019; Edwards et al., 2014; Manning

et al., 2019; Rossi et al., 2019; Szczerbowska-Boruchowska et al., 2012). Additionally, Raven et al. (2018) used XANES techniques to study sulfurization in sequentially extracted sediments from Pont d'Issole (France) suggesting that even small changes in primary productivity could lead to significant changes in OM preservation near critical redox thresholds. Similarly, other studies used XANES to study different S species in kerogens/bitumens (Dang et al., 2019; Kashiwabara et al., 2019; Meister et al., 2019; Mitra-Kirtley et al., 1999; Pomerantz et al., 2014; Vairavamurthy et al., 1994; Waldo et al., 1991; Wiltfong et al., 2005). However, these studies were conducted on processed (destroyed) samples and as such, there is a dearth of information on the presence of different forms/oxidation states of S and Fe and their spatial distribution in organic- and sulfur-rich mudstones.

1.6 Sulfurisation in Organic Rich Mudstones with Contrasting Diagenetic Materials

Early diagenetic materials such as, for example biogenic and non-biogenic silicates and carbonates, Fe, S and some trace elements tend to greatly influence the rate at which mudstones can be sulfurised (Taylor and Macquaker, 2000; Macquaker et al., 2014). Examples can be seen from the Kimmeridge Clay, Monterey and Whitby Mudstone Formations where, although they are typically deposited with analogous suites of reductants and oxidants, they ended up with varying amounts of OSCs, FeS_2 and different cement assemblages (see sections 1.6.1 to 1.6.3; Table 1.1). In-depth analyses, including on the micron-scales using synchrotron based techniques (X-ray imaging and XANES), of organic rich mudstones with contrasting diagenetic materials, are therefore needed to better understand the critical factor controlling the distribution of S, Fe and Fe sulfides (mainly FeS_2) in unusually organic and S-rich source rocks.

1.6.1 Monterey Formation: Diagenesis and Incorporation of Sulfur

The Monterey Formation (MF) is an exceptionally heterogeneous, predominantly biologically-derived marine deposit which was periodically starved of siliciclastic detritus (Table 1.1; Isaacs, 1989; Bohacs, 1990). It was deposited about 22 to 5 Ma (Miocene age) ago along the transform California margin (Blake et al., 1978; Barron, 1986), primarily on low-mid to upper-mid bathyal settings (continental slope), which narrowed upward in most sequences (Ingle, 1973; 1980; Barron, 1986; Isaacs and Rullkötter, 2001). Variations in sea level and the start of Miocene glaciation led to the deposition of four distinct sedimentary facies (clayey-siliceous, upper calcareous-siliceous, phosphatic and lower calcareous-siliceous members) making up the MF (Fig. 1.5; MacKinnon, 1989; Behl, 1999). The changes in sea level also brought about regional upwelling thus, increasing primary productivity and enhancing biological production (Barron, 1986; Behl, 1999; Isaacs and Rullkötter, 2001).

The scarcity of siliciclastic detritus (Isaacs, 1989; Bohacs, 1990) and the enhancement of biological production made the sediments dominated by biogenic materials such as diatoms, benthic and planktonic foraminifers, coccolithophores and OM (Isaacs, 1985; Isaacs and Petersen, 1987; Behl, 1999). Overtime, the highly reactive biologically-derived constituents of the MF (i.e. calcite, phosphate, silica and OM) have suffered series of paragenetic alterations with burial and by tectonic events (Behl, 1999).

During early diagenesis, the availability of OM at the sediment-water interface intensified microbial activities, mainly by sulfate and nitrate reducing microorganism (Macquaker et al., 2014; Piper and Isaacs, 2001). The discharge of phosphate from the decay and reworking of OM, the abundance of microbial mats, the presence of appreciable amounts of phosphate in the water column and the influx of phosphate from external sources due to upwelling enriched porewater with phosphate, which subsequently precipitated as apatite (Garrison et al., 1990; Föllmi et al., 2005; Macquaker et al., 2014). Calcite dominated foraminifers and coccolithophores are the primary carbonate components (Pisciotto, 1981). However, oxygen depletion due to microbial respiration led to the precipitation of a secondary carbonate material, the calcium-rich dolomite, which occurred as concretions, veins or disseminated rhombs (Pisciotto, 1981; Pisciotto and Mahoney, 1977). Contribution of large amounts of phytoplankton by primary producers to the sediments, subsequent dissolution of opaline diatom tests and the presence of carbonate and some clay minerals facilitated subsequent cementation by silica (Kastner et al., 1977; Behl, 1999; 2011). Furthermore, the intense reduction of sulfate by microbes progressively sulfurised the OM in succession starved of Fe (II) oxides (Macquaker et al., 2014) and silicate materials (Isaacs and Petersen, 1987; Jarvie and Lundell, 2001). Piper and Isaacs (2001) reported that the sediment where undisturbed owing to ocean-bottom dysoxia caused by the activities of nitrate reducers which significantly barred the existence of macroinfauna.

The OM in the MF is predominantly made up of amorphous marine algae. However, overwhelming fractions of terrestrial input are present locally (Isaacs and Magoon, 1984; Graham and William, 1985; Behl, 1999). The total organic carbon (TOC) means between 2 wt. % and 5 wt. % depending on sample variations (Isaacs and Petersen, 1987), but can be as high as 16.5 wt. % (Macquaker et al., 2014). Widespread ocean euxinia ensured the preservation of highly sulfurised type IIS kerogens in the MF (Behl, 1999; Macquaker et al., 2014; Orr, 1986; Rullköetter and Isaacs, 1996).

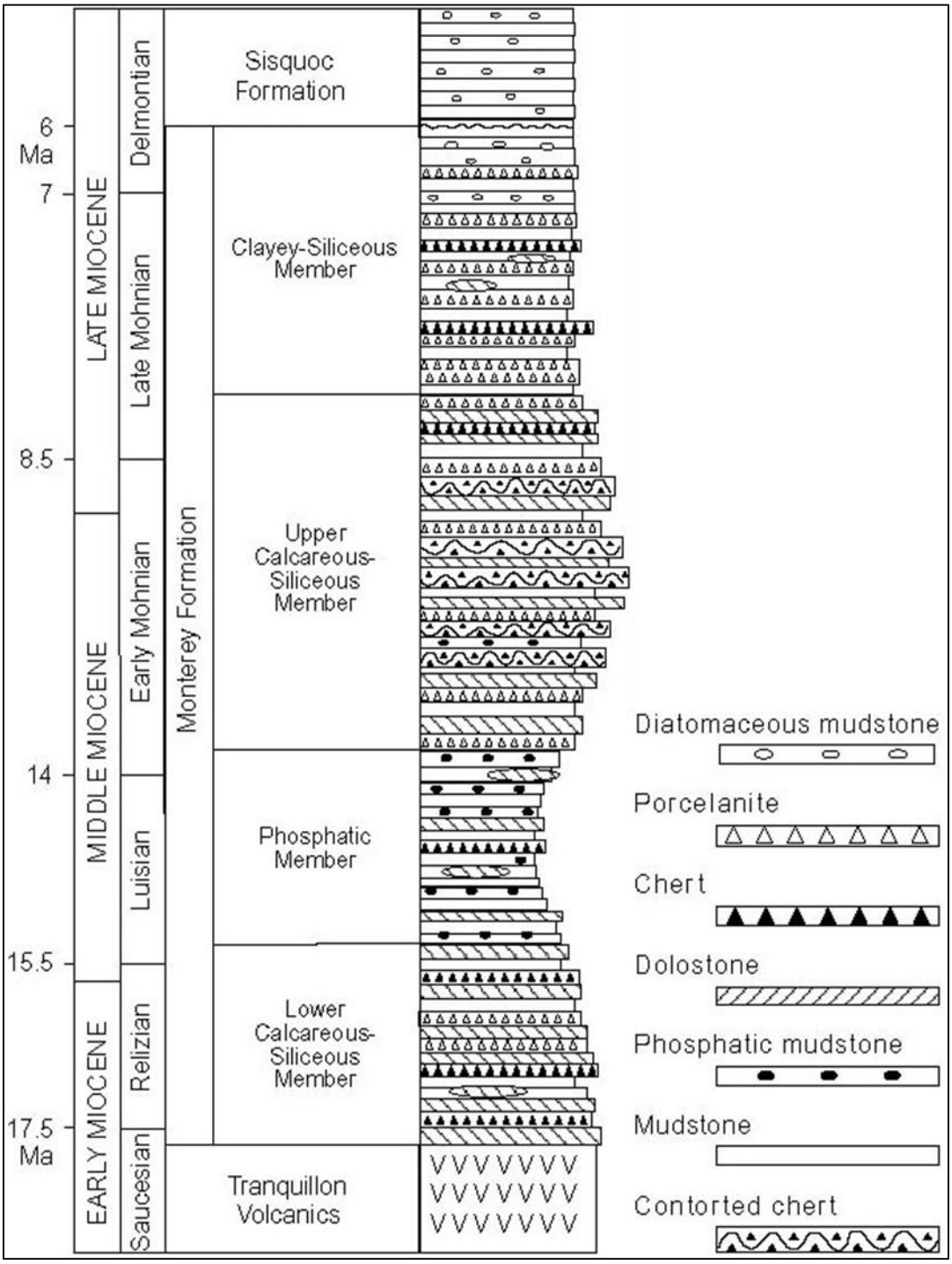

Figure 1.5: Stratigraphy of Monterey Formation in Santa Barbara basin (adapted from MacKinnon, 1989).

1.6.2 Kimmeridge Clay Formation: Diagenesis and Incorporation of Sulfur

The Kimmeridge Clay Formation (KCF), with TOC as high as 60 wt. % is the potential source rock of most North Sea oils (Lallier-Vergès et al., 1997; van Dongen et al., 2006). It is Jurassic in age and is characterised by distinct depositional cycles that typify about 250 m of its thickness (Lallier-Vergès et al., 1997; Tyson, 2004). The cyclicity is a result of commingling of variations in paleo-productivity, paleo-redox depositional conditions and sediment-related

dilution (Fig. 1.6; Lallier-Vergès et al., 1997; Morgans-Bell et al., 2001; Tyson, 2004; van Dongen et al., 2006). Herbin et al. (1993) noted that the cycles relate to both the massive accumulation and quality OM. Deposition occurred on the uppermost part of a mud-dominated continental shelf, under shallow marine conditions (Ziegler, 1990). The sediments are primarily made up of fine-grained siliciclastic detritus that comprise clay and silt size materials with little terrestrial OM (Table 1.1; Macquaker and Gawthorpe, 1993; Lallier-Vergès et al., 1997; Morgans-Bell et al., 2001). According to Macquaker et al. (1998), these materials were transported from high lands in southern England and northeast France to the basin. Biological production was prominent both in the water column and at the sediment-water interface (Tyson, 1996). As a result, the sediments were rich in biogenic materials such as coccolithophores, ammonites, calcispheres and foraminifers (Macquaker et al., 1998; Waterhouse, 1999).

The KCF suffered a complex diagenetic history encompassing the formation and dissolution of siliciclastic and non-siliciclastic materials (Scotchman, 1989; Shaw and Primmer, 1991). Several factors including, sedimentation rate, burial depth, subsidence, lithological features, and OM type influenced diagenesis (Scotchman, 1989). Storm activities ensured sediments were spread across the basin hence thin laminations and ripple marks were almost absent (Macquaker and Bohacs, 2007; Macquaker et al., 2014). However, some materials were transported to the ocean floor by suspension settling as pellets and flocs (Macquaker et al., 2010). During intervals of peak seafloor anoxia, places of low sedimentation rate, less subsidence and shallow burial, Fe oxide and reduced S reactions dominated (Scotchman, 1989) while places of high subsidence and sedimentation rates favoured methanogenesis and the incorporation of reduced S into OM with concomitant precipitation of Fe-rich calcite concretions (Scotchman, 1987).

OM is mainly algae and bacteria with some plant-derived input (Macquaker and Gawthorpe, 1993; Tyson, 1996; Morgans-Bell et al., 2001). Studies show OM in KCF comprise aliphatic hydrocarbon compounds and large amounts of carbohydrate derived OSCs (Farrimond et al., 1984; Lallier-Vergès et al., 1997; van Kaam-Peters et al., 1998; van Dongen et al., 2006).

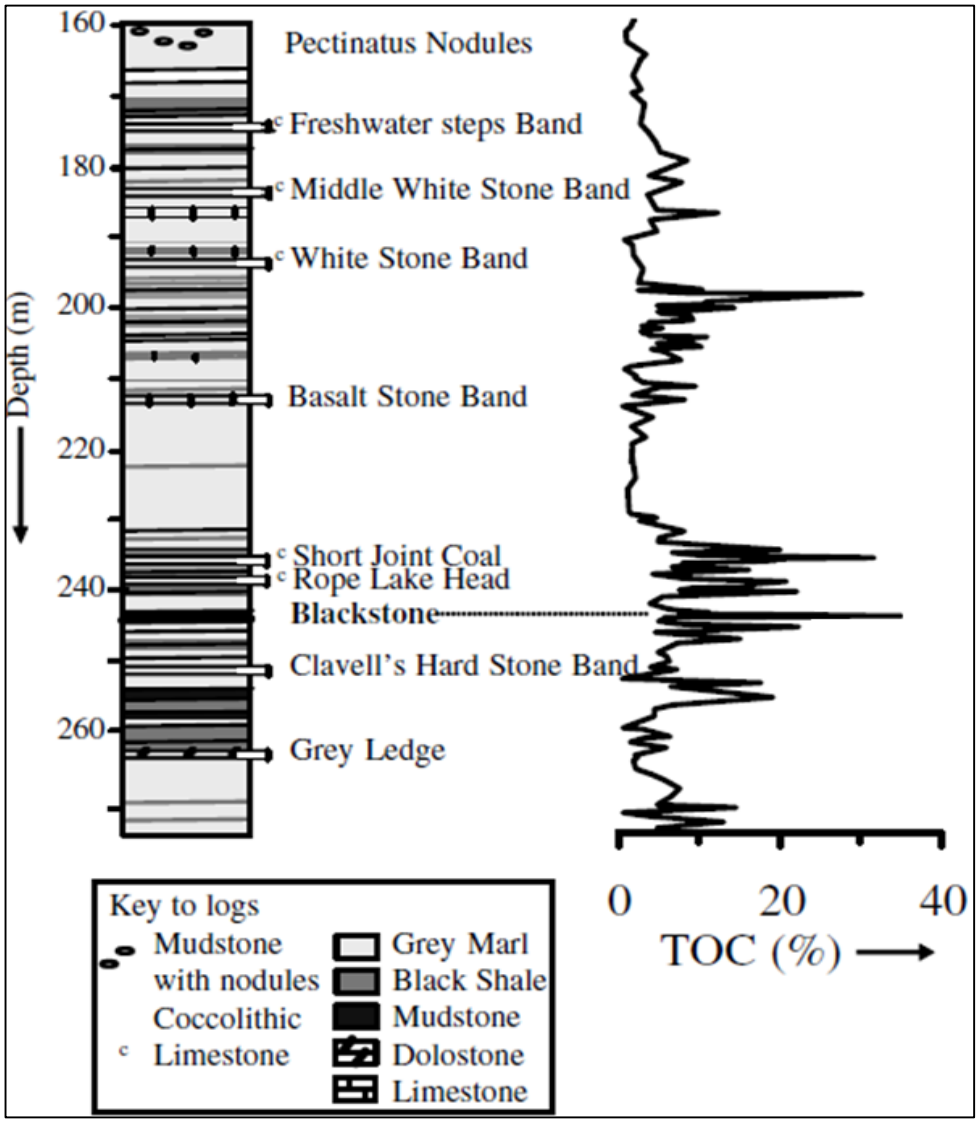

Figure 1.6: Stratigraphy of Upper Kimmeridge Clay Formation in Dorset with TOC values (adapted from Morgans-Bell et al., 2001; van Dongen et al., 2006).

1.6.3 Whitby Mudstone Formation: Diagenesis and Incorporation of Sulfur

The Whitby Mudstone Formation (WMF) is Jurassic in age and was deposited in the distal part of an epicontinental sea that spread over much of northwest Europe. It outcrops along the northeast coast of England and consist of a 70- 90 m bed of mudstones and shales typified by cemented layers and large carbonate concretions in some parts (Table 1.1; Pye and Krinsley, 1986). Powell (1984) characterised the WMF into five lithostratigraphic sub-units in descending order of age as follows; the Grey Shale (GS), Jet Rock (JR), Alum Shale, Peak Mudstone and Fox Cliff Siltstone members (Fig. 1.7). These members unconformably overlie the Cleveland Ironstone Formation which was deposited under shallow marine conditions (Hallam and Bradshaw, 1979; Hemingway, 1974; Rawson et al., 1983).

Morris (1979) used fossils and sedimentary structures to categorize the shale facies in WMF into three groups; (1) Normal shale facies, denoted by the lower beds of GS member, comprising bioturbated silty grey mudstones with numerous trace fossils and dispersed siderite concretions. (2) Restricted shale facies, denoted considerably by the Alum Shale member and the upper part of the GS member, comprising poorly laminated dark grey shales with dispersed carbonate concretions and minute bioturbation. (3) Bituminous shale facies, restricted to the JR member, denoted by finely laminated black shales with some FeS_2, massive calcite concretions and hardly any bioturbation.

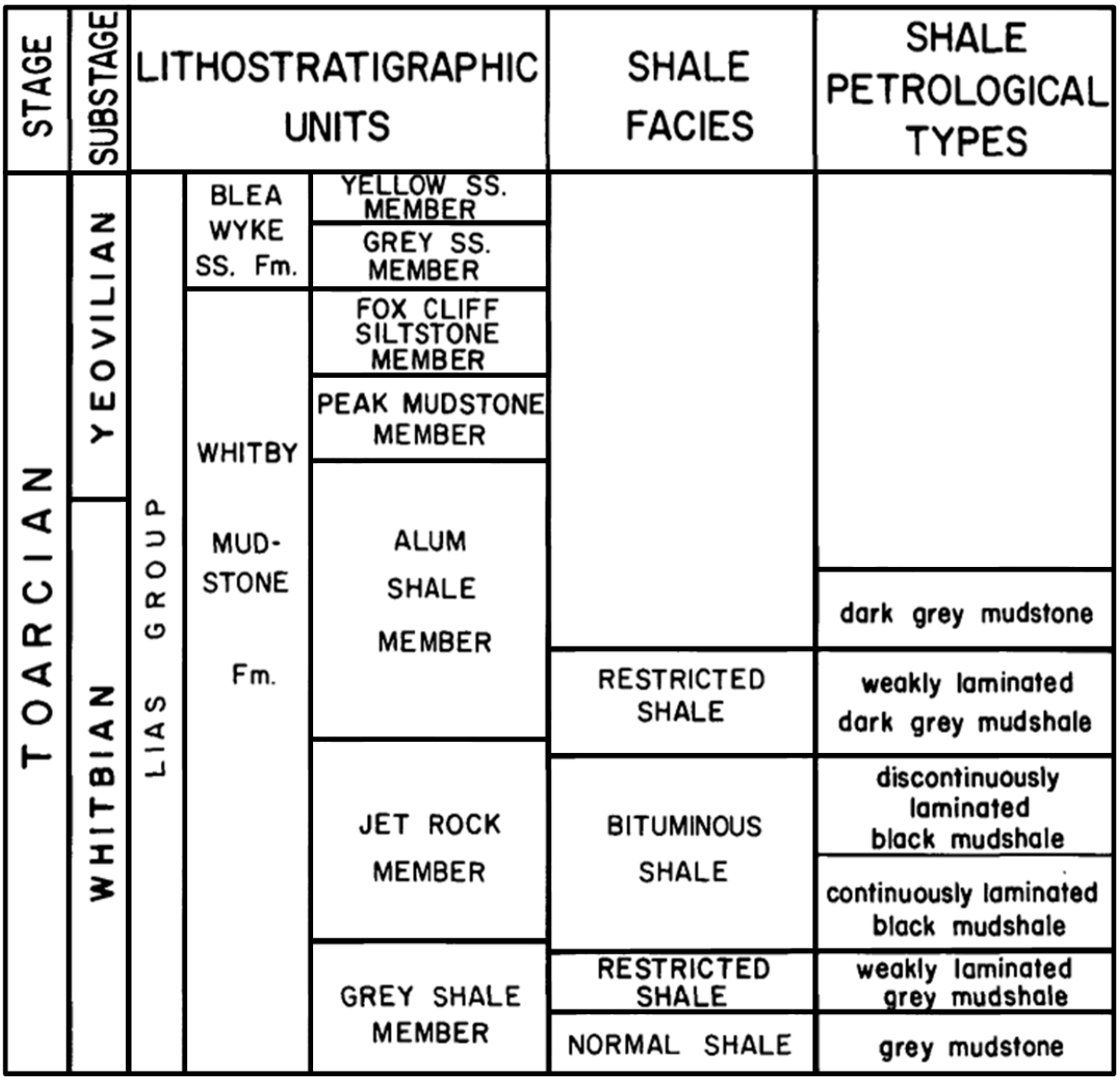

Figure 1.7: Stratigraphy of Whitby mudstone Formation in North Yorkshire (adapted from Powell, 1984; Morris, 1979; Pye and Krinsley, 1986).

Of the three identified shale facies the bituminous JR member is the most organic rich with TOC reaching as high as 14 wt. %. However, it is worthy of noting that three distinct organic

and S-rich layers classified as the lower, middle and upper S bands with TOCs reaching 6.8 wt. %, 4.7 wt. % and 3.5 wt. % respectively have been reported in the GS member (Salem, 2013).

The JR member and S-rich layers in the GS member are believed to have been accrued under organic-rich euxinic conditions which extends above the sediment surface (Berner, 1981; Maynard, 1982). Indeed, full biomarker inventory of the JR member and S-rich layers in the GS member showed the presence of diaryl isoprenoid, a derivative of isorenieratene (Bowden et al., 2006; Salem, 2013), which is an undisputed geochemical proxy for deciphering past euxinic marine conditions (Summons and Powell, 1987). Although, it is established that the JR member and S-rich layers in the GS member are deposited under euxinic conditions, there is no study yet documenting the presence of OSCs in them. However, iron sulfides, mainly FeS_2 are reported to be abundant in them (Rickard 1975; Berner, 1984; Salem, 2013). This means during diagenesis there was sufficient bioavailable Fe species that preferentially reacted with reduced S to form FeS_2 and none/limited amount was left to bind with OM. Nevertheless, this is a deduction from available literature and a further study is required to ascertain the presence of OSCs.

Table 1.1: Comparison of diagenetic materials between the Kimmeridge Clay (KCF), Monterey (MF) and Whitby Mudstone (MF) Formations (Sources: This study; Pye and Krinsley, 1986; van Dongen *et al*., 2006; Salem, 2013; Macquaker *et al.*, 2014)

Formation	Kerogen type/ TOC	Age	Paleo-redox conditions	Source materials	Presence of iron oxides	Pore-water buffering reactions	Diagenetic materials/ cements	Mechanical properties	Presence of pyrites	Organic sulfur
MF	Type IIS (amorphous marine algae) TOC: as high as 14 wt. %	Miocene	Oxic or anoxic/ euxinic depending on cycle	Predominantly biogenic (e.g. diatoms, coccoliths, forams) with some clay and terrestrial organic carbon.	Limited bioavailable iron sesquioxides	Less-effective silicate pore-water buffering	Apatite, carbonate and biogenic silica	Relatively Brittle	Limited	Present
KCF	Type II - IIS (algae, bacteria) TOC: as high as 52 wt. %	Jurassic	Anoxic/ euxinic	Predominantly siliciclastic materials (clay) with some biologically derived materials (e.g. bivalves, coccoliths, forams)	Abundant bioavailable iron sesquioxides	Effective silicate pore-water buffering	Silicate, ferroan carbonate and kaolinite	Relatively ductile	Abundant in some sections	Present
WMF	Type II (amorphous marine algae) TOC: as high as 6 wt. %	Jurassic	Oxic or sub-oxic/ anoxic depending on beds	Predominantly siliciclastic materials (clay) with some biologically derived material	Abundant bioavailable iron sesquioxides	Effective silicate pore-water buffering	Calcite, dolomite, kaolinite and siderite	Brittle	Abundant	Limited

1.7 Overall Aim and Objectives

1.7.1 Aim

As discussed earlier, preservation of OM in sediments is governed by several factors such as quality of organic input (Jones, 1987; Tyson, 2005), sedimentation rate (Canfield, 1994), density/activity of marine microbes (Pratt, 1984) and ocean redox conditions (Calvert et al., 1996). Some studies show that sulfurisation of OM in oxygen-depleted oceans play an important role in preservation of OM in marine sediments (Sinninghe Damsté and de Leeuw, 1990; van Kaam-Peters et al., 1998; Kok et al., 2000; van Dongen et al., 2003a, 2003b; van Dongen et al. 2006). However, it remains unclear which environmental conditions are solely responsible for high amounts of OM preservation through sulfurisation and why different mudstones deposited under sulfidic/euxinic conditions have varying amounts of OSCs and FeS_2. In addition, it remains unclear to what extent sulfurised OM is stable especially during influx of fresh Fe species or when ocean anoxia ceases and porewater becomes oxygenated. The exact timing and pathways of sulfurisation is also vaguely construed.

Therefore, the overall aim of this project is to investigate the critical factors influencing the formation of OSCs in the sedimentary record with a particular focus on the competition between iron sulfide (mainly FeS_2) formation and the sulfurisation of OM.

1.7.2 Objectives

To achieve the stated aim, the following objectives will be implemented.

i) To understand the critical factor controlling the distribution of S, Fe and iron sulfides (mainly FeS_2) in unusually organic and S-rich source rocks. For this, unusually organic and S-rich source rocks with contrasting compositions presented in section 1.6.1, 1.6.2 and 1.6.3 were selected as end-members for this study.

ii) To investigate the Monterey, Kimmeridge Clay and Whitby Mudstone Formations on micron-scales using synchrotron based techniques (X-ray imaging and XANES) to decipher the distribution of S and Fe species which can help in understanding which processes are vital during sulfurisation of OM and FeS_2 formation.

iii) To determine the stability of C-S bonds in OSCs during introduction of fresh Fe species. This will be done by sulfurising carbohydrates at mild temperatures and later adding Fe to observe any possible reactions and/or products formed.

1.7.3 Paper Status and Author Contributions

Paper 1 (Chapter 2): "Fundamental Controls on Organic Matter Preservation in Organic and Sulfur-Rich Hydrocarbon Source Rocks" – Prepared for submission to Marine and Petroleum Geology**.**

Y. Abubakar (principal author) collected/obtained samples with help from Prof K. G. Taylor, completed all experimental work, processed and analysed raw data, prepared figures and tables, interpreted results and drafted manuscript. Prof K. G. Taylor, Dr V. Coker, Prof R. A. Wogelius and Prof B. E. van Dongen provided conceptual guidance and reviewed manuscript.

Paper 2 (Chapter 3): "X-ray Imaging and Molecular Characterization of Sulfur in Organic and Sulfur-Rich Hydrocarbon Source Rocks" – Prepared for submission to Geochimica et Cosmochimica Acta.

Y. Abubakar (principal author) and Prof R. A. Wogelius completed X-ray imaging and XANES analyses. Y. Abubakar processed and analysed raw data, prepared figures and tables, interpreted results and drafted manuscript. Prof R. A. Wogelius, Dr V. Coker, Prof K. G. Taylor and Prof B. E. van Dongen provided conceptual guidance and reviewed manuscript.

Paper 3 (Chapter 4): "An experimental investigation of the stability of sulfurised carbohydrates" – Prepared for submission to Organic Geochemistry.

Y. Abubakar (principal author) completed sulfurisation and Fe experiments with help from Dr V. Coker and Prof B. E. van Dongen. Y. Abubakar and Prof R. A. Wogelius completed X-ray imaging and XANES analyses. Y. Abubakar processed and analysed raw data, prepared figures and tables, interpreted results and drafted manuscript. Dr V. Coker, Prof R. A. Wogelius, Prof K. G. Taylor and Prof B. E. van Dongen provided conceptual guidance and reviewed manuscript.

Reference

Adam, P., Schmid, J. C., Mycke, B., Strazielle, C., Connan, J., Huc, A., Riva, A., & Albrecht, P. (1993). Structural investigation of nonpoalr sulphur cross-linked macromolecules in petroleum. *Canadian Journal of Chemistry*, *57*, 3395–3419.

Adams, L. K., Macquaker, J. H. S., & Marshall, J. D. (2006). Iron(III)-Reduction in a Low-Organic-Carbon Brackish-Marine System. *Journal of Sedimentary Research*, *76*(6), 919–925. https://doi.org/10.2110/jsr.2006.080

Aizenshtat, Z., Krein, E. B., Vairavamurthy, M. A., & Goldstein, T. P. (1995). Role of Sulfur in the Transformations of Sedimentary Organic Matter: A Mechanistic Overview. In *Geochemical Transformations of Sedimentary Sulfur* (Vol. 612, pp. 2–16). American Chemical Society. https://doi.org/doi:10.1021/bk-1995-0612.ch002

Amrani, A. (2014). Organosulfur Compounds: Molecular and Isotopic Evolution from Biota to Oil and Gas. *Annual Review of Earth and Planetary Sciences*, *42*(1), 733–768. https://doi.org/10.1146/annurev-earth-050212-124126

Amrani, A., & Aizenshtat, Z. (2004a). Mechanisms of sulfur introduction chemically controlled: $\delta^{34}S$ imprint. *Organic Geochemistry*.

Amrani, A., & Aizenshtat, Z. (2004b). Reaction of polysulfide anions with α, β unsaturated isoprenoid aldehydes in aquatic media: Simulation of oceanic conditions. In *Organic Geochemistry* (Vol. 35, Issue 8, pp. 909–921).

Amrani, A., Said-Ahamed, W., Lewan, M. D., & Aizenshtat, Z. (2006). Experiments on $\delta^{34}S$ mixing between organic and inorganic sulfur species during thermal maturation. In *Geochimica et Cosmochimica Acta* (Vol. 70, Issue 20, pp. 5146–5161). https://doi.org/10.1016/j.gca.2006.07.030

Amrani, A., Sessions, A. L., & Adkins, J. F. (2009). Compound specific $\delta^{34}S$ analysis of volatile organics by coupled GC multicollector ICPMS. *Analytical Chemistry*, *81*(21), 9027–9034. https://doi.org/10.1021/ac9016538

Anderegg, W. R. L., Trugman, A. T., Badgley, G., Konings, A. G., & Shaw, J. (2020). Divergent forest sensitivity to repeated extreme droughts. *Nature Climate Change*, *10*(12), 1091–1095. https://doi.org/10.1038/s41558-020-00919-1

Anderson, T. F., & Pratt, L. M. (1995). Isotopic Evidence for the Origin of Organic Sulfur and Elemental Sulfur in Marine Sediments. *Geochemical Transformations of Sedimentary Sulfur*, *612*(8), 378–396. http://dx.doi.org/10.1021/bk-1995-0612.ch021

Anné, J., Edwards, N. P., Brigidi, F., Gueriau, P., Harvey, V. L., Geraki, K., Slimak, L., Buckley, M., & Wogelius, R. A. (2019). Advances in bone preservation: Identifying possible collagen preservation using sulfur speciation mapping. *Palaeogeography, Palaeoclimatology, Palaeoecology*, *520*, 181–187. https://doi.org/10.1016/j.palaeo.2019.01.030

Antler, G., Turchyn, A. V., Ono, S., Sivan, O., & Bosak, T. (2017). Combined ^{34}S, ^{33}S and ^{18}O Isotope Fractionations Record Different Intracellular Steps of Microbial Sulfate Reduction. *Geochimica et Cosmochimica Acta*, *203*, 364–380. https://doi.org/10.1016/j.gca.2017.01.015

Archer, D., Eby, M., Brovkin, V., Ridgwell, A., Cao, L., Mikolajewicz, U., Caldeira, K., Matsumoto, K., Munhoven, G., Montenegro, A., & Tokos, K. (2009). Atmospheric Lifetime of Fossil Fuel Carbon Dioxide. *Annual Review of Earth and Planetary Sciences*, *37*(1), 117–134. https://doi.org/10.1146/annurev.earth.031208.100206

Arrigo, K. R. (2007). Carbon cycle: Marine manipulations. *Nature*, *450*(7169), 491–492. https://doi.org/10.1038/450491a

Barron, J. A. (1986). Paleoceanographic and tectonic controls on deposition of the Monterey formation and related siliceous rocks in California. *Palaeogeography, Palaeoclimatology, Palaeoecology*, *53*(1), 27–45. https://doi.org/10.1016/0031-0182(86)90037-4

Behl, R. J. (1999). Since Bramlette (1946): The Miocene Monterey Formation of California revisited. *Geological Society of America Special Papers*, *338*(1946), 301–313. https://doi.org/10.1130/0-8137-2338-8.301

Behl, R. J. (2011). Chert spheroids of the Monterey Formation, California (USA): Early-diagenetic structures of bedded siliceous deposits. *Sedimentology*, *58*(2), 325–351. https://doi.org/10.1111/j.1365-3091.2010.01165.x

Berner, R. A. (1991). A model for atmospheric CO_2 over Phanerozoic time. In *American Journal of Science* (Vol. 291, Issue 4, pp. 339–376). https://doi.org/10.2475/ajs.291.4.339

Berner, Robert A. (1981). A New Geochemical Classification of Sedimentary Environments. *SEPM Journal of Sedimentary Research*, *Vol. 51*(2), 359–365. https://doi.org/10.1306/212F7C7F-2B24-11D7-8648000102C1865D

Berner, Robert A. (1984). Sedimentary pyrite formation: An update. *Geochimica et Cosmochimica Acta*, *48*(4), 605–615. https://doi.org/10.1016/0016-7037(84)90089-9

Berner, Robert A., & Caldeira, K. (1997). The need for mass balance and feedback in the geochemical carbon cycle. *Geology*, *25*(10), 955–956. http://geology.geoscienceworld.org/content/25/10/955

Berner, Robert A., & Raiswell, R. (1983). Burial of organic carbon and pyrite sulfur in sediments over phanerozoic time: a new theory. *Geochimica et Cosmochimica Acta*, *47*(5), 855–862. https://doi.org/10.1016/0016-7037(83)90151-5

Bertrand, P. P., Lallier-Vergès, E., Martinez, L., Pradier, B., Tremblay, P., Huc, A., Jouhannel, R., Tricart, J. P., Boussafir, M., Gelin, F., Lallier-Vergès, E., Derenne, S., Bertrand, P. P., Largeau, C., Borcovsky, D., Egenhoff, S., Fishman, N., Maletz, J., Boehlke, A., … Lowers, H. (1995). Electron microscopy and pyrolysis of kerogens from the Kimmeridge Clay Formation, UK: Source organisms, preservation processes, and origin of microcycles. *AAPG Bulletin*, *101*(18), 661–675. https://doi.org/10.1016/0016-7037(95)00273-3

Blair, N. E., & Aller, R. C. (2012). The Fate of Terrestrial Organic Carbon in the Marine Environment. *Annual Review of Marine Science*, *4*(1), 401–423. https://doi.org/10.1146/annurev-marine-120709-142717

Blake, M. C., Campbell, R. H., Dibblee, T. W., Jr., Howell, D. G., Nilsen, T. H., Normark, W. R., Vedder, J. C., and Silver, E. A. (1978). Neogene basin formation in relation to plate-tectonic evolution of the San Andreas Fault System, California. In *Association of Petroleum Geologists Bulletin* (Vol. 62, Issue 3). American Association of Petroleum Geologists.

Bohacs, K. M. (1990). Sequence stratigraphy of the Monterey Formation, Santa Barbara County: Integration of physical, chemical, and biofacies data from outcrop and subsurface. *SEPM, Core Workshop 14*, *74*, 139–200. https://doi.org/-

Boussafir, M., Gelin, F., Lallier-Vergès, E., Derenne, S., Bertrand, P., & Largeau, C. (1995). Electron microscopy and pyrolysis of kerogens from the Kimmeridge Clay Formation, UK: Source organisms, preservation processes, and origin of microcycles. *Geochimica et Cosmochimica Acta*, *59*(18), 3731–3747. https://doi.org/10.1016/0016-7037(95)00273-3

Bowden, S. A., Farrimond, P., Snape, C. E., & Love, G. D. (2006). Compositional differences in biomarker constituents of the hydrocarbon, resin, asphaltene and kerogen fractions: An example from the Jet Rock (Yorkshire, UK). *Organic Geochemistry*, *37*(3), 369–383. https://doi.org/10.1016/j.orggeochem.2005.08.024

Bradley, A. S., Leavitt, W. D., Schmidt, M., Knoll, A. H., Girguis, P. R., & Johnston, D. T. (2016). Patterns of sulfur isotope fractionation during microbial sulfate reduction. *Geobiology*, *14*(1). https://doi.org/10.1111/gbi.12149

Burdige, D. J. (2007). Preservation of organic matter in marine sediments: Controls, mechanisms, and an imbalance in sediment organic carbon budgets? *Chemical Reviews*, *107*(2), 467–485. https://doi.org/10.1021/cr050347q

Calvert, S. E. (1987). Oceanographic controls on the accumulation of organic matter in marine sediments. *Geological Society, London, Special Publications*, *26*, 137–151. https://doi.org/10.1144/GSL.SP.1987.026.01.08

Calvert, S. E., Bustin, R. M., & Ingall, E. D. (1996). Influence of water column anoxia and sediment supply on the burial and preservation of organic carbon in marine shales. *Geochimica et Cosmochimica Acta*, *60*(9), 1577–1593. https://doi.org/10.1016/0016-7037(96)00041-5

Calvert, Stephen E., & Pedersen, T. F. (1992). Organic carbon accumulation and preservation in marine sediments: how important is anoxia? In *Productivity, accumulation, and preservation in recent and ancient sediments* (pp. 231–263).

Canfield, D E. (1994). Factors Influencing Organic-Carbon Preservation in Marine- Sediments. *Chemical Geology*, *114*(3–4), 315–329. https://doi.org/10.1016/0009-2541(94)90061-2

Canfield, Donald E., Raiswell, R., Westrich, J. T., Reaves, C. M., & Berner, R. A. (1986). The use of chromium reduction in the analysis of reduced inorganic sulfur in sediments and shales. *Chemical Geology*, *54*(1–2), 149–155. https://doi.org/10.1016/0009-2541(86)90078-1

Castillo-Michel, A. H., G. Diaz-Sanchez, A., Martinez-Martinez, A., & Hesse, B. (2016). Investigations of Sulfur Chemical Status with Synchrotron Micro Focused X-ray fluorescence and X-ray Absorption Spectroscopy. *Protein & Peptide Letters*, *23*(3), 291–299. https://doi.org/10.2174/0929866523666160108120117

Coleman, M. L., Berner, R. A., Durand, B., Meadows, P. S., & Eglinton, G. (1985). Geochemistry of Diagenetic Non-Silicate Minerals Kinetic Considerations [and Discussion]. *Philosophical Transactions of the Royal Society A: Mathematical, Physical and Engineering Sciences*, *315*(1531), 39–56. https://doi.org/10.1098/rsta.1985.0028

Curtis, C. D., Burns, R. G., & Smith, J. V. (1977). Sedimentary Geochemistry: Environments and Processes Dominated by Involvement of an Aqueous Phase [and Discussion]. *Philosophical Transactions of the Royal Society A: Mathematical, Physical and Engineering Sciences*, *286*(1336), 353–372. https://doi.org/10.1098/rsta.1977.0123

Dang, D. H., Wang, W. W., Evans, R. D., Morgans-bell, H. S., Coe, A. L., Hesselbo, S. P., Jenkyns, H. C., Weedon, G. P., Marshall, J. E. A., Tyson, R. V., Williams, C. J., Tan, J., Sephton, M. A., Thompson, K. J., Kenward, P. A., Bauer, K. W., Warchola, T., Gauger, T., Martinez, R., … Fayek, M. (2019). Sulfur characterization in asphaltene, resin, and oil fractions of two crude oils. *Geochimica et Cosmochimica Acta*, *74*(4), 763–767. https://doi.org/10.1016/0016-7037(93)90389-E

Demaison, G. (1991). Anoxia vs. Productivity: What Controls the Formation of Organic-Carbon-Rich Sediments and Sedimentary Rocks?: Discussion (1). *AAPG Bulletin*, *75*, 499.

Demaison, G. J., & Moore, G. T. (1980). Anoxic environments and oil source bed genesis. *Organic Geochemistry*, *2*(1), 9–31. https://doi.org/10.1016/0146-6380(80)90017-0

Ducklow, H., & McCallister, S. (2004). The biogeochemistry of carbon dioxide in the coastal oceans. *The Sea*, *13*, 269–315.

Dufresne, J. L., & Bony, S. (2008). An assessment of the primary sources of spread of global warming estimates from coupled atmosphere-ocean models. *Journal of Climate*, *21*(19), 5135–5144. https://doi.org/10.1175/2008JCLI2239.1

Edwards, N. P., Manning, P. L., Bergmann, U., Larson, P. L., van Dongen, B. E., Sellers, W. I., Webb, S. M., Sokaras, D., Alonso-Mori, R., Ignatyev, K., Barden, H. E., van Veelen, A., Anné, J., Egerton, V. M., & Wogelius, R. a. (2014). Leaf metallome preserved over 50 million years. *Metallomics*, *6*(4), 774–782. https://doi.org/10.1039/c3mt00242j

Emerson, S., & Hedges, J. (2008). *Chemical oceanography and the marine carbon cycle*. Cambridge University Press.

Farrimond, P., Comet, P., Eglinton, G., Evershed, R. P., Hall, M. A., Park, D. W., & Wardroper, A. M. K. (1984). Organic geochemical study of the Upper Kimmeridge Clay of the Dorset type area. *Marine and Petroleum Geology*, *1*(4), 340–354. https://doi.org/10.1016/0264-8172(84)90135-1

Field, C B, Behrenfeld, M. J., Randerson, J. T., & Falkowski, P. (1998). Primary productivity of the biosphere: an integration of terrestrial and oceanic components. *Science*, *281*(5374), 237–240. https://doi.org/10.1126/science.281.5374.237

Field, Christopher B., & Raupach, M. R. (2004). *The global carbon cycle : integrating humans, climate, and the natural world*. Island Press.

Filley, T. R., Freeman, K. H., Wilkin, R. T., & Hatcher, P. G. (2002). Biogeochemical controls on reaction of sedimentary organic matter and aqueous sulfides in holocene sediments of Mud Lake, Florida. *Geochimica et Cosmochimica Acta*, *66*(6), 937–954. https://doi.org/10.1016/S0016-7037(01)00829-8

Föllmi, K. B., Badertscher, C., de Kaenel, E., Stille, P., John, C. M., Adatte, T., & Steinmann, P. (2005). Phosphogenesis and organic-carbon preservation in the Miocene Monterey Formation at Naples Beach, California - The Monterey hypothesis revisited. In *Bulletin of the Geological Society of America* (Vol. 117, Issues 5–6, pp. 589–619). https://doi.org/10.1130/B25524.1

Francois, R. (1987). A study of sulfur enrichment in the humic fraction of marine-sediments during early diagenesis. *Geochimica et Cosmochimica Acta*, *51*(1), 17–27.

Fukushima, K., Yasukawa, M., Muto, N., Uemura, H., & Ishiwatari, R. (1992). Formation of C20 isoprenoid thiophenes in modern sediments. *Organic Geochemistry*, *18*(1), 83–91. https://doi.org/10.1016/0146-6380(92)90146-O

Garrison, R. E., Kastner, M., & Reimers, C. E. (1990). Miocene phosphogenesis in California. *Phosphate Deposits of the World, Vol.3. Neogene to Modern Phosphorites*, 285–299.

Greenspan, S. E., Migliorini, G. H., Lyra, M. L., Pontes, M. R., Carvalho, T., Ribeiro, L. P., Moura-Campos, D., Haddad, C. F. B., Toledo, L. F., Romero, G. Q., & Becker, C. G. (2020). Warming drives ecological community changes linked to host-associated microbiome dysbiosis. *Nature Climate Change*, *10*(11), 1057–1061. https://doi.org/10.1038/s41558-020-0899-5

Grice, K., Schouten, S., Blokker, P., Derenne, S., Largeau, C., Nissenbaum, A., & Sinninghe Damsté, J. S. (2003). Structural and isotopic analysis of kerogens in sediments rich in free sulfurised Botryococcus braunii biomarkers. *Organic Geochemistry*, *34*(3), 471–482. https://doi.org/10.1016/S0146-6380(02)00187-0

Grotheer, H., Greenwood, P. F., McCulloch, M. T., Böttcher, M. E., & Grice, K. (2017). δ34S character of organosulfur compounds in kerogen and bitumen fractions of sedimentary rocks. In *Organic Geochemistry* (Vol. 110, pp. 60–64). https://doi.org/10.1016/j.orggeochem.2017.04.005

Hallam, A., & Bradshaw, M. J. (1979). Bituminous shales and oolitic ironstones as indicators of transgressions and regressions. *Journal of the Geological Society*, *136*(2), 157–164. https://doi.org/10.1144/gsjgs.136.2.0157

Hartgers, W. A., Lòpez, J. F., De Las Heras, F. X. C., & Grimalt, J. O. (1996). Sulphur-binding in recent environments. I. Lipid by-products from Ni2B desulphurization. *Organic Geochemistry*, *25*(5–7), 353–365. https://doi.org/10.1016/S0146-6380(96)00141-6

Heald, C. L., Henze, D. K., Horowitz, L. W., Feddema, J., Lamarque, J. F., Guenther, A., Hess, P. G., Vitt, F., Seinfeld, J. H., Godstein, A. H., & Fung, I. (2008). Predicted change in global secondary organic aerosol concentrations in response to future climate, emissions, and land use change. *Journal of Geophysical Research Atmospheres*, *113*(5), 0–16. https://doi.org/10.1029/2007JD009092

Hebting, Y., Adam, P., & Albrecht, P. (2003). Reductive desulfurization of allylic thiols by HS^-/H_2S in water gives clue to chemical reactions widespread in natural environments. *Organic Letters*, *5*(9), 1571–1574. https://doi.org/10.1021/ol034374j

Hedges, J. I., Keil, R. G., & Benner, R. (1997). What happens to terrestrial organic matter in the ocean? *Organic Geochemistry*, *27*(5–6), 195–212. https://doi.org/10.1016/S0146-6380(97)00066-1

Hedges, John I., Baldock, J. A., Gélinas, Y., Lee, C., Peterson, M., & Wakeham, S. G. (2001). Evidence for non-selective preservation of organic matter in sinking marine particles. *Nature*, *409*(6822), 801–804. https://doi.org/10.1038/35057247

Heitmann, T., & Blodau, C. (2006). Oxidation and incorporation of hydrogen sulfide by dissolved organic matter. *Chemical Geology*, *235*(1–2), 12–20. https://doi.org/10.1016/j.chemgeo.2006.05.011

Hemingway, J. (1974). Jurassic. In J. Hemingway & D. Rayner (Eds.), *The Geology and Mineral Resources of Yorkshire* (pp. 161–223). Yorkshire Geological Society.

Herbin, J.-P., Muller, C., Geyssant, J. R., Melieres, F., Penn, I. E., & the Yorkim group. (1993). Variation of the distribution of organic matter within a transgressive system tract: Kimmeridge Clay, (Jurassic), England. *Source Rocks in a Sequence Stratigraphic Framework*, *37*, 67–100.

Herndl, G. J., & Reinthaler, T. (2013). Microbial control of the dark end of the biological pump. *Nature Geoscience*, *6*(9), 718–724. https://doi.org/10.1038/ngeo1921

Horner-Devine, M. C., Leibold, M. A., Smith, V. H., & Bohannan, B. J. M. (2003). Bacterial diversity patterns along a gradient of primary productivity. *Ecology Letters*, *6*(7), 613–622. https://doi.org/10.1046/j.1461-0248.2003.00472.x

Houghton, R. (2003). The contemporary carbon cycle. *Treatise on Geochemistry*, *8*, 682. http://adsabs.harvard.edu/abs/2003TrGeo...8..473H

Hülse, D., Arndt, S., Wilson, J. D., Munhoven, G., & Ridgwell, A. (2017). Understanding the causes and consequences of past marine carbon cycling variability through models. *Earth-Science Reviews*, *171*, 349–382. https://doi.org/10.1016/j.earscirev.2017.06.004

Hunt, J. M. (1996). *Petroleum geochemistry and geology*. W.H. Freeman.

Ingle, J. (1973). Summary comments on Neogene biostratigraphy, physical stratigraphy, and palaeo-oceanography in the marginal northeastern Pacific Ocean. *Initial Reports of the Deep Sea Drilling Project, Washington DC, U.S Government Printing Office*, *18*, 949–960.

Ingle, J. C., Jr. (1980). Cenozoic paleobathymetry and depositional history of selected sequences within the southern California continental borderland. *Cushman Foundation for Foraminiferal Research Special Publication*, *19*, 163–195.

Isaacs, C. M. (1985). Abundance versus rates of accumulation in fine-grained strata of the Miocene Santa Barbara Basin, California. *Geo-Marine Letters: An International Journal of Marine Geology*, *5*(1), 25–30. https://doi.org/10.1007/BF02629793

Isaacs, C. M., & Rullkötter, J. (2001). *The Monterey Formation : from rocks to molecules*. Columbia University Press.

Isaacs, C., & Magoon, L. (1984). Thermal indicators of organic matter in the Sisquoc and Monterey formations, Santa Maria Basin, California. *Society of Economic Paleontologists and Mineralogists Annual Midyear Meeting Abstracts*, *1*, 40.

Isaacs, C., & Petersen, N. (1987). Petroleum in the Miocene Monterey Formation, California. In J. R. Hein (Ed.), *sedimentary rock-hosted ores and petroleum.* Van Nostrand Reinhold.

Isaacs1, C. M. (1989). Field trip guide to deposition and diagenesis of the Monterey Formation, Santa Barbara and Santa Maria areas, California. *USGS Open-File , Report*, 84–98.

Jarvie, D. M., & Lundell, L. L. (2001). Kerogen type and thermal transformation of organic matter in the Miocene Monterey Formation. In *The Monterey Formation, from Rocks to Molecules* (pp. 268–295).

Jones, R. W. (1987). Organic facies. *Advances in Petroleum Geochemisrty*, *2*, 1–80.

Kaplan, I. R., & Rittenberg, S. C. (1964). Microbiological Fractionation of Sulphur Isotopes. *Journal of General Microbiology*, *34*(1958), 195–212. https://doi.org/10.1099/00221287-34-2-195

Kashiwabara, T., Toda, R., Nakamura, K., Yasukawa, K., Fujinaga, K., Kubo, S., Nozaki, T., Takahashi, Y., Suzuki, K., Kato, Y., Bennett, W. W., Lombi, E., Burton, E. D., Johnston, S. G., Kappen, P., Howard, D. L., Canfield, D. E., Lenstra, W. K., Hermans, M., … Penner-hahn, J. E. (2019). Sulfur speciation in heavy petroleums: Information from X-ray absorption near-edge structure. *Geochimica et Cosmochimica Acta*, *25*(1), 181–187. https://doi.org/10.1016/0016-7037(91)90343-4

Kastner, M., Keene, J. B., & Gieskes, J. M. (1977). Diagenesis of siliceous oozes-I. Chemical controls on the rate of opal-A to opal-CT transformation-an experimental study. *Geochimica et Cosmochimica Acta*, *41*(8), 1041–1059. https://doi.org/10.1016/0016-7037(77)90099-0

Keeling, R., & Shertz, S. (1992). Atmospheric oxygen and implications for the global carbon cycle. *Nature*, *358*(27), 723–727.

Killops, S., & Killops, V. (2005). Introduction to Organic Geochemistry. *Introduction to Organic Geochemistry*, 30–70. https://doi.org/10.1002/9781118697214

Kohnen, M. E. L., Sinninghe-Damsté, J.S., ten Haven, H. L, & de Leeuw, J. W. (1989). Early incorportation of polysulphides in sedimentary organic matter. *Nature*, *341*, 640–641. https://doi.org/10.1038/341640a0

Kohnen, M. E. L., Sinninghe-Damsté, J. S., & De Leeuw, J. W. (1991). Biases from natural sulphurization in palaeoenvironmental reconstruction based on hydrocarbon biomarker distributions. *Nature*, *349*(6312), 775–778. https://doi.org/doi:10.1038/349775a0

Kohnen, M. E. L, Sinninghe Damsté, J. S., Kock-van Dalen, A. C., & de Leew, J. W. (1991). Di- or polysulphide-bound biomarkers in sulphur-rich geomacromolecules as revealed by selective chemolysis. *Geochimica et Cosmochimica Acta*, *55*(5), 1375–1394. https://doi.org/10.1016/0016-7037(91)90315-V

Kok, M. D., Rijpstra, W. I. C., Robertson, L., Volkman, J. K., & Sinninghe Damsté, J. S. (2000). Early steroid sulfurisation in surface sediments of a permanently stratified lake (Ace Lake, Antarctica). *Geochimica et Cosmochimica Acta*, *64*(8), 1425–1436. https://doi.org/10.1016/S0016-7037(99)00430-5

Kok, M. D., Schouten, S., & Sinninghe Damsté, J. S. (2000). Formation of insoluble, nonhydrolyzable, sulfur-rich macromolecules via incorporation of inorganic sulfur species into algal carbohydrates. *Geochimica et Cosmochimica Acta*, *64*(15), 2689–2699. https://doi.org/10.1016/S0016-7037(00)00382-3

Kolonic, S., Sinninghe Damsté, J. S., Bottcher, M. E., Kuypers, M. M. M., Kuhnt, W., Beckmann, B., Scheeder, G., & Wagner, T. (2002). Geochemical characterization of Cenomanian/Turonian black shales from the Tarfaya Basin (SW Morocco) - Relationships between palaeoenvironmental conditions and early sulphurization of sedimentary organic matter. *Journal of Petroleum Geology*, *25*(3), 325–350. https://doi.org/10.1111/j.1747-5457.2002.tb00012.x

Koopmans, M. P., Köster, J., van Kaam-Peters, H. M. E., Kenig, F., Schouten, S., Hartgers, W. A., de Leeuw, J. W., & Sinninghe Damsté, J. S. (1996). Diagenetic and catagenetic products of isorenieratene: Molecular indicators for photic zone anoxia. *Geochimica et Cosmochimica Acta*, *60*(22), 4467–4496. https://doi.org/10.1016/S0016-7037(96)00238-4

Koopmans, M. P., Köster, J., van Kaam-Peters, H. M. E., Kenig, F., Schouten, S., Hartgers, W. A., de Leeuw, J. W., & Sinninghe Damsté, J. S. (1996). Diagenetic and catagenetic products of isorenieratene: Molecular indicators for photic zone anoxia. *Geochimica et Cosmochimica Acta*, *60*(22), 4467–4496. https://doi.org/10.1016/S0016-7037(96)00238-4

Krein, E B, & Aizenshtat, Z. (1993). Phase Transfer-Catalyzed Reactions Between Polysulfide Anions and alpha,beta-Unsaturated Carbonyl Compounds. *J Org Chem*, *58*(15), 6103–6108.

Krein, Eitan B. (1993). Organic sulfur in the geosphere: analysis, structures and chemical processes. In Saul Patai and Zvi Rappoport (Ed.), *Sulphur-Containing Functional Groups (1993)* (pp. 975–1032). John Wiley & Sons, Inc. https://doi.org/10.1002/9780470034408.ch17

Krumbein, W., & Swart, P. (1983). The microbial carbon cycle. In W. Krumbein (Ed.), *Microbial Geochemistry* (1st ed., pp. 5–62). Blackwell Scientific Publications.

Kump, L. R., Brantley, S. L., & Arthur, M. A. (2000). Chemical Weathering, Atmospheric CO2, and Climate. *Annual Review of Earth and Planetary Sciences*, *28*(1), 611–667. https://doi.org/10.1146/annurev.earth.28.1.611

Kundzewicz, Z. W., Kanae, S., Seneviratne, S. I., Handmer, J., Nicholls, N., Peduzzi, P., Mechler, R., Bouwer, L. M., Arnell, N., Mach, K., Muir-Wood, R., Brakenridge, G. R., Kron, W., Benito, G., Honda, Y., Takahashi, K., & Sherstyukov, B. (2014). Flood risk and climate change global and regional perspectives. *Hydrological Sciences Journal*, *59*(1), 1–28. https://doi.org/10.1080/02626667.2013.857411

Lallier-Vergès, E., Hayes, J. M., Boussafir, M., Zaback, D. A., Tribovillard, N. P., Connan, J., & Bertrand, P. (1997). Productivity-induced sulphur enrichment of hydrocarbon-rich sediments from the Kimmeridge Clay Formation. *Chemical Geology*, *134*(4), 277–288. https://doi.org/http://dx.doi.org/10.1016/S0009-2541(96)00093-9

LaLonde, R. T., Ferrara, L. M., & Hayes, M. P. (1987). Low-temperature, polysulfide reactions of conjugated ene carbonyls: A reaction model for the geologic origin of S-heterocycles. *Organic Geochemistry*, *11*(6), 563–571. https://doi.org/10.1016/0146-6380(87)90010-6

Landa, M., Blain, S., & Christaki, U. (2015). Shifts in bacterial community composition associated with increased carbon cycling in a mosaic of phytoplankton blooms. *The ISME*, 1–12. https://doi.org/10.1038/ismej.2015.105

Lannuzel, D., Tedesco, L., van Leeuwe, M., Campbell, K., Flores, H., Delille, B., Miller, L., Stefels, J., Assmy, P., Bowman, J., Brown, K., Castellani, G., Chierici, M., Crabeck, O., Damm, E., Else, B., Fransson, A., Fripiat, F., Geilfus, N. X., … Wongpan, P. (2020). The future of Arctic sea-ice biogeochemistry and ice-associated ecosystems. *Nature Climate Change*, *10*(11), 983–992. https://doi.org/10.1038/s41558-020-00940-4

Larson, R. L. (1991). Geological consequences of superplumes. In *Geology* (Vol. 19, Issue 10, pp. 963–966). https://doi.org/10.1130/0091-7613(1991)019<0963:GCOS>2.3.CO

Larson, Roger L., & Erba, E. (1999). Onset of the mid-Cretaceous greenhouse in the Barremian-Aptian: Igneous events and the biological, sedimentary, and geochemical responses. *Paleoceanography*, *14*(6), 663–678. https://doi.org/10.1029/1999PA900040

Laubach, S. E., Olson, J. E., & Cross, M. R. (2009). Mechanical and fracture stratigraphy. *AAPG Bulletin*, *93*(11), 1413–1426. https://doi.org/10.1306/07270909094

Leckie, R. M., Bralower, T. J., & Cashman, R. (2002). Oceanic anoxic events and plankton evolution: Biotic response to tectonic forcing during the mid-Cretaceous. *Paleoceanography*, *17*(3), 13-1-13–29. https://doi.org/10.1029/2001PA000623

Li, M., Baker, B. J., Anantharaman, K., Jain, S., Breier, J. A., & Dick, G. J. (2015). Genomic and transcriptomic evidence for scavenging of diverse organic compounds by widespread deep-sea archaea. *Nature Communications*, *Accepted*(May), 1–6. https://doi.org/10.1038/ncomms9933

Li, M., Jain, S., & Dick, G. J. (2016). Genomic and transcriptomic resolution of organic matter utilization among deep-sea bacteria in guaymas basin hydrothermal plumes. *Frontiers in Microbiology*, *7*, 1125. https://doi.org/10.3389/fmicb.2016.01125

Li, X., Cutter, G. A., Thunell, R. C., Tappa, E., Gilhooly, W. P., Lyons, T. W., Astor, Y., & Scranton, M. I. (2011). Particulate sulfur species in the water column of the Cariaco Basin. *Geochimica et Cosmochimica Acta*, *75*(1), 148–163. https://doi.org/10.1016/j.gca.2010.09.039

Liu, Y., Goodrick, S., & Heilman, W. (2014). Wildland fire emissions, carbon, and climate: Wildfire-climate interactions. *Forest Ecology and Management*, *317*, 80–96. https://doi.org/10.1016/j.foreco.2013.02.020

Lorius, C., Jouzel, J., Raynaud, D., Hansen, J., & Treut, H. Le. (1990). The ice-core record: climate sensitivity and future greenhouse warming. *Nature*, *347*(6289), 139–145. https://doi.org/10.1038/347139a0

Luckge, A., Horsfield, B., Littke, R., & Scheeder, G. (2002). Organic matter preservation and sulfur uptake in sediments from the continental margin off Pakistan. *Organic Geochemistry*, *33*(4), 477–488. https://doi.org/10.1016/S0146-6380(01)00171-1

MacKinnon, T. C. (1989). Origin of the Miocene Monterey Formation in California. In J. W. R. and R. E. G. T. MacKinnon (Ed.), *Oil in the Monterey California Formation Los Angeles to Santa Maria, California July 20-24, 1989* (pp. 1–10). American Geophysical Union. https://doi.org/10.1029/FT311p0001

Macquaker, J. H. S., & Gawthorpe, R. L. (1993). Mudstone lithofacies in the Kimmeridge Clay Formation, Wessex Basin, southern England; implications for the origin and controls of the distribution of mudstones. *Journal of Sedimentary Research*, *63*(6), 1129–1143. https://doi.org/10.1306/D4267CC1-2B26-11D7-8648000102C1865D

Macquaker, J. H. S., Gawthorpe, R. L., Taylor, K. G., & Oates, M. J. (1998). Heterogeneity, stacking patterns and sequence stratigraphic interpretation in distal mudstone successions: examples from the Kimmeridge Clay Formation, U.K. In *Shales and mudstones: basin studies, sedimentology and paleontology* (pp. 163–186).

Macquaker, Joe H. S., & Bohacs, K. M. (2007). On the Accumulation of Mud. *Science*, *318*(5857), 1734–1735. https://doi.org/DOI: 10.1126/science.1151980

Macquaker, J. H S, Bentley, S. J., & Bohacs, K. M. (2010). Wave-enhanced sediment-gravity flows and mud dispersal across continental shelves: Reappraising sediment transport processes operating in ancient mudstone successions. *Geology*, *38*(10), 947–950. https://doi.org/10.1130/G31093.1

Macquaker, J. H S, Taylor, K. G., Keller, M., & Polya, D. (2014). Compositional controls on early diagenetic pathways in fine-grained sedimentary rocks: Implications for predicting unconventional reservoir attributes of mudstones. *AAPG Bulletin*, *98*(3), 587–603. https://doi.org/10.1306/08201311176

Mahoney, C., März, C., Buckman, J., Wagner, T., & Blanco-Velandia, V. O. (2019). Pyrite oxidation in shales: Implications for palaeo-redox proxies based on geochemical and SEM-EDX evidence. *Sedimentary Geology*, *389*, 186–199. https://doi.org/10.1016/j.sedgeo.2019.06.006

Mann, K. H., & Lazier, J. R. N. (2013). Dynamics of Marine Ecosystems: Biological-Physical Interactions in the Oceans: Third Edition. In *Dynamics of Marine Ecosystems: Biological-Physical Interactions in the Oceans: Third Edition*. https://doi.org/10.1002/9781118687901

Manning, P. L., Edwards, N. P., Bergmann, U., Anné, J., Sellers, W. I., van Veelen, A., Sokaras, D., Egerton, V. M., Alonso-Mori, R., Ignatyev, K., van Dongen, B. E., Wakamatsu, K., Ito, S., Knoll, F., & Wogelius, R. A. (2019). Pheomelanin pigment remnants mapped in fossils of an extinct mammal. *Nature Communications*, *10*(1), 1–13. https://doi.org/10.1038/s41467-019-10087-2

Maynard, J. B. (1982). Extension of Berner's "New geochemical classification of sedimentary environments" to ancient sediments. *Journal of Sedimentary Research*, *52*(4), 1325–1331. https://doi.org/10.1306/212F812F-2B24-11D7-8648000102C1865D

McCarren, J., Becker, J. W., Repeta, D. J., Shi, Y., Young, C. R., Malmstrom, R. R., Chisholm, S. W., & DeLong, E. F. (2010). Microbial community transcriptomes reveal microbes and metabolic pathways associated with dissolved organic matter turnover in the sea. *Proceedings of the National Academy of Sciences of the United States of America*, *107*(38), 16420–16427. https://doi.org/10.1073/pnas.1010732107

Mcnamara, M. E., van Dongen, B. E., Lockyer, N. P., Bull, I. d., & Orr, P. J. (2016). Fossilization of melanosomes via sulfurization. *Palaeontology*, *59*(3), 337–350. https://doi.org/10.1111/pala.12238

Meister, P., Brunner, B., Picard, A., Böttcher, M. E., Jørgensen, B. B., Kashiwabara, T., Toda, R., Nakamura, K., Yasukawa, K., Fujinaga, K., Kubo, S., Nozaki, T., Takahashi, Y., Suzuki, K., Kato, Y., Bennett, W. W., Hockmann, K., Johnston, S. G., Burton, E. D., … Penner-hahn, J. E. (2019). Sulfur speciation in heavy petroleums: Information from X-ray absorption near-edge structure. *Geochimica et Cosmochimica Acta*, *25*(1), 181–187. https://doi.org/10.1016/0016-7037(91)90343-4

Meshoulam, A., & Amrani, A. (2017). Sulfur isotope exchange between thiophenes and inorganic sulfur compounds under hydrous pyrolysis conditions. *Organic Geochemistry*, *103*, 79–87. https://doi.org/10.1016/j.orggeochem.2016.10.006

Michalopoulos, P., & Aller, R. C. (2004). Early diagenesis of biogenic silica in the Amazon delta: Alteration, authigenic clay formation, and storage. *Geochimica et Cosmochimica Acta*, *68*(5), 1061–1085. https://doi.org/10.1016/j.gca.2003.07.018

Mirza, M. M. Q. (2003). Climate change and extreme weather events: Can developing countries adapt? *Climate Policy*, *3*(3), 233–248. https://doi.org/10.1016/S1469-3062(03)00052-4

Mitra-Kirtley, S., Mullins, O. C., Ralston, C. Y., & Pareis, C. (1999). Sulfur characterization in asphaltene, resin, and oil fractions of two crude oils. *ACS Division of Fuel Chemistry, Preprints*, *44*(4), 763–767.

Moore, T. S., Murray, R. W., Kurtz, A. C., & Schrag, D. P. (2004). Anaerobic methane oxidation and the formation of dolomite. *Earth and Planetary Science Letters*, *229*(1–2), 141–154. https://doi.org/10.1016/j.epsl.2004.10.015

Mopper, K., & Degens, E. (1979). Organic carbon in the ocean: nature and cycling. In S. Bolin, B., Degens, E.T., Kempe & P. Ketnwe (Eds.), *The global carbon cycle* (pp. 293–316). Wiley.

Morgans-Bell, H. S., Coe, A. L., Hesselbo, S. P., Jenkyns, H. C., Weedon, G. P., Marshall, J. E. A., Tyson, R. V, & Williams, C. J. (2001). Integrated stratigraphy of the Kimmeridge Clay Formation (Upper Jurassic) based on exposures and boreholes in south Dorset, UK. *Geological Magazine*, *138*(05), 511–539. https://doi.org/10.1017/s0016756801005738

Morris, K. A. (1979). A classification of jurassic marine shale sequences: An example from the toarcian (lower jurassic) of Great Britain. *Palaeogeography, Palaeoclimatology, Palaeoecology*, *26*(C), 117–126. https://doi.org/10.1016/0031-0182(79)90144-5

Mossmann, J. R., Aplin, A. C., Curtis, C. D., & Coleman, M. L. (1991). Geochemistry of inorganic and organic sulphur in organic-rich sediments from the Peru Margin. *Geochimica et Cosmochimica Acta*, *55*(12), 3581–3595. https://doi.org/10.1016/0016-7037(91)90057-C

Naeher, S., Smittenberg, R. H., Gilli, A., Kirilova, E. P., Lotter, A. F., & Schubert, C. J. (2012). Impact of recent lake eutrophication on microbial community changes as revealed by high resolution lipid biomarkers in Rotsee (Switzerland). *Organic Geochemistry*, *49*, 86–95. https://doi.org/10.1016/j.orggeochem.2012.05.014

Nelson, B. C., Eglinton I., T., Seewald, J. S., Vairavamurthy, M. A., & Miknis, F. P. (1995). Transformations in Organic Sulfur Speciation During Maturation of Monterey Shale: Constraints from Laboratory Experiments. *Geochemical Transformations of Sedimentary Sulfur*, *612*(April), 138–166. https://doi.org/10.1021/bk-1995-0612.ch008

Oni, O. E., Schmidt, F., Miyatake, T., Kasten, S., Witt, M., Hinrichs, K. U., & Friedrich, M. W. (2015). Microbial communities and organic matter composition in surface and subsurface sediments of the Helgoland mud area, North Sea. *Frontiers in Microbiology*, *6*(NOV). https://doi.org/10.3389/fmicb.2015.01290

Orr, W. L., & Sinninghe Damste, J. S. (1990). Geochemistry of sulfur in petroleum systems. *Geochemistry of Sulfur in Fossil Fuels*, *429*, 2–29. https://doi.org/doi:10.1021/bk-1990-0429.ch001

Orr, Wilson L. (1986). Kerogen/asphaltene/sulfur relationships in sulfur-rich Monterey oils. *Organic Geochemistry*, *10*(1–3), 499–516. https://doi.org/10.1016/0146-6380(86)90049-5

Orr, Wilson L. (1978). Sulfur in heavy oils, oil sands and oil shales. *Oil Sand and Oil Shale Chemistry: New York, Verlag Chemie*, 223--243.

Ouverney, C. C., & Fuhrman, J. A. (2000). Marine planktonic archaea take up amino acids. *Applied and Environmental Microbiology*, *66*(11), 4829–4833. https://doi.org/10.1128/AEM.66.11.4829-4833.2000

Passier, H. F., Bosch, H.-J., Nijenhuis, I. A., Lourens, L. J., Böttcher, M. E., Leenders, A., Damsté, J. S. S., de Lange, G. J., & de Leeuw, J. W. (1999). Sulphidic Mediterranean surface waters during Pliocene sapropel formation. *Nature*, *397*(6715), 146–149. https://doi.org/Doi 10.1038/16441

Pedersen, T. F., & Calvert, S. E. (1990). Anoxia vs. productivity: what controls the formation of organic- carbon-rich sediments and sedimentary rocks? In *American Association of Petroleum Geologists Bulletin* (Vol. 74, Issue 4, pp. 454–466). https://doi.org/10.1306/0C9B282B-1710-11D7-8645000102C1865D

Perlinger, J. A., Kalluri, V. M., Venkatapathy, R., & Angst, W. (2002). Addition of hydrogen sulfide to juglone. *Environmental Science and Technology*, *36*(12), 2663–2669. https://doi.org/10.1021/es015602c

Peters, K. E., Walters, C. C., & Moldowan, J. M. (2005). The Biomarker Guide Part 1: Biomarkers and isotopes in the environment and human history. *The Biomarker Guide*, 361. https://doi.org/10.1016/0146-6380(93)90028-A

Piper, D., & Isaacs, C. (2001). The Monterey Formation: bottom-water redox conditions and photic-zone primary productivity. In *Monterey Formation from Rocks to Molecules.* (pp. 31–58). Columbia University Press.

Pisciotto, K. A. (1981). Review of Secondary Carbonates in the Monterey Formation, California. In R. G. Garrison, R. E., and Douglas (Ed.), *The Monterey Formation and related siliceous rocks of California* (pp. 273–283). Los Angeles, Pacific Section, Society of Economic Paleontologists and Mineralogists.

Pisciotto, K. A., & Mahoney, J. J. (1977). Isotopic survey of Diagenetic Carbonates, Deep Sea Drilling Project Leg 63. *Initial Reports of the DSDP*, *63*, 595–609.

Pomerantz, A. E., Bake, K. D., Craddock, P. R., Kurzenhauser, K. W., Kodalen, B. G., Mitra-Kirtley, S., & Bolin, T. B. (2014). Sulfur speciation in kerogen and bitumen from gas and oil shales. *Organic Geochemistry*, *68*, 5–12.

Powell, J. H. (1984). Lithostratigraphical nomenclature of the Lias Group in the Yorkshire Basin. *Proceedings of the Yorkshire Geological Society*, *45*(1–2), 51–57. https://doi.org/10.1144/pygs.45.1-2.51

Pratt, L. M. (1984). Influence of paleoenvironmental factors on preservation of organic matter in middle cretaceous greenhorn formation, pueblo, colorado. In *American Association of Petroleum Geologists Bulletin* (Vol. 68, Issue 9, pp. 1146–1159). https://doi.org/10.1306/AD4616E7-16F7-11D7-8645000102C1865D

Pye, K., & Krinsley, D. H. (1986). Microfabric, mineralogy and early diagenetic history of the Whitby Mudstone Formation (Toarcian), Cleveland Basin, U.K. *Geological Magazine*, *123*(03), 191. https://doi.org/10.1017/S0016756800034695

Qin, S. S., Zhu, M. X., Yang, G. P., & Wang, D. (2019). Atypical diagenesis of sulfur and iron in sediments of the river-dominated Bohai Sea (China). *Journal of Marine Systems*, *189*, 116–126. https://doi.org/10.1016/j.jmarsys.2018.10.004

Raiswell, R., & Anderson, T. F. (2005). Reactive iron enrichment in sediments deposited beneath euxinic bottom waters: constraints on supply by shelf recycling. *Geological Society, London, Special Publications*, *248*(1), 179–194. https://doi.org/10.1144/GSL.SP.2005.248.01.10

Raiswell, R., Canfield, D. E., & Berner, R. A. (1994). A comparison of iron extraction methods for the determination of degree of pyritisation and the recognition of iron-limited pyrite formation. *Chemical Geology*, *111*(1–4), 101–110. https://doi.org/10.1016/0009-2541(94)90084-1

Ramanathan, V., & Feng, Y. (2009). Air pollution, greenhouse gases and climate change: Global and regional perspectives. *Atmospheric Environment*, *43*(1), 37–50. https://doi.org/10.1016/j.atmosenv.2008.09.063

Raven, M. R., Keil, R. G., & Webb, S. M. (2020). *Microbial sulfate reduction and organic sulfur formation in sinking marine particles*. *6035*(December), 1–9.

Raven, M. R., Adkins, J. F., Werne, J. P., Lyons, T. W., & Sessions, A. L. (2015). Sulfur isotopic composition of individual organic compounds from Cariaco Basin sediments. *Organic Geochemistry*, *80*, 53–59. https://doi.org/10.1016/j.orggeochem.2015.01.002

Raven, M. R., Fike, D. A., Bradley, A. S., Gomes, M. L., Owens, J. D., & Webb, S. A. (2019). Paired organic matter and pyrite δ 34 S records reveal mechanisms of carbon, sulfur, and iron cycle disruption during Ocean Anoxic Event 2. *Earth and Planetary Science Letters*, *512*, 27–38. https://doi.org/10.1016/j.epsl.2019.01.048

Raven, M. R., Fike, D. A., Gomes, M. L., Webb, S. M., Bradley, A. S., & McClelland, H. L. O. (2018). Organic carbon burial during OAE2 driven by changes in the locus of organic matter sulfurization. *Nature Communications*, *9*(1). https://doi.org/10.1038/s41467-018-05943-6

Raven, M. R., Sessions, A. L., Adkins, J. F., & Thunell, R. C. (2016). Rapid organic matter sulfurization in sinking particles from the Cariaco Basin water column. *Geochimica et Cosmochimica Acta*, *190*, 175–190. https://doi.org/10.1016/j.gca.2016.06.030

Rawson, P. F., Greensmith, J. T., & Shalaby, S. E. (1983). Coarsening-upwards cycles in the uppermost Staithes and Cleveland Ironstone Formations (Lower Jurassic) of the Yorkshire coast, England. *Proceedings of the Geologists' Association*, *94*(1), 91–93. https://doi.org/10.1016/S0016-7878(83)80033-9

Riboulleau, A., Derenne, S., Sarret, G., Largeau, C., Baudin, F., & Connan, J. (2000). Pyrolytic and spectroscopic study of a sulphur-rich kerogen from the “Kashpir oil shales” (Upper Jurassic, Russian platform). *Organic Geochemistry*, *31*(12), 1641–1661. https://doi.org/10.1016/S0146-6380(00)00088-7

Rickard, D. T. (1975). Kinetics and mechanism of pyrite formation at low temperatures. *American Journal of Science*, *275*, 636–652.

Ridgwell, A., & Zeebe, R. E. (2005). The role of the global carbonate cycle in the regulation and evolution of the Earth system. In *Earth and Planetary Science Letters* (Vol. 234, Issues 3–4, pp. 299–315). https://doi.org/10.1016/j.epsl.2005.03.006

Riebesell, U., Schulz, K. G., Bellerby, R. G. J., Botros, M., Fritsche, P., Meyerhöfer, M., Neill, C., Nondal, G., Oschlies, A., Wohlers, J., & Zöllner, E. (2007). Enhanced biological carbon consumption in a high CO2 ocean. *Nature*, *450*(7169), 545–548. https://doi.org/10.1038/nature06267

Rossi, V., McNamara, M. E., Webb, S. M., Ito, S., & Wakamatsu, K. (2019). Tissue-specific geometry and chemistry of modern and fossilized melanosomes reveal internal anatomy of extinct vertebrates. *Proceedings of the National Academy of Sciences of the United States of America*, *116*(36), 17880–17889. https://doi.org/10.1073/pnas.1820285116

Ruddiman, W. F. (2001). *Earth’s climate : past and future*. W.H. Freeman.

Rullköetter, J., & Isaacs, C. (1996). Monterey source rock facies and petroleum formation-a synthesis of results of the cooperative Monterey organic geochemistry study. *American Association of Petroleum Geologists and Pacific Section SEPM (Society for Sedimentary Geology) Annual Meeting Abstracts*, *5*, 123. https://www.osti.gov/scitech/biblio/425841

Rullkötter, J. (2006). Organic matter: the driving force for early diagenesis. In M. Schulz, H. D. and Zabel (Ed.), *Marine geochemistry* (pp. 125–168). Springer Verlag. https://doi.org/10.1007/3-540-32144-6_4

Graham S. A., &William, L. A. (1985). Tectonic, Depositional, and Diagenetic History of Monterey Formation (Miocene), Central San Joaquin Basin, California. *American Association of Petroleum Geologists Bulletin*, *69*, 385–411. https://doi.org/10.1306/AD4624F7-16F7-11D7-8645000102C1865D

Salem, N. (2013). Geochemical characterisation of the Pliensbachian -Toarcian boundary during the onset of the Toarcian Oceanic Anoxic Event. North Yorkshire, UK, PhD Thesis, Newcastle University, UK.

Schaeffer, P., Adam, P., Philippe, E., Trendel, J. M., Schmid, J. C., Behrens, A., Connan, J., & Albrecht, P. (2006). The wide diversity of hopanoid sulfides evidenced by the structural identification of several novel hopanoid series. *Organic Geochemistry*, *37*(11), 1590–1616. https://doi.org/10.1016/j.orggeochem.2006.04.005

Schimel DS, Enting IG, Heimann M, Wigley TML, Raynaud D, Alves D, S. U. (1995). CO2 and the Carbon Cycle. In M. F. L. Houghton JT, H. N. Bruce J, Lee H, Callander BA, Haites E, & Maskell K (Eds.), *Climate change 1994: radiative forcing of climate change and an evaluation of the IPCC 1992 IS92 emission scenarios* (pp. 35–71). Cambridge University Press.

Schlesinger, W H. (1997). Biogeochemistry: an analysis of global change - 2nd ed. *Academic Press, San Diego*, 139–143.

Schlesinger, William H., & Bernhardt, E. S. (2013). Biogeochemistry. *Biogeochemistry*, *Dukes 2003*, 135–172. https://doi.org/10.1016/B978-0-12-385874-0.00005-4

Schmid, J. C., Connan, J., & Albrecht, P. (1987). Occurrence and geochemical significance of long-chain dialkylthiacyclopentanes. *Nature*, *329*(6134), 54–56. https://doi.org/10.1038/329054a0

Schouten, S., de Graaf, W., Sinninghe Damsté, J. S., van Driel, G. B., & de Leeuw, J. W. (1994). Laboratory simulation of natural sulphurization: II. Reaction of multi-functionalized lipids with inorganic polysulphides at low temperatures. *Organic Geochemistry*, *22*(3–5), 825–834. https://doi.org/10.1016/0146-6380(94)90142-2

Schouten, S., Eglinton, T. I., Sinninghe Damsté, J. S., & de Leeuw, J. W. (1995). Influence of Sulphur Cross-linking on the Molecular-Size Distribution of Sulphur-Rich Macromolecules in Bitumen. In *Geochemical Transformations of Sedimentary Sulfur* (Vol. 612, pp. 5–80). American Chemical Society. https://doi.org/doi:10.1021/bk-1995-0612.ch005

Schunck, H., Lavik, G., Desai, D. K., Großkopf, T., Kalvelage, T., Löscher, C. R., Paulmier, A., Contreras, S., Siegel, H., Holtappels, M., Rosenstiel, P., Schilhabel, M. B., Graco, M., Schmitz, R. A., Kuypers, M. M. M., & LaRoche, J. (2013). Giant Hydrogen Sulfide Plume in the Oxygen Minimum Zone off Peru Supports Chemolithoautotrophy. *PLoS ONE*, *8*(8). https://doi.org/10.1371/journal.pone.0068661

Schwarzwald, K., Poppick, A., Rugenstein, M., Bloch-johnson, J., & Mcinerney, D. (n.d.). *Changes in future precipitation mean and variability across scales*. 1–55. https://doi.org/10.1175/JCLI-D-20-0001.1.

Scotchman, I C. (1989). Diagenesis of the Kimmeridge Clay Formation, onshore UK. *Journal of the Geological Society*, *146*, 285–303. https://doi.org/10.1144/gsjgs.146.2.0283

Scotchman, I. C. (1987). Clay diagenesis in the Kimmeridge Clay Formation, onshore UK, and its relation to organic maturation. *Mineralogical Magazine*, *51*(62), 535–551.

Shaw, H. F., & Primmer, T. J. (1991). Diagenesis of mudrocks from the Kimmeridge Clay Formation of the Brae Area, UK North Sea. *Marine and Petroleum Geology*, *8*(3), 270–277. https://doi.org/10.1016/0264-8172(91)90081-B

Shawar, L., Halevy, I., Said-Ahmad, W., Feinstein, S., Boyko, V., Kamyshny, A., & Amrani, A. (2018). Dynamics of pyrite formation and organic matter sulfurization in organic-rich carbonate sediments. *Geochimica et Cosmochimica Acta*, *241*, 219–239. https://doi.org/10.1016/j.gca.2018.08.048

Sinninghe Damsté, J. S., Rijpstra, W. I. C., Kock-van Dalen, A. C., de Leeuw, J. W., & Schenck, P. A. (1989). Quenching of labile functionalised lipids by inorganic sulphur species: Evidence for the formation of sedimentary organic sulphur compounds at the early stages of diagenesis. *Geochimica et Cosmochimica Acta*, *53*(6), 1343–1355. https://doi.org/10.1016/0016-7037(89)90067-7

Sinninghe Damsté, J. S., ten Haven, H. L., de Leeuw, J. W., & Schenck, P. A. (1986). Organic geochemical studies of a Messinian evaporitic basin, northern Apennines (Italy)-II Isoprenoid and n-alkyl thiophenes and thiolanes. *Organic Geochemistry*, *10*(4–6), 791–805. https://doi.org/10.1016/S0146-6380(86)80016-X

Sinninghe Damsté, J. S, Kohnen, M. E. L., & de Leeuw, J. W. (1990). Thiophenic biomarkers for palaeoenvironmental assessment and molecular stratigraphy. *Nature*, *345*(6276), 609–611. https://doi.org/doi:10.1038/345609a0

Sinninghe Damsté, J. S., & de Leeuw, J. W. (1990). Analysis, structure and geochemical significance of organically-bound sulphur in the geosphere: State of the art and future research. *Organic Geochemistry*, *16*(4–6), 1077–1101. https://doi.org/10.1016/0146-6380(90)90145-P

Sinninghe Damsté, J. S., de Leeuw, J. W., Kock-van Dalen, A. C., de Zeeuw, M. A., de Lange, F., Rijpstra, W. I. C., & Schenck, P. A. (1987). The occurrence and identification of series of organic sulphur compounds in oils and sediment extracts. I. A study of Rozel Point Oil (U.S.A.). *Geochimica et Cosmochimica Acta*, *51*(9), 2369–2391. https://doi.org/10.1016/0016-7037(87)90291-2

Sinninghe Damsté, J. S., Eglinton, T. I., de Leeuw, J. W., & Schenck, P. A. (1989). Organic sulphur in macromolecular sedimentary organic matter: I. Structure and origin of sulphur-containing moieties in kerogen, asphaltenes and coal as revealed by flash pyrolysis. *Geochimica et Cosmochimica Acta*, *53*(4), 873–889. https://doi.org/10.1016/0016-7037(89)90032-X

Sinninghe Damsté, J. S., Rijpstra, W. I. C., de Leeuw, J. W., & Schenck, P. A. (1988). Origin of organic sulphur compounds and sulphur-containing high molecular weight substances in sediments and immature crude oils. *Organic Geochemistry*, *13*(4–6), 593–606. https://doi.org/10.1016/0146-6380(88)90079-4

Sinninghe Damsté, J. S., Kok, M. D., Köster, J., & Schouten, S. (1998). Sulfurized carbohydrates: An important sedimentary sink for organic carbon? *Earth and Planetary Science Letters*, *164*(1–2), 7–13. https://doi.org/10.1016/S0012-821X(98)00234-9

Sinnighe Damsté, J. S., Rijpstra, W. I. C., & Reichart, G. J. (2002). The influence of oxic degradation on the sedimentary biomaker record II. Evidence from Arabian Sea sediments. Geochimica et Cosmochimica Acta, 66(15), 2737–2754. https://doi.org/10.1016/S0016-7037(02)00865-7

Sinninghe Damsté, J. S., Rijpstra, W. I. C., Coolen, M. J. L., Schouten, S., & Volkman, J. K. (2007). Rapid sulfurisation of highly branched isoprenoid (HBI) alkenes in sulfidic Holocene sediments from Ellis Fjord, Antarctica. *Organic Geochemistry*, *38*(1), 128–139. https://doi.org/10.1016/j.orggeochem.2006.08.003

Smith, D. A., Sessions, A. L., Dawson, K. S., Dalleska, N., & Orphan, V. J. (2017). Rapid quantification and isotopic analysis of dissolved sulfur species. *Rapid Communications in Mass Spectrometry*, *31*(9), 791–803. https://doi.org/10.1002/rcm.7846

Smith, M. B., & March, J. (2001). March's advanced organic chemistry. In *Molecules* (Vol. 6, Issue 12). Wiley & Sons, Ltd. https://doi.org/10.3390/61201064

Speirs, J., McGlade, C., & Slade, R. (2015). Uncertainty in the availability of natural resources: Fossil fuels, critical metals and biomass. *Energy Policy*, *87*, 654–664. https://doi.org/10.1016/j.enpol.2015.02.031

Steinberg, M. M. H. M. (1999). Greenhouse gas carbon dioxide mitigation: science and technology. In *Greenhouse gas carbon dioxide mitigation: science and technology* (pp. 221–252).

Suess, E. (1980). Particulate organic carbon flux in the oceans—surface productivity and oxygen utilization. *Nature*, *288*(5788), 260–263. https://doi.org/10.1038/288260a0

Summons, R. E., & Powell, T. G. (1987). Identification of aryl isoprenoids in source rocks and crude oils: Biological markers for the green sulphur bacteria. *Geochimica et Cosmochimica Acta*, *51*(3), 557–566. https://doi.org/10.1016/0016-7037(87)90069-X

Sundquist, E. T., Ackerman, K. V, Parker, L., & Huntzinger, D. N. (2009). An Introduction to Global Carbon Cycle Management. In *Carbon sequestration and its role in the global carbon cycle* (pp. 1–23). https://doi.org/10.1029/2009GM000914

Szczerbowska-Boruchowska, M., Stegowski, Z., Lankosz, M., Szpak, M., & Adamek, D. (2012). A synchrotron radiation micro-X-ray absorption near edge structure study of sulfur speciation in human brain tumors - A methodological approach. *Journal of Analytical Atomic Spectrometry*, *27*(2), 239–247. https://doi.org/10.1039/c2ja10211k

Taylor, K. G., & Macquaker, J. H. S. (2000). Early diagenetic pyrite morphology in a mudstone-dominated succession: The Lower Jurassic Cleveland Ironstone Formation, eastern England. *Sedimentary Geology*, *131*(1–2), 77–86. https://doi.org/10.1016/S0037-0738(00)00002-6

Taylor, K. G., & Macquaker, J. H. S. (2011). Iron minerals in marine sediments record chemical environments. *Elements*, *7*(2), 113–118. https://doi.org/10.2113/gselements.7.2.113

Tegelaar, E. W., de Leeuw, J. W., Derenne, S., & Largeau, C. (1989). A reappraisal of kerogen formation. *Geochimica et Cosmochimica Acta*, *53*(11), 3103–3106. https://doi.org/10.1016/0016-7037(89)90191-9

Tissot, B. P., & Welte, D. H. (1984). Petroleum Formation and Occurrence. In *Second Revised and Enlarged Edition* (Vol. 66, Issue 37). https://doi.org/10.1029/EO066i037p00643

Turchyn, A. V., Antler, G., Byrne, D., Miller, M., & Hodell, D. A. (2015). Microbial sulfur metabolism evidenced from pore fluid isotope geochemistry at Site U1385. *Global and Planetary Change*, *141*, 82–90. https://doi.org/10.1016/j.gloplacha.2016.03.004

Tyson, R. V. (2005). The "Productivity Versus Preservation" Controversy: Cause, Flaws, and Resolution. *Deposition of Organic-Carbon-Rich Sediments: Models*, *82*, 17–33. https://doi.org/10.2110/pec.05.82.0017

Tyson, R. V. (2004). Variation in marine total organic carbon through the type Kimmeridge Clay Formation (Late Jurassic), Dorset, UK. *Journal of the Geological Society*, *161*, 667–673. https://doi.org/10.1144/0016-764903-078

Tyson, R. V. (1996). Sequence-stratigraphical interpretation of organic facies variations in marine siliciclastic systems: general principles and application to the onshore Kimmeridge Clay Formation, UK. *Geological Society, London, Special Publications*, *103*(1), 75–96. https://doi.org/10.1144/gsl.sp.1996.103.01.06

Urban, N. R., Ernst, K., & Bernasconi, S. (1999). Addition of sulfur to organic matter during early diagenesis of lake sediments. *Geochimica et Cosmochimica Acta*, *63*(6), 837–853. https://doi.org/10.1016/S0016-7037(98)00306-8

Vairavamurthy, A., Zhou, W., Eglinton, T., & Manowitz, B. (1994). Sulfonates: A novel class of organic sulfur compounds in marine sediments. *Geochimica et Cosmochimica Acta*, *58*(21), 4681–4687. https://doi.org/10.1016/0016-7037(94)90200-3

Valisolalao, J., Perakis, N., Chappe, B., & Albrecht, P. (1984). A novel sulfur containing C35 hopanoid in sediments. *Tetrahedron Letters*, *25*(11), 1183–1186. https://doi.org/10.1016/S0040-4039(01)91555-2

van Dongen, B. E., Rijpstra, W. I. C., Philippart, C. J. M., de Leeuw, J. W., & Sinninghe Damsté, J. S. (2000). Biomarkers in upper Holocene Eastern North Sea and Wadden Sea sediments. *Organic Geochemistry*, *31*(12), 1533–1543. https://doi.org/10.1016/S0146-6380(00)00125-X

van Dongen, B. E., Schouten, S., Baas, M., Geenevasen, J. A. J., & Sinninghe Damsté, J. S. (2003a). An experimental study of the low-temperature sulfurization of carbohydrates. *Organic Geochemistry*, *34*(8), 1129–1144. https://doi.org/10.1016/S0146-6380(03)00060-3

van Dongen, B. E., Schouten, S., & Sinninghe Damsté, J. S. (2003b). Sulfurization of carbohydrates results in a sulfur-rich, unresolved complex mixture in Kerogen pyrolysates. *Energy and Fuels*, *17*(4), 1109–1118. https://doi.org/10.1021/ef0202283

van Dongen, B. E., Schouten, S., & Sinninghe Damsté, J. S. (2006). Preservation of carbohydrates through sulfurization in a Jurassic euxinic shelf sea: Examination of the Blackstone Band TOC cycle in the Kimmeridge Clay Formation, UK. *Organic Geochemistry*, *37*(9), 1052–1073. https://doi.org/10.1016/j.orggeochem.2006.05.007

van Kaam-Peters, H. M. E., Schouten, S., de Leeuw, J. W., & Sinninghe Damsté, J. S. (1997). A molecular and carbon isotope biogeochemical study of biomarkers and kerogen pyrolysates of the Kimmeridge Clay Facies: Palaeoenvironmental implications. *Organic Geochemistry*, *27*(7–8), 399–422. https://doi.org/10.1016/S0146-6380(97)00084-3

van Kaam-Peters, H. M. E., Schouten, S., Köster, J., & Sinninghe Damstè, J. S. S. (1998). Controls on the molecular and carbon isotopic composition of organic matter deposited in a Kimmeridgian euxinic shelf sea: Evidence for preservation of carbohydrates through sulfurisation. *Geochimica et Cosmochimica Acta*, *62*(19–20), 3259–3283. https://doi.org/10.1016/S0016-7037(98)00231-2

Wagner, T., Hofmann, P., & Flögel, S. (2013). Marine black shale deposition and Hadley Cell dynamics: A conceptual framework for the Cretaceous Atlantic Ocean. *Marine and Petroleum Geology*, *43*, 222–238. https://doi.org/10.1016/j.marpetgeo.2013.02.005

Wagner, T., Kasten, S., & Kolonic, S. (2003). Non-steady state redox conditions in bottom and pore waters of the Mid-Cretaceous NW-African shelf at Tarfaya (SW-Morocco): Climate control and implications for synchrony of basin-wide oxidation of shallow waters during the CT-OAE2. *American Geophysical Union, Fall Meeting 2003, Abstract #PP41C-0847*.

Wakeham, S. G., Sinninghe Damsté, J. S., Kohnen, M. E. L., & de Leeuw, J. W. (1995). Organic sulfur compounds formed during early diagenesis in Black Sea sediments. *Geochimica et Cosmochimica Acta*, *59*(3), 521–533. https://doi.org/10.1016/0016-7037(94)00361-O

Wakeham, S. G., Sinninghe Damsté, J. S., Kohnen, M. E. L., & de Leeuw, J. W. (1995). Organic sulfur compounds formed during early diagenesis in Black Sea sediments. *Geochimica et Cosmochimica Acta*, *59*(3), 521–533. https://doi.org/10.1016/0016-7037(94)00361-O

Waldo, G. S., Carlson, R. M. K., Moldowan, J. M., Peters, K. E., & Penner-hahn, J. E. (1991). Sulfur speciation in heavy petroleums: Information from X-ray absorption near-edge structure. *Geochimica et Cosmochimica Acta*, *55*(3), 801–814. https://doi.org/10.1016/0016-7037(91)90343-4

Watanabe, K., & Kuwae, T. (2015). How organic carbon derived from multiple sources contributes to carbon sequestration processes in a shallow coastal system? *Global Change Biology*, *21*(7), 2612–2623. https://doi.org/10.1111/gcb.12924

Waterhouse, H. K. (1999). Orbital forcing of palynofacies in the Jurassic of France and the United Kingdom. *Geology*, *27*(6), 511–514. https://doi.org/10.1130/0091-7613(1999)027<0511:OFOPIT>2.3.CO;2

Werne, J. P., Hollander, D. J., Behrens, A., Schaeffer, P., Albrecht, P., & Sinninghe Damsté, J. S. (2000). Timing of early diagenetic sulfurization of organic matter: A precursor-product relationship in Holocene sediments of the anoxic Cariaco Basin, Venezuela. *Geochimica et Cosmochimica Acta*, *64*(10), 1741–1751. https://doi.org/10.1016/S0016-7037(99)00366-X

Werne, J. P., Hollander, D. J., Lyons, T. W., & Sinninghe Damsté, J. S. S. (2004). Organic sulfur biogeochemistry : Recent advances and future research directions. *Geological Society of America 4*, 135–150.

Werne, J. P., Hollander, D. J., Lyons, T. W., & Sinninghe Damsté, J. S. (2004). Organic sulfur biogeochemistry: Recent advances and future research directions. *Geological Society of America Special Papers*, *379*, 135–150. https://doi.org/10.1130/0-8137-2379-5.135

Werne, J. P., Lyons, T. W., Hollander, D. J., Formolo, M. J., & Sinninghe Damsté, J. S. (2003). Reduced sulfur in euxinic sediments of the Cariaco Basin: Sulfur isotope constraints on organic sulfur formation. *Chemical Geology*, *195*(1–4), 159–179. https://doi.org/10.1016/S0009-2541(02)00393-5

Werne, J. P., Lyons, T. W., Hollander, D. J., Schouten, S., Hopmans, E. C., & Sinninghe Damsté, J. S. (2008). Investigating pathways of diagenetic organic matter sulfurization using compound-specific sulfur isotope analysis. *Geochimica et Cosmochimica Acta*, *72*(14), 3489–3502. https://doi.org/10.1016/j.gca.2008.04.033

Wiltfong, R., Mitra-Kirtley, S., Mullins, O. C., Andrews, B., Fujisawa, G., & Larsen, J. W. (2005). Sulfur speciation in different kerogens by XANES spectroscopy. *Energy and Fuels*, *19*(5), 1971–1976. https://doi.org/10.1021/ef049753n

Zaback, D. A., & Pratt, L. M. (1992). Isotopic composition and speciation of sulfur in the Miocene Monterey Formation: Reevaluation of sulfur reactions during early diagenesis in marine environments. *Geochimica et Cosmochimica Acta*, *56*(2), 763–774. https://doi.org/10.1016/0016-7037(92)90096-2

Zheng, L., Chen, X., Dong, X., Wei, X., Jiang, C., Tang, Q., Bowles, M. W., MogolÍon, J. M., Kasten, S., Zabel, M., Hinrichs, K. U., Sim, M. S., Paris, G., Adkins, J. F., Orphan, V. J., Sessions, A. L., Wing, B. A., Halevy, I., Valiente, N., … Vaida, V. (2019). Decrypting the sulfur cycle in oceanic oxygen minimum zones. *Geochimica et Cosmochimica Acta*, *12*(1), 74–83. https://doi.org/10.1073/pnas.1702953114

Ziegler, P. (1990). Geological atlas of western and central Europe (2nd ed.). Shell International Petroleum.

Chapter 2

Project 1

Fundamental Controls on Organic Matter Preservation in Organic and Sulfur-Rich Hydrocarbon Source Rocks

Yusuf Abubakar [1, 2, *], Kevin G. Taylor[1], Victoria Coker[1], Roy A. Wogelius[1] and Bart E. van Dongen[1]

[1] Williamson Research Centre, Department of Earth and Environmental Sciences, University of Manchester, Oxford Road, Manchester, M13 9PL, UK

[2] Desert Research, Monitoring and Control Centre, Yobe State University, KM 7, Sir Kashim Road, Damaturu, Nigeria

[*]Correspondence: yusuf.abubakar@manchester.ac.uk; yusuf.abubakar@ysu.edu.ng

To be submitted to Marine and Petroleum Geology

Highlights

- Organic sulfur compounds were quantified for the first time in the Whitby Mudstone Formation.
- State-of-the-art electron microprobe imaging of total sulfur and iron in organic and sulfur-rich mudstones was feasible for the first time.
- Reaction between iron and sulfur is preferential over that sulfur and organic matter in iron dominated basins.
- Hydrogen over carbon and sulfur over carbon atomic ratios may not be reliable in assessing mudstones with high sulfur and low organic carbon.

Abstract

Incorporation of reduced inorganic sulfur (S) into organic matter (OM) in anoxic/euxinic environments is considered a vital route through which OM is sequestered in sediments for millions of years. However, precipitation of iron (Fe) sulfides, mainly pyrite (FeS_2), is believed to compete with OM preservation via sulfurisation. Multiple high resolution geochemical, petrographic and electron microprobe (EMPA) analyses were employed to better understand S controls on OM preservation with particular focus on FeS_2 precipitation in model organic and S-rich mudstones e.g., the Kimmeridge Clay (KCF), Monterey (MF) and Whitby Mudstone [Grey Shale (GS) and Jet Rock (JR) Members] Formations. Results indicate that S in the KCF and MF is mostly bound to OM as indicated by the relative abundance of organic sulfur compounds (OSCs) compared to other hydrocarbons in their pyrolysates. The relative low amounts of Fe in both the KCF and MF permitted extensive reaction of S and OM to occur efficiently, promoting preservation of high amounts OM through sulfurisation in these settings. EMPA imaging of total S and Fe in the studied mudstones was feasible for the first time and provided information about the distribution and nature of S and Fe. S signals in the KCF and MF were almost evenly spread across the whole imaged area, except for carbonate/phosphate-rich regions and Fe signals were relatively very low, indicating S in the KCF and MF is most likely bound to organics, supporting geochemical analyses. Contrary to the KCF and MF, S in the GS and JR, were not mostly organically bound as indicated by the relatively low/absence of OSCs and predominance of other hydrocarbons in their pyrolysates. The relative high amounts of Fe in both the GS and JR sequestered S as FeS_2, limiting S and OM reactions, hence, preservation through sulfurisation was less significant in these settings. S signals in the EMPA images of the GS and JR, although widespread, exist in discrete shapes/units ranging in geometry and size (from few nm up to 15 μm) and in most cases correlated with Fe when compared with their corresponding Fe EMPA images, indicating that the S in the GS and JR is not mostly bound to organics rather, it exists in discrete authigenic FeS_2, as supporting petrographic analyses. This study reported, for the first time, detailed distribution of OSCs in the MF, GS and JR, and compared/contrasted them with those previously observed in the KCF. This study further shows that state-of-the-art EMPA imaging of total S and Fe in organic and S-rich mudstones is feasible. Overall, the study supports preservation of OM through sulfurisation as an important pathway for massive sequestration of OM in the sedimentary record and, the abundance reactive Fe, could significantly hinder this process by preferentially reacting with reduced S, to form iron sulfides (mainly FeS_2), thus impeding reactions between

OM and S to occur efficiently. However, there is still a need to study S and Fe species (oxidation states) both at low and high resolutions to fully comprehend sulfurisation and FeS_2 formation processes.

Keywords/Phrases: Organic Matter Sulfurisation, Pyrite, Electron Microprobe Imaging, Kimmeridge Clay Formation, Monterey Formation, Whitby Mudstone Formation.

2.1 Introduction

Abundance of carbon dioxide (CO_2) in the atmosphere intensifies global/climate warming (Dufresne & Bony, 2008; Heald et al., 2008; Archer et al., 2009; Ramanathan & Feng, 2009; Aminu et al., 2017). However, this is naturally mitigated by the sequestration of CO_2 in sediments either as carbonate rocks or organic matter (OM; Li, 1972; Demaison & Moore, 1980; Demaison, 1991; Des Marais et al., 1992; van Cappellen & Canfield, 1993; Ruddy, 1997; Ruddiman, 2001; Kolonic et al., 2002; Ducklow & McCallister, 2004; Field & Raupach, 2004; Le Quéré & Metzl, 2004; Rullkötter, 2006; Emerson & Hedges, 2008; Wagner et al., 2013). Multiple processes/pathways have been reported through which CO_2 can be can preserved as OM in the sedimentary record (Müller & Suess, 1979; Demaison & Moore, 1980; Jenkyns, 1980, 1991; Suess, 1980; Arthur et al., 1984, 1987; Pratt, 1984; Pratt & King, 1986; Calvert, 1987; Canfield, 1989; Tegelaar et al., 1989; Pedersen & Calvert, 1990; Betts & Holland, 1991; Demaison, 1991; Calvert & Pedersen, 1992; van Cappellen & Canfield, 1993; Kolonic, et al., 2002; Rullkötter, 2006). One of these processes/pathways is the incorporation of reduced inorganic sulfur (S) into OM (i.e. preservation of OM through sulfurisation or natural vulcanisation) which, can enhance its preservation and, through this process, even labile OM such as carbohydrates can be preserved (Sinninghe Damsté et al., 1989; Tegelaar et al., 1989; Orr et al., 1990; Sinninghe Damsté & de Leeuw, 1990; Schouten et al., 1995; Koopmans et al., 1996; van Kaam-Peters et al., 1997, 1998, Werne et al., 2000, 2004, 2008; van Dongen et al., 2003a; 2003b; 2006). van Dongen et al (2006) for instance, showed that the presence of sulfurised carbohydrates in the kerogen of the Blackstone band of the Jurassic Kimmeridge Clay Formation contributed to the unusually high amounts of OM (up to 52 wt. %) preserved in this setting. Sulfurised organic compounds were also reported in other organic rich source rocks such as, the Miocene Monterey Formation (Orr, 1986; Zaback & Pratt, 1992; Nelson et al., 1995) and Jet Rock Member of the Whitby Mudstone Formation (Bowden et al., 2006; Salem, 2013). The incorporation of reduced S into sedimentary OM (i.e. sulfurisation of OM) is believed to be controlled by (1) the relative composition of porewater buffering rock materials like silicates (Michalopoulos & Aller, 2004) and carbonates (Moore et al., 2004), (2) the composition of reductants [the equilibrium between organic carbon (C) type inputs (marine against terrestrial) and biogenic methane] present in the water column and at the sediment-water interface used to enhanced microbial activity (Coleman et al., 1985), (3) the composition of oxidants in porewater (Curtis et al., 1977), (4) the abundance or otherwise of reduced sulfides (Coleman et al., 1985) and (5) the availability of reactive iron (Fe) oxides (L. K. Adams et al., 2006). The interplay between these factors during early diagenesis determines S incorporation

into OM and consequently its preservation in mudstones as S-rich OM (Macquaker et al., 2014). For instance, the presence of reactive clay minerals could trigger silicate- and carbonate-buffering reactions to occur and these reactions can reduce Fe (III) oxide, enriching porewater with Fe (II) oxide, thus naturally sequestering reduced S into Fe sulfides [e.g. pyrite (FeS_2)] and ultimately leading to S depleted OM being preserved (Raiswell et al., 1994; Macquaker et al., 2014). There seem to be a link between organic rich sediment composition, sulfurisation of OM, Fe sulfides and other diagenetic minerals precipitation. Examples can be seen in the Kimmeridge Clay, Monterey and Whitby Mudstone Formations where, although they are characteristically deposited with analogous suite of reductants and oxidants ending up with differing amounts of OM, organic sulfur compounds (OSCs), minerals (especially Fe sulfides) composition and cement assemblages of contrasting compositions (Howarth, 1962; Orr, 1986; Zaback & Pratt, 1992; Raiswell et al., 1993; Boussafir et al., 1995; Schouten et al., 1995; van Kaam-Peters et al., 1998; Sælen et al., 2000; Morgans-Bell et al., 2001; Bowden et al., 2006; van Dongen et al., 2006; Ghadeer & Macquaker, 2011; Ghadeer & Macquaker, 2012; Salem, 2013; Macquaker et al., 2014; Houben et al., 2016). However, it remains unclear what environmental, chemical and diagenetic factors seem to control these intricate diagenetic processes that control preservation of OM through sulfurisation.

Thus, the aims of this project are to (1) analyse and characterise a number of organic and sulfur-rich black shales with contrasting compositions to better understand the critical environmental, chemical and diagenetic factors that led to their formation using bulk and molecular geochemical, petrographic and electron microprobe techniques and (2) to compare the relative importance of preservation of OM through sulfurisation and Fe sulfides (mainly FeS_2) precipitation in these depositional environments.

2.2 Samples and Methods

2.2.1 Sample Description, Collection and Preparation

Samples were collected from three organic- and sulfur-rich hydrocarbon source rocks, the Kimmeridge Clay, Monterey and Whitby Mudstone Formations. These mudstones were deposited with a similar suite of oxidants and reductants but differ significantly in their post diagenetic characteristics such as OM and OSCs contents, mineral fabrics and sulfide minerals (Table 1.1; Howarth, 1962; Orr, 1986; Zaback & Pratt, 1992; Raiswell et al., 1993; Boussafir et al., 1995; Schouten et al., 1995; van Kaam-Peters et al., 1998; Sælen et al., 2000; Morgans-Bell et al., 2001; Bowden et al., 2006; van Dongen et al., 2006; Ghadeer & Macquaker, 2011; Ghadeer & Macquaker, 2012; Salem, 2013; Macquaker et al., 2014; Houben et al., 2016). The varying S pools in these mudstones makes them ideal for this study which seeks to investigate sulfur controls on OM preservation in mudstones.

The Kimmeridge Clay Formation (KCF) sample was collected from the Blackstone Band exposed at Clavell's Hard (*coordinates: 50° 36' 12" N, 2° 7' 26" W*), 1 km east of Kimmeridge Bay in Dorset, UK. The Blackstone Band is a Jurassic, relatively homogeneous dark brown, exceptionally organic-rich, fissile mudstone comprising shelly materials and FeS_2 nodules with intermittent hard, thin carbonate-rich layers (Scotchman, 1987, 1989; Shaw & Primmer, 1991; Macquaker & Gawthorpe, 1993; Morgans-Bell et al., 2001). The Blackstone band is the most organic-rich layer in the KCF and was characterised by the presence of other important diagenetic materials such as Fe, detrital silica and carbonate and kaolinite (See section 1.6.2; Table 1.1). The availability of these diagenetic materials in this bed compared to others in the KCF made it suitable for this study. The Monterey Formation (MF) sample was obtained from the repository of the United States Geological Survey, California, US and originated from the upper calcareous-siliceous member of the MF exposed at El Capitán beach (*coordinates: 34° 27' 41" N, 120° 1' 9" W*), Santa Barbara county, California, US. The upper calcareous-siliceous member of the MF is Miocene in age and it is a very organic rich, biogenic, calcareous, siliceous, phosphatic, and fossiliferous mudstone (Summons & Powell, 1987; Behl, 1999). It is the only layer in the MF (See section 1.6.1; Table 1.1) that contains almost all the diagenetic materials present in other layers of the MF thus, was selected for this study. The Whitby Mudstone Formation (WMF) samples were collected from the Jurassic Grey Shale (GS) and Jet Rock (JR) Members exposed between Staithes and Port Mulgrave (*coordinates: 54° 33' 27" N, 0° 46' 49" W*) in North Yorkshire, UK. The GS Member is a pyritic, fossiliferous siltstone and mudstone with bands of carbonate and Fe carbonate cements/concretions while the JR Member is a bituminous black shale with FeS_2,

massive calcite concretions and hardly any bioturbation (Morris, 1979; Powell, 1984; Pye & Krinsley, 1986). These members were selected for this study because they contain a diverse set of diagenetic materials absent in other beds of the WMF (Pye & Krinsley, 1986; Ghadeer & Macquaker 2011).

Rock samples were collected using a geological hammer and chisel. Samples were appropriately labelled in the field, orientations recorded, wrapped with aluminium foil, stored in designated sample bags and transported to the University of Manchester. All four samples were split and one half of each sample, labelled as (formation) archive hand specimen, was archived while the other half was trimmed to eliminate surficial contamination. The trimmed halves were further split into two using a rock cutting saw (cleaned with water and dichloromethane). Half of each split weighing about 50 g was finely powdered using a Tema mill (*Siebtechnik; Mundolsheim, France*) and freeze-dried for a series of bulk/molecule organic/inorganic geochemical analyses as described in detail in section 2.2.2.1 to 2.2.2.5. The mill's cup and lid were washed with detergent, rinsed with bidistilled water, dried and rinsed again with dichloromethane prior to milling each sample to avoid cross-contamination. 20 μm thick polished thin sections perpendicular to bedding plane with clear epoxy impregnation were prepared from the other splits. Thin sections were scanned with a Kodak esp® 1.2 scanner to provide high-resolution images (1200 x 1200 dpi) prior to petrographic and electron microprobe analyses described in detail in section 2.2.2.6 to 2.2.2.8.

2.2.2 Geochemical, Petrographic and Electron Microprobe Analyses

2.2.2.1 Total Organic Carbon (TOC), Total Inorganic Carbon (TIC) and Organic Elemental Carbon, Hydrogen, Nitrogen and Sulfur (CHNS) Analyses

TOC analysis was completed at Applied Petroleum Technology (APT), Norway using a LECO SC-632 instrument. 2 g of each powdered sample was treated with 10 % (vol.) hydrochloric acid to remove carbonate contents after which it was introduction into the LECO combustion oven. The combustion product CO_2, was detected by an infrared detector and used as a measure for total organic carbon (TOC). Analytical procedures followed the fourth edition of the Norwegian Industry Guide to Organic Geochemical Analyses (NIGOGA 4th Edition; Weiss et al., 2000). Reproducibility was tested by running a standard (Jet-Rock 1) after every other sample and checked against the acceptable range provided in NIGOGA 4th Edition (Weiss et al., 2000). TIC analysis was performed on a Shimadzu SSM-5000A (*Shimadzu, Japan*) instrument. 50 mg of powdered sample and a sodium carbonate standard were weighed into a ceramic boat and loaded into the designated inorganic C furnace. The furnace chamber is filled

with high-purity oxygen to ensure complete combustion (oxidation) of the sample and standard. Any inorganic C present in the sample (e.g. calcium carbonate/bicarbonate/CO_2) reacted with the phosphoric acid that was mixed with the sample and standard prior to being heated to around 200 ºC. This acid-base reaction produced CO_2 which was carried to an infrared detector by a stream of a high-purity inert carrier gas (helium). Peak area of the sample was measured and compared to the calibration curve obtained from a series of three sodium carbonate calibration standards. Unit was initially in mg C/50 mg sample thus, the number of mg of C in the sample was simply doubled to obtain a weight %. Error of ± 1 % is reported for both accuracy and precision. CHNS analysis was performed on a Thermo Scientific Flash 2000 (*Thermo Fisher Scientific, US*) organic elemental analyser. 2 mg of powdered freeze-dried samples were accurately weighed into tin containers which were placed into an autosampler tray continuously purged with a helium gas. Sample was dropped into a vertical quartz combustion reactor tube which maintains a temperature of 900 ºC. The helium carrier gas stream is enriched with pure oxygen as the sample was released into the furnace. The sample and tin container melt and the tin amplifies a violent reaction (flash combustion). This temporarily raises the temperature to about 1800 ºC. The gas mixture passes over a catalyst for complete oxidation after which flows through a layer of copper for removal of excess oxygen and reduction of nitrogen oxides to elemental nitrogen. The resulting gas mixture further flows to a chromatographic separation column in an oven with controlled temperature. At this stage, the gas components separate and elute as nitrogen, CO_2, water and sulfur dioxide. Quantitative determination of the elements was achieved with a thermal conductivity detector, signals were processed using Eager Xperience software package and results were presented in percent of C, H, N or S. For accuracy, standard reference materials were run before and after each analysis and results were measured with a possible error of ± 0.3 % for both accuracy and precision. Determination of CHNS in one was not possible thus CHN were determined first followed by S analysis.

2.2.2.2 Rock-Eval Pyrolysis

Rock-Eval pyrolysis was carried out at Applied Petroleum Technology (APT), Norway using a HAWK pyrolysis instrument (*Wildcat Technologies, US*) configured in standard mode. 100 mg of each powdered sample was pyrolysed in a helium inert atmosphere at a temperature programmed to start at 180 ºC then at 25 ºC min^{-1} to 650 ºC. The mass of the released volatile hydrocarbons (i.e. free hydrocarbons; S_1 peak in the pyrogram; expressed as mg HC/g sediment) at 300 ºC, non-volatile hydrocarbons (i.e. kerogen; S_2 peak in the pyrogram;

expressed as mg HC/g sediment) from 300 ºC to 550 ºC and CO_2 (i.e. oxygen; S_3 peak in the pyrogram; expressed as mg CO_2/g sediment) from start of pyrolysis to 390 ºC were measured using a flame ionisation detector (Espitalié et al., 1977). Tmax, the temperature at which maximum kerogen breakdown was achieved within the S_2 peak, considered a thermal maturity proxy, was recorded for all samples. Using the TOC data previously obtained for the samples, secondary Rock-Eval parameters; hydrogen index (HI; measure of OM type/quality), oxygen index (OI; measure of OM inertness), production potential (PP) and production index (PI) were calculated from the expressions HI = (S_2/TOC) × 100, OI = (S_3/TOC) × 100, PP = S_1 + S_2 and PI = S_1/S_1 + S_2 respectively (Tissot & Welte, 1984; Peters, 1986). Vitrinite reflectance (R_o) was estimated using 0.0180 x Tmax - 7.16 (Jarvie et al., 2001). Analytical procedures followed NIGOGA 4th Edition (Weiss et al., 2000) and reproducibility was tested by running a standard (Jet-Rock 1) after every other sample and checked against the acceptable range provided in NIGOGA 4th Edition (Weiss et al., 2000).

2.2.2.3 Pyrolysis-Gas Chromatography-Mass Spectrometry (Py-GC-MS)

Samples were analysed by Py-GC-MS using an Agilent GC-MSD system interfaced to a CDS-5200 Pyroprobe (*CDS Analytical, US*). 2 mg of powdered, freeze-dried, soxhlet extracted sample residues were weighed into pre-cleaned, fire polished quartz tubes with quartz wools placed at their bottoms and pyrolysed at 600 ºC for 20 s in a flow of helium. Products/moieties produced were transferred through a transfer line to an Agilent 7980A GC fitted with a Zebron ZB-5MS fused column (*Phenomenex, The Netherlands*; 95% dimethylpolysiloxane, 5% phenyl-arylene phase; 8 polarity; 350 ºC, 30 m length, 0.25 mm i.d., 0.25 μm film thickness) coupled to an Agilent 5975C MSD single quadrupole mass spectrometer (MS) run in the electron ionisation (EI) mode (Scanning a range of m/z 50 to 650 at 2.7 scans s-1; ionisation energy 70 eV; solvent delay 1 min). The pyrolysis transfer line and injector temperatures were set at 350 ºC, the valve oven at 325 ºC, the EI source at 230 ºC, the heated GC interface at 280 ºC and the MS quadrupole at 150 ºC. Samples were introduced in split mode (split ratio 20:1; split flow of 40 mL/min) and helium was used as the carrier gas. The oven temperature was programmed to hold at 40 ºC for 5 min then at 4 ºC min^{-1} to 300 ºC and kept for 15 min at this temperature for a total run time of 85 min. Data was analysed using MSD ChemStation (*Agilent, US*) and Xcalibur (*Thermo Fisher Scientific, US*) software packages and compounds/complexes were identified using the National Institute of Standard and Technology (*NIST, US*) mass spectral library. The 2-methylthiophene over toluene (2M/T), benzothiophenes over toluene (BT/T), 2,3-dimethylthiophene over 1,2-dimethylbenze + 1-

nonene [2,3DMT/(1,2DMB + 1Nonene)] and 2-ethylthiophene + 2,5-dimethylthiophene over 2-ethylthiophene + 2,5-dimethylthiophene + 2,4-dimethylthiophene + 2,3-dimethylthiophene [2ET + 2,5DMT/(2ET + 2,5DMT + 2,4DMT + 2,3DMT)] ratios were obtained from the relative abundance of the compounds identified (Eglinton et al., 1990; van Kaam-Peters et al., 1998; van Dongen et al., 2006). Pyrograms were processed and stacked in Origin (*OriginLab, US*).

2.2.2.4 X-ray Fluorescence (XRF)

XRF analysis was performed on a PANalytical Axios sequential X-ray fluorescence spectrometer (*Malvern Panalytical, UK*) to determine major and trace elements. Analysis was carried out on 12 g of freeze-dried, powdered samples mixed with 3 g of non-reactive wax binder and compressed to tablets, 3 cm in diameter using a pneumatic press. Prior to analysis, loss on ignition (LOI) was done on 1 g of powdered samples accurately weighed out into crucibles. The samples were heated to 105 ºC for 1 hr, cooled and reweighed. The sample were reheated to 1000 ºC for 1 hr, cooled and reweighed again. The former stage determines water loss while the later determines the loss of volatile matter, generally considered to be C, but can occasionally be mercury (Hg), arsenic (As), selenium (Se) and S. LOI data was entered into the XRF software (*Omnian; Malvern Panalytical, UK*) and when it has analysed a sample for major elements, it corrected for the weight loss (C) because C is too light an element to be seen by the XRF detector. Trace elements were analysed using the Pro-Trace Element Analytical application in the Malvern PANalytical software suite. Some elements were quantified in their oxides thus their actual amounts in the oxides were manually calculated. Analytical accuracy was 2 % to 5 % relative standard deviation (RSD) and uncertainty was typically < 1 % RSD for both major and trace elements. Detection limits are less than a few parts per million (mg/g).

2.2.2.5 X-ray Powder Diffraction (XRD)

XRD analysis was performed on a Bruker D8 Advance diffractometer equipped with a with Göbel Mirror and LynxEye sensitive detector operating at 40 kV / 40 mA (*Bruker, US*) and calibrated using aluminium, silicon and yttrium oxides. 0.2 g of freeze-dried, powdered samples were mixed with 1 ml of iso-amyl acetate, smeared evenly on glass slides and allowed to completely air-dry, after which were loaded immediately into the XRD instrument and analysed using a monochromatic Copper K-alpha X-ray with 1.5406 Å wavelength. Scans of the samples were collected from 5º to 70º (2θ) at a fixed incident angle of 2.5º, with a step size of 0.02º at a speed of 2 s $step^{-1}$. Diffraction patterns were collated and background subtracted using EVA version 4 software and peaks were identified using the International Centre for

Diffraction Data database. Mineral peak intensities were quantified using single-line fitting in TOPAS version 4.2 with a possible error of ± 1 % (vol.; *Bruker, US*).

2.2.2.6 Optical Microscopy

Optical microscopy was carried out on 20 μm thick polished thin sections with clear epoxy impregnation using a Nikon Eclipse LV100N POL polarising microscope with a 12 V - 50 W halogen lamp, built-in 12 V - 50 W DC transformer, NCB11 and ND8 filters and fitted with a Nikon DS - Fi2 camera. The microscope had various optical lenses (x 20, x 50, x 100, x 200 and x 500 magnifications) which allowed the snapping of quality micron (μm) to millimetre (mm) scale images for lithofacies characterisation.

2.2.2.7 Environmental Scanning Electron Microscopy-Energy Dispersive X-ray Spectroscopy (ESEM-EDS)

Backscattered ESEM-EDS imaging and elemental analysis was completed using a Quanta FEG 650 environmental scanning electron microscope (*FEI Instrument, US*) equipped with an energy dispersive X-ray spectroscopy unit (*Bruker x Flash 6130 Instrument, US)*, a concentric-backscatter (CBS) detector and Esprit 2.1 software. Thin sections analysed by optical microscopy were C coated (~ 9 nm) using a 108Carbon/A (*Cressington Scientific, UK*) C coater to provide a conductive coating to avoid surface charging and, loaded into the instrument's chamber. Scanning/imaging was done in the high vacuum mode using a voltage of 15 kV, 10 nA beam current, 0.30 mbar chamber pressure, 3 μs scanning speed, 3.50 spot size and 10.2 mm working distance.

2.2.2.8 Electron Microprobe Analysis (EMPA)

EMPA was performed on Cameca SX 100 electron probe micro-analyser equipped with a tungsten electron beam, five wavelength dispersive detectors, each fitted with a diffracting crystals and an energy dispersive spectrometer. C coated (~ 9 nm) thin sections were loaded into the instrument's chamber. Relative concentrations of S and Fe were mapped across a raster of 512 x 512 pixels in areas of interest on the thin sections using an instrument setup of 15 keV accelerating voltage, 20 nA beam current and spot sizes of 1 μm. The instrument was calibrated with well characterised mineral and synthetic standards prior to analysis.

2.3 Result

2.3.1 Petrography, Mineralogy and Geochemical analyses

The KCF sample is a homogenously brown mudstone with tiny lenses of ivory white (likely carbonate) materials ranging from few nanometres to 3 mm (Fig. 2.1a). The matrix of this sample predominantly consist of a mixture of amorphous and non-amorphous OM and some calcareous nannoplankton, FeS_2 and clay-size materials (Fig. 2.2a & b). The dark brown/opaque structures (round-like, stripy and wavy structures) are largely OM (Fig. 2.2a) and a few of the tiny black spots are a mixture of framboidal and euhedral FeS_2 as confirmed by ESEM-EDS analysis (Fig. 2.2b). Most of the light brown ripple-like structures across the whole imaged area are amorphous OM squash out of form, consistent with the unusually high organic carbon (OC; 52 wt. %) and minor amounts of inorganic carbon (IC; 1 wt. %) recorded in this sample (Fig. 2.2a; Table 2.1). Carbonate materials (ivory white structures) including calcareous faecal pellets and agglutinated foraminifer are present (Fig. 2.2a). XRD analysis indicate 48 wt. % and 4 wt. % of the carbonate materials are calcite and siderite, respectively (Table 2.2). Clay minerals are in the form of illite (22 wt. %) and kaolinite (3 wt. %). Quartz and FeS_2 are 16 wt. % and 7 wt. %, respectively (Table 2.2). Carbonate, silicate, phosphate and sulfide minerals are low compared to OM in KCF hence, in line with the relatively low amounts of silicon (Si; 4 wt. %), aluminium (Al; 2 wt. %), calcium (Ca; 4 wt. %), phosphorus (P; 0.2 wt. %) and Fe (1 wt. %) measured in the sample by XRF analysis (Fig. 2.2a & b; Table 2.2, 2.3). Other major elements such as, titanium (Ti; 0.1 wt. %), manganese (Mn; 0 wt. %), magnesium (Mg; 0.2 wt. %), sodium (Na; 0.1 wt. %) and potassium (K; 0.5 wt. %) are also considerably low in KCF (Table 2.3). Trace elements such as, cadmium (Cd; 1 wt. %), molybdenum (Mo; 85 wt. %) and uranium (U; 9 wt. %) are relatively high while barium (Ba; 83 wt. %), vanadium (V; 52 wt. %), zinc (Zn; 36 wt. %), copper (Cu; 33 wt. %), chromium (Cr; 40 wt. %), nickel (Ni; 67 wt. %) and thorium (Th; 2 wt. %) are relatively low compared to average shale values (Table 2.3; Wedepohl, 1971; Wedepohl, 2004).

Rock-Eval analysis shows that the KCF has high S_1 and S_2 peaks (12 and 356 mg HC/g rock respectively), low S_3 peak (1 mg CO_2/g TOC) and a Tmax value of 418 ºC, below the oil window (Table 2.1; oil window = 435 - 470 ºC; Peters, 1986). Estimated vitrinite reflectance (R_o = 0.0180 x Tmax - 7.16; Jarvie et al., 2001) indicate that the KCF, with an R_o of 0.4, is immature while its HI and OI values, 682 mg HC/g TOC and 1 mg CO_2/g TOC respectively, indicate it contains kerogen type 2 (Table 2.1; Tissot & Welte, 1984; Jones, 1987; Tyson, 2005). Production potential ($PP = S_1 + S_2$; Peters, 1986) of the KCF is high (368 mg HC/g rock)

while the production index (PI = $S_1/S_1 + S_2$; Peters, 1986) is 0, confirming immaturity status (Table 2.1; Peters, 1986). CHNS analysis indicate the presence of substantial amounts of S (7 wt. %; Table 2.1) while Py-GC-MS analysis reveals the presence of a wide of range of OSC moieties such as alkylated thiophenes and benzothiophenes (Fig. 2.3; Table 2.4), comparable to those reported in previous studies (van Kaam-Peters et al., 1998; van Dongen et al., 2006). Overall, the KCF is predominantly an organic and S-rich immature mudstone that contains some carbonate, silicate and FeS_2 but, starved of phosphate.

Table 2.1: Bulk geochemical data of the Kimmeridge Clay (KCF), Monterey (MF) and Whitby Mudstone [Grey Shale (GS) and Jet Rock (JR) members] Formations.

Data	KCF	MF	GS	JR
TOC (%)[a]	52.2	13.5	6.1	4.1
TIC (%)[b]	1.2	4.4	0.2	0.4
C (%)[c]	49.5	18.7	6.0	4.6
H (%)[c]	5.2	1.8	1.1	1.2
N (%)[c]	1.3	0.7	0.2	0.1
S (%)[c]	6.7	1.8	10.7	4.4
S_1 (mg/g)[d]	11.7	2.4	2.0	1.7
S_2 (mg/g) [d]	356	81	31	19
S_3 (mg/g)[d]	0.8	1.5	0.1	0.1
Tmax (ºC)[d]	418	402	431	437
VF (R_o)[e]	0.4	0.1	0.6	0.7
PP (mg/g)[f]	368	83	33	21
PI (wt ratio)[f]	0.03	0.03	0.06	0.08
HI (mg HC/g TOC)[f]	682	600	516	458
OI (mg CO_2/g TOC)[f]	1.4	10.8	1.5	1.2

[a] obtained from LECO analysis; [b] obtained from solid sample module analysis; [c] obtained from organic elemental (CHNS) analysis; [d] obtained from Rock-Eval analysis; [e] VF (R_o) = vitrinite reflectance, calculated using 0.0180 x Tmax - 7.16 (Jarvie et al., 2001); [f] parameters calculated from Rock-Eval data (PP = production potential, PI = production index, HI = hydrogen index, OI = oxygen index; Tissot & Welte, 1984; Peters, 1986).

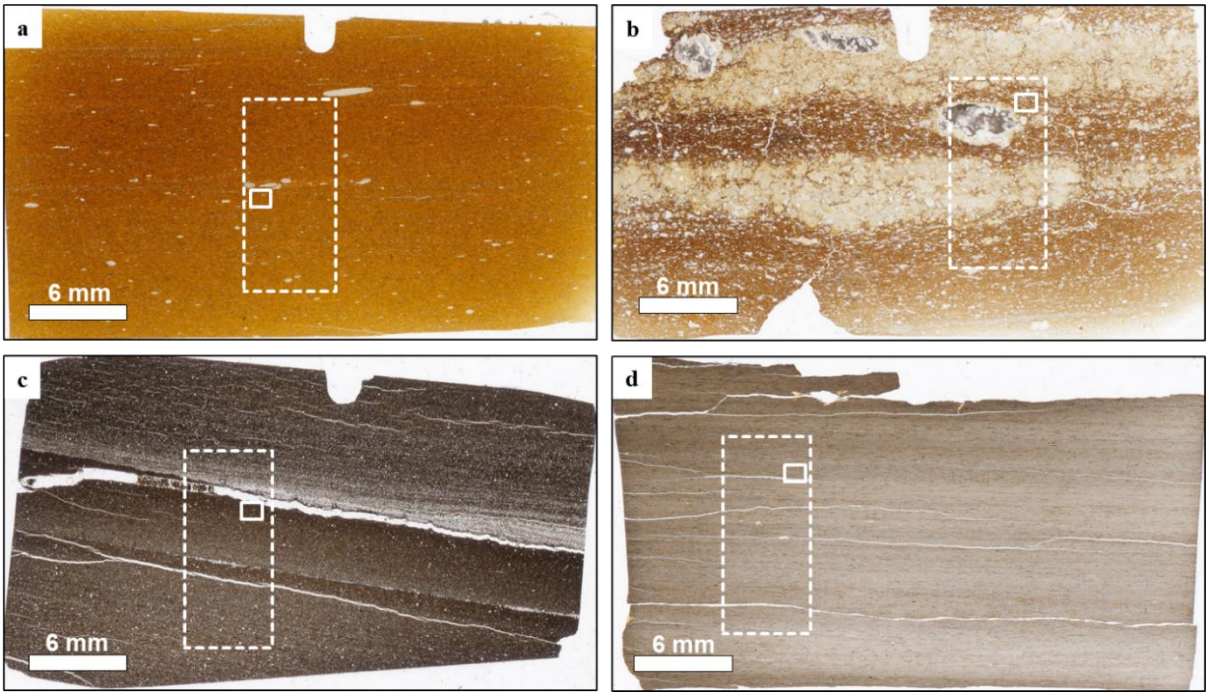

Figure 2.1: Scanned images of (a) Kimmeridge Clay Formation, (b) Monterey Formation, (c) Grey Shale and (d) Jet Rock members of the Whitby Mudstone Formations showing lithofacies variations in millimetre scales. Small solid squares in white are selected for detailed Optical and ESEM analyses as presented in Fig. 2.2 and large dashed squares in white for detailed EMPA analysis as presented in Fig. 2.4.

Table 2.2: Percentage weight of minerals in the Kimmeridge Clay (KCF), Monterey (MF) and Whitby Mudstone [Grey Shale (GS) and Jet Rock (JR) members] Formations as obtained from XRD analysis. Diffractograms are presented in supplementary information section (Fig. S2.5).

Mineral Class	Minerals (wt%)	KCF	MF	GS	JR
Carbonates	Calcite	48	57	0	3
	Siderite	4	0	< 1	0
Phosphate	Fluorapatite	0	18	0	0
Phyllosilicates	Clinochlore	0	0	5	1
	Illite	22	5	23	33
	Kaolinite	3	0	18	22
Sulfides	Gypsum	0	0	1	0
	Pyrite	7	< 1	17	10
Tectosilicates	Albite	0	10	7	6
	Quartz	16	9	29	25
	Total	100	100	100	100

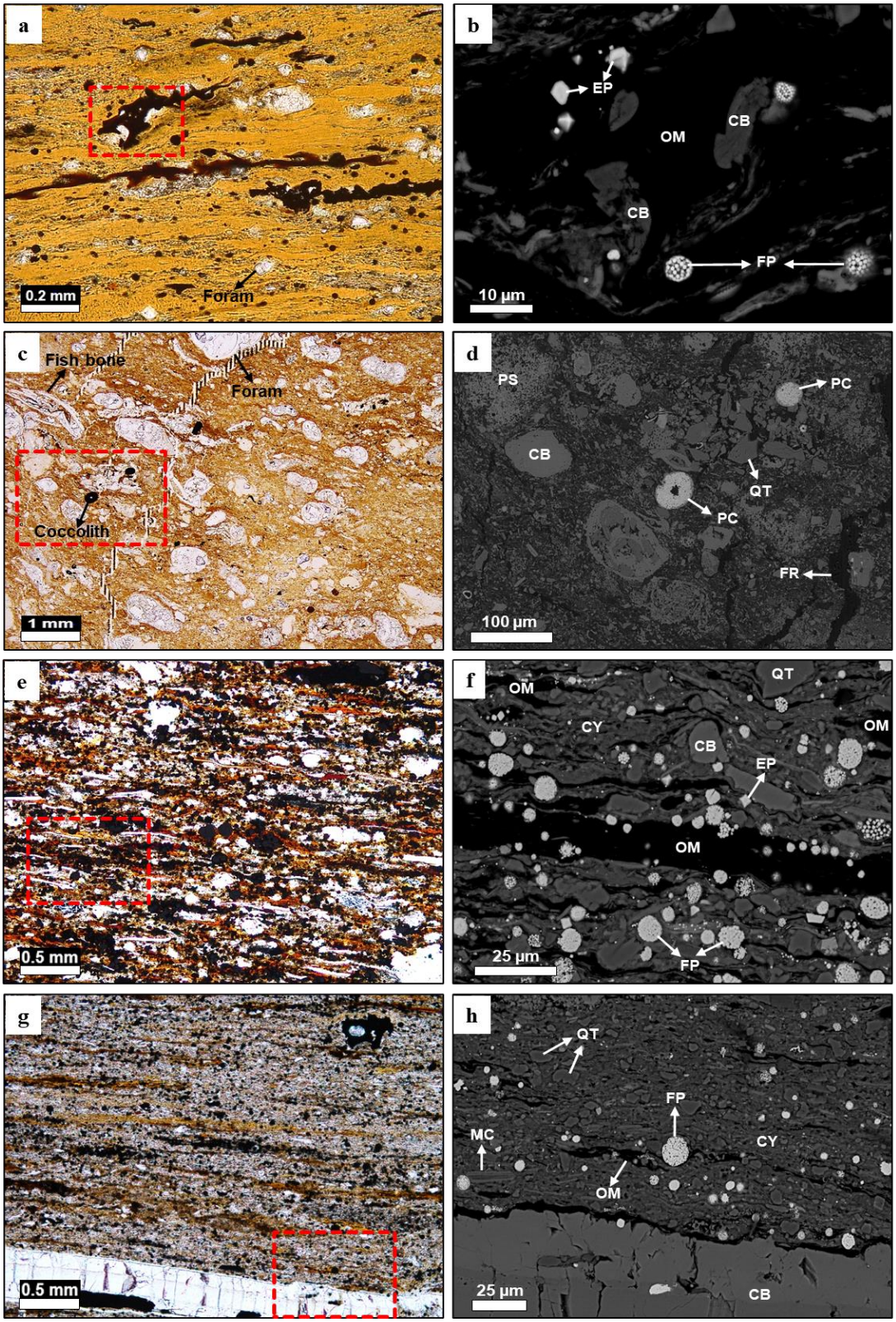

Figure 2.2: Paired optical and backscattered ESEM images of (a & b) Kimmeridge Clay Formation, (c & d) Monterey Formation, (e & f) Grey Shale and (g & h) Jet Rock members of the Whitby Mudstone Formations showing lithofacies variations in details at higher resolutions (nanometre to micron scales). Optical micrographs (a, c, e & g) were taken in areas marked with solid white line in figure 2.1 and red dashed squares in them are regions where ESEM-EDS analyses (b, d, f & h) were done. Abbreviations are; CB = carbonates, CY = clays, EF = euhedral pyrite, FP = framboidal pyrite, FR = fracture, MC = likely mica, OM = organic matter, PC = pyritised coccoliths, PS = phosphates and QT = quartz.

The MF in contrast to the KCF, is a heterogeneous dark brown mudstone with tiny fractures and numerous intercalations of ivory white bands ranging from a few nanometres to 5 mm in diameter and discrete (up to 3 mm in Ø) patches likely to be of biologically-derived marine origin (Fig. 2.1b). Matrix of this sample is mainly composed of substantial amorphous dark-light brown/yellowish OM, rip-up clasts, calcareous nannoplankton (mostly coccoliths), foraminifers, apatite concretions/cements, some diatom derived silicates and fractures, consistent with the high OC (14 wt. %) and appreciable IC (4 wt. %) recorded in this sample (Fig. 2.2c & d; Table 2.1). Few pyritised coccoliths are also present (Fig. 2.2d). XRD analysis indicate the presence of 57 wt. % calcite and 18 wt. % fluoroapatite, in line with the massive biological production observed in this sample (Fig. 2.2c & d; Table 2.2). Albite and quartz are 10 wt. % and 9 wt. % respectively and pyrite is < 1 wt. % likely due to the low Fe (1 wt. %) in the sample (Table 2.2 & 2.3). In contrast to the KCF, carbonate, phosphate and silicate minerals are abundant in MF, consistent with the relatively high amounts of Si (7 wt. %), Ca (21 wt. %) and P (4 wt. %) measured in the sample by XRF analysis (Fig. 2.2c & d; Table 2.2, 2.3). With the exception of Mg, Na, and K (all about 1 wt. %; all high in MF compared to the KCF), Al (2 wt. %), Fe (1 wt. %), Ti (0.1 wt. %) and Mn (0 wt. %) in MF are similar to those recorded in KCF (Table 2.3). Contrary to the KCF, Cd (4 wt. %), Cr (229 wt. %), Cu (72 wt. %), Ni (111 wt. %), U (32 wt. %), V (301 wt. %) and Zn (183 wt. %) in MF are substantially higher than average shale values (Table 2.3; Wedepohl, 1971; Wedepohl, 2004). Ba (411 wt. %) and Th (7 wt. %) are significantly high in MF compared to the KCF but, lower than average shale values while, Mo (34 wt. %) is low in MF compared to the KCF but, higher than average shale values (Table 2.3; Wedepohl, 1971; Wedepohl, 2004).

Rock-Eval analysis shows that the MF has high S_1 and high S_2 peaks (2 and 81 mg HC/g rock respectively), low S_3 peak (2 mg CO_2/g TOC) and a Tmax value of 402 ºC, below the oil window (Table 2.1; Peters, 1986). Estimated R_o of MF is 0.1, while its HI and OI values are, 600 mg HC/g TOC and 11 mg CO_2/g TOC respectively, indicating it is made up of an immature kerogen type 2 (Table 2.1; Tissot & Welte, 1984; Jarvie et al., 2001; Tyson, 2005). PP of the MF is high (83 mg HC/g rock) while PI is 0, confirming immaturity status (Table 2.1). CHNS analysis indicate the presence of S (2 wt. %; Table 2.1) while Py-GC-MS analysis reveals the presence of a wide of range of OSC moieties such as alkylated thiophenes and benzothiophenes comparable to those observed in the KCF (Fig. 2.3; Table 2.4). Overall, the MF is an organic and S-rich immature mudstone (although not as organic-rich as the KCF) with considerable amounts of carbonate, phosphate and silicate minerals but, unlike the KCF, starved of FeS_2.

Table 2.3: Major and trace elements in the Kimmeridge Clay (KCF), Monterey (MF) and Whitby Mudstone [Grey Shale (GS) and Jet Rock (JR) members] Formations as obtained from XRF analysis. Elements were analysed in their oxides from which their actual amounts were calculated.

Oxide/Element[a]	KCF	MF	GS	JR	Average Shale[b]
SiO_2	7.6	14.3	34.1	40.6	58.9
Si	3.5	6.7	15.9	19.0	
TiO_2	0.1	0.2	0.6	0.8	0.78
Ti	0.1	0.1	0.4	0.5	
Al_2O_3	3.6	3.8	16.2	20.5	16.7
Al	1.9	2.0	8.6	10.9	
Fe_2O_3	1.5	1.5	12.2	7.8	2.8
Fe	1.0	1.0	8.6	5.5	
MnO	0.0	0.0	0.1	0.0	0.09
Mn	0.0	0.0	0.1	0.0	
MgO	0.3	0.8	1.5	1.6	2.6
Mg	0.2	0.5	0.9	1.0	
CaO	5.1	29.6	0.4	2.2	2.2
Ca	3.7	21.2	0.3	1.6	
Na_2O	0.1	1.1	0.4	0.2	1.6
Na	0.1	0.8	0.3	0.1	
K_2O	0.6	0.9	1.8	3.1	3.6
K	0.5	0.7	1.5	2.5	
H_2O	1.5	2.5	1.0	2.0	5
H	0.2	0.3	0.1	0.2	
P_2O_5	0.4	8.4	0.1	0.2	0.16
P	0.2	3.7	0.0	0.1	
SO_3	11.5	5.1	12.4	5.9	n.d.
S	4.6	2.0	5.0	2.4	
LOI (CO_2)[c]	67.7	30.5	18.7	14.7	1.3
LOI (C)[c]	18.5	8.3	5.1	4.0	
Ba	83	410.8	230	428.3	580
Cd	1.0	3.7	6.3	6.1	0.13
Mo	84.7	34.0	40.4	25.6	1.3
V	51.6	301.0	149.3	169.0	130
Zn	35.5	182.8	99.3	107.6	95
Cu	33.2	71.9	82.5	29.9	45
Cr	39.9	228.8	156.9	120.9	90
Ni	67.1	110.9	170.0	90.3	68
U	8.7	32.3	9.2	11.9	3.7
Th	1.8	6.8	11.5	13.7	12

[a] major elements in weight percent (wt. %), trace elements in parts per million (ppm); [b] average shale data from Wedepohl (1971, 2004); [c] Loss on ignition (LOI), generally considered C but may contain S, Hg, As and Se.

Table 2.4: Thiophenes and benzothiophenes identified in the flash pyrolysates of Kimmeridge Clay (KCF), Monterey (MF) and Whitby Mudstone [Grey Shale (GS) and Jet Rock (JR) members] Formations as analysed by PyGCMS.

Peak[a]	Compound	Formula	Molecular Weight
1	Thiophene	C_4H_4S	84
2	2-methylthiophene	C_5H_6S	98
3	3-methylthiophene	C_5H_6S	98
4	2-ethylthiophene	C_6H_8S	112
5	2,5-dimethylthiophene	C_6H_8S	112
6	2,4-dimethylthiophene	C_6H_8S	112
7	2,3-dimethylthiophene	C_6H_8S	112
8	2-propylthiophene	$C_7H_{10}S$	126
9	2-ethyl-5-methylthiophene	$C_7H_{10}S$	126
10	2-ethyl-4-methylthiophene	$C_7H_{10}S$	126
11	2,3,5-trimethylthiophene	$C_7H_{10}S$	126
12	2,3,4-trimethylthiophene	$C_7H_{10}S$	126
13	2-methyl-5-propylthiophene	$C_8H_{12}S$	140
14	2,5-diethylthiophene	$C_8H_{12}S$	140
15	3,4-diethylthiophene	$C_8H_{12}S$	140
16	2-ethyl-5-propylthiophene	$C_9H_{14}S$	154
17	2-methylthieno[3,2-b]thiophene	$C_7H_6S_2$	154
18	Benzo[b]thiophene	C_8H_6S	134
19	2-methylbenzo[b]thiophene	C_9H_8S	148
20	4-methylbenzo[b)]thiophene	C_9H_8S	148
21	3-methylbenzo[b]thiophene	C_9H_8S	148
22	2,4-dimethylbenzo[b]thiophene	$C_{10}H_{10}S$	162
23	2,3-dimethylbenzo[b]thiophene	$C_{10}H_{10}S$	162
24	2-ethyl-7-methyl-1-benzothiophene	$C_{11}H_{11}S$	176

[a] Numbers refer to peaks in Figure 2.3.

The GS in contrast to both the KCF and MF, is largely a laminated, homogenous greyish-black mudstone with well-defined fractures ranging in diameter from few microns to 2 mm at low resolutions (Fig. 2.1c). However, at higher resolutions (nano - micron scales), it is a highly heterogeneous mudstone with varying components making up its fabric (Fig. 2.2e & f). The matrix of this sample consist of a mixture of numerous amorphous and non-amorphous (round-like, stripy and wavy structures) macerals (OM) varying in colour (black, brown, red and yellow), clay-size materials/minerals, pyrites and very low carbonate components (Fig. 2.2e & f), consistent with the high OC (6 wt. %) and very low IC (0.2 wt. %) measured in this sample (Table 2.1). Some of the black features in figure 2.2e are a mixture of framboidal and euhedral FeS_2, with framboidal FeS_2 dominating as confirmed by ESEM-EDS analysis (Fig. 2.2f). There

is no fossil in the imaged area but the GS has been reported to contain some fossils (Gunnar Sælen et al., 1996; Ghadeer & Macquaker, 2012). In contrast to both the KCF and MF, XRD analysis indicate the dominance of phyllosilicates (clay minerals = 23 wt. % illite and 18 wt. % kaolinite; chlorite group = 5 wt. % clinochlore) and tectosilicates (29 wt. % quartz and 7 wt. % albite) minerals over carbonate minerals in GS, in line with the petrographic analysis (Fig. 2.2e & f; Table 2.2). Sulfide minerals present are, FeS_2 (17 wt. %) and gypsum (1 wt. %) while carbonate materials are extremely low and mostly in the form of siderite (< 1 wt. %; Fig. 2.2e & f; Table 2.2). The abundance of silicate and sulfide minerals observed in GS gave rise to the high Si (16 wt. %), Al (9 wt. %) and Fe (9 wt. %) recorded in it compared to the KCF and MF while, the extremely low amounts of carbonates and the absence of phosphates in GS, explains the limited/absence of Ca (0.3 wt. %), P (0 wt. %) and IC (0.2 wt. %) measured in it compared to the KCF and MF (Fig. 2.2e & f; Table 2.1, 2.2 & 2.3). Mg (1 wt %), K (2 wt. %), Ti (0.4 wt. %) and Mn (0.1 wt. %) in GS are relatively higher than those recorded in the KCF and MF while, Na (0.3 wt. %) in it is relatively low compared to the MF but, relatively high compared to the KCF. Trace elements such as, Cd (6 wt. %), Cu (83 wt. %), Ni (170 wt. %) and Th (12 wt. %) in GS are high compared to the KCF and MF and, with the exception of Th, these elements are also high when compared to average shale values (Table 2.3; Wedepohl, 1971; Wedepohl, 2004). Ba (230 wt. %), Cr (157 wt. %), V (149 wt. %) and Zn (99 wt. %) are significantly high in GS compared to the KCF but, low by almost 50 % when compared to the MF (Table 2.3). Mo (40 wt. %) is low by almost 50 % in GS compared to the KCF but, relatively high compared to the MF while, U (9 wt. %) in GS is similar to the KCF but, significantly lower when compared to the MF (Table 2.3). Cr, V, Zn, Mo and U in GS are high while, Ba is low compared to average shale values (Table 2.3; Wedepohl, 1971; Wedepohl, 2004).

Rock-Eval analysis shows that the GS has high S_1 and high S_2 peaks (2 and 31 mg HC/g rock respectively), very low S_3 peak (0.1 mg CO_2/g TOC) and a Tmax value of 431 ºC, top of the oil window (Table 2.1; Peters, 1986). Estimated R_o of GS is 0.6, while its HI and OI values are, 516 mg HC/g TOC and 2 mg CO_2/g TOC respectively, indicating it is made up of a mature kerogen type 2 (Table 2.1; Tissot & Welte, 1984; Jarvie et al., 2001; Tyson, 2005). PP of GS is high (33 mg HC/g rock) while its PI is 0.1, confirming maturity status (Table 2.1; Peters, 1986). CHNS analysis indicate the presence of substantial amounts of S (11 wt. %; Table 2.1) while Py-GC-MS analysis reveals the presence of a wide of range of OSC moieties such as alkylated thiophenes and benzothiophenes comparable to those observed in the KCF and MF,

with the exception of thiophene, 3-methylthiophene, 2,5-dimethylthiophene, 2-ethyl-5-propylthiophene and 2-methylthieno[3,2-b]thiophene which are, either absent or below detection limit (Fig. 2.3; Table 2.4). Overall, the GS is an organic and S-rich mature mudstone (although not as organic-rich as the KCF and MF) and unlike the KCF and MF, predominantly consist of silicate and sulfide (mainly FeS_2) minerals and starved of carbonates and phosphates.

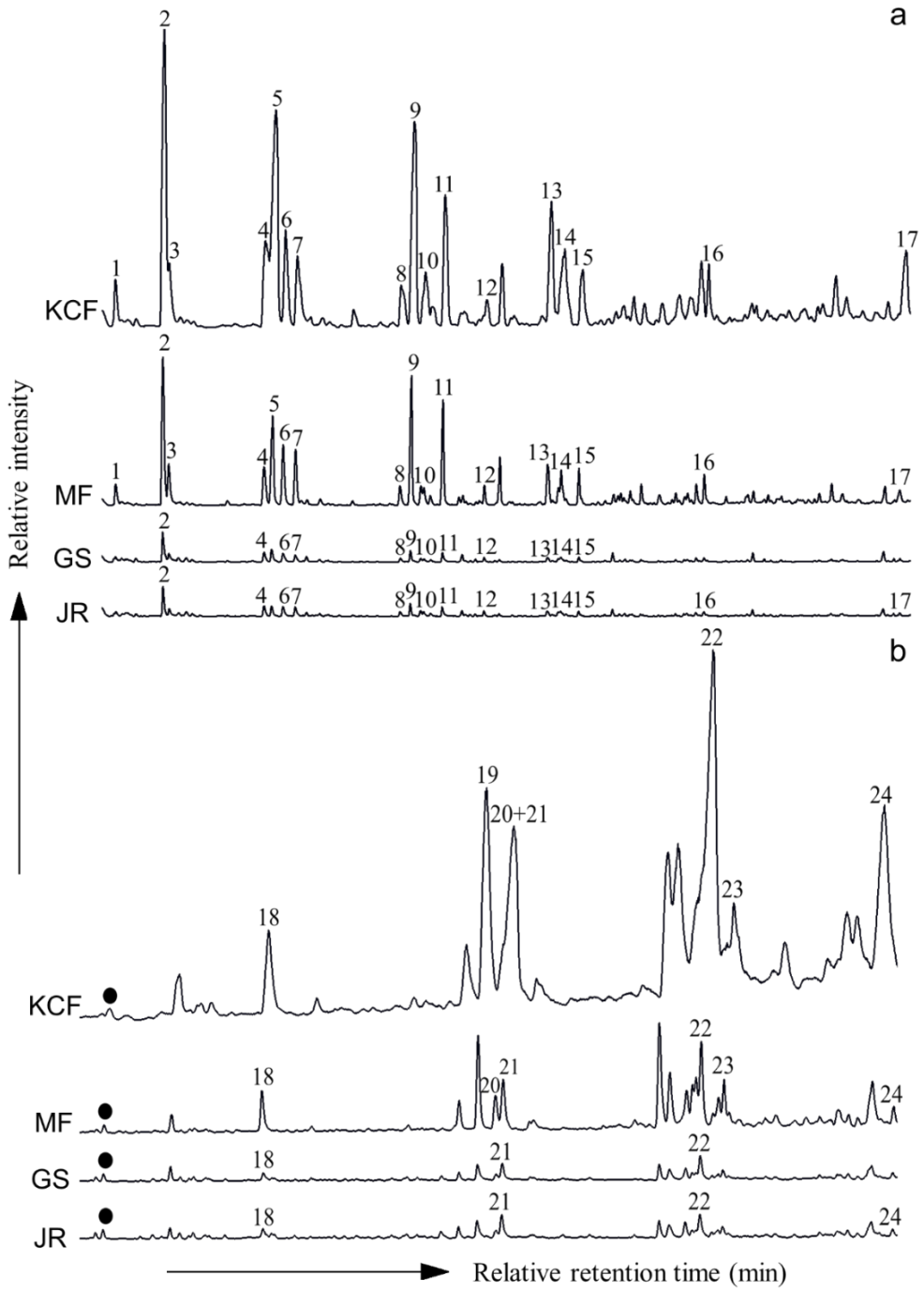

Figure 2.3: Distribution of (a) thiophenes and (b) benzothiophenes in the flash pyrolysates of Kimmeridge Clay (KCF), Monterey (MF) and Whitby Mudstone [Grey Shale (GS) and Jet Rock (JR) members] Formations as as revealed by the partial accurate mass chromatogram of m/z 84 + 97 + 98 + 111 + 112 + 125 + 126 + 139 + 140 + 153 + 154 and m/z 134+147+148+161+162 respectively. Numbers refer to compounds presented in Table 2.4. Filled circles are 1,2,3,4-Tetramethylbenzene.

In contrast to all the other samples (KCF, MF & GS), the JR at low resolutions, is a laminated, homogenous light brownish-grey mudstone (Fig. 2.1d). However, like the GS, it is highly heterogeneous at higher resolutions (nano - micron scales; Fig. 2.2g & h). The JR is characteristically structured into parallel and discontinuous wavily laminated stacked successions of very thin layers (10 nm - 5 µm) with periodic carbonate bands that are up to 0.5 mm in diameter (Fig. 2.1d; Fig. 2.2g & h). The matrix of JR, like the GS, is composed of a mixture of numerous amorphous and non-amorphous (round-like, stripy and wavy structures) macerals (OM) varying in colour (black/brown/yellow), consistent with the high OC (4 wt. %) and very low IC (0.4 wt. %) recorded in this sample (Fig. 2.2g & h; Table 2.1). Other lithofacies observed are, numerous fine grained quartz and clayey materials, few large detrital clays (mica; 25 µm), a carbonate band/layer and framboidal FeS_2 which constitute some of the black spherical structures in figure 2.2g as confirmed by ESEM-EDS analysis (Fig. 2.1d; Fig. 2.2g & h). Similar to the GS, XRD analysis of JR indicate the dominance of phyllosilicates (clay minerals = 33 wt. % illite and 22 wt. % kaolinite; chlorite group = 1 wt. % clinochlore) and tectosilicates (25 wt. % quartz and 6 wt. % albite) minerals over carbonate minerals, in line with the petrographic analysis (Fig. 2.2g & h; Table 2.2). However, in contrast to GS, pyrite (10 wt. %) and calcite (3 wt. %) are the only sulfide and carbonate minerals present in JR, respectively (Fig. 2.2g & h; Table 2.2). The abundance of silicate and sulfide minerals observed in JR gave rise to the high Si (19 wt. %), Al (11 wt. %) and Fe (6 wt. %) recorded in it while, the low/limited carbonate and phosphates minerals in JR, explains the low/limited amounts of Ca (2 wt. %), P (0.1 wt. %) and IC (0.4 wt. %) measured in it compared to the KCF and MF, but, similar when compared to GS except for Ca, which is relatively high in JR (Fig. 2.2g & h; Table 2.1, 2.2 & 2.3). Mg (1 wt %), K (3 wt. %) and Ti (1 wt. %) in JR are relatively higher than those recorded in the KCF and MF but, similar when compared to GS (Table 2.3). Na (0.1 wt. %) in JR is similar to those recorded in the KCF and GS but, high compared to the MF while, Mn (0 wt. %) is absent in JR, like in the KCF and MF. Trace elements such as, Ba (428 wt. %) and Th (14 wt. %) in JR are high compared to the KCF, MF and GS while, V (169 wt. %), Zn (108 wt. %) and U (12 wt. %) in JR are high compared to the KCF and GS but, low when compared to MF (Table 2.3). Cr (121 wt. %) and Ni (90 wt. %) in JR are low compared to the MF and GS but, high when compared to KCF while, Cd (6 wt. %) in JR is high compared to the KCF and MF but, similar when compared to GS (Table 2.3). Cu (30 wt. %) and Mo (26 wt. %) in JR are low compared to all samples (e.g. KCF, MF, GS; Table 2.3). With the exception Ba and Cu, all trace elements (e.g. Cd, Cr, V, Zn, Mo, Ni, U & Th) in JR are higher than average shale values (Table 2.3; Wedepohl, 1971; Wedepohl, 2004).

Rock-Eval analysis shows that the JR has high S_1 and high S_2 peaks (2 and 19 mg HC/g rock respectively), very low S_3 peak (0.1 mg CO_2/g TOC) and a Tmax value of 437 ºC, top of the oil window (Table 2.1; Peters, 1986). Estimated R_o of JR is 0.7, while its HI and OI values are, 458 mg HC/g TOC and 1 mg CO_2/g TOC respectively, indicating it is made up of a mature kerogen type 2 (Table 2.1; Tissot & Welte, 1984; Jarvie et al., 2001; Tyson, 2005). PP of GS is high (21 mg HC/g rock) while its PI is 0.1, confirming maturity status (Table 2.1; Peters, 1986). CHNS analysis indicate the presence of S (4 wt. %; Table 2.1) while Py-GC-MS analysis reveals the presence of a wide of range of OSC moieties such as alkylated thiophenes and benzothiophenes comparable to those observed in the GS (Fig. 2.3; Table 2.4). Overall, the JR is an organic and S-rich mature mudstone (although not as organic-rich as the KCF, MF and GS) and similar to the GS, predominantly consist of silicate and sulfide (mainly FeS_2) minerals and starved of carbonates and phosphates.

Collectively, petrographic, mineralogical and geochemical analyses indicate that the KCF and MF are more enriched in OC, OSCs and carbonate minerals and have less silicate and sulfide minerals compared to the GS and JR. In contrast, the GS and JR are more enriched in silicate and sulfide minerals and very lean in carbonate minerals compared to the KCF and MF. OC in the GS and JR is relatively considered high although, not as copious as in the KCF and MF. OSCs were equally present in the GS and JR although, not as abundant as in the KCF and MF.

2.3.2 Electron Microprobe Analysis (EMPA)

EMPA imaging completed on the areas marked in white dashed squares in Fig. 2.1 (a - d) reveal the abundance and spatial distribution of S and Fe in all the mudstones (Fig. 2.4). The images indicate widespread S and relatively low and discretely scattered Fe across the scanned section in the KCF (Fig. 2.4a & b), in line with the high amounts of S and low Fe measured in the sample using elemental XRF and CHNS analyses (Table 2.1 & 2.2). These data also explain the low iron sulfide (7 wt. % FeS_2) observed in the KCF using XRD and petrographic analyses (Fig. 2.2a & b; Table 2.2). EMPA images of the MF, like the KCF, indicate a relatively high concentration of S and low Fe across the imaged area with both elements being confined to the same areas of the sample with a heterogeneous distribution compared to the KCF (Fig. 2.4c & d). Where there is low Fe and S according to the EMPA, these regions were confirmed to be Ca and/or P-rich by optical and ESEM-EDS analyses (Fig. 2.1b; Fig. 2.2c & d). The presence of relative high S and low Fe is in line with previous elemental XRF and CHNS analyses (Table 2.1 & 2.3) and also consistent with the very low concentration of iron sulfide (< 1 wt. % FeS_2) observed in the MF using XRD and petrographic analyses (Fig. 2.2c & d; Table 2.2).

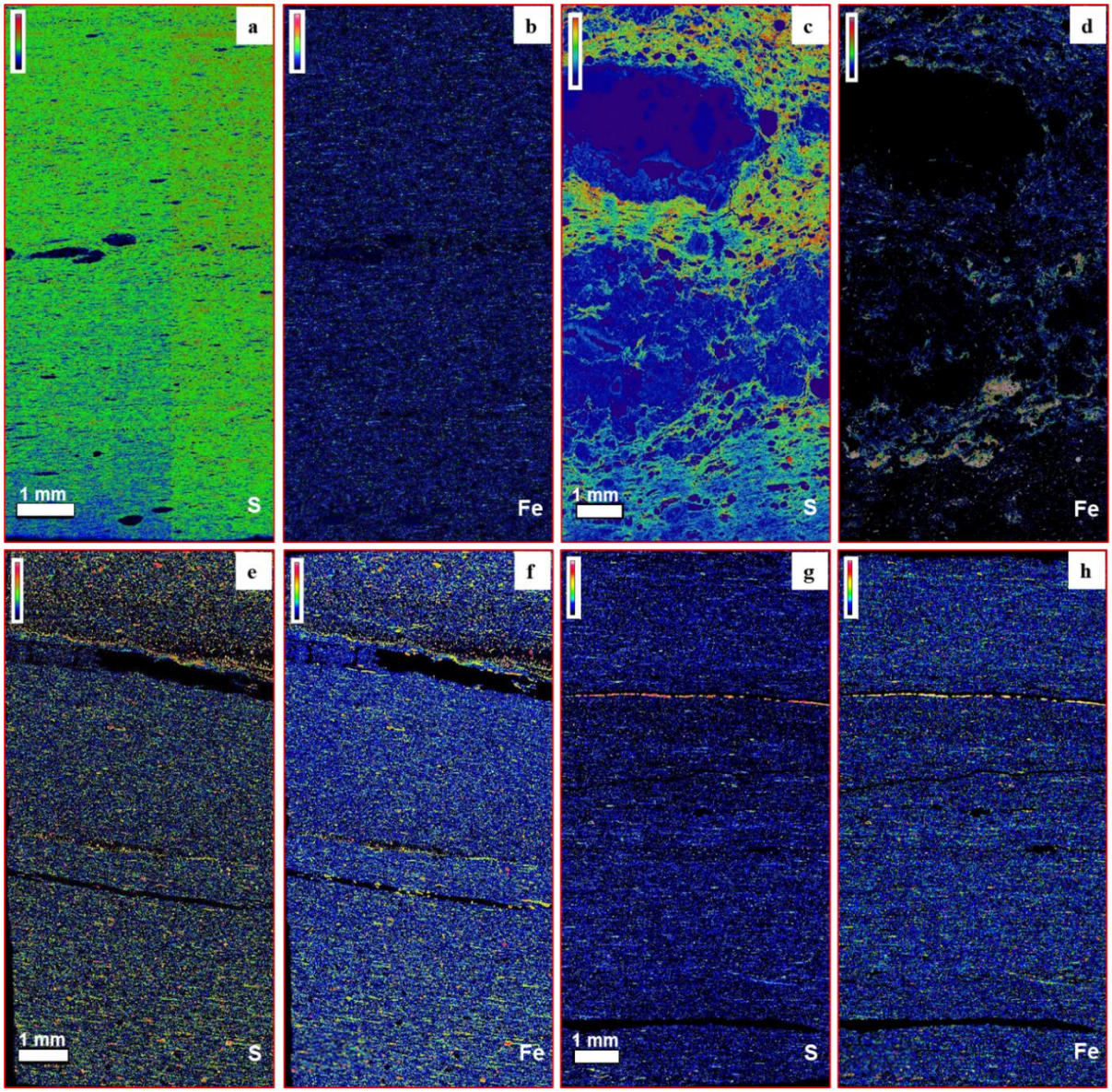

Figure 2.4: Electron microprobe images showing total S and F in the (a & b) Kimmeridge Clay, (c & d) Monterey and Whitby Mudstone [(e & f) Grey Shale and (g & h) Jet Rock] Formations, respectively. Imaging were completed on areas marked in white dashed squares in figure 2.1 (a - d).

In contrast to both the KCF and MF, EMPA images of the GS indicate relatively high spots of S and Fe signals distributed across the whole imaged area with the exception of certain fractured regions (Fig. 2.4e & f), in agreement with the high S and Fe measured in the sample using elemental XRF and CHNS analyses (Table 2.1 & 2.3), and also consistent with the enormous iron sulfide mineral (up to 17 wt. % FeS_2) observed in the GS using XRD and petrographic analyses (Fig. 2.2e & f; Table 2.2). The JR has an uneven distribution of S and Fe where both are concentrated together with certain bands/lenses showing strong signal and fractured regions displaying weak signals of both elements (Fig. 2.4g & h). Although, both S and Fe are relatively high, Fe signal appears to be stronger, in line with the high amounts Fe

compared S measured in this sample using elemental XRF and CHNS analyses (Table 2.1 & 2.3), and also consistent with the high iron sulfide mineral (up to 10 wt. % FeS_2) observed in the JR using XRD and petrographic analyses (Fig. 2.2e & f; Table 2.2). Collectively, the results show that EMPA can be used to image and determine the spatial distribution of S and Fe in organic and sulfur-rich mudstones. The data reveal the KCF and MF are relatively high in S and lean in Fe while the GS and JR are relatively high in both S and Fe.

2.4 Discussion

2.4.1 Organic Matter Source, Palaeo-productivity and Accumulation and Palaeo-redox

2.4.1.1 Organic Matter Source

The KCF, MF, GS and JR were all organic rich, with JR having the least OC (4 wt. %), which is still considered high (Table 2.1; Robert, 1988; Peters, 1986; Langford & Blanc-Valleron, 1990; Bordenave et al., 1993). With the exception of KCF, with HI value of 682 mg HC/g TOC, typical of kerogen type I/II, HI range between 600 - 458 mg HC/g TOC in the other mudstones, implying they contain kerogen type II (Table 2.1; Peters, 1986; Jones, 1987; Hunt, 1995). However, the organofacies/macerals in these mudstones differ (Fig. 2.2). The organic matter (OM) in the KCF is predominantly algal matter with minute terrigenous carbon as shown by optical examination (Fig. 2.2a), in line with previous study (van Kaam-Peters et al., 1998). The abundance of non-amorphous algal matter (dark brown), with some squashed out of form and disseminated (yellow ripple-like structures) throughout the optically examined section, translates to the high OC (52 wt. %) and HI (682 mg HC/g TOC) recorded in the KCF (Fig. 2.2a; Table 2.1). Similarly, OM in the MF is algal, but unlike the KCF it is mainly amorphous and widespread across the whole examined area (Fig. 2.2c). Although, biological production was enormous during the time of deposition of MF (Fig. 2.2c; Behl, 1999), its OC (14 wt. %; Table 2.1) and HI (600 mg HC/g TOC) are much lower compared to the KCF, implying preservation of OM was not efficient in MF and much of the produced organic carbon was remineralised. In contrast to both the KCF and MF, OM in the GS and JR exhibit similar characteristics (Fig. 2.2e & g). OM in both GS and JR is a mixture of different macerals (black, brown, red, yellow features in figure 2.2e & g) and, although discretely widespread across the whole optically examined area (2.2e & g), OC (6 and 4 wt. % respectively) and HI (516 and 458 mg HC/g TOC respectively) are relatively low in them compared to the KCF and MF (Table 2.1), suggesting the presence of appreciable fractions of terrestrial inert carbon in them. Overall, the KCF and MF were predominantly composed of algal OM with little or no terrigenous carbon input while OM in the GS and JR is a mix algal and terrestrial carbon.

2.4.1.2 Palaeo-productivity and Accumulation

Ba and P when normalised to Al, although with certain limitations, are widely used as palaeo-proxies to assess primary productivity owing to both having only one oxidation state (Brumsack, 1986; Föllmi et al., 1992; Ingall et al., 1993; van Cappellen & Ingall, 1994; Villamil, 1996; Schneider et al., 1997; Davis et al., 1999; Ganeshram, 1999; Mort et al., 2007; Henkel et al., 2012). Here, Ba is used because the mudstones under study, except for MF, are

all very low in P. Ba originates from barite in decaying marine phytoplankton and thus, is enriched in high productivity milieus (Goldberg & Arrhenius, 1958; Dymond et al., 1992; Francois et al., 1995; Dean et al., 1997), therefore, the Ba/Al ratio can be used as a primary productivity proxy. The Ba/Al ratio of MF is approximately fivefold higher compared to the other mudstones, with a value of 107 (Table 2.5), suggesting productivity was higher during deposition, in line with the large quantity of biological material observed in this unit (Fig. 2.1b & 2.2c). Ba/Al ratio of KCF and JR are similar, at 23 and 21, respectively, with GS having the lowest value at 14 however, all the mudstones have low Ba/Al values compared to average shale values (35; Table 2.5). Since barite is unstable in the absence of sulfate (Brumsack, 1986; Falkner et al., 1993; Ganeshram, 1999; McManus et al., 1998; Henkel et al., 2012), the Ba/Al ratio may be of use limited and, therefore additional trace metals were considered. Cu, Ni and Zn can be incorporated into OM, transported and preserved together with OM in sediments (Calvert & Pedersen, 1993; Jones & Manning, 1994; Whitfield, 2001; Achterberg et al., 2003; Algeo & Maynard, 2004; Böning et al., 2004). Although, these elements are also limited by the fact that they could be enriched in anoxic/euxinic settings due to their affinity to reduce S (Huerta-Diaz & Morse, 1992; Gregory et al., 2015), they are still commonly employed to access primary productivity (Nameroff et al., 2002; Tribovillard et al., 2006; Perkins et al., 2008). The Cu, Ni and Zn ratios show primary productivity was higher in MF followed by the KCF, GS and JR, in line with the Ba/Al ratios of the samples, except for JR where the Ba/Al is higher than GS (Table 2.5). TOC values of all the sample were normalised to their respective Al contents to correct for dilution by inorganic materials/clay, a process/proxy used to access organic carbon accumulation rates. TOC/Al values indicate OM accumulation rate was much higher in the KCF (15) followed by the MF (4), GS (0.4) and JR (0.2; Table 2.5), in line with the OC contents measured in the samples (Table 2.1). Although, the TOC/Al ratio presented here is perhaps not realistic owing to the different depositional settings of mudstones and varying clay (main source of Al) and carbonate contents in the samples, the TOC/Al ratio at least highlighted why OC was much higher in the KCF compared to the MF, even though its primary productivity was much lower to that of MF (Table 2.1 & 2.5), suggesting OM preservation in the KCF was enhanced compared to the other mudstones, in line with previous study (van Dongen et al., 2006).

2.4.1.3 Palaeo-redox

Redox-sensitive trace metals like U, V and Mo are used as palaeo-redox proxies due to their solubility in oxic settings and insolubility in anoxic/euxinic settings, resulting in their authigenic enrichment under anoxic conditions (Tribovillard et al., 2006). U, V and Mo in all the samples when normalised to Al where higher than Al normalised average shale values (Table 2.5; Wedepohl, 1971; 2004). However, when their enrichment factors (Brumsack, 2006; Tribovillard et al., 2006) were calculated and compared with average shale values, U and V show variable enrichments in the samples while Mo is enriched in all samples compared to average shale (Table 2.5). Algeo and Maynard (2004) and Scott and Lyons (2012) reported that Mo enrichment < 100 ppm indicate anoxic conditions with little or no reduced S while Mo enrichment > 100 ppm strongly indicate euxinic conditions. Therefore, the KCF and MF having Mo enrichments of up to 306 ppm and 114 ppm, respectively, indicate the mudstones were deposited under highly reduced conditions in the presence abundant reduced S, in line with previous geochemical and trace metal studies (van Kaam-Peters et al., 1998; Zaback & Pratt, 1992; van Dongen et al., 2006; Hancock et al., 2019; Mahoney et al., 2019). On the contrary, Mo is enriched by 32 ppm and 16 ppm in GS and JR, respectively, implying they were deposited predominantly under dysoxic/anoxic conditions. However, the presence of reduced S cannot be discount since FeS_2 have been observed in these settings (Fig. 2.2e, f, g & h). The variability of U and V enrichments in the samples called for an additional palaeo-redox proxy to support the Mo results. The ratio of U over Th (U/Th) is also commonly employed as a palaeo-redox proxy where ratios below 0.75, between 0.75 and 1.25 and above 1.25 indicate oxic, dysoxic and anoxic conditions, respectively (Adams & Weaver, 1958; Klinkhammer & Palmer, 1991; Jones & Manning, 1994). U/Th show a ratio of 4.8 for both KCF and MF and a ratio of approximately 1 for both GS and JR, indicating the former mudstones were deposited under extremely reducing condition and the later ones under dysoxic/anoxic, in line with the Mo results. However, the enrichment of Mn in GS compared to average shale suggest the sample was deposited under oxic conditions (Table 2.3; Calvert & Pedersen, 1993; Algeo & Maynard, 2004; März et al., 2009). Overall, the KCF and MF were deposited under anoxic, reduced S-rich (euxinic) conditions, GS under oxic/dysoxic conditions and JR dysoxic/anoxic conditions.

Table 2.5: Ratio/Enrichment factor of trace elements in the Kimmeridge Clay (KCF), Monterey (MF) and Whitby Mudstone [Grey Shale (GS) and Jet Rock (JR) members] Formations as obtained from XRF analysis. Aluminium and total organic carbon in weight percent (wt. %), trace elements in parts per million (ppm).

Ratio	KCF	MF	GS	JR	Average Shale[a]
Ba/Al	23.36	107.15	14.17	20.86	34.73
E.F[b]	0.7	3.1	0.4	0.6	
Cd/Al	0.3	1.0	0.4	0.3	0.01
E.F[b]	36.2	124.0	49.9	38.2	
Mo/Al	23.8	8.9	2.5	1.2	0.1
E.F[b]	306.2	113.9	32.0	16.0	
V/Al	14.5	78.5	9.2	8.2	7.8
E.F[b]	1.9	10.1	1.2	1.1	
Zn/Al	10.0	47.7	6.1	5.2	5.7
E.F[b]	1.8	8.4	1.1	0.9	
Cu/Al	9.3	18.8	5.1	1.5	2.7
E.F[b]	3.5	7.0	1.9	0.5	
Cr/Al	11.2	59.7	9.7	5.9	5.4
E.F[b]	2.1	11.1	1.8	1.1	
Ni/Al	18.9	28.9	10.5	4.4	4.1
E.F[b]	4.6	7.1	2.6	1.1	
U/Al	2.4	8.4	0.6	0.6	0.2
E.F[b]	11.1	38.0	2.6	2.6	
Th/Al	0.5	1.8	0.7	0.7	0.7
E.F[b]	0.7	2.5	1.0	0.9	
U/Th[c]	4.8	4.8	0.8	0.9	
TOC/Al	15	4	0.4	0.2	

[a] average shale data from Wedepohl (1971, 1991), [b] Enrichment factor calculated using EF = $(element/Al)_{sample}$ / $(element/Al)_{average\ shale}$ (Tribovillard et al, 2006; Brumsack, 2006). [c] adapted from Jones & Manning (1994).

2.4.2 Preservation of OM through Sulfurisation versus Pyrite Precipitation

Incorporation of reduced inorganic S into OM in anoxic environments has been widely reported as one of the effective ways through which OM is transported and stored in the fossil record. Through this process, even labile OM such as carbohydrates, which are readily remineralised can be preserved (Sinninghe Damsté et al., 1989; Sinninghe Damsté and de Leeuw, 1990; Orr

et al., 1990; Schouten et al., 1995; Koopmans et al., 1996; van Kaam-Peters et al., 1997, 1998; Werne et al., 2000; Grice et al., 2003; van Dongen et al., 2003a, 2003b; Werne et al., 2004; van Dongen et al., 2006; Werne et al., 2008). Since the KCF was deposited under euxinic conditions compared to the GS and JR and, the OM accumulation rate was significantly higher than that of GS and JR (as shown by TOC/Al ratio; Table 2.5), even though its primary productivity rate (as shown by Ba/Al ratio; Table 2.5) was to a certain extent similar to that GS and JR, the incorporation of reduced inorganic S was responsible for the enhanced preservation of OM (up to 52 wt. % OC) in the KCF, supporting previous studies (van Kaam-Peters et al., 1998; van Dongen et al., 2006). This is further supported by the high hydrogen over carbon (H/C; 1.3) and sulfur over carbon (S/C; 0.05) atomic ratios of the KCF, which indicate it contains kerogen type 2S (Table 2.6; Orr, 1986; Killops & Killops, 1993), consistent with previous studies (van Kaam-Peters et al., 1998; van Dongen et al, 2003). Interestingly, the H/C and S/C atomic ratios of GS and JR are significantly higher than that of the KCF (Table 2.6) which, suggest they are also made up of kerogen type II-S. However, the contribution of OSC moieties such as alkylated thiophenes and benzothiophenes observed in the flash pyrolysates of the GS and JR are very low compared to the KCF (Fig. 2.3; Table 2.4), as confirmed by the ratios of 2M/T (KCF = 2; GS = 0.4; JR = 0.5), BT/T (KCF = 3.2; GS = 0.1; JR = 0.2), 2,3DMT/[(1,2DMB + 1Nonene); KCF = 1.5; GS = 0.3; JR = 0.5] and 2ET+2,5DMT/[(2ET + 2,5DMT + 2,4DMT + 2,3DMT); KCF = 0.6; GS = 0.4; JR = 0.3; Table 2.6]. The high KCF ratios were also consistent with previous studies (van Kaam-Peters et al., 1998; van Dongen et al., 2006). The abundance of OSCs in the KCF compared to the GS and JR, explains why it generated petroleum at lower temperatures than the GS and JR, as shown by Tmax (KCF = 418 ºC; GS = 431 ºC; JR = 437 ºC; Table 2.1), consistent with previous studies (Fishman et al., 2012; Macquaker et al., 2014). The MF was deposited under euxinic conditions with OM accumulation rate significantly higher than that of the GS and JR but, significantly lower than that of the KCF, as shown by the TOC/Al ratio (Table 2.5). H/C (1.2) and S/C (0.04) atomic ratios of MF, indicate it contains kerogen type 2S (Table 2.6; Orr, 1986; Killops & Killops, 1993), consistent with previous study (Orr, 1986). This is further supported by the presence of a substantial amounts of a range of OSC moieties such as alkylated thiophenes and benzothiophenes observed in the flash pyrolysates (Fig. 2.3; Table 2.4), as confirmed by the high ratios of 2M/T (2.1), BT/T (0.9), 2,3DMT/[(1,2DMB + 1Nonene); 2.1] and 2ET+2,5DMT/[(2ET + 2,5DMT + 2,4DMT + 2,3DMT); 0.6; Table 2.6]. The abundance of OSCs in the MF was responsible for kerogen cracking at low temperatures (Tmax 402 ºC; Table 2.1), consistent with previous studies (Macquaker et al., 2014; Uguna et al., 2016). Our data indicate the use of H/C and S/C atomic

ratios as coined by Orr (1986) could be misleading if used to assess samples with high amounts S but, with low TOC.

Table 2.6: Atomic ratios of hydrogen over carbon and sulfur over carbon and ratios of 2-methylthiophene over toluene (2M/T), benzothiophenes over toluene (BT/T), 2,3-dimethylthiophene over 1,2-dimethylbenze + 1-nonene [2,3DMT/(1,2DMB + 1-Nonene)] and 2-ethylthiophene + 2,5-dimethylthiophene over 2-ethylthiophene + 2,5-dimethylthiophene + 2,4-dimethylthiophene + 2,3-dimethylthiophene [2ET + 2,5DMT/(2ET + 2,5DMT + 2,4DMT + 2,3DMT)] as obtained from CHNS and Py-GCMS analyses, respectively.

Ratios	KCF	MF	GS	JR
H/C	1.3	1.2	2.2	3.2
S/C	0.05	0.04	0.68	0.36
2M/T	2.0	2.1	0.4	0.5
BT/T	3.2	0.9	0.1	0.2
2,3DMT/ (1,2DMB+1-Nonene)	1.5	2.1	0.3	0.5
2ET+2,5DMT/ (2ET+2,5DMT+2,4DMT+2,3DMT)	0.6	0.6	0.4	0.3

Precipitation of iron sulfides, primarily FeS_2, has been suggested to be a competitor to OM preservation via sulfurization (Raiswell, 1982; Berner, 1984; Raiswell and Berner, 1985; Taylor and Macquaker, 2000; Jiang et al., 2017; Shawar et al., 2018; Raven et al., 2019). In euxinic basins were reactive Fe is present, reduced S can react with Fe to form iron sulfides, primarily FeS_2. The amounts of S in all samples is relatively high (Table 2.1 & 2.3). However, sulfurisation of OM was only significant in the KCF and MF and less significant in the GS and JR as indicated by the alkylated thiophenes and benzothiophenes ratio previously discussed (Table 2.6). This could be due to the presence of high amounts of Fe in the GS (9 wt. %) and JR (6 wt. %) compared to the KCF and MF, which both have 1 wt. % Fe (Table 2.3). The presence of high amounts of bioavailable Fe, reactive siliciclastic detritus and minute carbonate detritus in the GS and JR (Table 2.2 & 2.3) buffered porewater acidity caused by reduced S resulting in the precipitation of abundant authigenic FeS_2 (Table 2.2; Fig. 2.2f & h) via a number of thermodynamic pathways (Rickard & Luther, 2007). This led to the preservation of relative low amounts of S-lean OM that generated petroleum at relatively higher temperatures (Table 2.1; Tissot & Welte, 1984). In contrast to the GS and JR, the presence of very low amounts of bioavailable Fe, limited siliciclastic detritus and high carbonate detritus in the KCF and MF (Table 2.2 & 2.3) ensured high porewater acidity by reduced S, leading to preservation of high amounts of S-rich OM that generated petroleum at relatively lower temperatures (Table

2.1; Tissot & Welte, 1984) and thus, low/limited authigenic FeS_2 were formed in these mudstones (Table 2.2; Fig. 2.2b & d). S images obtained by electron microprobe analysis further provided information/insight about the distribution and nature of S in all the mudstones under study (Fig. 2.4). S signals in the S-rich OM samples (KCF & MF; Fig. 2.4a & c) were almost evenly spread across the whole imaged area, except for carbonate/phosphate-rich regions, consistent with the optical images which show OM in the KCF and MF are evenly distributed across the whole imaged area (Fig. 2.2a & c). Thus, suggesting the S in them is most likely bound to organics or in solution, in the case of this study organics as confirmed by previous results (Fig. 2.6; Table 2.1), especially since the KCF and MF are lean iron sulfides (Table 2.2). On the contrary, S signals in the S-lean OM samples (GS & JR; Fig. 2.4e & g) exhibit a different distribution pattern. Although widespread, S exist in discrete shapes/units ranging in geometry and size (from few nanometres up to 15 microns) and in most cases correlated with Fe when compared with their corresponding Fe electron microprobe images (Fig. 2.3f & h) thus, suggesting the S in the GS and JR were not mostly in solution or bound to organic compounds/complexes rather, they exist in discrete authigenic mineral phases, in the case of this study FeS_2 as confirmed by previous results (Table 2.2; Fig. 2.2f & h).

Collectively, the results in this study show that incorporation of reduced S into organic carbon enhances OM preservation even in low PP environments. However, the presence of oxidants such as sesquioxides of Fe could significantly hinder this process, for example, as in the case GS and JR were the presence of high amounts of Fe, sequestered much of the reduced S as FeS_2, impeding reactions between OM and S that could have led to formation of S-rich kerogen in GS and JR. In the contrary, the dearth of Fe in KCF and MF, permitted OM and S reactions to occur efficiently leading to formation of S-rich kerogens in the KCF and MF.

2.5 Conclusion

Multiple high resolution geochemical and petrographic analyses of mudstones from the Blackstone band of the Kimmeridge Clay Formation (KCF), upper calcareous-siliceous member of Monterey Formation (MF) and Grey Shale (GS) and Jet Rock (JR) members of the Whitby Mudstone Formation highlighted the contrasting chemical composition and physical nature of these mudstones. Results showed that sulfur (S) in the KCF and MF is mostly bound to organic matter (OM) as indicated by the relative abundance of organic S, mainly thiophenic compounds, compared to other hydrocarbons in their pyrolysates. The relatively low amounts of iron (Fe) in both the KCF and MF subdued the formation of FeS_2, thus were low/limited in both settings. Therefore, extensive reaction of S and OM in both KCF and MF occurred which

ensured the preservation of high amounts of S-rich kerogen in these settings. Electron microprobe (EMPA) mapping of total S and Fe in the studied organic and S-rich mudstones was feasible for the first time and provided information/insight about the distribution and nature of S and Fe. S signals in the KCF and MF were almost evenly spread across the whole imaged area, except for carbonate/phosphate-rich regions and Fe signals were relatively very low, indicating S in the KCF and MF is most likely bound to organics, as supported by the multiple geochemical analyses. Contrary to the KCF and MF, S in the GS and JR, were not mostly organically bound as indicated by the relatively low/absence of thiophenic compounds and predominance of other hydrocarbons in their pyrolysates. The relatively high amounts of Fe in both the GS and JR sequestered S as pyrites (FeS_2), resulting in the diminution of reaction between S and OM thus, preservation through sulfurisation in these setting was less significant compared to the KCF and MF and this reflected in their measured kerogen compositions. Furthermore, S signals in the EMPA images of the GS and JR exhibit a different distribution pattern. Although widespread, S exist in discrete shapes/units ranging in geometry and size (from few nm up to 15 μm) and in most cases correlated with Fe when compared with their corresponding Fe EMPA images, indicating that the S in the GS and JR was not mostly bound to organic compounds/complexes rather, they exist in discrete authigenic FeS_2, as supported by petrographic and geochemical analyses.

Overall, this study reported, for the first time, detailed distribution of OSCs in the MF, GS and JR, and compared/contrasted them with those observed in the KCF by previous studies. This study further shows that state-of-the-art EMPA elemental mapping of total S and Fe in organic and S-rich mudstones is feasible. Results support preservation of OM through sulfurisation as an important pathway for massive sequestration of OM in the sedimentary record as previously reported and, the presence of oxidants such as, sesquioxides of Fe, could significantly hinder this process by preferentially reacting with reduced S, to form iron sulfides (mainly FeS_2), thus impeding reactions between OM and S to occur efficiently. Although, the abundance of reactive Fe could have a dominant control on preservation through sulfurisation, there is still a need to study S and Fe species (oxidation states) both at low and high resolutions to fully comprehend sulfurisation and FeS_2 formation processes.

Acknowledgement

Petroleum Technology Development Fund (Nigeria) is thanked for funding YA (16PhD153), We thank Heath Bagshaw, John Waters, and John Fellowes for training YA on FTIR, XRD

and EMPA respectively, Paul Lythgoe for help with XRF and Alastair Bewsher for help with TIC.

Reference

Achterberg, E. P., Van Den Berg, C. M. G., & Colombo, C. (2003). High resolution monitoring of dissolved Cu and Co in coastal surface waters of the western North Sea. *Continental Shelf Research*, *23*(6), 611–623. https://doi.org/10.1016/S0278-4343(03)00003-7

Adams, J. A. S., & Weaver, C. E. (1958). Thorium-to-Uranium Ratios as Indicators of Sedimentary Processes: Example of Concept of Geochemical Facies1. *AAPG Bulletin*, *42*(2), 387–430. https://doi.org/10.1306/0BDA5A89-16BD-11D7-8645000102C1865D

Adams, L. K., Macquaker, J. H. S., & Marshall, J. D. (2006). Iron(III)-Reduction in a Low-Organic-Carbon Brackish-Marine System. *Journal of Sedimentary Research*, *76*(6), 919–925. https://doi.org/10.2110/jsr.2006.080

Algeo, T. J., & Maynard, J. B. (2004). Trace-element behavior and redox facies in core shales of Upper Pennsylvanian Kansas-type cyclothems. *Chemical Geology*, *206*(3–4), 289–318. https://doi.org/10.1016/j.chemgeo.2003.12.009

Aminu, M. D., Nabavi, S. A., Rochelle, C. A., & Manovic, V. (2017). A review of developments in carbon dioxide storage. *Applied Energy*, *208*(September), 1389–1419. https://doi.org/10.1016/j.apenergy.2017.09.015

Archer, D., Eby, M., Brovkin, V., Ridgwell, A., Cao, L., Mikolajewicz, U., Caldeira, K., Matsumoto, K., Munhoven, G., Montenegro, A., & Tokos, K. (2009). Atmospheric Lifetime of Fossil Fuel Carbon Dioxide. *Annual Review of Earth and Planetary Sciences*, *37*(1), 117–134. https://doi.org/10.1146/annurev.earth.031208.100206

Arthur, M. A., Dean, W. E., & Stow, D. A. V. (1984). Models for the deposition of Mesozoic-Cenozoic fine-grained organic-carbon-rich sediment in the deep sea. *Geological Society, London, Special Publications*, *15*(1), 527–560. https://doi.org/10.1144/gsl.sp.1984.015.01.34

Arthur, M. A., Schlanger, S. O., & Jenkyns, H. C. (1987). The Cenomanian-Turonian Oceanic Anoxic Event, II. Palaeoceanographic controls on organic-matter production and preservation. *Geological Society, London, Special Publications*, *26*(1), 401–420. https://doi.org/10.1144/GSL.SP.1987.026.01.25

Behl, R. J. (1999). Since Bramlette (1946): The Miocene Monterey Formation of California revisited. *Geological Society of America Special Papers*, *338*(1946), 301–313. https://doi.org/10.1130/0-8137-2338-8.301

Berner, R. A. (1984). Sedimentary pyrite formation: An update. *Geochimica et Cosmochimica Acta*, *48*(4), 605–615. https://doi.org/10.1016/0016-7037(84)90089-9

Betts, J. N., & Holland, H. D. (1991). The oxygen content of ocean bottom waters, the burial efficiency of organic carbon, and the regulation of atmospheric oxygen. *Global and Planetary Change*, *5*(1–2), 5–18. https://doi.org/10.1016/0921-8181(91)90123-E

Böning, P., Brumsack, H. J., Böttcher, M. E., Schnetger, B., Kriete, C., Kallmeyer, J., & Borchers, S. L. (2004). Geochemistry of Peruvian near-surface sediments. *Geochimica et Cosmochimica Acta*, *68*(21), 4429–4451.

Bordenave, M. L., Espitalié, J., Laplat, P., Oudin, J. L., & Vandenbrouke, M. (1993). Screening techniques for source rock evaluation. In M. L. Bordenave (Ed.), *Applied petroleum geochemistry* (pp. 217–279). Editions Technip.

Boussafir, M., Gelin, F., Lallier-Vergès, E., Derenne, S., Bertrand, P., & Largeau, C. (1995). Electron microscopy and pyrolysis of kerogens from the Kimmeridge Clay Formation, UK: Source organisms, preservation processes, and origin of microcycles. *Geochimica et Cosmochimica Acta*, *59*(18), 3731–3747. https://doi.org/10.1016/0016-7037(95)00273-3

Bowden, S. A., Farrimond, P., Snape, C. E., & Love, G. D. (2006). Compositional differences in biomarker constituents of the hydrocarbon, resin, asphaltene and kerogen fractions: An example from the Jet Rock (Yorkshire, UK). *Organic Geochemistry*, *37*(3), 369–383. https://doi.org/10.1016/j.orggeochem.2005.08.024

Brumsack, H. J. (1986). The inorganic geochemistry of Cretaceous black shales (DSDP Leg 41) in comparison to modern upwelling sediments from the Gulf of California. *North Atlantic Palaeoceanography*, *21*, 447–462.

Brumsack, Hans J. (2006). The trace metal content of recent organic carbon-rich sediments: Implications for Cretaceous black shale formation. *Palaeogeography, Palaeoclimatology, Palaeoecology*, *232*(2–4), 344–361. https://doi.org/10.1016/j.palaeo.2005.05.011

Calvert, S. E. (1987). Oceanographic controls on the accumulation of organic matter in marine sediments. *Geological Society, London, Special Publications*, *26*, 137–151. https://doi.org/10.1144/GSL.SP.1987.026.01.08

Calvert, S. E., & Pedersen, T. F. (1993). Geochemistry of Recent oxic and anoxic marine sediments: Implications for the geological record. *Marine Geology*, *113*(1–2), 67–88. https://doi.org/10.1016/0025-3227(93)90150-T

Calvert, Stephen E., & Pedersen, T. F. (1992). Organic carbon accumulation and preservation in marine sediments: how important is anoxia? In *Productivity, accumulation, and preservation in recent and ancient sediments* (pp. 231–263).

Canfield, D. E. (1989). Sulfate reduction and oxic respiration in marine sediments: implications for organic carbon preservation in euxinic environments. *Deep Sea Research Part A. Oceanographic Research Papers*, *36*(1), 121–138. https://doi.org/10.1016/0198-0149(89)90022-8

Coleman, M. L., Berner, R. A., Durand, B., Meadows, P. S., & Eglinton, G. (1985). Geochemistry of Diagenetic Non-Silicate Minerals Kinetic Considerations [and Discussion]. *Philosophical Transactions of the Royal Society A: Mathematical, Physical and Engineering Sciences*, *315*(1531), 39–56. https://doi.org/10.1098/rsta.1985.0028

Curtis, C. D., Burns, R. G., & Smith, J. V. (1977). Sedimentary Geochemistry: Environments and Processes Dominated by Involvement of an Aqueous Phase [and Discussion]. *Philosophical Transactions of the Royal Society A: Mathematical, Physical and Engineering Sciences*, *286*(1336), 353–372. https://doi.org/10.1098/rsta.1977.0123

Davis, C., Pratt, L. M., Sliter, W. V, Mompart, L., & Murat, B. (1999). Factors influencing organic carbon and trace metal accumulation in the Upper Cretaceous La Luna Formation of the western Maracaibo Basin, Venezuela. In E. Barrera & C. C. Johnson (Eds.), *Evolution of the Cretaceous Ocean-Climate System* (p. 203). Geological Society of America. https://doi.org/10.1130/0-8137-2332-9.203

Dean, W. E., Gardner, J. V., & Piper, D. Z. (1997). Inorganic geochemical indicators of glacial-interglacial changes in productivity and anoxia on the California continental margin. *Geochimica et Cosmochimica Acta*, *61*(21), 4507–4518. https://doi.org/10.1016/S0016-7037(97)00237-8

Demaison, G. (1991). Anoxia vs. Productivity: What Controls the Formation of Organic-Carbon-Rich Sediments and Sedimentary Rocks?: Discussion (1). *AAPG Bulletin*, *75*, 499. http://archives.datapages.com/data/doi/10.1306/0C9B2821-1710-11D7-8645000102C1865D

Demaison, G. J., & Moore, G. T. (1980). Anoxic environments and oil source bed genesis. *Organic Geochemistry*, *2*(1), 9–31. https://doi.org/10.1016/0146-6380(80)90017-0

Des Marais, D. J., Strauss, H., Summons, R., & Hayes, J. (1992). Carbon isotope evidence for the stepwise oxidation of the Proterozoic environment. *Nature*, *359*(6396), 605.

Ducklow, H., & McCallister, S. (2004). The biogeochemistry of carbon dioxide in the coastal oceans. *The Sea*, *13*, 269–315.

Dufresne, J. L., & Bony, S. (2008). An assessment of the primary sources of spread of global warming estimates from coupled atmosphere-ocean models. *Journal of Climate*, *21*(19), 5135–5144. https://doi.org/10.1175/2008JCLI2239.1

Dymond, J., Suess, E., & Lyle, M. (1992). Abstract . We used sediment traps to define the higher barium contents in the intermediate and combined our particle flux data with existing water linkages to ocean productivity and the degree of. *Paleoceanography*, *7*(2), 163–181.

Eglinton, T. I., Sinninghe Damsté, J. S., Kohnen, M. E. L., & de Leeuw, J. W. (1990). Rapid estimation of the organic sulphur content of kerogens, coals and asphaltenes by pyrolysis-gas chromatography. *Fuel*, *69*(11), 1394–1404. https://doi.org/10.1016/0016-2361(90)90121-6

Emerson, S., & Hedges, J. (2008). *Chemical oceanography and the marine carbon cycle*. Cambridge University Press.

Espitalié, J., Laporte, J. L., Madec, M., Marquis, F., Leplat, P., Paulet, J., & Boutefeu, A. (1977). Méthode rapide de caractérisation des roches mètres, de leur potentiel pétrolier et de leur degré d'évolution. *Rev. Inst. Fr. Pét.*, *32*(1), 23–42. https://doi.org/10.2516/ogst:1977002

Falkner, K. K., klinkhammer, G. P., Bowers, T. S., Todd, J. F., Lewis, B. L., Landing, W. M., & Edmond, J. M. (1993). The behavior of barium in anoxic marine waters. *Geochimica et Cosmochimica Acta*, *57*(3), 537–554. https://doi.org/10.1016/0016-7037(93)90366-5

Field, C. B., & Raupach, M. R. (2004). *The global carbon cycle : integrating humans, climate, and the natural world*. Island Press.

Fishman, N. S., Hackley, P. C., Lowers, H. A., Hill, R. J., Egenhoff, S. O., Eberl, D. D., & Blum, A. E. (2012). The nature of porosity in organic-rich mudstones of the Upper Jurassic Kimmeridge Clay Formation, North Sea, offshore United Kingdom. *International Journal of Coal Geology*, *103*, 32–50. https://doi.org/10.1016/j.coal.2012.07.012

Föllmi, K. B., Garrison, R. E., Ramirez, P. C., Zambrano-Ortiz, F., Kennedy, W. J., & Lehner, B. L. (1992). Cyclic phosphate-rich successions in the upper Cretaceous of Colombia. *Palaeogeography, Palaeoclimatology, Palaeoecology*, *93*(3–4), 151–182.

Francois, R., Honjo, S., Manganini, S. J., & Ravizza, G. E. (1995). Biogenic barium fluxes to the deep sea Implications for paleoproductivity reconstruction. *Global Biochemical Cycles*, *9*(2), 289–303.

Ganeshram, R. S. (1999). Factors Controlling the Burial of Organic Carbon in Laminated and Bioturbated Sediments off NW Mexico: Implications for hydrocarbon preservation. *Geochimica et Cosmochimica Acta*, *63*, 1723–1734. https://doi.org/10.1180/minmag.1998.62a.1.262

Ghadeer, S. G., & Macquaker, J. H. S. (2012). The role of event beds in the preservation of organic carbon in fine-grained sediments: Analyses of the sedimentological processes operating during deposition of the Whitby Mudstone Formation (Toarcian, Lower Jurassic) preserved in northeast England. *Marine and Petroleum Geology*, *35*(1), 309–320. https://doi.org/10.1016/j.marpetgeo.2012.01.001

Ghadeer, S. G., & Macquaker, J. H. S. (2011). Sediment transport processes in an ancient mud-dominated succession: A comparison of processes operating in marine offshore settings and anoxic basinal environments. *Journal of the Geological Society*, *168*(5), 1121–1132. https://doi.org/10.1144/0016-76492010-016

Goldberg, E. D., & Arrhenius, G.O.S. (1958). Chemistry of Pacific pelagic sediments. *Geochimica et Cosmochimica Acta*, *13*(2–3), 153–212. https://doi.org/10.1016/0016-7037(58)90046-2

Gregory, D. D., Large, R. R., Halpin, J. A., Baturina, E. L., Lyons, T. W., Wu, S., Danyushevsky, L., Sack, P. J., Chappaz, A., Maslennikov, V. V, & Bull, S. W. (2015). Trace Element Content of Sedimentary Pyrite in Black Shales. *Economic Geology*, *110*(6), 1389–1410. https://doi.org/10.2113/econgeo.110.6.1389

Grice, K., Schouten, S., Blokker, P., Derenne, S., Largeau, C., Nissenbaum, A., & Sinninghe Damsté, J. S. (2003). Structural and isotopic analysis of kerogens in sediments rich in free sulfurised Botryococcus braunii biomarkers. *Organic Geochemistry*, *34*(3), 471–482. https://doi.org/10.1016/S0146-6380(02)00187-0

Hancock, L. G., Hardisty, D. S., Behl, R. J., & Lyons, T. W. (2019). A multi-basin redox reconstruction for the Miocene Monterey Formation, California, USA. *Palaeogeography, Palaeoclimatology, Palaeoecology*, *520*(September 2018), 114–127. https://doi.org/10.1016/j.palaeo.2019.01.031

Heald, C. L., Henze, D. K., Horowitz, L. W., Feddema, J., Lamarque, J. F., Guenther, A., Hess, P. G., Vitt, F., Seinfeld, J. H., Godstein, A. H., & Fung, I. (2008). Predicted change in global secondary organic aerosol concentrations in response to future climate, emissions, and land use change. *Journal of Geophysical Research Atmospheres*, *113*(5), 0–16. https://doi.org/10.1029/2007JD009092

Henkel, S., Mogollón, J. M., Nöthen, K., Franke, C., Bogus, K., Robin, E., Bahr, A., Blumenberg, M., Pape, T., Seifert, R., März, C., de Lange, G. J., & Kasten, S. (2012). Diagenetic barium cycling in Black Sea sediments - A case study for anoxic marine environments. *Geochimica et Cosmochimica Acta*, *88*, 88–105. https://doi.org/10.1016/j.gca.2012.04.021

Houben, M. E., Barnhoorn, A., Lie-A-Fat, J., Ravestein, T., Peach, C. J., & Drury, M. R. (2016). Microstructural characteristics of the Whitby Mudstone Formation (UK). *Marine and Petroleum Geology*, *70*, 185–200. https://doi.org/10.1016/j.marpetgeo.2015.11.011

Howarth, M. K. (1962). The Jet Rock Series and Alum Shale Series of the Yorkshire Coast. *Proceedings of the Yorkshire Geological Society*, *33*(18), 381–422.

Huerta-Diaz, M. A., & Morse, J. W. (1992). Pyritization of trace metals in anoxic marine sediments: RN - Geochim. Cosmochim. Acta, v. 56, p. 2681-2702. *Geochimica et Cosmochimica Acta*, *56*(7), 2681–2702.

Hunt, J. M. (1995). *Petroleum geochemistry and geology*. WH Freeman Company.

Ingall, E. D., Bustin, R. M., & Van Cappellen, P. (1993). Influence of water column anoxia on the burial and preservation of carbon and phosphorus in marine shales. *Geochimica et Cosmochimica Acta*, *57*(2), 303–316. https://doi.org/10.1016/0016-7037(93)90433-W

Jarvie, D. M., Claxton, B. L., Henk, F., & Breyer, J. T. (2001). Oil and shale gas from the Barnett Shale, Fort Worth basin, Texas. *AAPG Bulletin*, *85*(13), A100.

Jenkyns, H. C. (1980). Cretaceous anoxic events: from continents to oceans. *Journal of the Geological Society*, *137*(2), 171–188. https://doi.org/10.1144/gsjgs.137.2.0171

Jenkyns, H. C. (1991). Impact of Cretaceous sea level rise and anoxic events on the Mesozoic carbonate platform of Yugoslavia. In *American Association of Petroleum Geologists Bulletin* (Vol. 75, Issue 6, pp. 1007–1017). https://doi.org/10.1306/0C9B28AD-1710-11D7-8645000102C1865D

Jiang, S., Mokhtari, M., & Borrok, D. M. (2017). Incorporating the effect of pyrite on total organic carbon estimation in eagle ford shale. *Society of Petroleum Engineers - SPE Liquids - Rich Basins Conference - North America 2017*. https://doi.org/10.2118/187484-ms

Jones, B., & Manning, D. A. C. (1994). Comparison of geochemical indices used for the interpretation of palaeoredox conditions in ancient mudstones. *Chemical Geology*, *111*(1–4), 111–129. https://doi.org/10.1016/0009-2541(94)90085-X

Jones, R. W. (1987). Organic facies. In J. Brooks & D. Welte (Eds.), *Advanced in Petroleum Geochemistry* (Vol. 2, pp. 1–90). Academic Press.

Killops, S. D., & Killops, V. J. (1993). *An introduction to organic geochemistry*. Longman Scientific and Technical.

Klinkhammer, G. P., & Palmer, M. R. (1991). Uranium in the oceans: Where it goes and why. *Geochimica et Cosmochimica Acta*, *55*(7), 1799–1806. https://doi.org/10.1016/0016-7037(91)90024-Y

Kolonic, S., Sinninghe Damsté, J. S., Bottcher, M. E., Kuypers, M. M. M., Kuhnt, W., Beckmann, B., Scheeder, G., & Wagner, T. (2002). Geochemical characterization of Cenomanian/Turonian black shales from the Tarfaya Basin (SW Morocco) - Relationships between palaeoenvironmental conditions and early sulphurization of sedimentary organic matter. *Journal of Petroleum Geology*, *25*(3), 325–350. https://doi.org/10.1111/j.1747-5457.2002.tb00012.x

Kolonic, S., Sinninghe Damsté, J. S., Böttcher, M. E., Kuypers, M. M. M., Kuhnt, W., Beckmann, B., Scheeder, G., & Wagner, T. (2002). Geochemical characterization of Cenomanian/Turonian black shales from the Tarfaya Basin (SW Morocco). *Journal of Petroleum Geology*, *25*(3), 325–350. https://doi.org/10.1111/j.1747-5457.2002.tb00012.x

Koopmans, M. P., Köster, J., Van Kaam-Peters, H. M. E., Kenig, F., Schouten, S., Hartgers, W. A., De Leeuw, J. W., & Sinninghe Damsté, J. S. (1996). Diagenetic and catagenetic products of isorenieratene: Molecular indicators for photic zone anoxia. *Geochimica et Cosmochimica Acta*, *60*(22), 4467–4496. https://doi.org/10.1016/S0016-7037(96)00238-4

Langford, F. F., & Blanc-Valleron, M.-M. (1990). Interpreting Rock-Eval pyrolysis data using graphs of pyrolizable hydrocarbons vs. total organic carbon. *AAPG Bulletin*, *74*(6), 799–804.

Le Quéré, C., & Metzl, N. (2004). Natural processes regulating the ocean uptake of CO_2. In M. R. Field, C.B. and Raupach (Ed.), *The Global Carbon Cycle: Integrating Humans, Climate, and the Natural World* (1st ed., pp. 243–255). Island Press.

Li, Y. (1972). Geochemical mass balance among lithosphere, hydrosphere, and atmosphere. *American Journal of Science*, *272*(2), 119–137.

Macquaker, J. H. S., & Gawthorpe, R. L. (1993). Mudstone lithofacies in the Kimmeridge Clay Formation, Wessex Basin, southern England; implications for the origin and controls of the distribution of mudstones. *Journal of Sedimentary Research*, *63*(6), 1129–1143. https://doi.org/10.1306/D4267CC1-2B26-11D7-8648000102C1865D

Macquaker, J. H. S., Taylor, K. G., Keller, M., & Polya, D. (2014). Compositional controls on early diagenetic pathways in fine-grained sedimentary rocks: Implications for predicting unconventional reservoir attributes of mudstones. *AAPG Bulletin*, *98*(3), 587–603. https://doi.org/10.1306/08201311176

Mahoney, C., März, C., Buckman, J., Wagner, T., & Blanco-Velandia, V. O. (2019). Pyrite oxidation in shales: Implications for palaeo-redox proxies based on geochemical and SEM-EDX evidence. *Sedimentary Geology*, *389*, 186–199. https://doi.org/10.1016/j.sedgeo.2019.06.006

März, C., Beckmann, B., Franke, C., Vogt, C., Wagner, T., & Kasten, S. (2009). Geochemical environment of the Coniacian-Santonian western tropical Atlantic at Demerara Rise. *Palaeogeography, Palaeoclimatology, Palaeoecology*, *273*(3–4), 286–301. https://doi.org/10.1016/j.palaeo.2008.05.004

McManus, J., Berelson, W. M., Klinkhammer, G. P., Johnson, K. S., Coale, K. H., Anderson, R. F., Kumar, N., Burdige, D. J., Hammond, D. E., Brumsack, H. J., McCorkle, D. C., & Rushdi, A. (1998). Geochemistry of barium in marine sediments: Implications for its use as a paleoproxy. *Geochimica et Cosmochimica Acta*, *62*(21–22), 3453–3473. https://doi.org/10.1016/s0016-7037(98)00248-8

Michalopoulos, P., & Aller, R. C. (2004). Early diagenesis of biogenic silica in the Amazon delta: Alteration, authigenic clay formation, and storage. *Geochimica et Cosmochimica Acta*, *68*(5), 1061–1085. https://doi.org/10.1016/j.gca.2003.07.018

Moore, T. S., Murray, R. W., Kurtz, A. C., & Schrag, D. P. (2004). Anaerobic methane oxidation and the formation of dolomite. *Earth and Planetary Science Letters*, *229*(1–2), 141–154. https://doi.org/10.1016/j.epsl.2004.10.015

Morgans-Bell, H. S., Coe, A. L., Hesselbo, S. P., Jenkyns, H. C., Weedon, G. P., Marshall, J. E. A., Tyson, R. V, & Williams, C. J. (2001). Integrated stratigraphy of the Kimmeridge Clay Formation (Upper Jurassic) based on exposures and boreholes in south Dorset, UK. *Geological Magazine*, *138*(05), 511–539. https://doi.org/10.1017/s0016756801005738

Morris, K. A. (1979). A classification of jurassic marine shale sequences: An example from the toarcian (lower jurassic) of Great Britain. *Palaeogeography, Palaeoclimatology, Palaeoecology*, *26*(C), 117–126. https://doi.org/10.1016/0031-0182(79)90144-5

Mort, H. P., Adatte, T., Föllmi, K. B., Keller, G., Steinmann, P., Matera, V., Berner, Z., & Stüben, D. (2007). Phosphorus and the roles of productivity and nutrient recycling during oceanic anoxic event 2. *Geology*, *35*(6), 483–486. https://doi.org/10.1130/G23475A.1

Müller, P. J., & Suess, E. (1979). Productivity, sedimentation rate, and sedimentary organic matter in the oceans-I. Organic carbon preservation. *Deep Sea Research Part A, Oceanographic Research Papers*, *26*(12), 1347–1362. https://doi.org/10.1016/0198-0149(79)90003-7

Nameroff, T. J., Balistrieri, L. S., & Murray, J. W. (2002). Suboxic trace metal geochemistry in the eastern tropical North Pacific. *Geochimica et Cosmochimica Acta*, *66*(7), 1139–1158. https://doi.org/10.1016/S0016-7037(01)00843-2

Nelson, B. C., Eglinton I., T., Seewald, J. S., Vairavamurthy, M. A., & Miknis, F. P. (1995). Transformations in Organic Sulfur Speciation During Maturation of Monterey Shale: Constraints from Laboratory Experiments. *Geochemical Transformations of Sedimentary Sulfur*, *612*, 138–166. https://doi.org/10.1021/bk-1995-0612.ch008

Orr, W. L. (1986). Kerogen/asphaltene/sulfur relationships in sulfur-rich Monterey oils. *Organic Geochemistry*, *10*(1–3), 499–516. https://doi.org/10.1016/0146-6380(86)90049-5

Orr, W. L., White, C. M. (Curt M. ., American Chemical Society. Division of Geochemistry., & American Chemical Society. Meeting (197th : 1989 : Dallas, T. . (1990). *Geochemistry of sulfur in fossil fuels : developed from a symposium sponsored by the Division of Geochemistry at the 197th National Meeting of the American Chemical Society, Dallas, Texas, April 9-14, 1989*. American Chemical Society.

Pedersen, T. F., & Calvert, S. E. (1990). Anoxia vs. productivity: what controls the formation of organic- carbon-rich sediments and sedimentary rocks? In *American Association of Petroleum Geologists Bulletin* (Vol. 74, Issue 4, pp. 454–466). https://doi.org/10.1306/0C9B282B-1710-11D7-8645000102C1865D

Perkins, R. B., Piper, D. Z., & Mason, C. E. (2008). Trace-element budgets in the Ohio/Sunbury shales of Kentucky: Constraints on ocean circulation and primary productivity in the Devonian-Mississippian Appalachian Basin. *Palaeogeography, Palaeoclimatology, Palaeoecology*, *265*(1–2), 14–29. https://doi.org/10.1016/j.palaeo.2008.04.012

Peters, K. E. (1986). Guidelines for Evaluating Petroleum Source Rock Using Programmed Pyrolysis1. *AAPG Bulletin*, *70*(3), 318–329. https://doi.org/10.1306/94885688-1704-11D7-8645000102C1865D

Powell, J. H. (1984). Lithostratigraphical nomenclature of the Lias Group in the Yorkshire Basin. *Proceedings of the Yorkshire Geological Society*, *45*(1–2), 51–57. https://doi.org/10.1144/pygs.45.1-2.51

Pratt, L. M. (1984). Influence of paleoenvironmental factors on preservation of organic matter in middle cretaceous greenhorn formation, pueblo, colorado. In *American Association of Petroleum Geologists Bulletin* (Vol. 68, Issue 9, pp. 1146–1159). https://doi.org/10.1306/AD4616E7-16F7-11D7-8645000102C1865D

Pratt, L. M., & King, J. D. (1986). Variable marine productivity and high eolian input recorded by rhythmic black shales in Mid-Cretaceous pelagic deposits from central Italy. *Paleoceanography*, *1*(4), 507–522. https://doi.org/10.1029/PA001i004p00507

Pye, K., & Krinsley, D. H. (1986). Microfabric, mineralogy and early diagenetic history of the Whitby Mudstone Formation (Toarcian), Cleveland Basin, U.K. *Geological Magazine*, *123*(03), 191. https://doi.org/10.1017/S0016756800034695

Raiswell, R. (1982). Pyrite texture, isotopic composition and the availability of iron. In *American Journal of Science* (Vol. 282, Issue 8, pp. 1244–1263). https://doi.org/10.2475/ajs.282.8.1244

Raiswell, R., & Berner, R. A. (1985). Pyrite formation in euxinic and semi-euxinic sediments. In *American Journal of Science* (Vol. 285, Issue 8, pp. 710–724). https://doi.org/10.2475/ajs.285.8.710

Raiswell, R., Bottrell, S. H., Al-Biatty, H. J., & Tan, M. M. (1993). The influence of bottom water oxygenation and reactive iron content on sulfur incorporation into bitumens from Jurassic marine shales. In *American Journal of Science* (Vol. 293, Issue 6, pp. 569–596). https://doi.org/10.2475/ajs.293.6.569

Raiswell, R., Canfield, D. E., & Berner, R. A. (1994). A comparison of iron extraction methods for the determination of degree of pyritisation and the recognition of iron-limited pyrite formation. *Chemical Geology*, *111*(1–4), 101–110. https://doi.org/10.1016/0009-2541(94)90084-1

Ramanathan, V., & Feng, Y. (2009). Air pollution, greenhouse gases and climate change: Global and regional perspectives. *Atmospheric Environment*, *43*(1), 37–50. https://doi.org/10.1016/j.atmosenv.2008.09.063

Raven, M. R., Fike, D. A., Bradley, A. S., Gomes, M. L., Owens, J. D., & Webb, S. A. (2019). Paired organic matter and pyrite δ 34 S records reveal mechanisms of carbon, sulfur, and iron cycle disruption during Ocean Anoxic Event 2. *Earth and Planetary Science Letters*, *512*, 27–38. https://doi.org/10.1016/j.epsl.2019.01.048

Rickard, D., & Luther, G. W. (2007). Chemistry of iron sulfides. In *Chemical Reviews* (Vol. 107, Issue 2). https://doi.org/10.1021/cr0503658

Robert, P. (1988). *Organic metamorphism and geothermal history: microscopic study of organic matter and thermal evolution of sedimentary basins* (1st ed., Vol. 3). Springer.

Ruddiman, W. F. (2001). *Earth's climate : past and future*. W.H. Freeman.

Ruddy, G. (1997). An overview of carbon and sulphur cycling in marine sediments. In Jickells T.D. and Rae J. E. (Ed.), *Biogeochemistry of intertidal sediments* (1st ed.). Cambridge University Press.

Rullkötter, J. (2006). Organic matter: the driving force for early diagenesis. In M. Schulz, H. D. and Zabel (Ed.), *Marine geochemistry* (pp. 125–168). Springer Verlag. https://doi.org/10.1007/3-540-32144-6_4

Sælen, G., Tyson, R. V., Telnæs, N., & Talbot, M. R. (2000). Contrasting watermass conditions during deposition of the Whitby Mudstone (Lower Jurassic) and Kimmeridge Clay (Upper Jurassic) formations, UK. *Palaeogeography, Palaeoclimatology, Palaeoecology*, *163*(3–4), 163–196. https://doi.org/10.1016/S0031-0182(00)00150-4

Sælen, Gunnar, Doyle, P., & Talbot, M. R. (1996). Stable-isotope analyses of belemnite rostra from the Whitby Mudstone Fm., England: Surface water conditions during deposition of a marine black shale. *Palaios*, *11*(2), 97–117. https://doi.org/10.2307/3515065

Salem, N. (2013). Geochemical characterisation of the Pliensbachian -Toarcian boundary during the onset of the Toarcian Oceanic Anoxic Event. North Yorkshire, UK (Issue February). *Newcastle University*, UK.

Schneider, R. R., Price, B., Müller, P. J., Kroon, D., & Alexander, I. (1997). Monsoon related variations in Zaire (Congo) sediment load and influence of fluvial silicate supply on marine productivity in the east equatorial Atlantic during the last 200,000 years. *Paleoceanography*, *12*(3), 463–481. https://doi.org/10.1029/96PA03640

Schouten, S., Sinninghe Damsté, J. S., Baas, M., Kock-van Dalen, A. C., Kohnen, M. E. L., & de Leeuw, J. W. (1995). Quantitative assessment of mono- and polysulphide-linked carbon skeletons in sulphur-rich macromolecular aggregates present in bitumens and oils. *Organic Geochemistry*, *23*(8), 765–775. https://doi.org/10.1016/0146-6380(95)00055-J

Schouten, S., Sinninghe Damsté, J. S., & de Leeuw, J. W. (1995). A novel triterpenoid carbon skeleton in immature sulphur-rich sediments. *Geochimica et Cosmochimica Acta*, *59*(5), 953–958. https://doi.org/10.1016/0016-7037(95)00013-5

Scotchman, I. C. (1989). Diagenesis of the Kimmeridge Clay Formation, onshore UK. *Journal of the Geological Society*, *146*, 285–303. https://doi.org/10.1144/gsjgs.146.2.0283

Scotchman, I. C. (1987). Clay diagenesis in the Kimmeridge Clay Formation, onshore UK, and its relation to organic maturation. *Mineralogical Magazine*, *51*(62), 535–551. http://www.minersoc.org/pages/Archive-MM/Volume_51/51-362-535.pdf

Scott, C., & Lyons, T. W. (2012). Contrasting molybdenum cycling and isotopic properties in euxinic versus non-euxinic sediments and sedimentary rocks: Refining the paleoproxies. *Chemical Geology*, *324–325*, 19–27. https://doi.org/10.1016/j.chemgeo.2012.05.012

Shaw, H. F., & Primmer, T. J. (1991). Diagenesis of mudrocks from the Kimmeridge Clay Formation of the Brae Area, UK North Sea. *Marine and Petroleum Geology*, *8*(3), 270–277. https://doi.org/10.1016/0264-8172(91)90081-B

Shawar, L., Halevy, I., Said-Ahmad, W., Feinstein, S., Boyko, V., Kamyshny, A., & Amrani, A. (2018). Dynamics of pyrite formation and organic matter sulfurization in organic-rich carbonate sediments. *Geochimica et Cosmochimica Acta*, *241*, 219–239. https://doi.org/10.1016/j.gca.2018.08.048

Sinninghe Damsté, J. S., & de Leeuw, J. W. (1990). Analysis, structure and geochemical significance of organically-bound sulphur in the geosphere: State of the art and future research. *Organic Geochemistry*, *16*(4–6), 1077–1101. https://doi.org/10.1016/0146-6380(90)90145-P

Sinninghe Damsté, J. S., Rijpstra, W. I. C., de Leeuw, J. W., & Schenck, P. A. (1989). The occurrence and identification of series of organic sulphur compounds in oils and sediment extracts: II. Their presence in samples from hypersaline and non-hypersaline palaeoenvironments and possible application as source, palaeoenvironmental and matur. *Geochimica et Cosmochimica Acta*, *53*(6), 1323–1341. https://doi.org/10.1016/0016-7037(89)90066-5

Suess, E. (1980). Particulate organic carbon flux in the oceans—surface productivity and oxygen utilization. *Nature*, *288*(5788), 260–263. https://doi.org/10.1038/288260a0

Summons, R. E., & Powell, T. G. (1987). Identification of aryl isoprenoids in source rocks and crude oils: Biological markers for the green sulphur bacteria. *Geochimica et Cosmochimica Acta*, *51*(3), 557–566. https://doi.org/10.1016/0016-7037(87)90069-X

Taylor, K. G., & Macquaker, J. H. S. (2000). Early diagenetic pyrite morphology in a mudstone-dominated succession: The Lower Jurassic Cleveland Ironstone Formation, eastern England. *Sedimentary Geology*, *131*(1–2), 77–86. https://doi.org/10.1016/S0037-0738(00)00002-6

Tegelaar, E. W., de Leeuw, J. W., Derenne, S., & Largeau, C. (1989). A reappraisal of kerogen formation. *Geochimica et Cosmochimica Acta*, *53*(11), 3103–3106. https://doi.org/10.1016/0016-7037(89)90191-9

Tissot, B. P., & Welte, D. H. (1984a). Petroleum Formation and Occurrence, A New Approach to Oil and Gas Exploration, Second Edition. *Springer-Verlag Berlin Heidelberg New York 1978*, 720.

Tissot, B. P., & Welte, D. H. (1984b). Petroleum Formation and Occurrence. In *Second Revised and Enlarged Edition* (Vol. 66, Issue 37). https://doi.org/10.1029/EO066i037p00643

Tribovillard, N., Algeo, T. J., Lyons, T., & Riboulleau, A. (2006). Trace metals as paleoredox and paleoproductivity proxies: An update. *Chemical Geology*, *232*(1–2), 12–32. https://doi.org/10.1016/j.chemgeo.2006.02.012

Tyson, R. V. (2005). The "Productivity Versus Preservation" Controversy: Cause, Flaws, and Resolution. *Deposition of Organic-Carbon-Rich Sediments: Models*, *82*, 17–33. https://doi.org/10.2110/pec.05.82.0017

Uguna, C. N., Carr, A. D., Snape, C. E., Meredith, W., Scotchman, I. C., Murray, A., & Vane, C. H. (2016). Impact of high water pressure on oil generation and maturation in Kimmeridge Clay and Monterey source rocks: Implications for petroleum retention and gas generation in shale gas systems. *Marine and Petroleum Geology*, *73*, 72–85. https://doi.org/10.1016/j.marpetgeo.2016.02.028

van Cappellen, P., & Canfield, D. E. (1993). Lack of evidence for enhanced preservation of sedimentary organic matter in the oxygen minimum of the Gulf of California: Comment and Reply. *Geology*, *21*(6), 570–571. https://doi.org/10.1130/0091-7613(1993)021<0570:LOEFEP>2.3.CO;2

van Cappellen, P., & Ingall, E. D. (1994). Benthic phosphorus regeneration, net primary production, and ocean anoxia: A model of the coupled marine biogeochemical cycles of carbon and phosphorus. *Paleoceanography*, *9*(5), 677–692. https://doi.org/10.1029/94PA01455

van Dongen, B. E., Schouten, S., Baas, M., Geenevasen, J. A. J., & Sinninghe Damsté, J. S. (2003). An experimental study of the low-temperature sulfurization of carbohydrates. *Organic Geochemistry*, *34*(8), 1129–1144. https://doi.org/10.1016/S0146-6380(03)00060-3

van Dongen, B. E., Schouten, S., & Sinninghe Damsté, J. S. (2003). Sulfurization of carbohydrates results in a sulfur-rich, unresolved complex mixture in Kerogen pyrolysates. *Energy and Fuels*, *17*(4), 1109–1118. https://doi.org/10.1021/ef0202283

van Dongen, B. E., Schouten, S., & Sinninghe Damsté, J. S. (2006). Preservation of carbohydrates through sulfurization in a Jurassic euxinic shelf sea: Examination of the Blackstone Band TOC cycle in the Kimmeridge Clay Formation, UK. *Organic Geochemistry*, *37*(9), 1052–1073. https://doi.org/10.1016/j.orggeochem.2006.05.007

van Kaam-Peters, H. M. E., Schouten, S., de Leeuw, J. W., & Sinninghe Damsté, J. S. (1997). A molecular and carbon isotope biogeochemical study of biomarkers and kerogen pyrolysates of the Kimmeridge Clay Facies: Palaeoenvironmental implications. *Organic Geochemistry*, *27*(7–8), 399–422. https://doi.org/10.1016/S0146-6380(97)00084-3

van Kaam-Peters, H. M. E., Schouten, S., Köster, J., & Sinninghe Damstè, J. S. (1998). Controls on the molecular and carbon isotopic composition of organic matter deposited in a Kimmeridgian euxinic shelf sea: Evidence for preservation of carbohydrates through sulfurisation. *Geochimica et Cosmochimica Acta*, *62*(19–20), 3259–3283. https://doi.org/10.1016/S0016-7037(98)00231-2

Villamil, T. (1996). Depositional and geochemical cyclicity in the cretaceous fine-grained strata of colombia. A model for organic matter content. In *CT y F - Ciencia, Tecnologia y Futuro* (Vol. 1, Issue 2, pp. 5–23).

Wagner, T., Hofmann, P., & Flögel, S. (2013). Marine black shale deposition and Hadley Cell dynamics: A conceptual framework for the Cretaceous Atlantic Ocean. *Marine and Petroleum Geology*, *43*, 222–238. https://doi.org/10.1016/j.marpetgeo.2013.02.005

Wedepohl, K. H. (1971). Environmental Influences on the Chemical Composition of Shales and Clays. *Physics and Chemistry of the Earth*, *8*, 307–333.

Wedepohl, K. H. (2004). The Composition of Earth's Upper Crust, Natural Cycles of Elements, Natural Resources. In *Elements and Their Compounds in the Environment* (pp. 2–16). https://doi.org/https://doi.org/10.1002/9783527619634.ch1

Weiss, H. M., Wilhelms, a, Mills, N., Scotchmer, J., Hall, P. B., Lind, K., & Brekke, T. (2000). The Norwegian Industry Guide to Organic Geochemical Analyses. *Norsk Hydro Statoil Geolab Nor SINTEF Petroleum Research and the Norwegian Petroleum Directorate*, 1–102.

Werne, J. P., Hollander, D. J., Behrens, A., Schaeffer, P., Albrecht, P., & Sinninghe Damsté, J. S. (2000). Timing of early diagenetic sulfurization of organic matter: A precursor-product relationship in Holocene sediments of the anoxic Cariaco Basin, Venezuela. *Geochimica et Cosmochimica Acta*, *64*(10), 1741–1751. https://doi.org/10.1016/S0016-7037(99)00366-X

Werne, J. P., Hollander, D. J., Lyons, T. W., & Sinninghe Damsté, J. S. (2004). Organic sulfur biogeochemistry: Recent advances and future research directions. *Geological Society of America Special Papers*, *379*, 135–150. https://doi.org/10.1130/0-8137-2379-5.135

Werne, J. P., Lyons, T. W., Hollander, D. J., Schouten, S., Hopmans, E. C., & Sinninghe Damsté, J. S. (2008). Investigating pathways of diagenetic organic matter sulfurization using compound-specific sulfur isotope analysis. *Geochimica et Cosmochimica Acta*, *72*(14), 3489–3502. https://doi.org/10.1016/j.gca.2008.04.033

Whitfield, M. (2001). Interactions between phytoplankton and trace metals in the ocean. In *Advances in Marine Biology* (Vol. 41, Issue C). https://doi.org/10.1016/S0065-2881(01)41002-9

Zaback, D. A., & Pratt, L. M. (1992). Isotopic composition and speciation of sulfur in the Miocene Monterey Formation: Reevaluation of sulfur reactions during early diagenesis in marine environments. *Geochimica et Cosmochimica Acta*, *56*(2), 763–774. https://doi.org/10.1016/0016-7037(92)90096-2

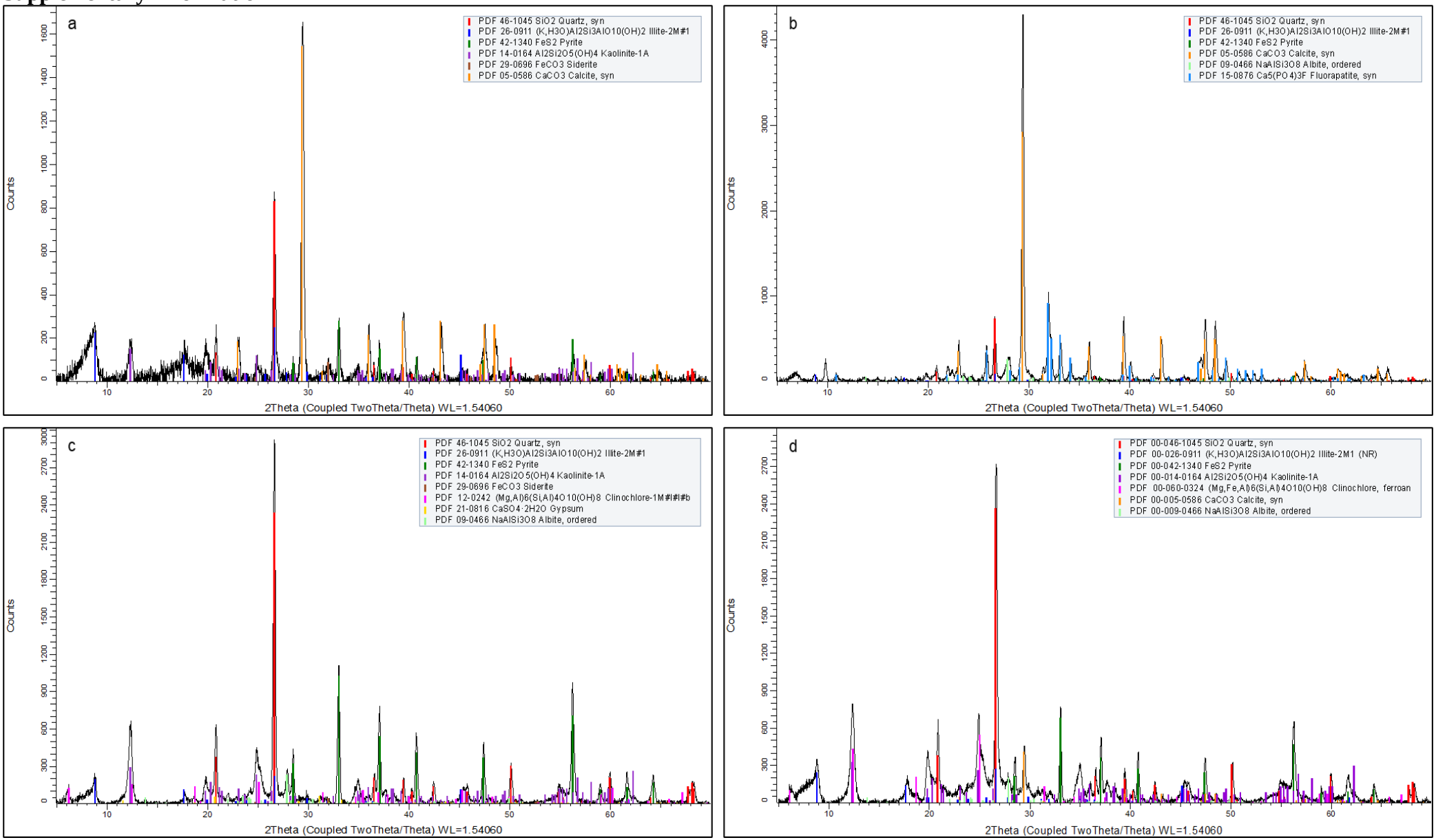

Figure S2.5: Diffractograms of (a) Kimmeridge Clay Formation, (b) Monterey Formation, (c) Grey Shale and (d) Jet Rock members of the Whitby Mudstone Formations as obtained by XRD analyses. Quantitative data is presented in figure 2.2.

Chapter 3

Project 2

X-ray Imaging and Molecular Characterization of Sulfur and Iron in Organic and Sulfur-Rich Hydrocarbon Source Rocks

Yusuf Abubakar [1, 2, *], Roy A. Wogelius[1], Victoria Coker[1], Kevin G. Taylor[1] and Bart E. van Dongen[1]

[1] Department of Earth and Environmental Sciences, School of Natural Sciences and Williamson Research Centre for Molecular Environmental Science, University of Manchester, Oxford Road, Manchester, M13 9PL, UK

[2] Desert Research, Monitoring and Control Centre, Yobe State University, KM 7, Sir Kashim Road, Damaturu, Nigeria

[*]Correspondence: yusuf.abubakar@manchester.ac.uk; yusuf.abubakar@ysu.edu.ng

To be submitted to Geochimica et Cosmochimica Acta

Highlights

- First ever mapping and characterisation of sulfur and iron oxidation states in organic and sulfur-rich mudstones using novel state-of-the-art synchrotron-based techniques.
- Sulfur, iron and other important diagenetic elements such as silicon, phosphorus and calcium were non-destructively, spatially-resolved across mudstones to improving our understanding of sulfurisation and iron sulfide formation processes.
- Analyses indicate there was a period in time when euxinic bottom water prevailed in the Grey Shale Member of the Whitby Mudstone Formation than previously recognised.

Abstract

Preservation through sulfurisation has been widely reported as one of the important pathways through which organic matter (OM) is transported and stored in the geosphere. However, the formation of iron sulfides, primarily pyrite (FeS_2), is suggested to be a competitor to this process. There is still a dearth of spatial information on sulfur (S) and iron (Fe) inventories (oxidation states) at high resolution that could improve our understanding of sulfurisation and FeS_2 formation processes as well as the environmental conditions during time of deposition. Organic- and S-rich mudstones from the Kimmeridge Clay, Monterey and Whitby Mudstone Formations were analysed using novel state-of-the-art synchrotron-based techniques (X-ray fluorescence imaging and X-ray absorption near edge structure analyses). Detailed analyses at high resolution (µm to mm scale) indicate that the presence of sulfurised OM in the Kimmeridge Clay Formation is widespread, in line with the presence of stable euxinic conditions in the water column over a relatively long period of time and a relatively low influx of reactive Fe, promoting the preservation of substantial amounts of OM through sulfurisation. In contrast, analyses indicate that the presence of sulfurised OM was transitional in the Monterey Formation, in line with fluctuating redox conditions in the water column over time, and insignificant in the Whitby Mudstone Formation, likely due to the abundance of reactive Fe outcompeting the formation of sulfurised OM. This study presents, for the first time, the use of synchrotron-based techniques to non-destructively, spatially resolve (chemically map) and provide detailed information about S and Fe oxidation states in the mudstones studied. These results improved our understanding of environmental conditions during the time of deposition of the studied mudstones at higher resolution than previously reported. The novel techniques can also be employed to study other mudstones and thereby their depositional settings may be more accurately reconstructed.

Keywords/Phrases: Organic Matter Sulfurisation, Pyrite, Kimmeridge Clay Formation, Monterey Formation, Whitby Mudstone Formation, X-Ray Fluorescence Imaging, X-Ray Absorption Near Edge Structure.

3.1 Introduction

Preservation through sulfurisation has been widely reported as one of the important pathways through which organic matter (OM) is transported and stored in the geosphere (Tegelaar et al., 1989; Koopmans et al., 1996; Sinninghe Damsté et al., 1998; Grice et al., 2003; van Dongen et al., 2006). However, the formation of iron (Fe) sulfides, primarily pyrite (FeS_2), is suggested to be a competitor to OM preservation via sulfurisation (Raiswell, 1982; Berner, 1984; Raiswell & Berner, 1985; Taylor & Macquaker, 2000; Jiang et al., 2017; Shawar et al., 2018; Raven et al., 2019). A lot of attention has been given to understand how sulfurisation of OM and FeS_2 precipitation occur and what processes are involved (Berner & Raiswell, 1983; Raiswell & Al-Biatty, 1989; Canfield et al., 1998; Werne et al., 2004; Amrani, 2014; Macquaker et al., 2014). However, little information is available to explain the competition between these two processes due to; (1) the large suite of organic sulfur compounds (OSCs) observed in sediments (Sinninghe Damsté et al., 1987), (2) the metabolic and abiotic chemical reactions that operate simultaneously to form OSCs and FeS_2 (Raven et al., 2016a), and (3) the possibility of an influx of Fe oxides at later times which can serve as a sink for reduced sulfur (S; Raiswell & Anderson, 2005). Although most studies associate sulfurisation of OM with sediments, recent analyses show that this process can already start in the water column (Raven et al., 2016b, 2020). Fe sulfide formation has been reported to also occur in the water column (Balistrieri et al., 1992; Murray, 1995; Luther et al., 2003) This suggests sulfurisation of OM may precede Fe sulfide formation or both processes could occur simultaneously, contrary to conventional thought that Fe sulfide formation is always favoured over OM sulfurization in Fe-rich oceans and porewater.

Multiple geochemical techniques have been used to improve our understanding of the evolution of OSCs and FeS_2 in organic- and S-rich mudstones (hydrocarbon source rocks). Conventional techniques such as gas chromatography-mass spectrometry and pyrolysis-gas chromatography-mass spectrometry (GC-MS and Py-GC-MS) already provide detailed molecular information on the presence, origin and formation of OSCs in mudstones/sediments (Sinninghe Damsté et al., 1987; Orr et al., 1990; Sinninghe Damsté & de Leeuw, 1990; Kohnen et al., 1991; Hartgers et al., 1996; Koopmans et al., 1996; van Kaam-Peters et al., 1998; Isaacs and Rullkötter, 2001; Grice et al., 2003; Bowden et al., 2006; van Dongen et al, 2006; Zheng et al., 2019) and, for instance, confirm that sulfurisation of carbohydrates largely caused the preservation of massive amounts of OM in the Kimmeridge Clay Formation (Sinninghe Damsté et al., 1998; van Kaam-Peters et al., 1998; van Dongen et al., 2006). S isotopic studies also significantly enhance our

understanding of OM sulfurisation and FeS_2 formation, particularly related to the origin of the S and the timing of the process (Werne et al., 2003, 2004, 2008; Amrani et al., 2009; Raven et al., 2016a; Grotheer et al., 2017; Meshoulam & Amrani, 2017; Smith et al., 2017; Shawar et al., 2018; Zheng et al., 2019; Wang et al., 2019). Other techniques such as X-ray diffraction (XRD), X-ray fluorescence (XRF) and sequential extractions provide detailed information on the affinity of S to other elements, such as Fe, Mo, Zn, and Cd, and the various mineral phases in which S can exist (Pye & Krinsley, 1986; Dicen et al., 2019; He et al., 2019). However, the aforementioned techniques give only limited information, particularly spatial detail at the millimetre/micron scale, whereas to fully comprehend sulfurisation processes more detailed information is required with regards the S and Fe availability, distribution, coordination and inventory.

To obtain detailed spatial information on both S and Fe in the sedimentary record a wide range of imaging techniques, such as optical microscopy, environmental scanning electron microscopy-energy dispersive spectroscopy (ESEM-EDS), electron microprobe (EPMA) and Fourier transform infrared spectroscopy (FTIR in reflectance mode), have been used to improve our understanding of the fate of S and Fe in mudstones during and after diagenesis (Bertrand et al., 1995; Taylor & Macquaker, 2000; Taylor & Macquaker, 2011; Macquaker et al., 2014; Mahoney et al., 2019). These imaging techniques provide some spatial information on mineral phases and to some extent help in the quantification of S and Fe in mudstones/sediments. Macquaker et al. (2014), for instance, employed ESEM-EDS to document abundance and distribution of S in the Kimmeridge Clay and Monterey Formations. Similarly, Mahoney et al. (2019) also used ESEM-EDS to analyse S and Fe in the Kimmeridge Clay and Chipaque (Colombia) Formations. However, these imaging techniques are limited in providing well-defined spatially resolved chemical-redox information of the key elements including S and Fe.

Bulk, molecular, isotopic and imaging analyses provide us with invaluable information about S and Fe in mudstones/sediments. However, in order to fully comprehend OM sulfurisation and FeS_2 formation processes, vital information such S and Fe oxidation states and their spatial distribution in sediment in required. Recently, studies have employed state-of-the-art synchrotron-based techniques such as X-ray absorption spectroscopy (XAS) to study S, Fe and other elements in fossils and their extant equivalents (Edwards et al., 2014; Barden et al., 2015; Anné et al., 2019; Manning et al., 2019). Using, for instance, X-ray absorption near edge structure (XANES) analysis the different S and Fe species in some fossils and human organs

(e.g. brain) can be revealed (Szczerbowska-Boruchowska et al., 2012; Manning et al., 2019). Additionally, X-ray fluorescence imaging (elemental) helped to spatially map S and Fe species in fossils (Edwards et al., 2014; Castillo-Michel et al., 2016; Anné et al., 2019; Manning et al., 2019; Rossi et al., 2019; Szczerbowska-Boruchowska et al., 2012). Raven et al., 2018 used XANES to study sulfurisation in sequentially extracted sediments from Pont d'Issole (France) suggesting that even small changes in primary productivity could lead to significant changes in OM preservation near critical redox thresholds. Similarly, other studies used XANES to study different S species in kerogens/bitumens (Waldo et al., 1991; Vairavamurthy et al., 1994; Mitra-Kirtley et al., 1999; Wiltfong et al., 2005; Pomerantz et al., 2014; Dang et al., 2019; Kashiwabara et al., 2019; Meister et al., 2019). However, these studies were conducted on processed (destroyed) samples and as such, there is a dearth of information on the presence of different forms/oxidation states of S and Fe and their spatial distribution in organic- and S-rich mudstones.

The aims of this study are therefore to determine (1) if state-of-the-art X-ray Absorption Spectrometry (X-ray imaging and XANES) techniques can be used to non-destructively map and provide detailed information about S and Fe species in organic- and S-rich mudstones and (2) to improve our understanding of sulfurization and iron sulfide (e.g. FeS_2) formation processes during the deposition of these mudstones.

3.2 Materials and Methods

3.2.1 Sample Descriptions

For this study, samples were collected from three organic- and S-rich hydrocarbon source rocks/mudstones, the Kimmeridge Clay Formation, Monterey Formation and Whitby Mudstone Formation. The Kimmeridge Clay Formation sample was collected from the Blackstone band exposed at Clavell's Hard (Fig. 3.1), 1 km east of Kimmeridge Bay in Dorset, UK. The Blackstone band is a relatively homogeneous dark brown, exceptionally organic-rich, laminated, fissile mudstone comprising shelly materials and FeS_2 nodules with intermittent hard, thin carbonate-rich layers (Scotchman, 1987, 1989; Shaw & Primmer, 1991; Macquaker & Gawthorpe, 1993; Morgans-Bell et al., 2001) and bulk analyses indicates a high organic carbon (OC) and S content, 52 wt. % and 7 wt. %, respectively (Chapter 2, Table 2.1; Table 3.1). Py-GC-MS analysis showed a relative high amount of S containing compounds in the pyrolysate, as illustrated by a 2-methylthiophene to toluene ratio of 2 (Chapter 2, Table 2.6; Table 3.1), in line with preservation of OM (predominantly carbohydrates) through sulfurisation (van Kaam-Peters et al., 1998; van Dongen et al., 2006). In addition, previous analyses confirmed the presence of low amounts of FeS_2 and Fe (Chapter 2, Table 2.2 & 2.3; Table 3.1). The Monterey Formation sample was obtained from the repository of the United States Geological Survey, California, US and originated from the middle interval of the Monterey Formation exposed at El Capitán beach (Fig. 3.1), Santa Barbara county, California, US. It is a very organic-rich, biogenic, siliceous-phosphatic, calcareous and fossiliferous mudstone (Behl, 1999; Summons & Powell, 1987) and bulk analyses indicate an OC and S content that is substantially lower compared to the Kimmeridge Clay Formation sample; 14 wt. % and 2 wt. %, respectively (Chapter 2, Table 2.1; Table 3.1). Comparable to the sample from the Kimmeridge Clay Formation, the Monterey Formation sample is also characterised by a substantial amount of OSCs in the pyrolysate as indicated by a 2-methylthiophene to toluene ratio of 2.1, but there is an absence of FeS_2, although a few pyritised micro fossils were observed only low amounts Fe were measured (Chapter 2, Table 2.2, 2.3 & Table 2.1; Table 3.1). The final sample is from the Whitby Mudstone Formation and was collected from the Grey Shale Member exposed at Staithes in North Yorkshire, UK (Fig. 3.1). The Grey Shale Member is a pyritic, fossiliferous siltstone and mudstone with bands of carbonate and Fe carbonate cements/concretions (Powell, 1984; Pye & Krinsley, 1986) and bulk analyses indicated the lowest OC but highest S content of all three mudstones, 6 wt. % and 11 wt. %, respectively (Chapter 2, Table 2.1; Table 3.1). In contrast to the other two mudstones, this sample is characterised by a low contribution of OSCs in the pyrolysate as illustrated by a 2-

methylthiophene to toluene ratio of 0.4 but, the presence of a high amount of FeS_2 and Fe (Chapter 2, Table 2.2, 2.3 & Table 2.1; Table 3.1).

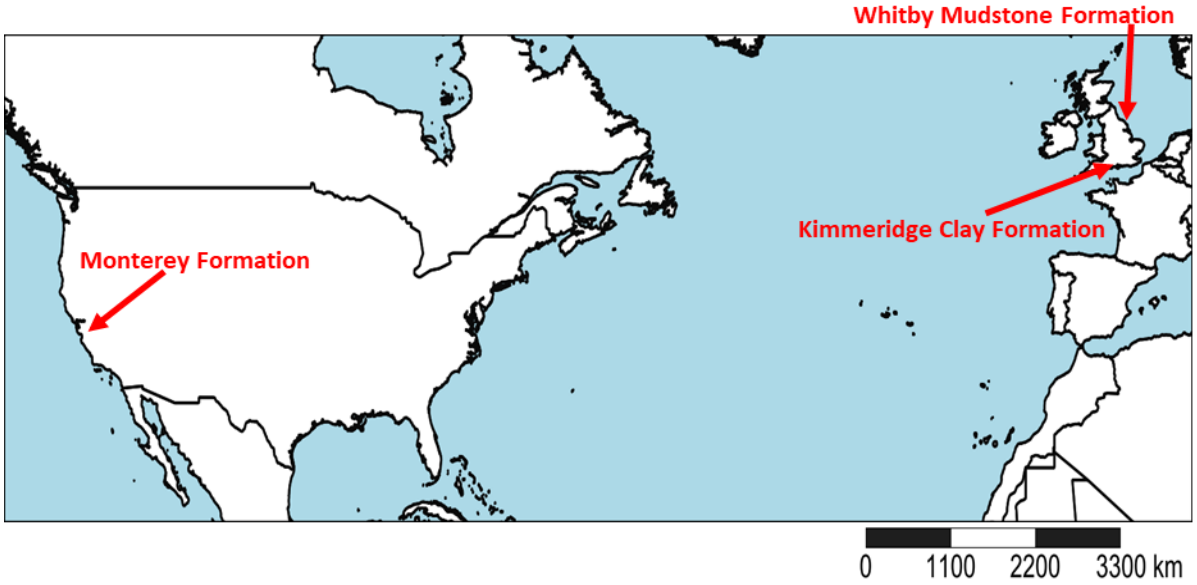

Figure 3.1: Map showing sample locations for the mudstones analysed in this study

Table 3.1: Age, location and geochemical data of mudstones from the Monterey, Kimmeridge Clay and Whitby Mudstone Formations analysed in present study.

Samples	Monterey Formation	Kimmeridge Clay Formation	Whitby Mudstone Formation
Geological Age[a]	Miocene	Jurassic	Jurassic
Location	El Capitán beach (USA)	Clavell's Hard (UK)	Staithes (UK)
Longitude Latitude	34º 27' 41" N 120º 1' 9" W	50º 36' 12" N 2º 7' 26" W	54º 33' 27" N 0º 46' 49" W
Organic Carbon (wt. %)[b]	13.5	52.0	6.1
Iron (wt. %)[b]	1.0	1.0	8.6
Calcium (wt. %)[b]	21.2	3.7	0.3
Phosphorous (wt. %)[b]	3.7	0.2	0.03
Sulfur (wt. %)[b]	2.0	6.7	10.7
2MT/T Ratio[b, c]	2.1	2.0	0.4
HI (mg HC/g TOC)[b],[d]	600.4	682.2	515.8
OI (mg HC/g TOC)[b],[d]	10.81	1.44	1.48
Tmax (ºC)[b],[d]	402	418	431

[a] as described in Powell, 1984; Behl, 1999 & Morgans-Bell et al., 2001; [b] see Chapter 2 for details; [c] 2-methylthiphene over toluene ratio (2M/T), calculated from Py-GC-MS analysis ; [d] calculated from Rock-Eval parameters (HI = hydrogen index; OI = oxygen index & Tmax = temperature at maximum kerogen yield; Tissot & Welte, 1984).

3.2.2 Sample Preparation

Rock samples were collected using a geological hammer and chisel. Samples were appropriately labelled in the field, orientations recorded, wrapped with aluminium foil, stored in designated sample bags and transported to the University of Manchester. All three samples were split and one half of each sample, labelled as (formation) archive hand specimen, was archived while the other half was trimmed to eliminate surficial contamination. The trimmed halves were further split in two using a rock cutting saw (cleaned with water and dichloromethane) and 20 μm thick polished thin sections perpendicular to bedding with clear epoxy impregnation were prepared from half of each trimmed sample while the other trimmed halves were used for analyses reported elsewhere (see Chapter 2). Thin sections were scanned with a Kodak esp® 1.2 scanner to provide high-resolution images (1200x1200 dpi). The formations archive hand specimens were photographed using a 12-megapixel camera with a quad-LED true tone flash with aperture widened to f/2.8.

3.2.3 X-ray Absorption Spectroscopy

3.2.3.1 Synchrotron Rapid Scanning X-ray Fluorescence (SRS-XRF)

SRS-XRF mapping for S was completed at wiggler beamline 6-2 of the Stanford Synchrotron Radiation Lightsource (SSRL), a subsidiary of the Stanford linear accelerator centre of the US national acceleratory laboratory in California. A detailed technical description of SRS-XRF is provided elsewhere (Edwards et al., 2018) but method and parameters employed are reported here. All experiments were performed in ambient conditions and initial analyses were done with hand specimens to ensure the excitation volume was entirely within the rock matrix for all elements. To improve spatial resolution prepared thin sections were also analysed/mapped. The hand specimens were mounted on an X-Y motorised stage 6.2 cm away from the pinhole and fixed at an incident angle 45º to the beam and the detector at a scattering angle 90º to the beam with a 70 mm air path. The hand specimens were scanned with an incident beam energy of 2.5 keV, a 0.1 mm diameter pinhole aperture, 0.1 mm step size, and 5 ms dwell time. Thin sections were mounted onto an X-Y motorised metal case and sealed within a polythene bag that was kept purged with a constant flow of helium to create a low density atmosphere to minimise the absorption of incident and fluoresced X-rays by air. The metal case was set at an incident angle 45º to the beam and the detector at a scattering angle 64º to the beam with a 15 mm air path. The thin sections were scanned with an incident beam energy of 2.56 keV, a 0.035 mm diameter pinhole aperture, 0.035 mm step size, and 5 ms dwell time. All map intensities were scaled from 0 to 250 counts. Fluoresced X-rays were detected using a single element

lithium drifted (Vortex) silicon detector. Data was processed and analysed using Sam Webb's Microprobe Analysis Toolkit (SMAK version 1.40; Webb, 2011) Software.

3.2.3.2 Micro-Focus X-Ray Fluorescence (MF-XRF)

MF-XRF mapping for S and Fe was performed at beamline I18 at Diamond Light Source (DLS), the UK's national synchrotron light source science facility in Oxfordshire. Thin sections were mounted onto a motorised stage and sealed within a polythene bag that is kept purged with a constant flow of helium to create a low-density atmosphere to minimise the absorption of incident and fluoresced X-rays by air. Thin sections were scanned with an incident beam energy of 8 keV, 0.01 mm X and Y step sizes, 0.05 s per pixel to acquire small-scale elemental maps for S and Fe at 10 micron (μm) resolution. Fluoresced X-rays were detected by a combination of a double-crystal Si(111) monochromator, Kirkpatrick–Baez mirrors and a four element Vortex silicon drift detector. S and Fe maps were processed using the ROI imaging tool in PyMCA X-ray Fluorescence Toolkit (version 5.5.3; Solé et al., 2007) and DAWN (version 2.18; Basham et al., 2015) by defining the X-ray emission energy of an element in the recorded energy dispersive X-ray spectra.

3.2.3.3 X-Ray Absorption Near Edge Structure (XANES)

S K-edge XANES and Fe K-edge XANES analyses were carried out at SSRL beamline 6-2 and DLS beamline I18, respectively. Thin sections were prepared directly from the samples. S and Fe standards [elemental S, pyrite S, cysteine, disulfide (oxidised glutathione), benzothiazole, methionine sulfoxide, pyrite Fe] were prepared by smearing the standards onto glass slides with ethanol. Sections/slides were placed on a motorised stage sealed within a polythene bag that was kept purged with a constant flow of helium, to create a low density atmosphere to minimise the absorption of incident and fluoresced X-rays by air. Photo-oxidation by the X-ray beam was minimised by employing a defocused beam, rapid scan speeds and by changing the area analysed by slightly moving the beam between scans. Fe K-edge XANES data was acquired in fluorescence mode using a defocussed beam with slit apertures of 50 μm (horizontal) and 500 μm (vertical) and a four element Si drift Vortex fluorescence detector set at scattering angle of 90º. S K-edge XANES was acquired in fluorescence mode using a single element Vortex silicon drift detector set at a scattering angle ~ 60º. S XANES data averaging was done using Sam Webb's SIXPack software package (version 1.40; Webb, 2005). All other XANES spectral analysis (background subtractions and normalisations) and linear combination fitting was accomplished using the Athena application, a component of the Demeter suite of XAS analytical tools (Ravel & Newville, 2005).

3.3 Results and Discussion

3.3.1 Synchrotron Rapid Scanning–X-Ray Fluorescence and (Sulfur) X-ray Absorption Near Edge Structure analysis

3.3.1.1 Monterey and Kimmeridge Clay Formations Hand Specimens

The Monterey Formation hand specimen (Monterey HS; Fig. 3.2a) is dark brown (mostly OM and some silicate minerals as confirmed by petrography and XRD analyses; see Chapter 2, Fig. 2.2c & d; Table 2.2) with numerous intercalations of ivory white bands ranging from a few microns to 5 mm in diameter and discrete (up to 1 cm in Ø) patches of biologically-derived marine origin as confirmed by petrography and XRD analyses (see Chapter 2, Fig. 2.2c & d; Table 2.2). The dark brown and ivory white layers will henceforth be referred to as dark and light layers. SRS-XRF imaging of the Monterey HS shows the presence of S across the whole scanned section with the highest relative concentrations in the dark, silicate rich, layers (Fig. 3.2b). In contrast, most of the light bands and patches were confirmed to contain relative high amounts of phosphorus (P; Fig. 3.2c) or Chorine (Cl; Fig. 3.2d).

S K-edge XANES imaging of a selected area of the Monterey HS (square outlined in white in Fig. 3.2a) indicates that S oxidation states can be resolved. Forty-two XANES spectra were obtained at different spots within the region of interest and these were averaged and show the presence of different forms of S with maxima at 2472.1 eV, 2473.8 eV and 2482.0 eV (Fig. 3.3). Comparison with spectra of selected standards indicate this is consistent with the presence of benzothiazole, methionine sulfoxide and sulfate, respectively (Fig. 3.3). Linear combination fitting (LCF) of the averaged spectra against a range of selected standards (7 S standards) reveals on average 61 % of S in the scanned area is organically bound, for example, in the benzothiazole and methionine sulfoxide form (Table 3.2). These organic S forms, together with total sulfur and sulfate can be spatially resolved (chemically mapped) across the region of interest at their specific energies (Fig. 3.4). The chemical maps obtained indicate however that the concentration of the sulfate type S (Fig. 3.4b) may be locally predominant when compared to the intermediate (organic) forms of S (Fig. 3.4c & d), particularly in regions forming what appear to be dewatering structures. It is likely that these structures were planes of weakness in Monterey HS along which sulfate-rich overlying sea water were introduced. The absence of dewatering structures in the maps for organic forms of S (Fig. 3.4c & d) suggest that sulfate was possibly introduced after the organic S forms were already present. The diagenetic history of the Monterey Formation is characterised by a series of chemical reactions including sulfide oxidation and sulfate reduction (Macquaker et al., 2014; Hancock et al., 2019; Nelson et al.,

2019), which could have contributed to the sulfate type S that dominated the dewatering structures.

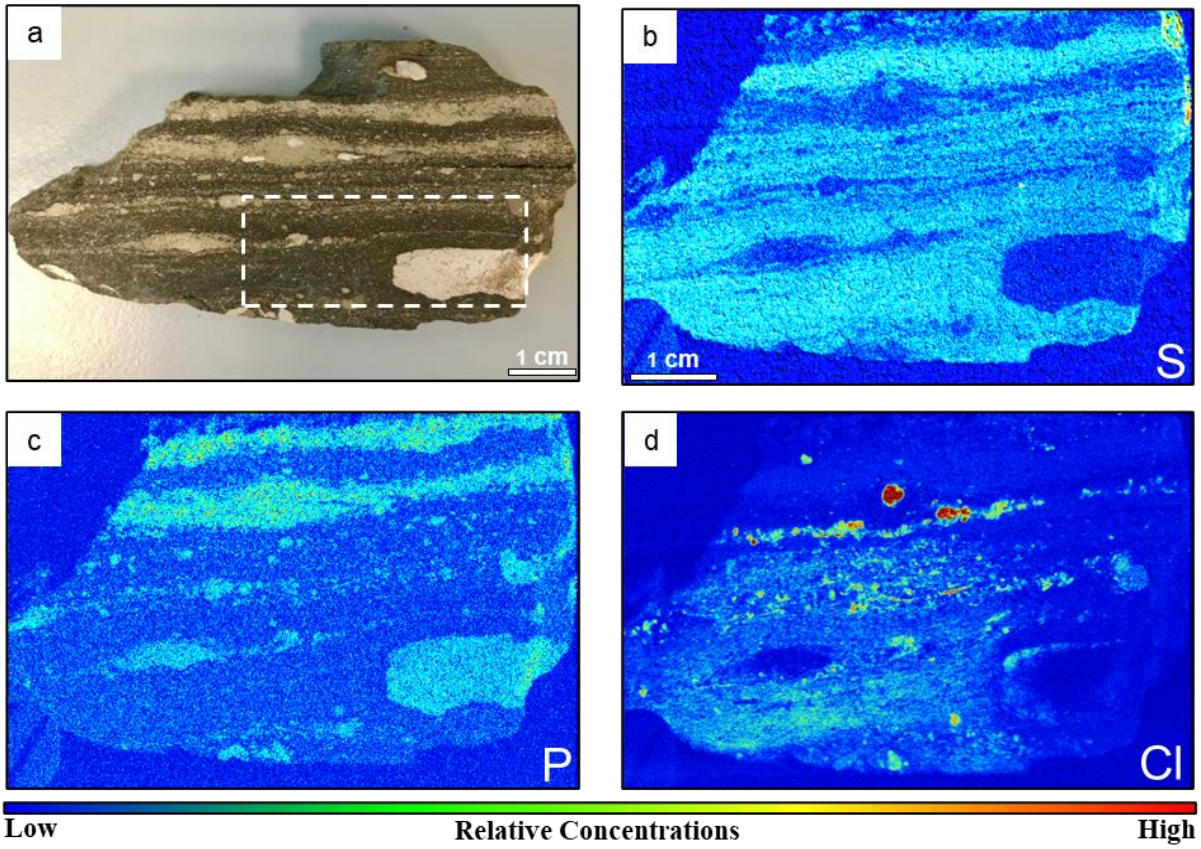

Figure 3.2: Optical image (a) with area outlined in white selected for detailed S K-edge XANES and SRS-XRF analyses as presented in Fig. 3.3 and 3.4, respectively and X-ray fluorescence images of the Monterey Formation hand specimen (9 x 5 cm) showing (b-d) spatially-resolved maps of total sulfur, phosphorus and chlorine obtained at a single incident beam energy of 2500 eV.

The Kimmeridge Clay Formation (Blackstone band) hand specimen (Kimmeridge HS; Fig 3.5a) is, in contrast to Monterey HS, homogeneously black (predominantly OM and some silicate) with tiny lenses of carbonate materials as confirmed by petrography and XRD analyses (see Chapter 2, Fig. 2.2a & b, Table 2.2). SRS-XRF imaging of a selected area (square outlined in white in Fig. 3.5a) indicates a relatively uniform distribution of S across the whole area with only few lenses lean in S (Fig. 3.5b). S K-edge XANES (66 spectra averaged) of the Kimmeridge HS compared with the spectra of selected S standards reveals the presence of elemental S and pyrite S as well as methionine sulfoxide, benzothiazole and sulfate type S (Table 3.2; Fig. 3.3), comparable to what was observed in Monterey HS. However, in contrast to the Monterey HS analyses, the presence of cysteine (amino acid with a thiol side chain) and disulfide (oxidised glutathione) type S (Fig. 3.3). LCF indicates the dominance of organic forms of S (methionine sulfoxide, cysteine, disulfide and benzothiazole), with a combined percentage of 56 %, implying that 50 % of the S in the Kimmeridge HS is organically bound

(Table 3.2). Also present are substantial contributions of elemental S (28 %) and pyrite S (14%) but only a minor contribution of sulfate type of S (3 %). The latter indicates that the Blackstone band, in line with previous analyses (Sinninghe Damsté et al., 1998; van Kaam-Peters et al., 1998; van Dongen et al., 2006), was deposited under prevailing anoxic conditions when sulfate reduction was high, allowing the reduced S to bind to OM leading to the preservation of unusually high amounts of OM through sulfurization.

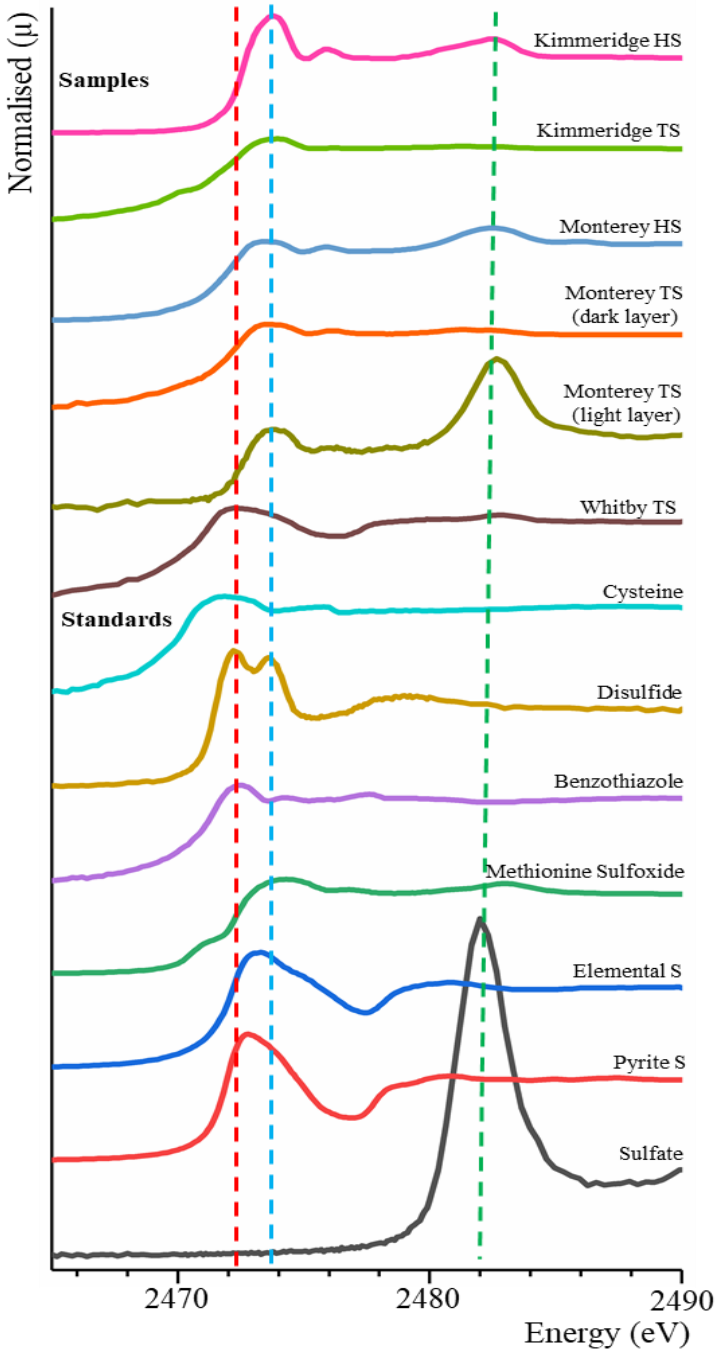

Figure 3.3: S K-edge XANES spectra of hand specimens (HS) and thin sections (TS) of the Monterey, Kimmeridge Clay and Whitby Mudstone Formation together with selected sulfur standards (elemental S, pyrite S, cysteine, disulfide, benzothiazole, methionine sulfoxide and sulfate). The vertical dashed red, blue and green lines represent absorption spectrum maxima for reduced S, intermediate S species and sulfate respectively.

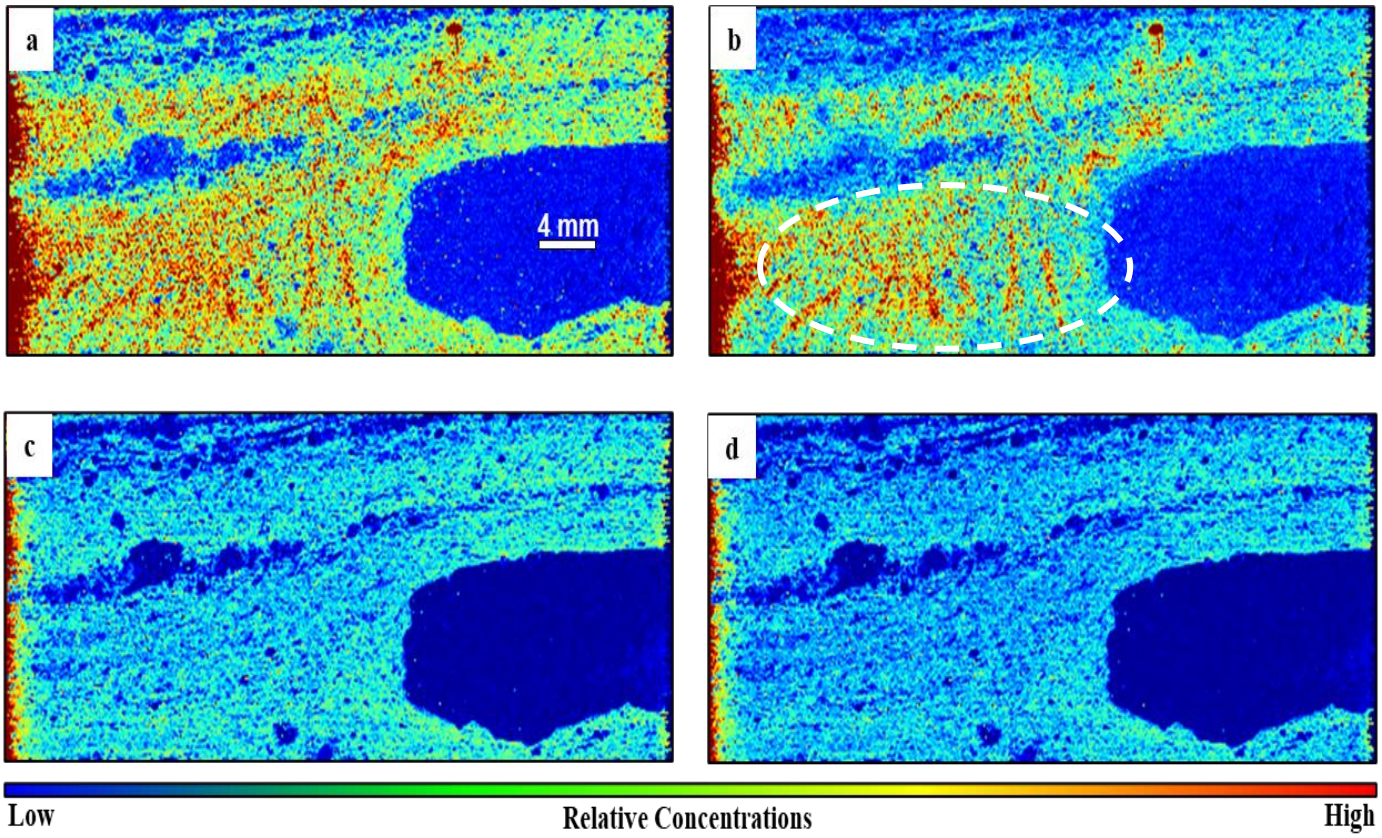

Figure 3.4: X-ray fluorescence images of the area outlined in white in figure 3.2a of the Monterey Formation hand specimen (9 x 5 cm) showing different sulfur oxidation states; (a) total sulfur (b) sulfate (c) methionine sulfoxide and (d) benzothiazole obtained at energies 2500.0 eV, 2482.0 eV, 2473.8 eV and 2472.1 eV, respectively. White dashed circle in (b) indicate possible dewatering structures.

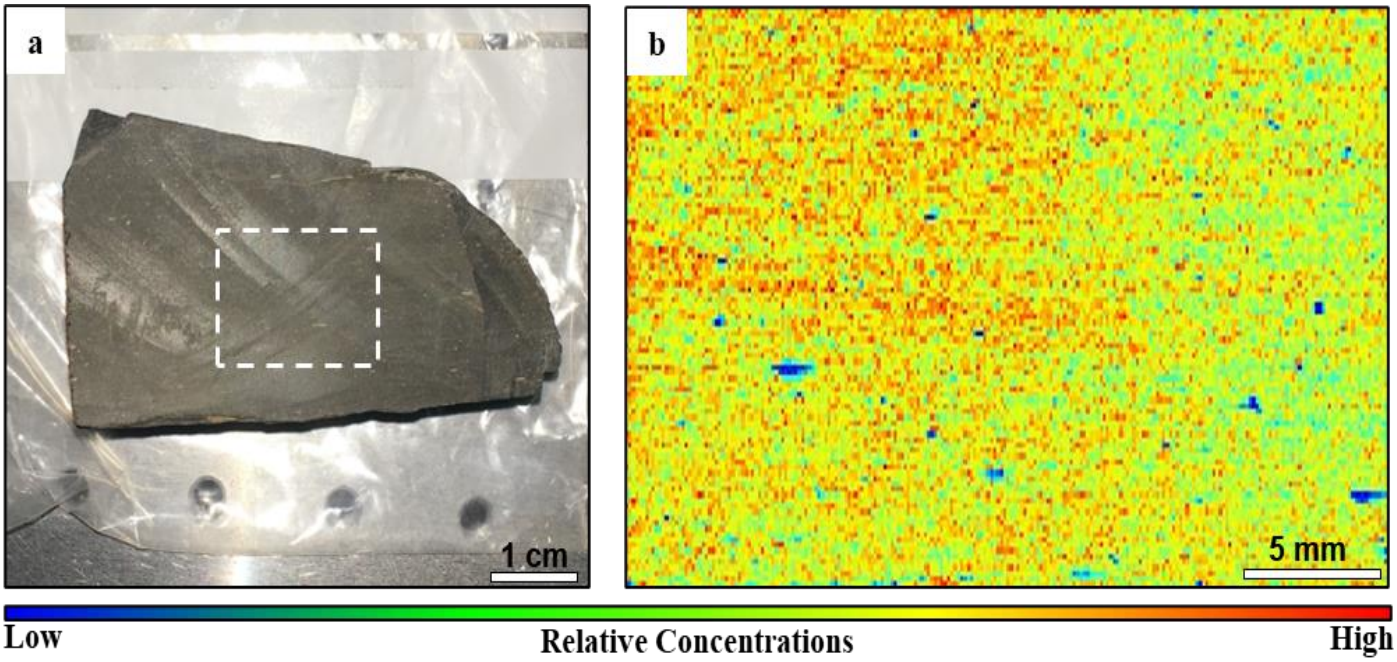

Figure 3.5: (a) Optical image of the Kimmeridge Clay Formation (Blackstone band) hand specimen (6 x 4 cm) and (b) X-ray fluorescence image of the area outlined in white in panel 'a' showing a map of total sulfur obtained at a single incident beam energy of 2500 eV.

Table 3.2: Linear combination fitting (LCF) for Kimmeridge Clay, Monterey and Whitby Mudstone Formations against selected S standards. Weights are in percentage; HS = Hand specimen; TS = Thin section; n.d. = Not detected.

	Standards	Kimmeridge HS	Kimmeridge TS	Monterey HS	Monterey TS		Whitby TS
					Dark (Si) Region	Light (P) Region	
1	Elemental S	28	6.0	21	10	n.d.	43
2	Pyrite S	14	<1.0	13	<1.0	n.d.	25
3	Cysteine	<1.0	3.0	n.d.	2.0	1.0	n.d.
4	Disulfide	5.0	<1.0	n.d.	n.d.	n.d.	2.0
5	Benzothiazole	6.0	61	22	42	3.0	3.0
6	Methionine Sulfoxide	44	29	39	44	25	n.d.
7	Sulfate	3.0	1.0	5.0	1.0	71	27

Combined these results indicate that SRS-XRF imaging and S K-edge XANES analyses of organic- and sulfur-rich mudstones at low spatial resolution (cm scale) are feasible. Specifically, the data reveals a dominance of organic S compared to the other S species as well as a low contribution of sulfate type S in both samples analysed. However, for conclusion to be drawn on to the conditions during the time of deposition there is a need to study these mudstones at a higher resolution (at the µm - mm scale) using thin sections prepared from these mudstones (see below).

3.3.1.2 Thin Section Analyses

Detailed, high resolution (µm - mm scale) SRS-XRF chemical mapping of S, Si and P and S were conducted on thin sections prepared from the Kimmeridge Clay (Kimmeridge TS), Monterey (Monterey TS) and Whitby Mudstone (Whitby TS) Formations (Fig. 3.6). SRS-XRF chemical maps of the Kimmeridge TS reveal a widespread S distribution throughout Kimmeridge TS with lower signals within discrete lenses (Fig 3.6d), in line with the analysis of the Kimmeridge HS, together with a uniform presence of silicate throughout the whole section and the presence or relative low amount of P (Fig. 3.6m & p). From the chemical maps, there appears to be a correlation between Si and S as S tends to concentrate more in the Si-rich layers. The detailed S K-edge maps to determine species distribution of the S indicate that organic S (Org. S; 2473.9 eV) is abundant across the Kimmeridge TS while sulfate (2482.6 eV) is relatively low (Fig. 3.6g & h). S K-edge XANES analysis (average of 17 spectra) of the Kimmeridge TS using LCF indicates a dominance of benzothiazole S (up to 61 %) over methionine sulfoxide S (29 %) and less of disulfide S (< 1 %; oxidised glutathione) compared to Kimmeridge HS. There was a minor contribution from elemental S, cysteine S and pyrite S

with 6 %, 3 % and < 1 % by weight, respectively (Fig. 3.3, Table 3.2). The abundance of organic S compounds is in line with the analyses of the Kimmeridge HS and supports that OM in the Kimmeridge Clay Formation is primarily preserved through sulfurisation (van Kaam-Peters et al., 1998; van Dongen et al., 2006).

The SRS-XRF chemical maps of the Monterey TS reveal a distinct S pattern across the section, with relatively high concentrations in the dark layers and lower concentrations in the light layers as shown in the optical (scanned) image, in line with what was observed in the Monterey HS (Fig. 3.6b & e). The S K-edge chemical maps of the Monterey TS show that much of S is in the organic S (Org. S; 2473.9 eV) form as shown by the strong signal compared to the sulfate type S (sulfate: 2482.6 eV; Fig. 3.6i & j). As mentioned previously this likely indicates that sulfate reduction was not significant at certain periods in time. Si and P mapping indicate that the majority of Si is concentrated in the darker layers while P dominates the light layers (Fig. 3.6n & q cf. to Fig. 3.6b). In line with these, an average S K-edge XANES spectrum obtained from the light P rich layers and matched against selected S standards (LCF analysis) indicates a dominance of sulfate (71 %), substantial amounts of methionine sulfoxide type S (25 %) and the minor presence of benzothiazole (3 %; Fig. 3.3, Table 3.2). In contrast, the average spectrum of the dark Si-rich layers has relatively low amounts of sulfate (1 %) but, is abundant in the organic species of S such as methionine sulfoxide (44 %), benzothiazole (42 %) and cysteine (2 %) along with elemental S (10 %; Fig. 3.3, Table 3.2). Interestingly, the S maps of organic and sulfate type S indicate comparable distribution patterns with organic S being mainly concentrated in the dark Si-rich layers, while sulfate dominates the light P-rich layers (Fig. 3.6i, j, n & q). Combined, this indicates that preservation through sulfurisation did play a role in the Monterey Formation albeit not as continuously as in the Kimmeridge Clay Formation.

The SRS-XRF chemical maps of the Whitby TS reveal an abundance of total S (Fig. 3.6f), the presence of Si in layers and the complete absence of P (Fig. 3.6o & r). Here, S K-edge chemical maps acquired at 2473.9 eV (reduced S) and 2482.6 eV (sulfate) reveal high concentrations of reduced S and the presence of a relatively lower sulfate signal (Fig. 3.6k & 3.6l). The S K-edge XANES (average of 13 spectra) confirms the higher levels of reduced S species and the results, matched against selected S standards (LCF analysis), indicate a dominance of elemental S (43 %), pyrite S (25 %) and sulfate type S (27 %). Only a minor contribution of organic S in the form of benzothiazole S (3 % wt) and disulfide S (2 %) could be detected. It is worth noting that organic S and reduced inorganic S may exhibit spectral overlap when mapped at 2473.9

eV, however, in the case of the Whitby Mudstone Formation, XANES analysis confirmed S is predominantly non-organically bound while in the Kimmeridge Clay and the Monterey Formations S is predominantly organically bound. These findings are in line with previous analyses, indicating that the Whitby Mudstone Formation is lean in organic S (see Chapter 2, Table 2.6; Bowden et al., 2006).

Combined these results indicate that SRS-XRF chemical mapping and S K-edge XANES analyses at high resolution (µm - mm scale) are feasible. The outcomes of these analyses support the importance of sulfurisation as a pathway to preservation of OM in the Kimmeridge Clay and Monterey Formations but this process may be rather insignificant in the Whitby Mudstone Formation. As previously discussed, iron sulfide formation, primarily FeS_2, is suggested to be a competitor to the sulfurisation processes. Therefore, there is a need to map Fe, which largely controls this process, as well as elements such as Ca and P which can buffer chemical reactions during diagenesis. To further this work, Micro-Focus X-ray imaging and Fe K-edge XANES were completed on these key mudstone samples.

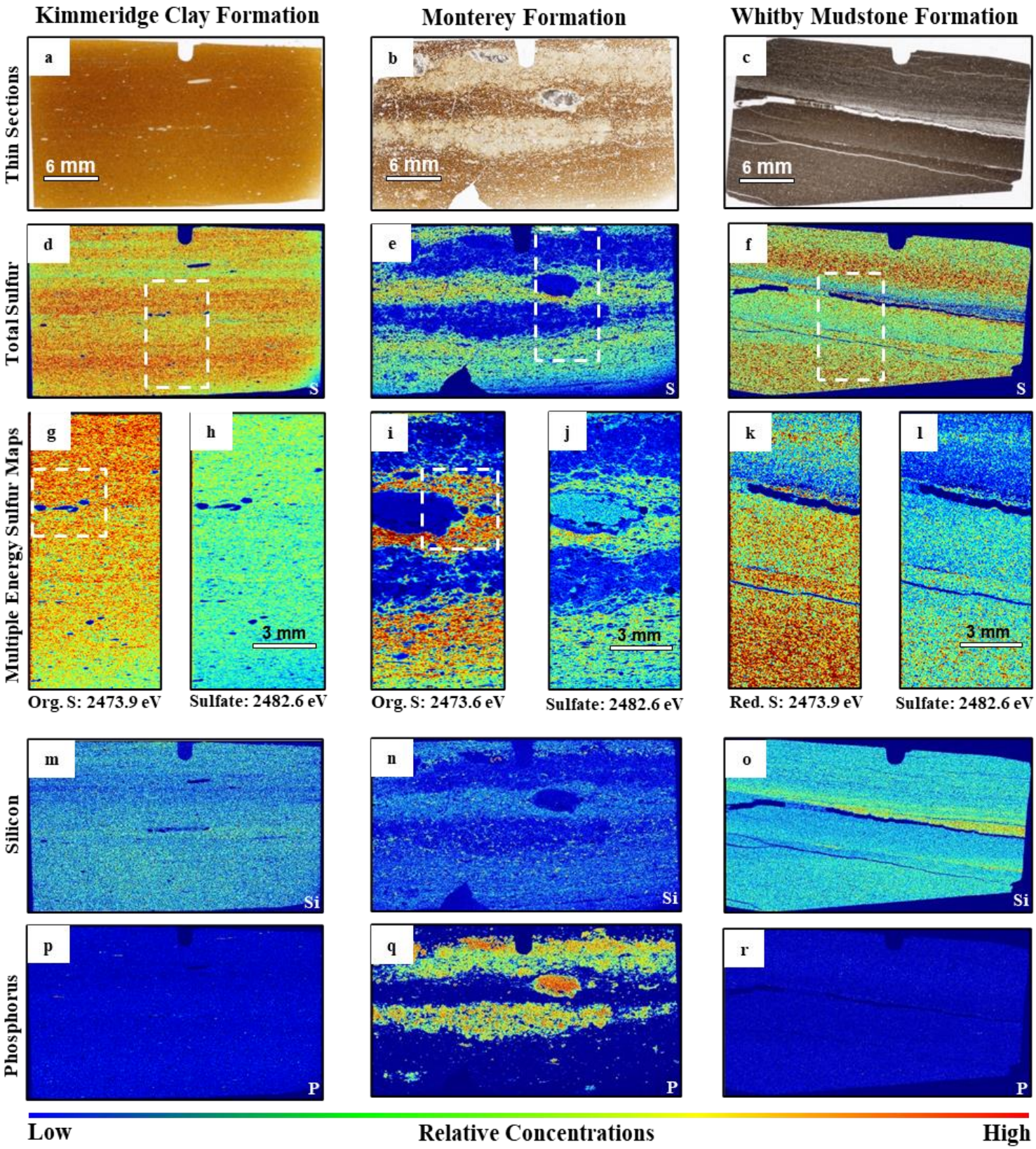

Figure 3.6: (a-c) Scanned images and (d-f) Single energy X-ray images of Kimmeridge Clay, Monterey and Whitby Mudstone Formations showing total S maps obtained at 2500 eV. (g-l; areas outlined in white in d-f) showing S K-edge images of organic S (Org. S) for the Kimmeridge Clay and Monterey Formations and reduced S (Red. S) for Whitby Mudstone Formations and sulfate obtained at 2473.9 and 2482.6 eV, respectively. (m-o) and (p-r) Single energy X-ray images showing spatially-resolved maps of Si and P in the Kimmeridge Clay, Monterey and Whitby Mudstone Formations acquired with a single incident beam energy of 2500 eV, respectively.

3.3.2 Micro-focus X-ray Fluorescence (MF-XRF) and Fe K-edge X-ray Absorption Near Edge Structure (XANES)

MF-XRF imaging completed on the areas marked in white squares with an incident beam energy of 8000 eV in figure 3.6g, i and the whole of figure 3.6k reveal the spatial distribution of Fe with respect to S and the presence of Ca and/or P (Fig. 3.7). Results indicate a relative high S signal across the whole scanned area in the Kimmeridge TS, supporting the SRS-XRF analysis (Fig. 3.7ai). A relatively low Fe signal can be detected, discretely dispersed across the whole section analysed, with substantial amounts of Ca concentrating in defined (Fig. 3.7aii - aiii). This is in line with previous elemental XRF and CHNS analyses presented in Table 3.1. By overlaying the S, Fe and Ca maps (Fig. 3.7aiv), it can be seen that Ca does not appear to correlate with S or Fe and Fe is only partly correlated to S and does not correlate in those areas indicated in red in Fig. 3.7aiv. Fe K-edge XANES were collected at 3 points as marked on the combined map (Kimmeridge TS1 - TS3; Fig. 3.7aiv). Kimmeridge TS1 and TS3 are points where S and Fe correlated, while Kimmeridge TS2 is an Fe-rich only point. Fe K-edge XANES show that Kimmeridge TS1 is a form of reduced Fe with reduced S coordination well-matched to the FeS_2 standard analysed (Fig. 3.8). In contrast Kimmeridge TS3, although correlated with S, does not show a good fit with FeS_2 and is more likely an oxidised Fe specie (Fig. 3.8). The Kimmeridge TS2 spectrum to some extant matches the siderite ($FeCO_3$) standard (Fig. 3.8) but could also be considered to be Fe substituted into calcite ($CaCO_3$) due to the presence of high concentrations of Ca at this location.

The MF-XRF chemical maps of the Monterey TS show high amounts of S and Ca and/or P across the whole section in line with SRS-XRF analysis but a relatively low Fe contribution and only a few localised discrete Fe areas could be observed at the top of the section (Fig. 3.7bi - biii). This is in line with previous work using elemental XRF and CHNS analyses presented in Table 3.1. An overlay of the maps for Fe, S and Ca and/or P indicates that S and Ca/P are largely uncorrelated and unlike the Kimmeridge TS, Fe is largely uncorrelated with S except for few bright spots at the top of the section (Fig. 3.7biv). Fe K-edge XANES collected at points on the combined map indicate that Monterey TS2 matches well to the FeS_2 standard analysed (Fig. 3.8). This is in line with previous petrography and ESEM-EDX analyses that reveal Monterey TS2 is a pyritised microfossil (coccolith; see Chapter 2, Fig. 2.2c & d). The other two Fe K-edge XANES, TS1 and TS3, do not fit the FeS_2 and indicate the presence of oxidised Fe.

In contrast to both the Kimmeridge TS and Monterey TS, MF-XRF elemental maps of the Whitby TS show that both S and Fe are presence in relatively high abundances and widespread across the scanned area (Fig. 3.7ci - cii). Ca on the other hand is only presence in relatively low abundances and concentrated within fracture zones (Fig. 3.7ciii), supporting previous work using elemental XRF and CHNS analyses (Table 3.1). An overlay of the S, Fe and Ca maps indicates that Fe is strongly correlated with S across the whole map with a few Ca-rich lenses and a few discretely dispersed non S correlated Fe-rich spots (Fig. 3.7civ). Fe K-edge XANES collected at points on the combined map (Whitby TS1 to TS3) indicate that Whitby TS2 and TS3 agree well with the $FeCO_3$ and FeS_2 standards, respectively, while Whitby TS1, although spatially correlated with S, is likely to be a species of oxidised Fe (Fig. 3.8). The widespread correlation of S and Fe observed in Whitby TS (yellow colours in Fig. 3.7civ) is in agreement with previous studies that show the Whitby Mudstone Formation contain substantial amounts of iron sulfides (see Chapter 2, Fig. 2.2e & f).

Combined, these results indicate that MF-XRF and Fe K-edge XANES of these types of mudstones are feasible and the outcomes support the SRS-XRF analyses. The data indicates that Fe is abundant in the Whitby Mudstone Formation and most of it is bound to (or correlated with) S. In contrast, the presence of Fe in the other mudstones is much lower but what is there is either, comparable to the Whitby Mudstone Formation, largely bound to S (the Kimmeridge Clay Formation) or does not show a correlation with S (the Monterey Formation).

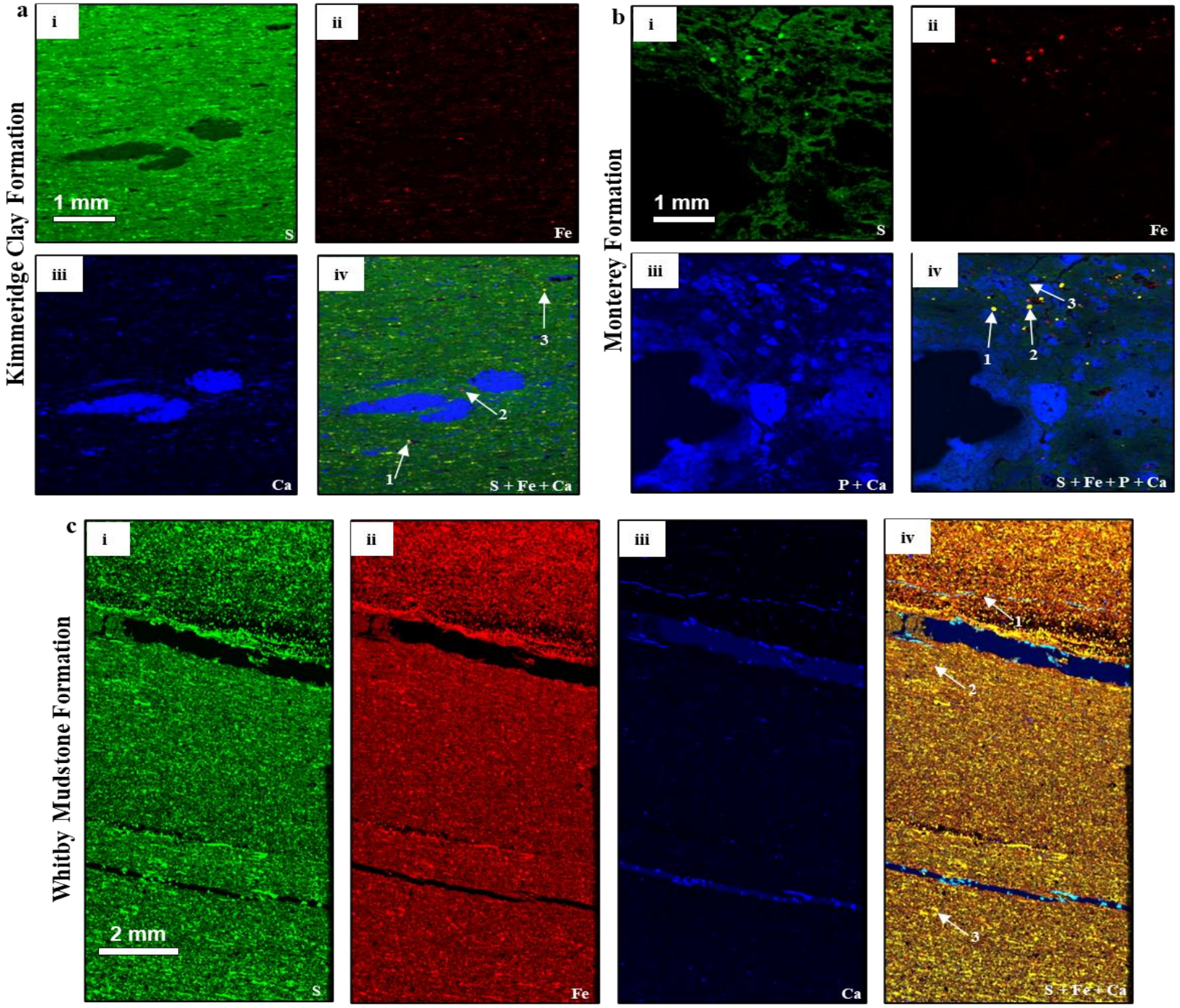

Figure 3.7: Micro-Focus spatially resolved X-ray images of the Kimmeridge Clay, Monterey and Whitby Mudstone Formations (areas marked in white squares in figure 3.6g and i and the whole of figure 3.6k) obtained at 8000 eV showing (ai, bi & ci) total S, (aii, bii & cii) total Fe, (aiii, biii & ciii) total Ca/P and (aiv, biv & civ) combined total S, Fe and Ca/P maps. The coloration in the combined maps refer to: yellow = S correlated to Fe, green = S, red = Fe and Ca and/or P = blue). Arrowed numbers on the map correlate to the Fe K-edge XANES spectra of the different mudstones as presented in figure 3.8.

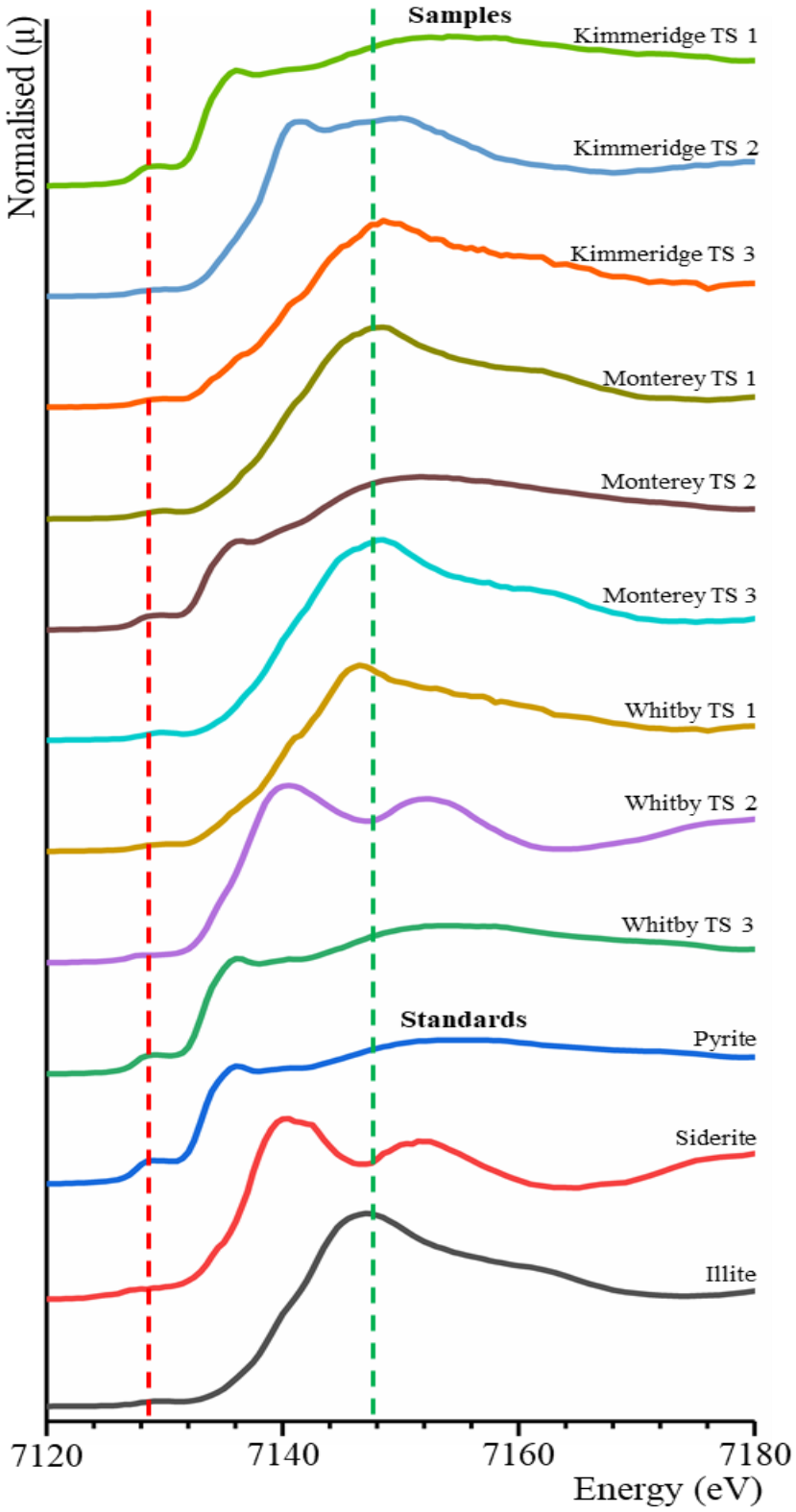

Figure 3.8: Fe K-edge XANES spectra for the thin section of the Kimmeridge Clay, Monterey and Whitby Mudstone Formations and selected Fe standards (pyrite Fe, siderite, and illite). The vertical dashed red and green lines represent absorption spectrum maxima for reduced Fe, and oxidised respectively.

3.3.3 Implications for Environmental Conditions During the Time of Deposition of the Analysed Mudstones

van Dongen et al. (2006) previously proposed that, based on a combination of bulk and molecular analyses, the Blackstone Band of the Kimmeridge Clay Formation was deposited when the environmental conditions were such that euxinic conditions extend into the photic zone of the water column, resulting in photic zone euxinia. The oxygen exposure time of the settling OM under these conditions is minimal leading to a substantial fraction of the labile OM (carbohydrates) reaching the ocean floor and being preserved through sulfurisation. However, based on these analyses occasional short-lived oxygenation could not be excluded. These potential seasonal oxygenation events would increase the time that the sinking OM in the water column was exposed to oxygen and would reduce the relative amounts of preserved OM (carbohydrates) substantially. In our work, XRF imaging at high resolution (µm to mm scale) and S K-edge XANES of the Kimmeridge Clay formation indicate a uniform presence of sulfurized OM throughout the whole section as, for instance can be seen in Fig.'s 3.6d and 3.6g. A uniform distribution excludes the possibility of short-lived oxygenation events and supports the presence of constant stable euxinic conditions in the water column over a relatively long period of time (Ma), at least during the deposition of the Blackstone band, corroborating previous studies (van Kaam-Peters et al., 1998; Tyson, 2004; van Dongen et al., 2006; Gallois et al., 2019). In addition, information from MF-XRF and Fe K-edge XANES further indicates a relative low influx of reactive Fe, which would be a sink for reduced inorganic S in the Blackstone Band section (Fig. 3.7aii). Therefore, there was likely an excess of reduced inorganic S available, leading to the preservation of S-rich kerogen at all times.

The analyses of the Monterey Formation showed the presence of dark Si layers rich in organic S intercalating with light P layers lean in organic S (Fig. 3.6e, i & j) indicating that the euxinic conditions that leads to sulfide availability and the subsequent preservation of OM through sulfurisation did not persist for long periods of time. In fact, the presence of the light P layers lean in organic S confirm that there were periods in time when (sub)oxic conditions dominated the water column leading to profuse biological production as characterised by the abundance of apatite cements (Macquaker et al., 2014). This indicate that even at high resolution (µ - mm scales) preservation through sulfurization was not continuous in the Monterey Formation and there were sharp transitions between (sub)oxic and anoxic/euxinic conditions during the time of deposition in line with recent analyses of sections of the Monterey Formation (Hancock et al., 2019). Analyses also show that the presence of reactive Fe is low in the Monterey

Formation (Fig. 3.7bii) indicating that the lack of OM accumulation through sulfurisation in the Monterey Formation was not due to the presence of Fe but rather the occasional remineralisation of OM during peak ocean oxygenation episodes. To summarise, preservation through sulfurisation played an important role in the preservation of OM in the Monterey Formation (Isaacs et al., 2019; Jarvie & Lundell, 2001; Macquaker et al., 2014; Wilson L. Orr, 1986), again leading to the preservation of S-rich kerogen, but it was a more discontinuous process compared to the formation of the Kimmeridge Blackstone Band.

The Whitby Mudstone Formation was reported to have been deposited during persistent oxic conditions (Ghadeer & Macquaker, 2011), but when analysed at high resolution (µm - mm scales), abundance of reduced S was observed throughout the whole section (Fig. 3.6k), indicating there was a period in time when anoxic/euxinic conditions prevailed. However, in contrast to the Kimmeridge and Monterey Formations, much of the available reduced S during this euxinic period preferentially reacted with reactive Fe to form iron sulfides (e.g. FeS_2: Fig. 3.7civ) and only limited amounts of reduced S was available to react with OM. This indicates that preservation of OM through sulfurisation was not a significant process in the diagenetic history of the Whitby Mudstone Formation. Indeed previous studies reported the abundance of FeS_2 and low OM contents (Pye & Krinsley, 1986; Sælen et al., 2000; Houben et al., 2016) and our analyses confirm these earlier observations.

Collectively, these results indicate that synchrotron-based techniques (X-ray imaging and XANES) can be used to study elemental composition (e.g. S, Fe, Si, Ca, P), their various species (oxidation states) and the relative spatial abundance of the species in the mudstones analysed. This improves our understanding of preservation through sulfurisation and iron sulfide formation (e.g. FeS_2) during the time of mudstone deposition at high resolution (µm - mm scales) not previously analysed. Therefore, these techniques are a new set of tools to study mudstones and sediments from other depositional settings to decipher and spatially resolve (map) elemental/chemical inventories in them to reconstruct their palaeo-environmental depositional conditions.

3.4 Conclusion

Analyses of organic- and sulfur-rich mudstones from the Kimmeridge Clay, Monterey and Whitby Mudstone Formations using novel state-of-the-art synchrotron-based techniques (XRF imaging and X-ray absorption near edge structure analysis) indicate for the first time that these techniques can be used to non-destructively map and provide detailed information about S and

Fe species in these mudstones. Detailed analyses at high resolution (µm to mm scale) indicate that S-rich OM in the Kimmeridge Clay Formation is widespread, in line with the presence of stable euxinic conditions in the water column over a relatively long period of time and a relatively low influx of reactive Fe, promoting the preservation of substantial amounts of OM through sulfurisation. In contrast, analyses indicate that the presence of sulfurized OM was transitional in the Monterey Formation, in line with fluctuating redox conditions in the water column over time, likely due to profuse biological production. Finally, sulfurisation was insignificant in the Whitby Mudstone formation, likely due to the abundance of reactive Fe outcompeting the formation of sulfurised OM.

Acknowledgement

The Petroleum Technology Development Fund (Nigeria) is thanked for funding YA (16PhD153), Diamond Lightsource (DLS, UK) for beamtime award (SP22220). We gratefully thank Nick Edwards (Stanford Synchrotron Radiation Lightsource) and Tina Geraki (DLS) for help with XAS data collection, Fred Mosselmans (DLS) for the providing pyrite and siderite data and Caroline Slomp and Thilo Behrends for providing the illite data (both presented in figure 3.8).

Reference

Amrani, A. (2014). Organosulfur Compounds: Molecular and Isotopic Evolution from Biota to Oil and Gas. *Annual Review of Earth and Planetary Sciences*, *42*(1), 733–768. https://doi.org/10.1146/annurev-earth-050212-124126

Amrani, A., Sessions, A. L., & Adkins, J. F. (2009). Compound specific $\delta^{34}S$ analysis of volatile organics by coupled GC multicollector ICPMS. *Analytical Chemistry*, *81*(21), 9027–9034. https://doi.org/10.1021/ac9016538

Anné, J., Edwards, N. P., Brigidi, F., Gueriau, P., Harvey, V. L., Geraki, K., Slimak, L., Buckley, M., & Wogelius, R. A. (2019). Advances in bone preservation: Identifying possible collagen preservation using sulfur speciation mapping. *Palaeogeography, Palaeoclimatology, Palaeoecology*, *520*, 181–187.

Balistrieri, L. S., Murray, J. W., & Paul, B. (1992). The cycling of iron and manganese in the water column of Lake Sammamish, Washington. *Limnology and Oceanography*, *37*(3), 510–528. https://doi.org/10.4319/lo.1992.37.3.0510

Barden, H. E., Bergmann, U., Edwards, N. P., Egerton, V. M., Manning, P. L., Perry, S., van Veelen, A., Wogelius, R. A., & van Dongen, B. E. (2015). Bacteria or melanosomes? A geochemical analysis of micro-bodies on a tadpole from the Oligocene Enspel Formation of Germany. *Palaeobiodiversity and Palaeoenvironments*, *95*(1), 33–45. https://doi.org/10.1007/s12549-014-0177-5

Basham, M., Filik, J., Wharmby, M. T., Chang, P. C. Y., El Kassaby, B., Gerring, M., Aishima, J., Levik, K., Pulford, B. C. A., Sikharulidze, I., Sneddon, D., Webber, M., Dhesi, S. S., Maccherozzi, F., Svensson, O., Brockhauser, S., Náray, G., & Ashton, A. W. (2015). Data Analysis WorkbeNch (DAWN). *Journal of Synchrotron Radiation*, *22*(3), 853–858. https://doi.org/10.1107/S1600577515002283

Behl, R. J. (1999). Since Bramlette (1946): The Miocene Monterey Formation of California revisited. *Geological Society of America Special Papers*, *338*(1946), 301–313. https://doi.org/10.1130/0-8137-2338-8.301

Berner, R. A. (1984). Sedimentary pyrite formation: An update. *Geochimica et Cosmochimica Acta*, *48*(4), 605–615. https://doi.org/10.1016/0016-7037(84)90089-9

Berner, R. A., & Raiswell, R. (1983). Burial of organic carbon and pyrite sulfur in sediments over phanerozoic time: a new theory. *Geochimica et Cosmochimica Acta*, *47*(5), 855–862. https://doi.org/10.1016/0016-7037(83)90151-5

Bertrand, P. P., Lallier-Vergès, E., Martinez, L., Pradier, B., Tremblay, P., Huc, A., Jouhannel, R., Tricart, J. P., Boussafir, M., Gelin, F., Lallier-Vergès, E., Derenne, S., Bertrand, P. P., Largeau, C., Borcovsky, D., Egenhoff, S., Fishman, N., Maletz, J., Boehlke, A., … Lowers, H. (1995). Electron microscopy and pyrolysis of kerogens from the Kimmeridge Clay Formation, UK: Source organisms, preservation processes, and origin of microcycles. *AAPG Bulletin*, *101*(18), 661–675.

Bowden, S. A., Farrimond, P., Snape, C. E., & Love, G. D. (2006). Compositional differences in biomarker constituents of the hydrocarbon, resin, asphaltene and kerogen fractions: An example from the Jet Rock (Yorkshire, UK). *Organic Geochemistry*, *37*(3), 369–383. https://doi.org/10.1016/j.orggeochem.2005.08.024

Canfield, D. E. (1994). Factors influencing organic carbon preservation in marine sediments. *Chemical Geology*, *114*(3–4), 315–329. https://doi.org/10.1016/0009-2541(94)90061-2

Canheld, D. E., Boudreau, B. P., Mucci, A., & Gundersen, J. K. (1998). The early diagenetic formation of organic sulfur in the sediments of Mangrove Lake, Bermuda. *Geochimica et Cosmochimica Acta*, *62*(5), 767–781. https://doi.org/10.1016/S0016-7037(98)00032-5

Castillo-Michel, A. H., Diaz-Sanchez, G. A., Martinez-Martinez, A., & Hesse, B. (2016). Investigations of Sulfur Chemical Status with Synchrotron Micro Focused X-ray fluorescence and X-ray Absorption Spectroscopy. *Protein & Peptide Letters*, *23*(3), 291–299. https://doi.org/10.2174/0929866523666160108120117

Dang, D. H., Wang, W. W., Evans, R. D., Morgans-bell, H. S., Coe, A. L., Hesselbo, S. P., Jenkyns, H. C., Weedon, G. P., Marshall, J. E. A., Tyson, R. V., Williams, C. J., Tan, J., Sephton, M. A., Thompson, K. J., Kenward, P. A., Bauer, K. W., Warchola, T., Gauger, T., Martinez, R., … Fayek, M. (2019). Sulfur characterization in asphaltene, resin, and oil fractions of two crude oils. *Geochimica et Cosmochimica Acta*, *74*(4), 763–767. https://doi.org/10.1016/0016-7037(93)90389-E

Dicen, G. P., Navarrete, I. A., Rallos, R. V., Salmo, S. G., & Garcia, M. C. A. (2019). The role of reactive iron in long-term carbon sequestration in mangrove sediments. *Journal of Soils and Sediments*, *19*(1), 501–510. https://doi.org/10.1007/s11368-018-2051-y

Edwards, N. P., Manning, P. L., Bergmann, U., Larson, P. L., van Dongen, B. E., Sellers, W. I., Webb, S. M., Sokaras, D., Alonso-Mori, R., Ignatyev, K., Barden, H. E., van Veelen, A., Anné, J., Egerton, V. M., & Wogelius, R. a. (2014). Leaf metallome preserved over 50 million years. *Metallomics*, *6*(4), 774–782. https://doi.org/10.1039/c3mt00242j

Edwards, Nicholas P., Webb, S. M., Krest, C. M., van Campen, D., Manning, P. L., Wogelius, R. A., Bergmann, U., & IUCr. (2018). A new synchrotron rapid-scanning X-ray fluorescence (SRS-XRF) imaging station at SSRL beamline 6-2. *Journal of Synchrotron Radiation*, *25*(5), 1565–1573. https://doi.org/10.1107/S1600577518010202

Gallois, R., Lallier-Vergès, E., Hayes, J. M., Boussafir, M., Zaback, D. A., Tribovillard, N. P., Connan, J., Bertrand, P., Burnham, A. K., Atar, E., März, C., Aplin, A. C., Dellwig, O., Herringshaw, L. G., Lamoureux-Var, V., Leng, M. J., Schnetger, B., Wagner, T., Lees, J. A., … Williams, C. J. (2019). Accumulation of organic matter in the Kimmeridge Clay formation (KCF): an update fossilisation model for marine petroleum source-rocks. *Marine and Petroleum Geology*, *73*(4), 110–134. https://doi.org/http://dx.doi.org/10.1016/S0016-7878(00)80019-X

Ghadeer, S. G., & Macquaker, J. H. S. (2011). Sediment transport processes in an ancient mud-dominated succession: A comparison of processes operating in marine offshore settings and anoxic basinal environments. *Journal of the Geological Society*, *168*(5), 1121–1132. https://doi.org/10.1144/0016-76492010-016

Grice, K., Schouten, S., Blokker, P., Derenne, S., Largeau, C., Nissenbaum, A., & Sinninghe Damsté, J. S. (2003). Structural and isotopic analysis of kerogens in sediments rich in free sulfurised Botryococcus braunii biomarkers. *Organic Geochemistry*, *34*(3), 471–482. https://doi.org/10.1016/S0146-6380(02)00187-0

Grotheer, H., Greenwood, P. F., McCulloch, M. T., Böttcher, M. E., & Grice, K. (2017). $\delta^{34}S$ character of organosulfur compounds in kerogen and bitumen fractions of sedimentary rocks. In *Organic Geochemistry* (Vol. 110, pp. 60–64). https://doi.org/10.1016/j.orggeochem.2017.04.005

Hancock, L. G., Hardisty, D. S., Behl, R. J., & Lyons, T. W. (2019). A multi-basin redox reconstruction for the Miocene Monterey Formation, California, USA. *Palaeogeography, Palaeoclimatology, Palaeoecology*, *520*(September 2018), 114–127. https://doi.org/10.1016/j.palaeo.2019.01.031

Hartgers, W. A., Lòpez, J. F., De Las Heras, F. X. C., & Grimalt, J. O. (1996). Sulphur-binding in recent environments. I. Lipid by-products from Ni2B desulphurization. *Organic Geochemistry*, *25*(5–7), 353–365. https://doi.org/10.1016/S0146-6380(96)00141-6

He, Q., An, Y., Sun, F., & Lai, C. (2019). Genesis of pyrite concretions: Constraints from mineral and geochemical features of longtan formation in Anhui province, eastern China. *Minerals*, *9*(8). https://doi.org/10.3390/min9080467

Houben, M. E., Barnhoorn, A., Lie-A-Fat, J., Ravestein, T., Peach, C. J., & Drury, M. R. (2016). Microstructural characteristics of the Whitby Mudstone Formation (UK). *Marine and Petroleum Geology*, *70*, 185–200. https://doi.org/10.1016/j.marpetgeo.2015.11.011

Isaacs, C. M., & Rullkötter, J. (2001). *The Monterey Formation : from rocks to molecules*. Columbia University Press.

Isaacs, C. M., Ma, H., Zhao, B., Li, L., Xie, F., Zhou, H., Zheng, Q., Wang, X., He, J., Changwei, L., Hiatt, E. E., Pufahl, P. K., Guimarães da Silva, L., Zaback, D. A., Pratt, L. M., Orr, W. L., Rubio-Rincón, F. J., Welles, L., Lopez-Vazquez, C. M., … Yu, W. (2019). Transformations in Organic Sulfur Speciation During Maturation of Monterey Shale: Constraints from Laboratory Experiments. *Palaeogeography, Palaeoclimatology, Palaeoecology*, *612*(February), 138-166 SE – 8. https://doi.org/doi:10.1021/bk-1995-0612.ch008

Jarvie, D. M., & Lundell, L. L. (2001). Kerogen type and thermal transformation of organic matter in the Miocene Monterey Formation. In *The Monterey Formation, from Rocks to Molecules* (pp. 268–295).

Jiang, S., Mokhtari, M., & Borrok, D. M. (2017). Incorporating the effect of pyrite on total organic carbon estimation in eagle ford shale. *Society of Petroleum Engineers - SPE Liquids - Rich Basins Conference - North America 2017*. https://doi.org/10.2118/187484-ms

Kashiwabara, T., Toda, R., Nakamura, K., Yasukawa, K., Fujinaga, K., Kubo, S., Nozaki, T., Takahashi, Y., Suzuki, K., Kato, Y., Bennett, W. W., Lombi, E., Burton, E. D., Johnston, S. G., Kappen, P., Howard, D. L., Canfield, D. E., Lenstra, W. K., Hermans, M., … Penner-hahn, J. E. (2019). Sulfur speciation in heavy petroleums: Information from X-ray absorption near-edge structure. *Geochimica et Cosmochimica Acta*, *25*(1), 181–187. https://doi.org/10.1016/0016-7037(91)90343-4

Kohnen, M. E. L., Sinninghe Damsté, J. S., Ten Haven, H. L., kock.-Van Dalen, A. C., Schouten, S., & De Leeuw, J. W. (1991). Identification and geochemical significance of cyclic di-and trisulphides with linear and acyclic isoprenoid carbon skeletons in immature sediments. *Geochimica et Cosmochimica Acta*, *55*(12), 3685–3695. https://doi.org/10.1016/0016-7037(91)90067-F

Koopmans, M. P., Köster, J., van Kaam-Peters, H. M. E., Kenig, F., Schouten, S., Hartgers, W. A., De Leeuw, J. W., & Sinninghe Damsté, J. S. (1996). Diagenetic and catagenetic products of isorenieratene: Molecular indicators for photic zone anoxia. *Geochimica et Cosmochimica Acta*, *60*(22), 4467–4496. https://doi.org/10.1016/S0016-7037(96)00238-4

Luther, G. W., Glazer, B., Ma, S., Trouwborst, R., Shultz, B. R., Druschel, G., & Kraiya, C. (2003). Iron and sulfur chemistry in a stratified lake: Evidence for iron-rich sulfide complexes. *Aquatic Geochemistry*, *9*(2), 87–110. https://doi.org/10.1023/B:AQUA.0000019466.62564.94

Macquaker, J. H. S., & Gawthorpe, R. L. (1993). Mudstone lithofacies in the Kimmeridge Clay Formation, Wessex Basin, southern England; implications for the origin and controls of the distribution of mudstones. *Journal of Sedimentary Research*, *63*(6), 1129–1143. https://doi.org/10.1306/D4267CC1-2B26-11D7-8648000102C1865D

Macquaker, J. H. S., Taylor, K. G., Keller, M., & Polya, D. (2014). Compositional controls on early diagenetic pathways in fine-grained sedimentary rocks: Implications for predicting unconventional reservoir attributes of mudstones. *AAPG Bulletin*, *98*(3), 587–603. https://doi.org/10.1306/08201311176

Mahoney, C., März, C., Buckman, J., Wagner, T., & Blanco-Velandia, V. O. (2019). Pyrite oxidation in shales: Implications for palaeo-redox proxies based on geochemical and SEM-EDX evidence. *Sedimentary Geology*, *389*, 186–199. https://doi.org/10.1016/j.sedgeo.2019.06.006

Manning, P. L., Edwards, N. P., Bergmann, U., Anné, J., Sellers, W. I., van Veelen, A., Sokaras, D., Egerton, V. M., Alonso-Mori, R., Ignatyev, K., van Dongen, B. E., Wakamatsu, K., Ito, S., Knoll, F., & Wogelius, R. A. (2019). Pheomelanin pigment remnants mapped in fossils of an extinct mammal. *Nature Communications*, *10*(1), 1–13. https://doi.org/10.1038/s41467-019-10087-2

Meister, P., Brunner, B., Picard, A., Böttcher, M. E., Jørgensen, B. B., Kashiwabara, T., Toda, R., Nakamura, K., Yasukawa, K., Fujinaga, K., Kubo, S., Nozaki, T., Takahashi, Y., Suzuki, K., Kato, Y., Bennett, W. W., Hockmann, K., Johnston, S. G., Burton, E. D., … Penner-hahn, J. E. (2019). Sulfur speciation in heavy petroleums: Information from X-ray absorption near-edge structure. *Geochimica et Cosmochimica Acta*, *25*(1), 181–187. https://doi.org/10.1016/0016-7037(91)90343-4

Meshoulam, A., & Amrani, A. (2017). Sulfur isotope exchange between thiophenes and inorganic sulfur compounds under hydrous pyrolysis conditions. *Organic Geochemistry*, *103*, 79–87. https://doi.org/10.1016/j.orggeochem.2016.10.006

Mitra-Kirtley, S., Mullins, O. C., Ralston, C. Y., & Pareis, C. (1999). Sulfur characterization in asphaltene, resin, and oil fractions of two crude oils. *ACS Division of Fuel Chemistry, Preprints*, *44*(4), 763–767.

Morgans-Bell, H. S., Coe, A. L., Hesselbo, S. P., Jenkyns, H. C., Weedon, G. P., Marshall, J. E. A., Tyson, R. V, & Williams, C. J. (2001). Integrated stratigraphy of the Kimmeridge Clay Formation (Upper Jurassic) based on exposures and boreholes in south Dorset, UK. *Geological Magazine*, *138*(05), 511–539. https://doi.org/10.1017/s0016756801005738

Murray, T. E. (1995). The correlation between iron sulfide precipitation and hypolimnetic phosphorus accumulation during one summer in a softwater lake. *Canadian Journal of Fisheries and Aquatic Sciences*, *52*(6), 1190–1194. https://doi.org/10.1139/f95-115

Nelson, B. C., Eglinton I., T., Seewald, J. S., Vairavamurthy, M. A., Miknis, F. P., Su, M., Han, F., Wu, Y., Yan, Z., Lv, Z., Tian, D., Wang, S., Hu, S., Shen, Z., Li, Z., Brandano, M., Ronca, S., Di Bella, L., An, S. U., … Coleman, M. (2019). Coupled iron and phosphorus release from seasonally hypoxic Louisiana shelf sediment. *Palaeogeography, Palaeoclimatology, Palaeoecology*, *665*(February), 112–128. https://doi.org/10.1016/j.still.2019.02.012

Orr, W. L., & Sinninghe Damste, J. S. (1990). Geochemistry of sulfur in petroleum systems. *Geochemistry of Sulfur in Fossil Fuels*, *429*, 2–29. https://doi.org/doi:10.1021/bk-1990-0429.ch001

Orr, Wilson L. (1986). Kerogen/asphaltene/sulfur relationships in sulfur-rich Monterey oils. *Organic Geochemistry*, *10*(1–3), 499–516. https://doi.org/10.1016/0146-6380(86)90049-5

Orr, Wilson L., White, C. M. (1990). Geochemistry of sulfur in fossil fuels : developed from a symposium sponsored by the Division of Geochemistry at the 197th National Meeting of the American Chemical Society, Dallas, Texas. *American Chemical Society*, *9-14*, (1989).

Pomerantz, A. E., Bake, K. D., Craddock, P. R., Kurzenhauser, K. W., Kodalen, B. G., Mitra-Kirtley, S., & Bolin, T. B. (2014). Sulfur speciation in kerogen and bitumen from gas and oil shales. *Organic Geochemistry*, *68*, 5–12. https://doi.org/10.1016/j.orggeochem.2013.12.011

Powell, J. H. (1984). Lithostratigraphical nomenclature of the Lias Group in the Yorkshire Basin. *Proceedings of the Yorkshire Geological Society*, *45*(1–2), 51–57. https://doi.org/10.1144/pygs.45.1-2.51

Pye, K., & Krinsley, D. H. (1986). Microfabric, mineralogy and early diagenetic history of the Whitby Mudstone Formation (Toarcian), Cleveland Basin, U.K. *Geological Magazine*, *123*(03), 191. https://doi.org/10.1017/S0016756800034695

Raiswell, R. (1982). Pyrite texture, isotopic composition and the availability of iron. In *American Journal of Science* (Vol. 282, Issue 8, pp. 1244–1263). https://doi.org/10.2475/ajs.282.8.1244

Raiswell, R., & Al-Biatty, H. J. (1989). Depositional and diagenetic C-S-Fe signatures in early Paleozoic normal marine shales. *Geochimica et Cosmochimica Acta*, *53*(5), 1147–1152. https://doi.org/10.1016/0016-7037(89)90220-2

Raiswell, R., & Anderson, T. F. (2005). Reactive iron enrichment in sediments deposited beneath euxinic bottom waters: constraints on supply by shelf recycling. *Geological Society, London, Special Publications*, *248*(1), 179–194. https://doi.org/10.1144/GSL.SP.2005.248.01.10

Raiswell, R., & Berner, R. A. (1985). Pyrite formation in euxinic and semi-euxinic sediments. In *American Journal of Science* (Vol. 285, Issue 8, pp. 710–724). https://doi.org/10.2475/ajs.285.8.710

Ravel, B., & Newville, M. (2005). ATHENA, ARTEMIS, HEPHAESTUS: data analysis for X-ray absorption spectroscopy using IFEFFIT. *Journal of Synchrotron Radiation*, *12*(4), 537–541. https://doi.org/10.1107/S0909049505012719

Raven, M. R., Sessions, A. L., Fischer, W. W., & Adkins, J. F. (2016a). Sedimentary pyrite $\delta^{34}S$ differs from porewater sulfide in Santa Barbara Basin: Proposed role of organic sulfur. *Geochimica et Cosmochimica Acta*, *186*. https://doi.org/10.1016/j.gca.2016.04.037

Raven, M. R., Sessions, A. L., Adkins, J. F., & Thunell, R. C. (2016b). Rapid organic matter sulfurization in sinking particles from the Cariaco Basin water column. *Geochimica et Cosmochimica Acta*, *190*, 175–190. https://doi.org/10.1016/j.gca.2016.06.030

Raven, M. R, Keil, R. G., & Webb, S. M. (2020). *Microbial sulfate reduction and organic sulfur formation in sinking marine particles*. *6035*(December), 1–9.

Raven, M. R., Fike, D. A., Bradley, A. S., Gomes, M. L., Owens, J. D., & Webb, S. A. (2019). Paired organic matter and pyrite δ 34 S records reveal mechanisms of carbon, sulfur, and iron cycle disruption during Ocean Anoxic Event 2. *Earth and Planetary Science Letters*, *512*, 27–38. https://doi.org/10.1016/j.epsl.2019.01.048

Raven, M. R., Fike, D. A., Gomes, M. L., Webb, S. M., Bradley, A. S., & McClelland, H. L. O. (2018). Organic carbon burial during OAE2 driven by changes in the locus of organic matter sulfurization. *Nature Communications*, *9*(1). https://doi.org/10.1038/s41467-018-05943-6

Rossi, V., McNamara, M. E., Webb, S. M., Ito, S., & Wakamatsu, K. (2019). Tissue-specific geometry and chemistry of modern and fossilized melanosomes reveal internal anatomy of extinct vertebrates. *Proceedings of the National Academy of Sciences of the United States of America*, *116*(36), 17880–17889. https://doi.org/10.1073/pnas.1820285116

Sælen, G., Tyson, R. V., Telnæs, N., & Talbot, M. R. (2000). Contrasting watermass conditions during deposition of the Whitby Mudstone (Lower Jurassic) and Kimmeridge Clay (Upper Jurassic) formations, UK. *Palaeogeography, Palaeoclimatology, Palaeoecology*, *163*(3–4), 163–196. https://doi.org/10.1016/S0031-0182(00)00150-4

Scotchman, I. C. (1989). Diagenesis of the Kimmeridge Clay Formation, onshore UK. *Journal of the Geological Society*, *146*, 285–303. https://doi.org/10.1144/gsjgs.146.2.0283

Scotchman, I. C. (1987). Clay diagenesis in the Kimmeridge Clay Formation, onshore UK, and its relation to organic maturation. *Mineralogical Magazine*, *51*(62), 535–551. http://www.minersoc.org/pages/Archive-MM/Volume_51/51-362-535.pdf

Shaw, H. F., & Primmer, T. J. (1991). Diagenesis of mudrocks from the Kimmeridge Clay Formation of the Brae Area, UK North Sea. *Marine and Petroleum Geology*, *8*(3), 270–277. https://doi.org/10.1016/0264-8172(91)90081-B

Shawar, L., Halevy, I., Said-Ahmad, W., Feinstein, S., Boyko, V., Kamyshny, A., & Amrani, A. (2018). Dynamics of pyrite formation and organic matter sulfurization in organic-rich carbonate sediments. *Geochimica et Cosmochimica Acta*, *241*, 219–239. https://doi.org/10.1016/j.gca.2018.08.048

Sinninghe Damsté, J. S., & de Leeuw, J. W. (1990). Analysis, structure and geochemical significance of organically-bound sulphur in the geosphere: State of the art and future research. *Organic Geochemistry*, *16*(4–6), 1077–1101. https://doi.org/10.1016/0146-6380(90)90145-P

Sinninghe Damsté, J. S., de Leeuw, J. W., Kock-Van Dalen, A. C., de Zeeuw, M. A., Lange, F. D, Irene, W., Rijpstra, C., & Schenck, P. A. (1987). The occurrence and identification of series of organic sulphur compounds in oils and sediment extracts. I. A study of Rozel Point Oil (U.S.A.). *Geochimica et Cosmochimica Acta*, *51*(9), 2369–2391. https://doi.org/10.1016/0016-7037(87)90291-2

Sinninghe Damsté, J. S., Kok, M. D., Köster, J., & Schouten, S. (1998). Sulfurized carbohydrates: An important sedimentary sink for organic carbon? *Earth and Planetary Science Letters*, *164*(1–2), 7–13. https://doi.org/10.1016/S0012-821X(98)00234-9

Smith, D. A., Sessions, A. L., Dawson, K. S., Dalleska, N., & Orphan, V. J. (2017). Rapid quantification and isotopic analysis of dissolved sulfur species. *Rapid Communications in Mass Spectrometry*, *31*(9), 791–803. https://doi.org/10.1002/rcm.7846

Solé, V. A., Papillon, E., Cotte, M., Walter, P., & Susini, J. (2007). A multiplatform code for the analysis of energy-dispersive X-ray fluorescence spectra. *Spectrochimica Acta Part B: Atomic Spectroscopy*, *62*(1), 63–68. https://doi.org/https://doi.org/10.1016/j.sab.2006.12.002

Summons, R. E., & Powell, T. G. (1987). Identification of aryl isoprenoids in source rocks and crude oils: Biological markers for the green sulphur bacteria. *Geochimica et Cosmochimica Acta*, *51*(3), 557–566. https://doi.org/10.1016/0016-7037(87)90069-X

Szczerbowska-Boruchowska, M., Stegowski, Z., Lankosz, M., Szpak, M., & Adamek, D. (2012). A synchrotron radiation micro-X-ray absorption near edge structure study of sulfur speciation in human brain tumors - A methodological approach. *Journal of Analytical Atomic Spectrometry*, *27*(2), 239–247. https://doi.org/10.1039/c2ja10211k

Taylor, K. G., & Macquaker, J. H. S. (2000). Early diagenetic pyrite morphology in a mudstone-dominated succession: The Lower Jurassic Cleveland Ironstone Formation, eastern England. *Sedimentary Geology*, *131*(1–2), 77–86. https://doi.org/10.1016/S0037-0738(00)00002-6

Taylor, Kevin G., & Macquaker, J. H. S. (2011). Iron minerals in marine sediments record chemical environments. *Elements*, *7*(2), 113–118. https://doi.org/10.2113/gselements.7.2.113

Tegelaar, E. W., de Leeuw, J. W., Derenne, S., & Largeau, C. (1989). A reappraisal of kerogen formation. *Geochimica et Cosmochimica Acta*, *53*(11), 3103–3106. https://doi.org/10.1016/0016-7037(89)90191-9

Tissot, B. P., & Welte, D. H. (1984). Petroleum Formation and Occurrence, A New Approach to Oil and Gas Exploration, Second Edition. *Springer-Verlag Berlin Heidelberg New York 1978*, 720.

Tyson, R. V. (2004). Variation in marine total organic carbon through the type Kimmeridge Clay Formation (Late Jurassic), Dorset, UK. *Journal of the Geological Society*, *161*, 667–673. https://doi.org/10.1144/0016-764903-078

Vairavamurthy, A., Zhou, W., Eglinton, T., & Manowitz, B. (1994). Sulfonates: A novel class of organic sulfur compounds in marine sediments. *Geochimica et Cosmochimica Acta*, *58*(21), 4681–4687. https://doi.org/10.1016/0016-7037(94)90200-3

van Dongen, B. E., Schouten, S., & Sinninghe Damsté, J. S. (2006). Preservation of carbohydrates through sulfurization in a Jurassic euxinic shelf sea: Examination of the Blackstone Band TOC cycle in the Kimmeridge Clay Formation, UK. *Organic Geochemistry*, *37*(9), 1052–1073. https://doi.org/10.1016/j.orggeochem.2006.05.007

van Kaam-Peters, H. M. E., Schouten, S., Köster, J., & Sinninghe Damstè, J. S. S. (1998). Controls on the molecular and carbon isotopic composition of organic matter deposited in a Kimmeridgian euxinic shelf sea: Evidence for preservation of carbohydrates through sulfurisation. *Geochimica et Cosmochimica Acta*, *62*(19–20), 3259–3283. https://doi.org/10.1016/S0016-7037(98)00231-2

Waldo, G. S., Carlson, R. M. K., Moldowan, J. M., Peters, K. E., & Penner-hahn, J. E. (1991). Sulfur speciation in heavy petroleums: Information from X-ray absorption near-edge structure. *Geochimica et Cosmochimica Acta*, *55*(3), 801–814. https://doi.org/10.1016/0016-7037(91)90343-4

Wang, P., Algeo, T. J., Zhou, Q., Yu, W., Du, Y., Qin, Y., Xu, Y., Yuan, L., & Pan, W. (2019). Large accumulations of 34S-enriched pyrite in a low-sulfate marine basin: The Sturtian Nanhua Basin, South China. *Precambrian Research*, *335*, 105504. https://doi.org/10.1016/j.precamres.2019.105504

Webb, S. M. (2005). SIXPack a Graphical User Interface for XAS Analysis Using IFEFFIT. *Physica Scripta*, 1011. https://doi.org/10.1238/physica.topical.115a01011

Webb, S. M. (2011). The MicroAnalysis Toolkit: X-ray Fluorescence Image Processing Software. *AIP Conference Proceedings*, *1365*(1), 196–199. https://doi.org/10.1063/1.3625338

Werne, J. P., Hollander, D. J., Lyons, T. W., & Sinninghe Damsté, J. S. (2004). Organic sulfur biogeochemistry: Recent advances and future research directions. *Geological Society of America Special Papers*, *379*, 135–150. https://doi.org/10.1130/0-8137-2379-5.135

Werne, J. P., Lyons, T. W., Hollander, D. J., Formolo, M. J., & Sinninghe Damsté, J. S. (2003). Reduced sulfur in euxinic sediments of the Cariaco Basin: Sulfur isotope constraints on organic sulfur formation. *Chemical Geology*, *195*(1–4), 159–179. https://doi.org/10.1016/S0009-2541(02)00393-5

Werne, J. P., Lyons, T. W., Hollander, D. J., Schouten, S., Hopmans, E. C., & Sinninghe Damsté, J. S. (2008). Investigating pathways of diagenetic organic matter sulfurization using compound-specific sulfur isotope analysis. *Geochimica et Cosmochimica Acta*, *72*(14), 3489–3502. https://doi.org/10.1016/j.gca.2008.04.033

Wiltfong, R., Mitra-Kirtley, S., Mullins, O. C., Andrews, B., Fujisawa, G., & Larsen, J. W. (2005). Sulfur speciation in different kerogens by XANES spectroscopy. *Energy and Fuels*, *19*(5), 1971–1976. https://doi.org/10.1021/ef049753n

Zheng, L., Chen, X., Dong, X., Wei, X., Jiang, C., Tang, Q., Bowles, M. W., MogolÍon, J. M., Kasten, S., Zabel, M., Hinrichs, K. U., Sim, M. S., Paris, G., Adkins, J. F., Orphan, V. J., Sessions, A. L., Wing, B. A., Halevy, I., Valiente, N., … Vaida, V. (2019). Decrypting the sulfur cycle in oceanic oxygen minimum zones. *Geochimica et Cosmochimica Acta*, *12*(1), 74–83. https://doi.org/10.1073/pnas.1702953114

Chapter 4

Project 3

An experimental investigation of the stability of sulfurised carbohydrates

Yusuf Abubakar [1, 2, *], Victoria Coker[1], Roy A. Wogelius[1] Kevin G. Taylor[1], and Bart E. van Dongen[1]

[1] Williamson Research Centre, Department of Earth and Environmental Sciences, University of Manchester, Oxford Road, Manchester, M13 9PL, UK

[2] Desert Research, Monitoring and Control Centre, Yobe State University, KM 7, Sir Kashim Road, Damaturu, Nigeria

[*]Correspondence: yusuf.abubakar@manchester.ac.uk; yusuf.abubakar@ysu.edu.ng

To be submitted to Organic Geochemistry

Highlights

- Stability of carbon-sulfur bonds in sulfurised organic matter is tested for the first time.
- Metastable FeS materials were formed during reaction of sulfurized glucose with iron(II) chloride.
- Metastable FeS materials transformed to a more stable iron sulfide (likely pyrite).
- Sulfurised glucose still present after iron(II) chloride treatment.

Abstract

Sulfurisation of organic matter (OM) is considered an important process through which enormous amounts of carbon (C) is preserved in the sedimentary record. However, this process is believed to be controlled by the availability of iron (Fe). In anoxic/euxinic oceans where sulfate is reduced and reactive Fe is present, reaction between reduced inorganic sulfur (S) and Fe species is preferential over OM. This process is continuous until all Fe in a system is exhausted after which remnant reduced S can react with OM to form S-rich OM that can survive remineralisation and be preserved. This is a widely accepted concept, however, it remains unclear to what extent sulfurised OM is stable especially during an influx of fresh, reactive Fe species to ocean and porewater. We completed a series of experiments reacting sulfurised glucose (carbohydrate type OM) with iron(II) chloride. Results indicate, for the first time, that some S in the sulfurised glucose was utilised by Fe to form metastable FeS materials, which were subsequently converted to minerals with co-ordination of S and Fe that is similar to the co-ordination environment and oxidation state of S and Fe in S^{-2} Fe sulfide minerals (likely pyrrhotite or troilite). Some of these S^{-2} minerals further converted to form traces of a more stable S^{-1} iron sulfides (likely pyrite). However, there was still sulfurised glucose in the product after Fe treatment. This suggest that potentially (specific) parts of the S originally bound to the glucose were lost during the experiments. The metastable FeS materials were likely either formed from that part of the sulfurised glucose with weak S-S bonds, while the stronger C-S bonds were stable, and could be preserved for millions of years. However, it cannot be excluded that it is a matter of time before all S in the sulfurised glucose would be stripped off to form iron sulfides. Overall, reaction between OM and S could be said to be partially reversible in the presence of reactive Fe species.

Keywords/Phrases: Organic Matter, Organic Sulfur Compounds, Sulfur, Iron, Pyrite, X-ray Fluorescence Imaging, X Absorption Near Edge Structure.

4.1 Introduction

Global biogeochemical cycles of carbon (C), sulfur (S), oxygen (O) and iron (Fe) are interlinked through a series of biotic and abiotic processes that occur on a range of timescales (Berner, 1989; Werne et al. 2004; Gill et al. 2007; Hurtgen et al. 2009; Couture et al. 2016). These elements and the way they interact are essential for the sustenance of life on earth (Walker, 1986; Berner, 2005, 2006). Many studies have reported that during sedimentary deposition of OM, marine biota scavenge it for their metabolic activities (Ouverney & Fuhrman, 2000; McCarren et al., 2010; Herndl & Reinthaler, 2013; Landa et al., 2015; Li et al., 2015; Li et al., 2016), thus increasing the size of their population and activities (Horner-Devine et al., 2003; Mann & Lazier, 2013; Naeher et al., 2012; Oni et al., 2015). With time, dissolved O in the water column reduces due to respiration and the remaining non-remineralised OM reaches the ocean bottom where portions may get preserved for millions of years (Demaison & Moore, 1980; Jenkyns, 1980; Wagreich et al., 2011).

Several factors, such as upwelling (nutrient supply), water column residence time, sedimentation rate, ocean circulation and basin geometry control OM preservation in the sedimentary record (Demaison & Moore, 1980; Arthur et al., 1984; Pratt, 1984; Pratt & King, 1986; Arthur et al., 1987). However, another important factor for the effective preservation of OM in the fossil record is the presence/absence of reduced S in the water column/sediments. During the expansion of the microbial communities, as part of their activities, sulfate in the ocean is reduced to sulfide (Canfield et al., 1986; Filley et al., 2002; Luckge et al., 2002; Werne et al., 2003; Schunck et al., 2013; Turchyn et al., 2015; Bradley et al., 2016; Antler et al., 2017), which can react with OM, making it less labile for remineralisation and hence ultimately improving the OM preservation potential (Demaison & Moore, 1980; Sinninghe Damsté & de Leeuw, 1990; van Kaam-Peters et al., 1998; Werne et al., 2003; Amrani & Aizenshtat, 2004; van Dongen et al., 2006). Through this sulfurisation process, even labile organic C such as carbohydrates could be preserved (Sinninghe Damsté et al., 1998; Kok et al., 2000; van Dongen etal., 2006). van Dongen et al. (2006), for example, proposed that the reaction of S with carbohydrate type C was responsible for the unusual accumulation of organic C (up to 52 wt %) in the Blackstone band of the Jurassic Kimmeridge Clay Formation. Sulfurised organic compounds were also reported in other organic C-rich source rocks, such as the Miocene Monterey Formation (Orr, 1986; Zaback & Pratt, 1992; Nelson et al., 1995) and in many exploited petroleum source rocks (Orr, 1978, 1986; Waldo et al., 1991).

However, in the presence of bioavailable Fe, the reduced S reacts preferentially with Fe to initially precipitate metastable Fe monosulfide minerals such as amorphous FeS or mackinawite (tetragonal FeS; Schoonen & Barnes, 1991) and subsequently transforms to a more stable iron disulfide [(e.g. pyrite (FeS_2)] through a number of thermodynamic pathways (Rickard & Luther, 2007; Rickard, 2019).

Although it is well established that sulfurisation of OM is one of the key pathways for the effective preservation of OM, there is little known about the fate or stability of sulfurised OM after it is formed (i.e. reversibility of S and OM reaction). It remains, for instance, unclear what happens to the freshly produced sulfurised OM during influx of fresh bioavailable iron species from aeolian dust, glacial melts and/or continental run offs into sediments and porewater.

The aims of this study are therefore, (1) to investigate the stability of C-S bonds in sulfurised OM (carbohydrates) after the introduction of Fe^{2+} under anoxic conditions and (2) to understand the kinetics of any subsequent iron sulfide (e.g. FeS_2) formation from an organic S or polysulfide precursor.

4.2 Materials and Methods

4.2.1 Materials

The elements/compounds used in this study were D-glucose (Sigma Aldrich), elemental S (S8; Sigma Aldrich), sodium hydrosulfide hydrate ($NaHS \cdot xH_2O$; Sigma Aldrich), ammonium polysulfide ($H_8N_2S_3$; Fisher Scientific), iron (II) chloride tetrahydrate ($FeCl_2 \cdot 4H_2O$; Sigma Aldrich), and copper flakes (Elementar).

4.2.2 Glucose Sulfurisation

D-glucose sulfurisation was completed according to an established protocol (Kok et al., 2000; van Dongen et al., 2003). In this study, the size of the sulfurisation reaction was increased by a factor of 40 compared to that of van Dongen et al., (2003) to obtain sufficient material for further experiments and geochemical analyses. In short, 8 g of D-glucose was mixed with 22.4 g $NaHS \bullet xH_2O$ and 0.64 g S_8 in 240 ml of bidistilled deionised water (H_2O) in a high specification airtight jar, the solution was flushed with N_2 in a glove box (95 % N_2 / 5 % H_2) to create an anoxic environment, closed and stirred for 4 weeks at 50 ºC. The solution was left to cool at room temperature, activated copper flakes were added to remove remnant S_8, filtered with 0.22 μm polyethersulfone, freeze dried and stored for analyses and Fe experiments. The formation of sulfurised glucose material was established using a combination of pyrolysis-gas chromatography-mass spectrometry (Py-GC-MS), attenuated total reflectance-Fourier transform infrared spectroscopy (ATR-FTIR) and elemental carbon, hydrogen, nitrogen and sulfur (CHNS) analyses.

4.2.3 Molecular and Elemental Analyses of Sulfurised Glucose

4.2.3.1 Pyrolysis-Gas Chromatography-Mass Spectrometry (Py-GC-MS)

Samples were analysed by Py-GC-MS using an Agilent GC-MSD system interfaced to a CDS-5200 Pyroprobe (*CDS Analytical, US*). 2 mg of freeze-dried sulfurised glucose was weighed into pre-cleaned fire-polished quartz tubes with quartz wool placed at its bottom and pyrolysed at 600 ºC for 20 s in a flow of helium. Products/moieties produced were transferred through a heated transfer line to an Agilent 7980A GC fitted with a Zebron ZB-5MS fused column (*Phenomenex, The Netherlands*; 95% dimethylpolysiloxane, 5% phenyl-arylene phase; 8 polarity; 350 ºC, 30 m length, 0.25 mm i.d., 0.25 μm film thickness) coupled to an Agilent 5975C MSD single quadrupole mass spectrometer (MS) run in the electron ionisation (EI) mode (Scanning a range of m/z 50 to 650 at 2.7 scans s^{-1}; ionisation energy 70 eV; solvent delay 1 min). The pyrolysis transfer line and injector temperatures were set at 350 ºC, the valve oven at 325 ºC, the EI source at 230 ºC, the heated GC interface at 280 ºC and the MS

quadrupole at 150 ºC. Sample was introduced in split mode (split ratio 20:1; split flow of 40 mL/min) and helium was used as the carrier gas. The oven temperature was programmed to hold at 40 ºC for 5 min then increase 4 ºC min^{-1} to 300 ºC and kept for 15 min at this temperature for a total run time of 85 min. Thiophene and alkylated thiophenes were quantified by integration of their peaks in the partial accurate mass chromatograms of *m/z* 84 + 97 + 98 + 111 + 112 + 125 + 126 + 139 + 140 + 153 + 154. The different isomers were identified based on their relative retention time, mass spectral data and in comparison with previous studies (Sinninghe Damsté et al., 1988; Kok et al., 2000; van Dongen et al., 2003).

4.2.3.2 Attenuated Total Reflectance - Fourier Transform Infrared (ATR-FTIR) Spectroscopy

ATR-FTIR point analysis was completed using a PerkinElmer Spotlight 400 instrument (*Perkin Elmer, US*) with a contact attenuated total reflectance (ATR) crystal attachment with a 100 μm^2 aperture, 4 cm^{-1} resolution, a spectral wave range of 4000 - 650 cm^{-1} (3 - 15 μm) and a deuterated triglycine sulfate detector. IR spectra (average of 4 scans) were collected on ca. 100 μg of freeze-dried sulfurised glucose without prior sample preparation. Spectral background subtractions were completed via an automated protocol and peaks were identified using the Bio-Rad KnowItAll Informatics System 2020 multi-technique database and identification was verified by comparison with published values (Coates, 2006; Ibrahim et al., 2006). IR spectra of pure D-glucose was also collected and analysed as described above for comparison. Spectra were processed and stacked in Origin (*OriginLab, US*).

4.2.3.3 Organic Elemental Carbon, Hydrogen, Nitrogen and Sulfur (CHNS) Analyses

CHNS determination was performed on a Thermo Scientific Flash 2000 (*Thermo Fisher Scientific, US*) organic elemental analyser. 2 mg of freeze-dried sulfurised glucose was accurately weighed into tin containers which were placed into an autosampler tray continuously purged with helium gas. Samples were dropped into a vertical quartz combustion reactor tube which was maintained at a temperature of 900 ºC. The helium carrier gas stream was enriched with pure O as the sample was released into the furnace. For analysis, the sample and tin container melt and the tin amplifies a violent reaction (flash combustion). This temporarily raises the temperature to about 1800 ºC. The gas mixture passes over a catalyst for complete oxidation after which, it flows through a layer of copper for removal of excess O and reduction of nitrogen oxides to elemental nitrogen. The resulting gas mixture further flows to a chromatographic separation column in an oven with controlled temperature. At this stage, the gas components separate and elute as nitrogen, carbon dioxide, water and sulfur dioxide. Quantitative determination of the elements was achieved with a thermal conductivity detector,

signals were processed using Eager Xperience software package and results were presented in percent of C, H, N or S. For accuracy of results, standard reference materials were run before and after each analysis. Determination of CHNS in one run was not possible thus CHN were determined first and then followed by S analysis. A possible error of ± 0.3 % for both accuracy and precision is reported.

4.2.4 Iron Experiments

1 g of freeze-dried sulfurised glucose (see section 4.2.2) containing 8.7 mg of S (as determine by CHNS analysis) was dissolved in 2.7 ml of N_2 purged distilled deionised H_2O to make a 1 M S concentration in an airtight serum bottle in a glove box under an anoxic atmosphere (95 % N_2 / 5 % H_2). A pH of 10 was recorded after complete dissolution. The bottle was sealed with a butyl rubber stopper and a metal crimp. 683 µl taken from a 1 M stock solution of $FeCl_2 \cdot 4H_2O$ was injected into the dissolved sulfurised glucose using a syringe and needle, resulting in a 4:1 S to Fe ratio (see appendix 4.1 for detail calculations of concentrations). The 4:1 S to Fe ratio was considered based on the stoichiometry of FeS_2 and literature suggesting synthesis of Fe sulfides from a precursor excess in S (Gartman & Luther, 2013). The solution was shaken for 10 min to achieve complete mixing of S and Fe. Addition of Fe immediately turned the brown looking dissolved sulfurised glucose to black and reduced the pH to 7.4, similar to that of sediments in the natural environment (Berner, 1967; Herlihy & Mills, 1986) thus, further pH adjustment with sodium hydroxide was not needed. As control experiments, $H_8N_2S_3$ and pure D-glucose were equally subjected to the same $FeCl_2$ treatment. In the case of $H_8N_2S_3$, 1.8 ml (see appendix 4.1 for detail calculations of concentrations) was reacted with 683 µl of $FeCl_2 \cdot 4H_2O$ to make 4:1 S to Fe ratio and 0.9 ml of N_2 purged twice-distilled deionised H_2O was added to round up the solution to 2.7 ml. For the D-glucose, 1 g was dissolved in 2.7 ml N_2 bubbled bidistilled deionised H_2O followed by addition of 683 µl of $FeCl_2 \cdot 4H_2O$. All experiments were completed in triplicate for reproducibility, and were gently shaken in a Stuart SI500 orbital incubator (*Cole-Parmer, UK*) at 30 ºC for 4 weeks. The incubator was covered to avoid any photo-oxidation during the 4 weeks' period. Prior to experiments, concentrations of S and Fe were determined by inductively coupled plasma-atomic emission spectroscopy (ICP-AES) using aliquots from separate 1 M stock solutions of the sulfurised glucose and $FeCl_2 \cdot 4H_2O$ respectively as described in detail in section 4.2.5.

After 4 weeks, bottles were open in a glove box (95 % N_2 / 5 % H_2) and liquid phases from all experiment were gently removed using a syringe and needle for further analysis. Aliquots from the liquid phases were analysed immediately by ICP-AES for the concentrations of S and Fe

as described in detail in section 4.2.5. The remnant liquid phases of the sulfurised glucose experiments were freeze-dried and analysed by Py-GC-MS and CHNS as described earlier. The solid phases were analysed by grazing-incidence X-ray diffraction (XRD), environmental scanning electron microscopy-energy dispersive spectroscopy (ESEM-EDS), micro-focus X-ray fluorescence (MF-XRF) and X-ray absorption near edge structure (XANES) analyses. The original non-Fe reacted sulfurised glucose was also analysed by MF-XRF and XANES for comparison.

4.2.5 Chemical and Mineralogical Analyses of Iron Experiments

4.2.5.1 Liquid Phases

4.2.5.1.1 Inductively Coupled Plasma-Atomic Emission Spectroscopy (ICP-AES)

ICP-AES analysis was undertaken using a dual view Optima 5300DV instrument (Perkin-Elmer, US) with a detection limit of 10-15 μg/L or approximately 50 ppb. Liquid samples of sulfurised glucose and $FeCl_2 \cdot 4H_2O$ before and after experiments were digested with 2% nitric acid (HNO_3) to achieve complete dissolution and were subsequently run and measured as total S and Fe in percentage. A standard was run before and after measurements to check for any instrumental drift.

4.2.5.2 Solid Phases

4.2.5.1.2 Grazing-Incidence X-ray Diffraction (XRD)

Grazing-incidence XRD was performed on a Bruker D8 Advance diffractometer equipped with a with Göbel Mirror and LynxEye sensitive detector operating at 40 kV / 40 mA. Solid phases from all experiments were smeared evenly on glass slides and allowed to completely dry in a glove box (95 % N_2 / 5 % H_2) to avoid oxidation, after which were loaded immediately into the XRD instrument and analysed using an incident monochromatic Cu K-alpha X-ray beam with 1.5406 Å wavelength. Scans of the solids were collected from 5º to 70º (2θ) at a fixed incident angle of 2.5º, with a step size of 0.02º at a speed of 2 s $step^{-1}$. Diffraction patterns were collated and background subtracted using EVA version 4 software package (*Bruker AXS, UK*) and peaks were identified using the International Centre for Diffraction Data (ICDD) Powder Diffraction File database.

4.2.5.1.3 Environmental Scanning Electron Microscopy-Energy Dispersive X-ray Spectroscopy (ESEM-EDS)

Backscattered ESEM-EDS imaging and elemental analysis were completed using a Quanta FEG 650 environmental scanning electron microscope (*FEI Instrument, US*) equipped with an energy dispersive X-ray spectroscopy unit (*Bruker x Flash 6130 Instrument, (US)*, Esprit 2.1

software) and a concentric-backscatter (CBS) detector. Solids from the Fe-treated sulfurised glucose or control experiments were smeared evenly on 12.5 mm stubs with a carbon layer and allowed to completely dry in a glove box (95 % N_2 / 5 % H_2) to avoid oxidation, and loaded immediately into the ESEM-EDS chamber. Scanning/Imaging was done in the high vacuum mode using a voltage of 15 kV, 0.30 mbar chamber pressure, 3 μs scanning speed, 3.50 spot size and 10.2 mm working distance.

4.2.6 Micro-Focus X-Ray Fluorescence (MF-XRF)

MF-XRF mapping for S and Fe was performed at beamline I18 at the Diamond Light Source (DLS), the UK's national synchrotron light source science facility in Oxfordshire. Solid phases from the Fe-treated sulfurised glucose and $H_8N_2S_3$ control experiments were smeared evenly on glass slides and allowed to completely dry in a glove box (95 % N_2 / 5 % H_2) to avoid oxidation. Slides were mounted onto a motorised stage and sealed within a polythene bag that is kept purged with a constant flow of helium to create a low-density inert atmosphere to minimise the absorption of incident and fluoresced X-rays by air. Samples were scanned with an incident beam energy of 8 keV, 0.01 mm X and Y step sizes, 0.05 s dwell time per pixel to acquire small-scale elemental maps for S and Fe at 10 micron (μm) resolution. Beam path included a double-crystal Si(111) monochromator, Kirkpatrick–Baez mirrors. A four element Vortex silicon drift detector was used to detect fluoresced X-rays. S and Fe maps were processed using the ROI imaging tool in PyMCA X-ray Fluorescence Toolkit (version 5.5.3; Solé et al., 2007) and DAWN (version 2.18; Basham et al., 2015) by defining the X-ray emission energy of an element in the recorded EDS spectra.

4.2.7 X-Ray Absorption Near Edge Structure (XANES)

S K-edge XANES and Fe K-edge XANES analyses were carried out DLS beamline I18. For this, experimental samples (solid phases) and a set of S and Fe standards [including elemental S, pyrite (S and Fe), cysteine, disulfide (oxidised glutathione), benzothiazole, methionine sulfoxide, sulfate, and pyrite] were smeared onto glass slides (slurry of solid phases were directly smeared onto glass slides while standards were smeared using ethanol). Slides were placed on a motorised stage sealed within a polythene bag that was kept purged with a constant flow of helium, to create a low density inert atmosphere to minimise the absorption of incident and fluoresced X-rays by air. Photo-oxidation by the X-ray beam was minimised by employing a defocused beam, rapid scan speeds and by changing the area analysed by slightly moving the beam between scans. S K-edge and Fe K-edge XANES data were acquired in fluorescence mode using a defocussed beam with slit apertures of 50 μm (horizontal) and 500 μm (vertical)

and a four element Si drift Vortex fluorescence detector set at scattering angle of 90°. XANES spectral analysis (background subtractions and normalisations) and linear combination fitting was accomplished using the Athena application, a component of the Demeter suite of XAS analytical tools (Ravel & Newville, 2005).

4.3 Results and Discussion

4.3.1 Formation of Sulfurised Glucose

Sulfurised carbohydrate OM was synthesised under controlled inert (nitrogen) conditions by reacting pure D-glucose with $NaSH{\cdot}H_2O$ and S_8 for 4 weeks. Removal of excess S_8 with activated Cu curls and subsequent freeze-drying yielded a brown material with a strong garlic-like smell in-line with previous studies (Kok et al., 2000; van Dongen et al., 2003). Elemental analysis shows the amount of C, H and S was 12.6 wt. %, 5.4 wt. % and 8.7 wt. %, respectively.

To confirm the formation of sulfurised glucose the material obtained after sulfurisation was analysed by FTIR Spectroscopy and compared to the infrared spectrum of pure D-glucose. FTIR spectroscopy of pure D-glucose shows the presence of a strong, sharp absorption peak at 3404 cm^{-1} (OH1) and a strong broad peak between 3400 cm^{-1} and 3200 cm^{-1} (OH2) denoting the existence of a free and hydrogen bonded OH (alcohol) groups respectively (Fig 4.1a; Table 4.1). Strong peaks at 1111 cm^{-1}, 1049 cm^{-1} and 993 cm^{-1} were attributed to the CO stretch of alcohols. Two strong peaks; a symmetric one at 2945 cm^{-1} and an antisymmetric one at 2914 cm^{-1} indicate the presence of CH (alkane) groups. Likewise, a medium, asymmetric peak at 1458 cm^{-1} and a symmetric one at 1372 cm^{-1} and three weak deformed peaks at 1340 cm^{-1}, 1203 cm^{-1} and 1079 cm^{-1} show the presence of CH_2, and CH (alkane) groups respectively. The medium skeletal peaks at 1224 cm^{-1}, 1146 cm^{-1} and 731 cm^{-1} and a medium deformation peak at 1014 cm^{-1} were assigned to the CC (alkane) groups while the peak at 650 cm^{-1} is attributed to the bending of CH_2. Lastly, the COC stretching bands of ether groups were observed at 916 cm^{-1}, 838 cm^{-1} and 775 cm^{-1}, in line with previous studies (Zhbankov et al., 1995; Ibrahim et al., 2006; Yusoff et al., 2020).

In contrast, FTIR spectroscopy of the sulfurised glucose indicates an absence of the free OH and substantial reduction of the hydrogen bonded OH at 3404 cm^{-1} and between 3400 cm^{-1} and 3200 cm^{-1}, respectively (Fig 4.1b; Table 4.1). The spectrum is further characterised by an absence of the CH (alkane) stretches at 2945 cm^{-1} and 2914 cm^{-1}, the presence of a weak deformed peak at 2495 cm^{-1} likely being the SH of thiols, and medium and strong *ν* C=O stretches at 1776 cm^{-1} and 1587 cm^{-1} consistent with the presence of a cyclic, 4-membered ring ketone and β-diketone respectively. In addition, strong antisymmetric peaks at 1411 cm^{-1} and 1335 cm^{-1} may be assigned to the S=O stretch of sulfate and sulfone, respectively, while another weak peak at 1050 cm^{-1} can be attributed to the S=O stretch of sulfoxide. The strong peaks at 1121 cm^{-1} and 668 cm^{-1} are most probably the C=S and CS stretches of alkyl thioketone and thioether respectively. Finally, a strong peak at 1001 cm^{-1} is ascribed to CH

deformation of an alkene group while the strong and weak peaks at 878 cm^{-1} and 770 cm^{-1} were assigned to the SO stretches of sulfuric esters. The presence of copious double bonded C, S and O suggests that the starting material is a complex sulfurised OM, significantly different from the original D-Glucose. Furthermore, the presence of alkyl thioketone supports previous studies that reported carbonyl functional groups react preferentially with inorganic sulfur species compared to hydroxyl groups which are relatively inert (Schouten et al., 1993; Schneckenburger et al., 1998; van Dongen et al., 2003).

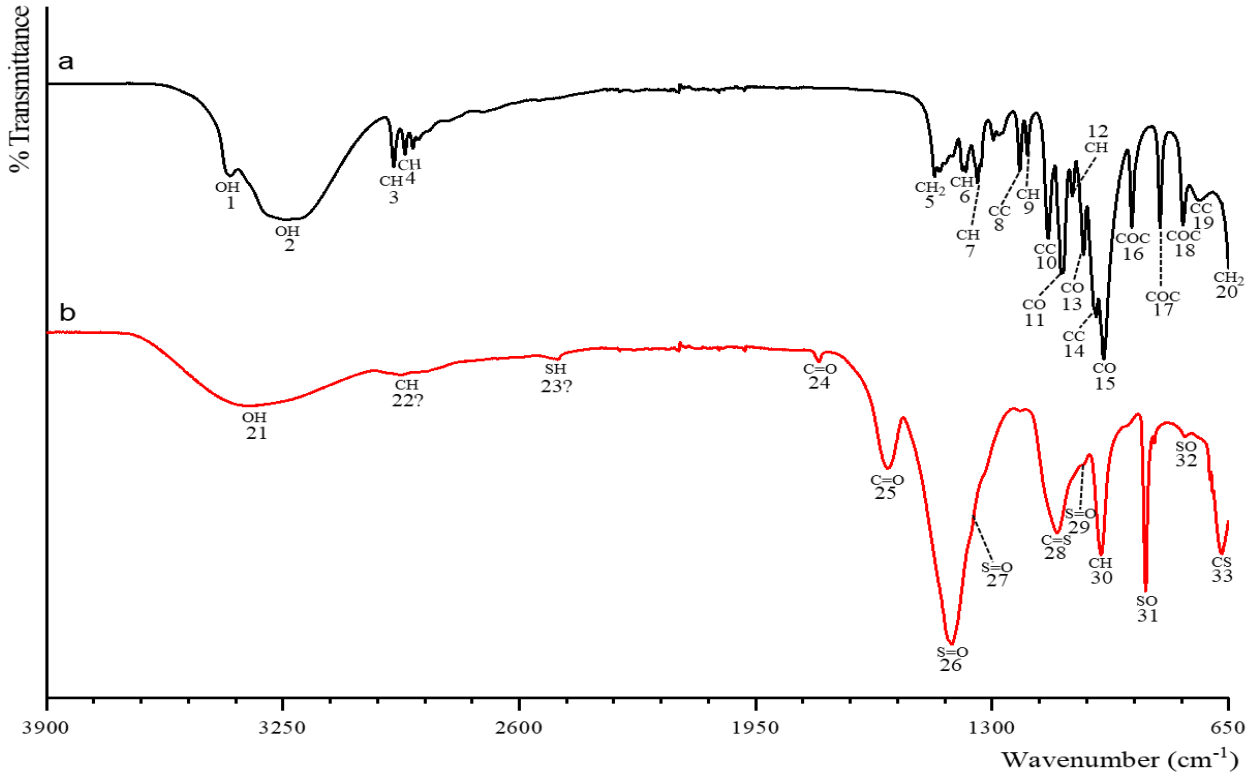

Figure 4.1: Infrared spectrum of (a) pure and (b) sulfurised D-glucose. Marks on peaks denote chemical bonds and numbers represent detailed information as presented in Table 4.1.

Table 4.1: Infrared absorption bands of the pure and sulfurised D-glucose (presented in figure 4.1) as identified using the Bio-Rad KnowItAll Informatics System 2020 multi-technique database and comparison with literature (Coates, 2006; Ibrahim et al., 2006) AS = Antisymmetric, S = Symmetric, ? = Uncertainty.

Peak	Classification	Chemical Group	Bond Mixture	Dominant Bond	Wavenumber Range (cm^{-1})	Specific Wavenumber (cm^{-1})	Intensity	Vibration
1	Alcohol	Free OH	-	OH	3430 -3375	3404	Strong	Stretch
2	"	$(R)_2CH$-OH (H bonded)	-	OH	3400 - 3200	3238	Variable	Stretch
3	Alkane	R-$(CH_2)_4$-C	-	CH	2944 - 2936	2945	Strong	S Stretch
4	"	R-$(CH_2)_4$-C	-	CH	2914 - 2906	2914	Strong	AS Stretch
5	"	R-$(CH_2)_4$-OR	$\delta CH_2 + \delta OCH + \delta CCH$	CH_2	1475 - 1435	1458	Medium	AS Stretch
6	"	R-$(CH_2)_4$-OR	$\delta OCH + \delta COH + \delta CCH$	CH	1380 – 1375	1372	Medium	S stretch
7	"	R-$(CH_2)_4$-OR	$\delta CCH + \delta OCH$ in plane	CH	1350 – 1320	1340	Weak	Deformation
8	"	R-$(CH_2)_4$-OR	$\delta CH + \delta OH$ in plane	CC	1250 - 1200	1224	Medium	Skeletal
9	"	R-$(CH_2)_4$-OR	$\delta CH + \delta OH$ in plane	CH	1208-1200	1203	Weak	Skeletal
10	"	R-$(CH_2)_4$-OR	CO + CC	CC	1160 - 1135	1146	Variable	Skeletal
11	Alcohol	$(R)_2CH$-OH (H bonded)	-	CO	1125 - 1090	1111	Strong	Stretch
12	Alkane	R-$(CH_2)_4$-OR	CH in plane H bend	CH	1086 - 1078	1079	Weak	Bend
13	Alcohol	$(R)_2CH$-OH	CO + CC	CO	1075 – 1000	1049	Strong	Stretch
14	Alkane	R-$(CH_2)_4$-OR	CO + CC	CC	1048 – 1000	1014	Medium	Deformation
15	Alcohol	$(R)_2CH$-OH	CO + CC	CO	990 - 1060	993	Strong	Stretch

16	Ether	R-O-R'	CO + CCH + C-O-C 5-ring ether	COC	920 – 905	916	Medium	S stretch
17	"	R-O-R'	C-O-C 3-ring ether	COC	880 – 805	838	Strong	Deformation
18	"	R-O-R'	δCCO + δCCH	COC	803 – 761	775	Medium	S stretching
19	Alkane	$R-(CH_2)_4-C$	-	CC	750 – 720	731	Medium	Skeletal
20	"	$R-(CH_2)_4-C$	-	CH_2	664-640	650	Variable	Bending
21	Alcohol	$(R)_2CH-OH$ (H bonded)	-	OH	3400 - 3200	3238	Variable	Stretch
22[?]	Alkane	$R-(CH_2)_4-OR$	-	CH	2936 - 2916	2945	Strong	AS Stretch
23[?]	Thiols	R-SH	-	SH	2469 - 2530	2495	Weak	Deformation
24	Cyclic, 4-ring ketone	R-C(=O)-R'	-	C=O	1790 - 1760	1776	Medium	Stretch
25	Ketone (β-Diketone)	R-C(=O)-R'	-	C=O	1640 - 1540	1587	Strong	Stretch
26	Sulfate	$O-SO_2-O$	-	S=O	1450 - 1350	1411	Strong	AS Stretch
27	Sulfone	$R-SO_2-R$	-	S=O	1350 - 1300	1335	Strong	Stretch
28	Alkyl thioketone	$R_2C=S$	-	C=S	1200 - 1050	1121	Medium - Strong	Stretch
29	Sulfoxide	R-S(=O)-R'	-	S=O	1060 - 1020	1050	Weak	Stretch
30	Alkene	$R-CH=CH_2$	-	CH	1032 - 975	1001	Strong	Deformation
31	Sulfuric esters	O_4SR_2	-	SO	700 - 900	878	Strong	Stretch
32	"	O_4SR_2	-	SO	700 - 900	770	Weak	Stretch
33	Thioether	R-S-R'	-	CS	710 - 570	668	Strong	Stretch

Additional Py-GC-MS analyses of the sulfurised glucose indicates the presence of a series of C_0-C_4 alkylated thiophenic compounds comparable to those observed by Kok et al. (2000) and van Dongen et al. (2003) indicating that the sulfurisation of glucose was achieved (Fig. 4.2a.). Kok et al. (2000) further noted the thiophenic compounds would not have formed if the inorganic S species were not physically bound to the glucose.

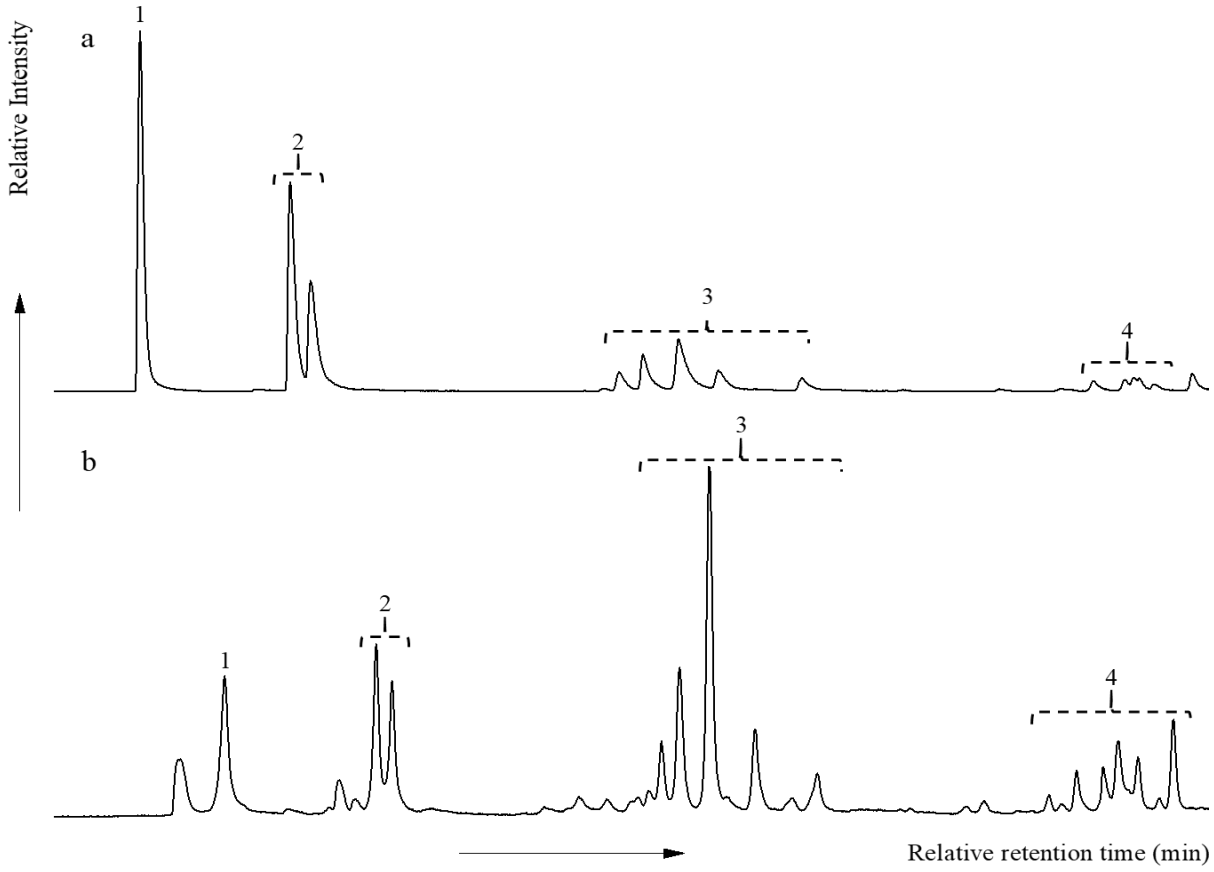

Figure 4.2: Distribution of thiophenes in the pyrolysates of (a) sulfurised D-glucose and (b) sulfurised D-glucose treated with iron as revealed by the partial accurate mass chromatograms of m/z 84 + 97 + 98 + 111 + 112 + 125 + 126 + 139 + 140 + 153 + 154. Peak assignments are (1) thiophene (2) methylthiophenes (3) ethyl and/or dimethylthiophenes and (4) propyl and/or trimethylthiophenes. The shift in relative retention time between the two pyrograms is due to a different column used for both analyses.

4.3.2 Iron Treatment of Pure Glucose, Sulfurised Glucose and Polysulfide

To investigate the fate and stability of sulfurised OM commonly found in the sedimentary record, the sulfurised glucose was reacted with $FeCl_2$ under controlled inert (nitrogen) conditions for 5 weeks and in triplicate for reproducibility. In all cases this yielded a black liquid phase with greyish-black debris (solid phase) which was partly in suspension with the remainder settled out, suggesting the formation of iron sulfides and/or other minerals. As control experiments, ammonium polysulfide ($H_8N_2S_3$) and pure D-glucose were subjected to

the same $FeCl_2$ treatment. The $H_8N_2S_3$ control experiment yielded a product similar (i.e. physical observation) to the starting material while the D-glucose control experiment solution remained clear and no solid material was formed indicating, although other reactions could have happened, no iron sulfide formation occurred.

4.3.2.1 Liquid Phases

CHNS analyses on the freeze-dried liquid phase of the Fe-treated sulfurised glucose indicates that the initial amount of sulfur (8.7 wt. %) in the original sulfurised glucose was removed by approximately 50 % with final concentrations ranging between 4.0 wt. % and 4.8 wt. %. Similarly, ICP-AES analysis of the liquid phase also indicates that only half of the original S (380 - 450 mg/L) is still present in the liquid phase at the end of the experiment (170 - 210 mg/L; Table 4.2). S in the Fe-treated polysulfide (control experiment) was lower by approximately 40 % while the final concentrations of Fe in both the Fe-treated sulfurised glucose and polysulfide were lower by 10 % - 20 % (Table 4.2), indicating the possibility of the formation of Fe sulfides. The concentration of Fe in solution in the Fe-treated pure glucose control experiment remained constant throughout the whole experiment (99 mg/L; Table 4.2), implying Fe may not react directly with glucose and thus discounting the possibility of formation of other Fe non-sulfide minerals.

Table 4.2: Initial and final concentrations of sulfur and iron in the liquid phase of the experiments obtained from ICP-AES analysis.

Experiment	ICP-AES (mg/L)			
	Sulfur		Iron	
	initial	final	initial	final
Sulfurised Glucose	380 - 450	170 - 210 (45 - 47)[b]	180 - 210	165 - 170 (92 - 80)[b]
Pure Glucose[a]	n.d.[c]	n.d.[c]	220	218 (99)[b]
Polysulfide[a]	406	243 (60)[b]	224	188 (84)[b]

[a] Controls. [b] Approximate percentage of the original S and Fe remaining in brackets.
[c] Not determined.

Since the amount of S utilised by Fe in the Fe-treated sulfurised glucose was only reduced by half of the initial amount used, 50 % of the remaining S is still in the liquid phases. Py-GC-MS of the freeze-dried liquid phase showed the presence of alkylated thiophenic compounds, similar to those observed in the original sulfurised glucose (Fig. 4.2b), indicating that although sulfurised glucose and Fe reactions could have occurred, not all the sulfurised glucose was

utilised by the Fe. Interestingly, a change in the distribution pattern of the thiophenes was observed with a relative increase in the presence of ethyl and/or dimethylthiophenes and propyl and/or trimethylthiophenes if compared to the thiophenes and methylthiophenes (Fig. 4.2b). This suggest that potentially specific parts of the S originally bound to the carbohydrate material were lost during the experiments.

4.3.2.2 Solid Phases

Since elemental CHNS and ICP-AES analyses indicated a reduction in the amount of S and Fe in the liquid phases of both the Fe-treated sulfurised glucose and polysulfide, the mineralogy of the solid phases were characterized using XRD. XRD analysis of the Fe-treated sulfurised glucose showed the presence of ferrotochilinite [$6FeS \cdot 5Fe(OH)_2$] a dark bronze, monoclinic iron monosulfide (FeS) mineral formed at low temperatures (Pekov et al., 2013) and ivsite [$Na_3H(SO_4)_2$], a colourless (whitish in powdered form), monoclinic sulfate-rich mineral with Na and H (Fig. 4.3a; Filatov et al., 2016). Other minerals identified were maghemite (γ-Fe_2O_3), a brownish low temperature oxidation product of magnetite (Kim et al., 2012; Ruíz-Baltazar et al., 2015) and halite (NaCl) which was formed by the reaction of Na and Cl from NaHS and $FeCl_2$ used in the experiments dominate the spectrum with an additional set of peaks at 10º, 24º, 25º and 38º that could be glucose (Fig. 4.3a). In contrast, XRD analysis of the Fe-treated polysulfide showed the presence of salammoniac (ammonium chloride) and a dominance of S_8 (Fig. 4.3b). The physico-chemical properties of the minerals observed are consistent with the chemistry of the reactants and the conditions under which the experiments were completed as well as the elemental CHNS and ICP-AES results. Furthermore, although iron sulfides such as pyrite, troilite, pyrrhotite and greigite have not been observed, their formation cannot be discounted owing to the limitation of XRD analyses, which has ~ 2 % detection limit for mixed materials (Norton, 2015). ESEM-backscattered (BS) electron imaging and EDS analysis of the Fe-treated sulfurised glucose show a large grey asterisk-like crystal and dark large structures with curvy edges indicating the presence of NaCl and S respectively (Fig. 4.4a & c). Also present were structures resembling the ferrotochilinite crystals reported by Pekov et al., 2013 (structures with a question mark in Fig. 4.4a) and many tiny circle and/or oval shaped amorphous spots ranging from 1 µm to 5 µm were observed. These spots were regions where S and Fe correlated as indicated by EDS (e.g. arrowed 1 & 2 in Fig. 4.4a & c). These spots could be iron monosulfides as previous studies suggest iron sulfides formed at low temperatures show no crystals (Sweeney & Kaplan, 1973). A BS electron image of the Fe-treated polysulfide also showed the presence of S as denoted by the presence of dark large

structures with curvy edges in line with what was observed in the Fe-treated sulfurised glucose (Fig. 4.4b). However, in contrast to the Fe-treated sulfurised glucose, spots where S and Fe correlated (arrowed 3 & 4) were mostly crystalline (Fig. 4.4c). The presence of Si in the samples could potentially arise from leaching of the glassware used in the experiment or from the glass slides. Overall, the ESEM-EDS result is consistent with the XRD result and the chemistry of the elements/compounds used for the experiment. However, information on the oxidation states of the S and Fe is required to fully understand the series of possible minerals phases formed.

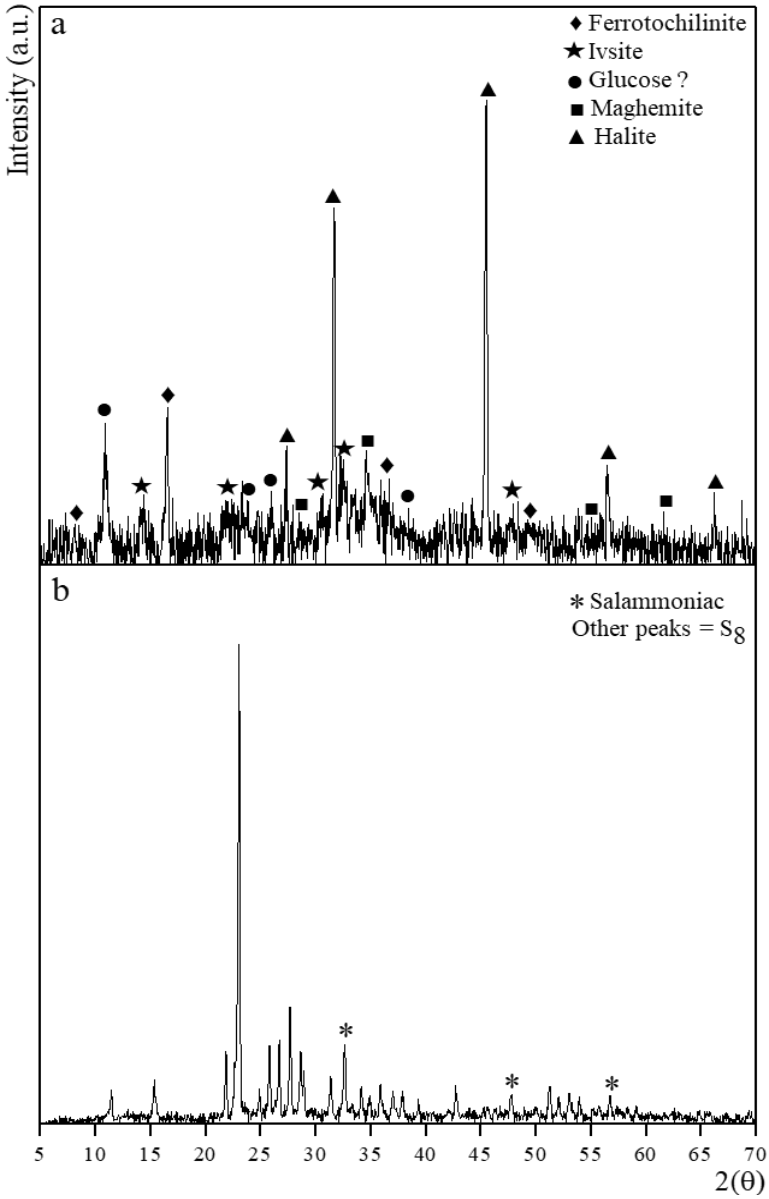

Figure 4.3: Diffractograms of solid phases of Fe-treated (a) sulfurised D-glucose and (b) ammonium polysulfide. Experiments were completed in triplicate and XRD patterns were all the same hence only one was of the triplets is presented here.

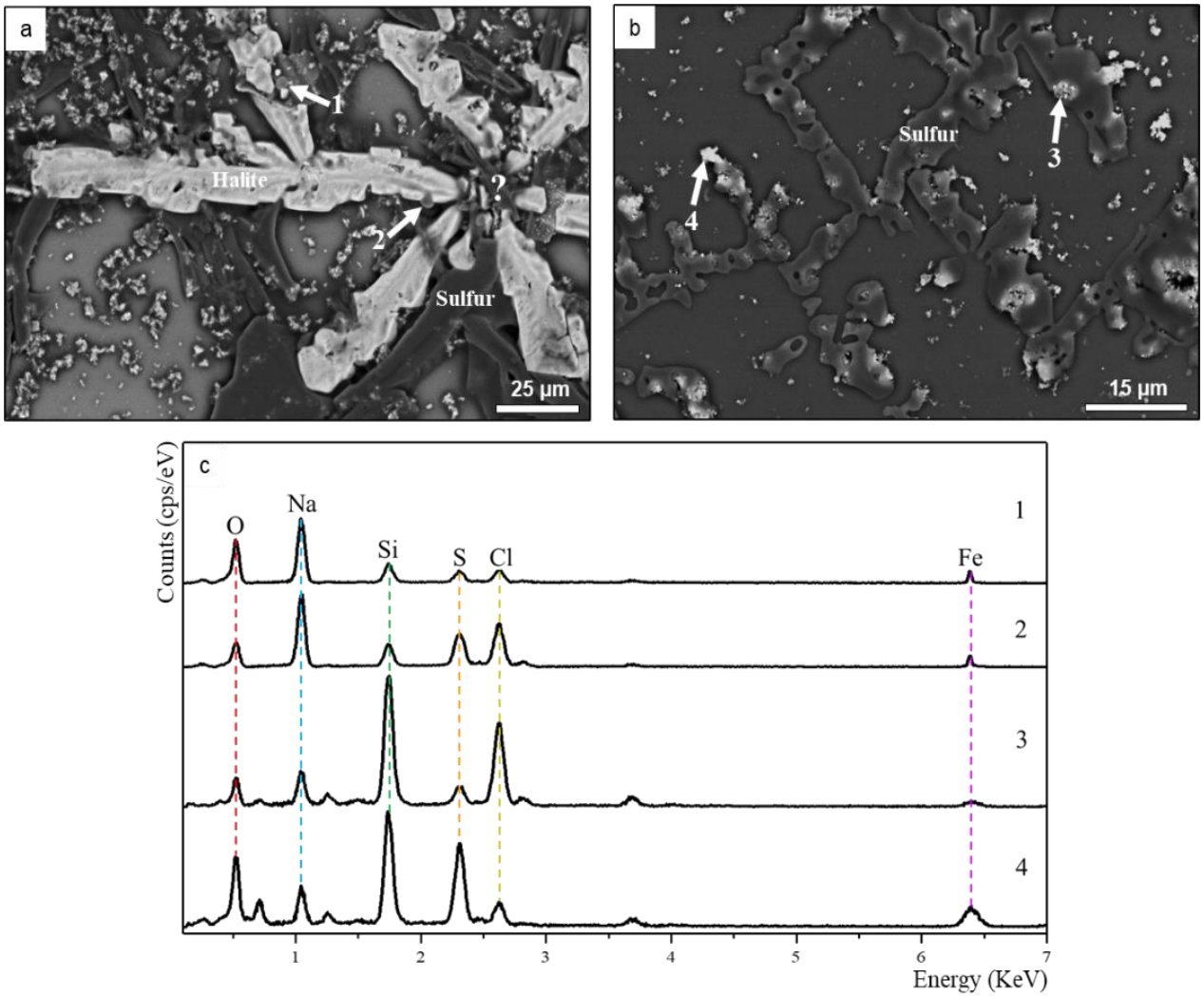

Figure 4.4: High resolution backscattered electron images of solid phases of Fe-treated (a) sulfurised carbohydrate and (b) ammonium polysulfide (c) show ESEM-EDS spectra collected from numbered arrowed numbers in (a) and (b). White asterisk-like crystal is halite and structure designated with question mark is similar to ferrotochilinite as reported by Pekov et al. (2013).

4.3.3 Micro-Focus X-ray imaging and X-ray Absorption Near Edge Spectroscopy

MF-XRF imaging of the sulfurised glucose was carried out with the same relative intensity for the fluorescence emission of S (red) and Si (bluish-green) at a number of key incident energies [2470.7 eV (fully reduced S), 2473.70 eV, 2479.0 eV and 2483.3 eV (fully oxidised sulfate type S)] to understand S species present and their distribution. Results of the imaging indicate that all of the S species are distributed similarly across the mapped area with a relatively strong sulfate signal (Fig. 4.5a - d). Sulfate appears to be abundant although the experiments were completed strictly under anoxic conditions and this suggest a partial reduction of the fully reduced S could have occurred or the original S species used in the experiments were partially oxidized. Si shows up better in the lowest energy map because there was less fully reduced

sulfur compared to the other species and thus less background. This is unequivocally in line with the FTIR analysis which shows the dominance of S-O and S=O stretches denoting the prevalence of sulfate and other oxidised S species (Fig. 4.1b, Table 4.1).

The MF-XRF chemical mapping of the solid phase of the Fe-treated sulfurised glucose was completed to understand the changes in the abundance and distribution of S and Fe after Fe treatment. Results show S (green) and Fe (red) across the whole scanned area with skeletal precipitates (possibly halite) showing a strong signal in the S image while relatively high concentration Fe spots ranging from 1 µm up to 0.2 mm in size, discretely dispersed in the Fe map (Fig. 4.5e & f). The combined S and Fe chemical map indicates a strong correlation between these elements in some spots (Fig. 4.5g; orange spots) consistent with previous ESEM-EDS analyses. S K-edge XANES spectra (average of 26 spectra) taken within these orange spots show, besides the presence of the original sulfate, an evolution to different forms of S (Fig. 4.6a; S. glucose + Fe spectra). In the S. Glucose + Fe spectrum both the sulfate and organic S contributions to the spectrum were lower compared to the S. Glucose spectrum thus indicating a significant shift in the S speciation towards a more reduced profile, in line with the anoxic experimental conditions. Much of the organic S was fully reduced to S with a formal valence of minus 2 (S^{-2}) as indicated by its energy shift from 2473.60 eV to 2470.26 eV, an energy lower than that of the pyrite S standard (2472.88 eV) with S^{-1} formal valence, suggesting the presence of an S^{-2} component comparable to pyrrhotite S or troilite S. Linear combination fitting (LCF) and comparison with spectra from previous studies indicate that the sulfate was partially reduced to sulfonate (black dashed circle on S. glucose + Fe spectra in Fig. 4.6; Vairavamurthy et al., 1994, 1997; Morgan et al., 2012; Greenfield et al., 2015; Birdwell et al., 2018; Kashiwabara et al., 2019). LCF also indicated the presence of minute amounts of pyrite S (7 %), elemental S (2 %) and unresolved organic type S which could be the remnant of unreduced original sulfurised glucose. Fe K-edge XANES analyses were taken at 3 points where S K-edge XANES had been obtained (Fig. 4.5g; arrows with numbers 1 - 3). These spectra (averaged to a spectrum) indicate a close fit with the FeS and pyrrhotite/troilite Fe standards (Fig. 4.6b; S. glucose + Fe spectra). LCF against the FeS, pyrrhotite/troilite Fe and pyrite Fe standards show that the Fe-treated sulfurised glucose consist of about 57 % FeS, 33 % pyrrhotite/troilite Fe like component and 10 % pyrite Fe, consistent with the S K edge XANES analysis. XRD analysis previously indicated the possible presence of maghemite and, as it is a non S mineral, Fe could be present in places but not bound to S, which could account for enhancing the peak at 7128 eV in the Fe-treated sulfurised glucose spectra.

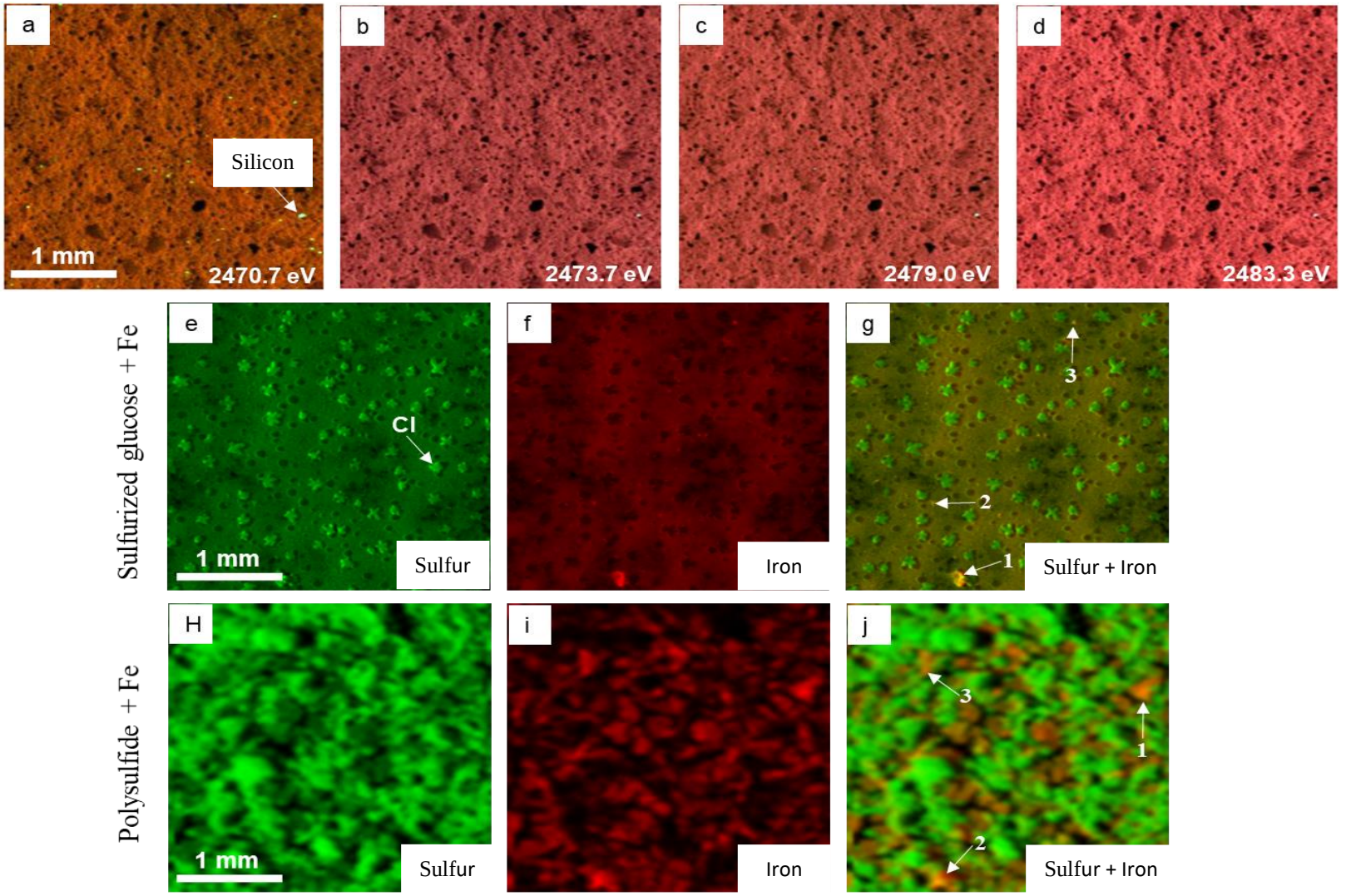

Figure 4.5: Micro-focus spatially resolved X-ray images of (a-d) sulfurised glucose mapped at 2470.7, 2473.7, 2479.0 and 2483.3 eVs, (e-g) Fe-treated sulfurised glucose maps windowed for total S (green), total Fe (red) and combined total S and Fe (yellow) and (h-j) Fe-treated polysulfide maps windowed for total S (green), total Fe (red) and combined total S and Fe (yellow). Maps were obtained at 8000 eV. Arrowed numbers indicate where Fe XANES were taken.

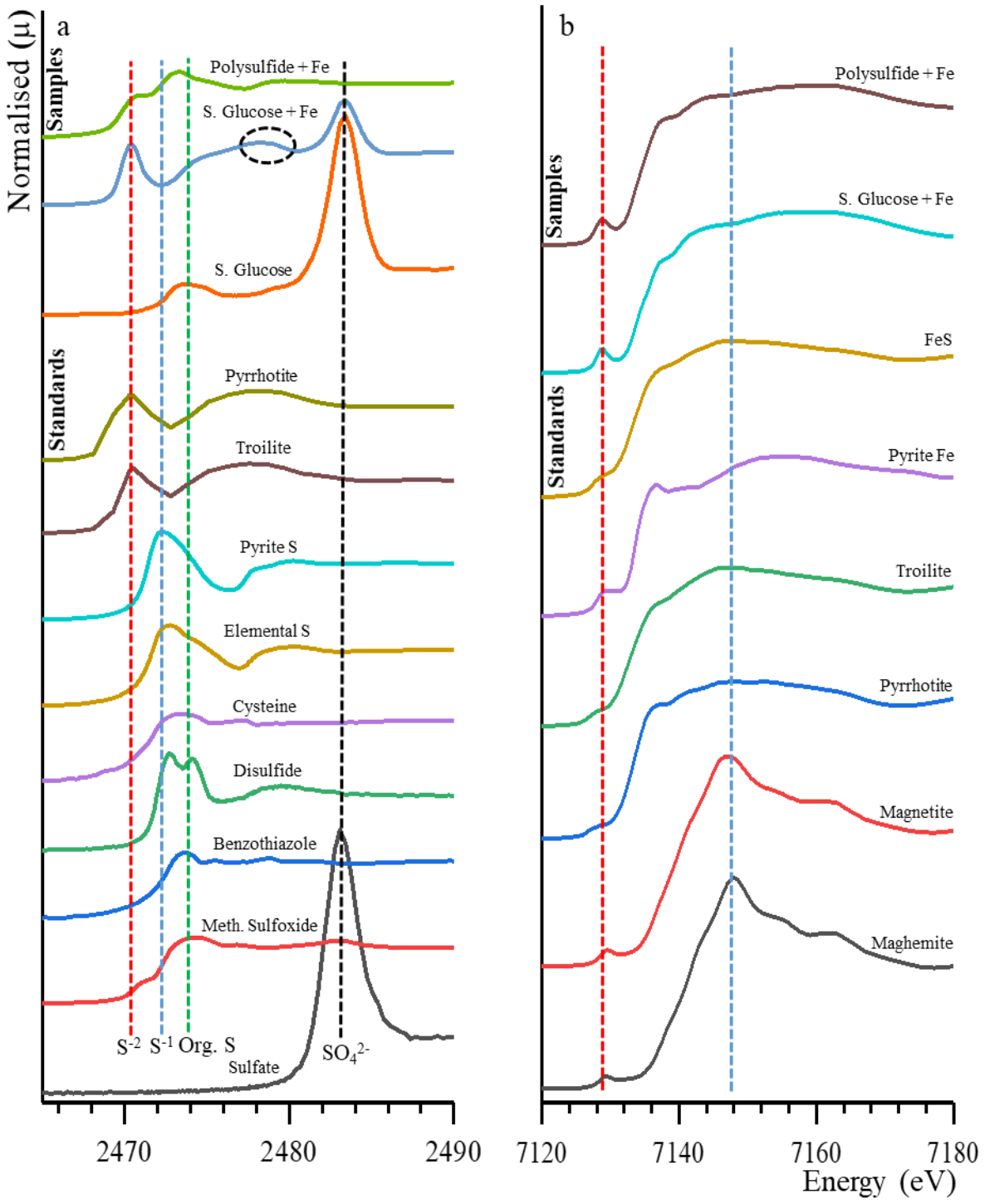

Figure 4.6: (a) S K-edge XANES spectra of sulfurised glucose, Fe-treated sulfurised glucose and Fe-treated polysulfide and standards (b) Fe K-edge XANES spectra of Fe-treated sulfurised glucose and Fe-treated polysulfide and standards. The vertical dashed red blue, green, black lines and the circled dashed lines in (a) represent absorption spectrum of S^{-2}, S^{-1}, organic S, sulfate and sulfonate respectively. The vertical dashed red and blue lines represent absorption spectrum maxima for reduced Fe and oxidised respectively.

MF-XRF chemical mapping of the solid phase of the Fe-treated polysulfide showed relatively high concentrations of S (green; 1 µm - 0.5 mm in size) and Fe (red; 1 µm - 0.3 mm in size) across the whole scanned area (Fig. 4.5h & i). The combined S and Fe chemical map showed a more intense S and Fe correlation compared to the Fe-treated sulfurised glucose (Fig. 4.5j; orange spots) consistent with previous ESEM-EDS analyses. S K-edge XANES spectra (averaged of 29 spectra) taken on the S and Fe correlated regions of interest showed the presence of S^{-2} and S^{-1} components and a complete absence of sulfate type S (polysulfide + Fe spectra; Fig. 4.6a). Some intermediate S species (e.g. peak/hump at 2473.0 eV and 2478.0 eV) were not assigned due to time limitations which left us unable to collect S K-edge XANES spectra on the original non Fe polysulfide for comparisons. However, LCF of the Fe-treated polysulfide and comparison with the S^{-2} (pyrrhotite and troilite), S^{-1} (pyrite S) and elemental S standards show 64 %, 27 % and 9 % were S^{-2} components, pyrite S and elemental S, respectively. LCF with organic type S was not completed because the polysulfide used was inorganic. Fe K-edge XANES analysis, average of 3 points collected where S K-edge XANES were previously obtained on the combined chemical map (Fig. 4.5j; arrowed numbers 1 - 3), show a close fit with the FeS and pyrrhotite/troilite Fe standards (polysulfide + Fe spectra; Fig. 4.6b) directly comparable to the Fe K-edge XANES analysis of the Fe-treated sulfurised glucose. LCF against the FeS, pyrrhotite/troilite Fe and pyrite Fe standards reveal that the Fe-treated polysulfide consisted of 37 % FeS, 42 % pyrrhotite/troilite Fe like component and 21% pyrite Fe, indicating a low FeS concentration and high pyrrhotite/troilite Fe like component and pyrite Fe contribution if compared to the Fe K-edge XANES spectral analysis of the Fe-treated sulfurised glucose.

Combined, these results indicate that Fe sulfides could be formed directly from sulfurised carbohydrate (glucose) and polysulfides in the presence of reactive Fe. The addition of Fe to sulfurised glucose and the polysulfide led to a mix of S and Fe speciation. Much of the S in both experiments (especially organic S in the case of Fe-treated sulfurised glucose) were reduced to a mixture of S^{-2} and S^{-1} components with S^{-2} moieties dominating. Some of these moieties combined with Fe to form a pyrrhotite/troilite like mineral solid phase and trace amounts of the intermediate pyrite S.

4.3.4 Implications for Sulfurised Carbohydrate (Glucose) Stability and Iron Sulfide Formation in the Natural Environment

Synthesis of FeS_2 from a metastable FeS precursors is known to be a rapid process (Berner, 1969; Sweeney and Kaplan, 1973; Rickard, 1975; Luther, 1991; Gartman and Luther, 2013; Rickard, 2019). Luther (1991) proposed that direct and instantaneous formation of FeS_2 from a polysulfide precursor is almost unachievable, thus FeS precursors form first after which FeS_2 precipitation ensues depending on pH, temperature and time. Rickard (2019) further proposed that the characteristics of FeS_2 formation are consistent with the LaMer model (LaMer & Dinegar, 1950; LaMer, 1952; Wilkin & Barnes, 1997) which involves; (i) a slow nucleation phase which require a big energy cost to step over in order to start the formation of a metastable FeS nuclei/precursor (Schoonen and Barnes, 1991), (ii) a rapid nucleation phase where exponential conversation of FeS to FeS_2 occurs (Read, 1968; Rickard & Luther, 2007) and (iii) a nucleation decline phase due to exhaustion of nutrients/reactants (Rickard & Luther, 2007). Our experiment/result is consistent with the LaMer model and the proposal of Luther (1991). Addition of Fe to the sulfurised glucose and polysulfide immediately turned the solutions black marking the beginning of the slow phase of metastable FeS (pyrite precursor) formation as confirmed by XRD and ESEM-EDS analyses. Fe K-edge XANES analysis in this study suggest that under specific conditions (pH 7.4, 30 ºC and 5 weeks) there was sufficient time and chemical exchange to allow the nucleation of very small poorly formed FeS nuclei/precursors, which started to stabilise by converting to minerals with co-ordination of S and Fe that is similar to the co-ordination environment and oxidation state of S and Fe in pyrrhotite and troilite (S^{-2} minerals). Some amounts of these S^{-2} minerals further converted to form traces of a more stable S^{-1} iron sulfide which is likely to be FeS_2. The conversion of FeS to S^{-2} components was more significant in the Fe-treated polysulfide compared to the Fe-treated sulfurised glucose. This could be due to the presence of the OM in the Fe-treated sulfurised glucose which has been reported to subdue FeS reactivity when in excess (Morgan et al., 2012).

Collectively, these results indicate that sulfurised carbohydrates are partly unstable in the presence of reactive Fe owing to the formation of Fe sulfides after Fe treatment. However, the presence of sulfurised glucose in the product after Fe treatment suggests that the Fe sulfide materials were likely either formed from that part of the sulfurised carbohydrate with weak S-S bonds, while the stronger C-S bonds were stable, and could be preserved or it could be a matter of time before Fe strips off all S in the sulfurised carbohydrate to form Fe sulfides.

4.4 Conclusion

Series of experiments were completed to investigate the stability of sulfurised OM in the presence of reactive Fe. Product of Fe-treated sulfurised glucose was analysed using a combination of bulk/molecular geochemical, petrographic and synchrotron-based analyses. Results indicate, for the first time, that some S in the sulfurised glucose was utilised by Fe to form metastable FeS materials, which were subsequently converted to minerals with co-ordination of S and Fe that is similar to the co-ordination environment and oxidation state of S and Fe in S^{-2} Fe sulfide minerals (likely pyrrhotite or troilite). Some of these S^{-2} minerals further converted to form traces of a more stable S^{-1} iron sulfides likely FeS_2. However, there was still sulfurised glucose in the product after Fe treatment, suggesting that potentially (specific) parts of the S originally bound to the glucose were lost during the experiments. The metastable FeS materials were likely either formed from that part of the sulfurised glucose with weak S-S bonds, while the stronger C-S bonds were stable, and could be preserved for millions of years. However, it cannot be excluded that it is a matter of time before all S in the sulfurised glucose would be stripped off to form iron sulfides. Overall, reaction between OM and S could be said to be partially reversible in the presence of reactive Fe species.

Acknowledgement

Petroleum Technology Development Fund (Nigeria) is thanked for funding YA (16PhD153), Diamond Lightsource (DLS, UK) for beamtime award (SP22220). We gratefully thank Tina Geraki (DLS) for help with XAS data collection, John Waters for help with XRD and Paul Lythgoe for help with ICP-AES.

Reference

Amrani, A., & Aizenshtat, Z. (2004). Reaction of polysulfide anions with α, β, unsaturated isoprenoid aldehydes in aquatic media: Simulation of oceanic conditions. *Organic Geochemistry 35, 8*, 909–921. https://doi.org/10.1016/j.orggeochem.2004.04.002

Antler, G., Turchyn, A. V., Ono, S., Sivan, O., & Bosak, T. (2017). Combined ^{34}S, ^{33}S and ^{18}O Isotope Fractionations Record Different Intracellular Steps of Microbial Sulfate Reduction. *Geochimica et Cosmochimica Acta*, *203*, 364–380. https://doi.org/10.1016/j.gca.2017.01.015

Arthur, M. A., Dean, W. E., & Stow, D. A. V. (1984). Models for the deposition of Mesozoic-Cenozoic fine-grained organic-carbon-rich sediment in the deep sea. *Geological Society, London, Special Publications*, *15*(1), 527–560. https://doi.org/10.1144/gsl.sp.1984.015.01.34

Arthur, M. A., Schlanger, S. O., & Jenkyns, H. C. (1987). The Cenomanian-Turonian Oceanic Anoxic Event, II. Palaeoceanographic controls on organic-matter production and preservation. *Geological Society, London, Special Publications*, *26*(1), 401–420. https://doi.org/10.1144/GSL.SP.1987.026.01.25

Basham, M., Filik, J., Wharmby, M. T., Chang, P. C. Y., El Kassaby, B., Gerring, M., Aishima, J., Levik, K., Pulford, B. C. A., Sikharulidze, I., Sneddon, D., Webber, M., Dhesi, S. S., Maccherozzi, F., Svensson, O., Brockhauser, S., Náray, G., & Ashton, A. W. (2015). Data Analysis WorkbeNch (DAWN). *Journal of Synchrotron Radiation*, *22*(3), 853–858. https://doi.org/10.1107/S1600577515002283

Berner, R. A. (1967). Diagenesis of iron sulfides in recent marine sediments. *American Association for the Advancement of Science*, *83*, 268–272.

Berner, R. A. (1969). The synthesis of framboidal pyrite. *Economic Geology*, *64*(4), 383–384. https://doi.org/10.2113/gsecongeo.64.4.383

Berner, R. A. (1989). Biogeochemical cycles of carbon and sulfur and their effect on atmospheric oxygen over phanerozoic time. *Global and Planetary Change*, *1*(1–2), 97–122. https://doi.org/10.1016/0921-8181(89)90018-0

Berner, R. A. (2005). The carbon and sulfur cycles and atmospheric oxygen from middle Permian to middle Triassic. *Geochimica et Cosmochimica Acta*, *69*(13), 3211–3217. https://doi.org/10.1016/j.gca.2005.03.021

Berner, R. A. (2006). Carbon, sulfur and O_2 across the Permian-Triassic boundary. *Journal of Geochemical Exploration*, *88*(1-3 SPEC. ISS.), 416–418. https://doi.org/10.1016/j.gexplo.2005.08.088

Birdwell, J. E., Lewan, M. D., Bake, K. D., Bolin, T. B., Craddock, P. R., Forsythe, J. C., & Pomerantz, A. E. (2018). Evolution of sulfur speciation in bitumen through hydrous pyrolysis induced thermal maturation of Jordanian Ghareb Formation oil shale. *Fuel*, *219*(September 2017), 214–222. https://doi.org/10.1016/j.fuel.2018.01.107

Bradley, A. S., Leavitt, W. D., Schmidt, M., Knoll, A. H., Girguis, P. R., & Johnston, D. T. (2016). Patterns of sulfur isotope fractionation during microbial sulfate reduction. *Geobiology*, *14*(1). https://doi.org/10.1111/gbi.12149

Canfield, D. E., Raiswell, R., Westrich, J. T., Reaves, C. M., & Berner, R. A. (1986). The use of chromium reduction in the analysis of reduced inorganic sulfur in sediments and shales. *Chemical Geology*, *54*(1–2), 149–155. https://doi.org/10.1016/0009-2541(86)90078-1

Coates, J. (2006). Interpretation of Infrared Spectra, A Practical Approach. In *Encyclopedia of Analytical Chemistry*. https://doi.org/doi:10.1002/9780470027318.a5606

Couture, R. M., Fischer, R., Van Cappellen, P., & Gobeil, C. (2016). Non-steady state diagenesis of organic and inorganic sulfur in lake sediments. *Geochimica et Cosmochimica Acta*, *194*. https://doi.org/10.1016/j.gca.2016.08.029

Demaison, G. J., & Moore, G. T. (1980). Anoxic environments and oil source bed genesis. *Organic Geochemistry*, *2*(1), 9–31. https://doi.org/10.1016/0146-6380(80)90017-0

Filatov, S. K., Karpov, G. A., Shablinskii, A. P., Krivovichev, S. V., Vergasova, L. P., & Antonov, A. V. (2016). Ivsite, Na3H(SO4)2, a new mineral from volcanic exhalations of fumaroles of the Fissure Tolbachik Eruption of the 50th Anniversary of the Institute of Volcanology and Seismology, Far East Branch, Russian Academy of Sciences. *Doklady Earth Sciences*, *468*(2), 632–635. https://doi.org/10.1134/S1028334X16060179

Filley, T. R., Freeman, K. H., Wilkin, R. T., & Hatcher, P. G. (2002). Biogeochemical controls on reaction of sedimentary organic matter and aqueous sulfides in holocene sediments of Mud Lake, Florida. *Geochimica et Cosmochimica Acta*, *66*(6), 937–954. https://doi.org/10.1016/S0016-7037(01)00829-8

Gartman, A., & Luther, G. W. (2013). Comparison of pyrite (FeS2) synthesis mechanisms to reproduce natural FeS2 nanoparticles found at hydrothermal vents. *Geochimica et Cosmochimica Acta*, *120*, 447–458. https://doi.org/10.1016/j.gca.2013.06.016

Gill, B. C., Lyons, T. W., & Saltzman, M. R. (2007). Parallel, high-resolution carbon and sulfur isotope records of the evolving Paleozoic marine sulfur reservoir. *Palaeogeography, Palaeoclimatology, Palaeoecology*, *256*(3–4), 156–173. https://doi.org/10.1016/j.palaeo.2007.02.030

Greenfield, M. L., Byrne, M., Mitra-Kirtley, S., Kercher, E. M., Bolin, T. B., Wu, T., Craddock, P. R., Bake, K. D., & Pomerantz, A. E. (2015). XANES measurements of sulfur chemistry during asphalt oxidation. *Fuel*, *162*, 179–185. https://doi.org/10.1016/j.fuel.2015.08.074

Herlihy, A. T., Mills, A. L., & Hall, C. (1986). The pH regime of sediments underlying acidified waters. *Biogeochemistry 2(1*), 377–381.

Herndl, G. J., & Reinthaler, T. (2013). Microbial control of the dark end of the biological pump. *Nature Geoscience*, *6*(9), 718–724. https://doi.org/10.1038/ngeo1921

Horner-Devine, M. C., Leibold, M. A., Smith, V. H., & Bohannan, B. J. M. (2003). Bacterial diversity patterns along a gradient of primary productivity. *Ecology Letters*, *6*(7), 613–622. https://doi.org/10.1046/j.1461-0248.2003.00472.x

Hurtgen, M. T., Pruss, S. B., & Knoll, A. H. (2009). Evaluating the relationship between the carbon and sulfur cycles in the later Cambrian ocean: An example from the Port au Port Group, western Newfoundland, Canada. *Earth and Planetary Science Letters*, *281*(3–4), 288–297. https://doi.org/10.1016/j.epsl.2009.02.033

Ibrahim, M., Alaam, M., El-Haes, H., Jalbout, A. F., & De Leon, A. (2006). Analysis of the structure and vibrational spectra of glucose and fructose. *Ecletica Quimica*, *31*(3), 15–21. https://doi.org/10.1590/S0100-46702006000300002

Jenkyns, H. C. (1980). Cretaceous anoxic events: from continents to oceans. *Journal of the Geological Society*, *137*(2), 171–188. https://doi.org/10.1144/gsjgs.137.2.0171

Kashiwabara, T., Toda, R., Nakamura, K., Yasukawa, K., Fujinaga, K., Kubo, S., Nozaki, T., Takahashi, Y., Suzuki, K., Kato, Y., Bennett, W. W., Lombi, E., Burton, E. D., Johnston, S. G., Kappen, P., Howard, D. L., Canfield, D. E., Lenstra, W. K., Hermans, M., … Penner-hahn, J. E. (2019). Sulfur speciation in heavy petroleums: Information from X-ray absorption near-edge structure. *Geochimica et Cosmochimica Acta*, *25*(1), 181–187. https://doi.org/10.1016/0016-7037(91)90343-4

Kim, W., Suh, C. Y., Cho, S. W., Roh, K. M., Kwon, H., Song, K., & Shon, I. J. (2012). A new method for the identification and quantification of magnetite-maghemite mixture using conventional X-ray diffraction technique. *Talanta*, *94*, 348–352. https://doi.org/10.1016/j.talanta.2012.03.001

Kok, M. D., Schouten, S., & Sinninghe Damsté, J. S. (2000). Formation of insoluble, nonhydrolyzable, sulfur-rich macromolecules via incorporation of inorganic sulfur species into algal carbohydrates. *Geochimica et Cosmochimica Acta*, *64*(15), 2689–2699. https://doi.org/10.1016/S0016-7037(00)00382-3

LaMer, V. K., & Dinegar, R. H. (1950). Theory, Production and Mechanism of Formation of Monodispersed Hydrosols. *Journal of the American Chemical Society*, *72*(11), 4847–4854. https://doi.org/10.1021/ja01167a001

LaMer, V. K. (1952). Nucleation in Phase Transitions. *Industrial & Engineering Chemistry*, *44*(6), 1270–1277. https://doi.org/10.1021/ie50510a027

Landa, M., Blain, S., & Christaki, U. (2015). Shifts in bacterial community composition associated with increased carbon cycling in a mosaic of phytoplankton blooms. *The ISME …*, 1–12. https://doi.org/10.1038/ismej.2015.105

Li, M., Baker, B. J., Anantharaman, K., Jain, S., Breier, J. A., & Dick, G. J. (2015). Genomic and transcriptomic evidence for scavenging of diverse organic compounds by widespread deep-sea archaea. *Nature Communications*, *Accepted*(May), 1–6. https://doi.org/10.1038/ncomms9933

Li, M., Jain, S., & Dick, G. J. (2016). Genomic and transcriptomic resolution of organic matter utilization among deep-sea bacteria in guaymas basin hydrothermal plumes. *Frontiers in Microbiology*, *7*, 1125. https://doi.org/10.3389/fmicb.2016.01125

Luckge, A., Horsfield, B., Littke, R., & Scheeder, G. (2002). Organic matter preservation and sulfur uptake in sediments from the continental margin off Pakistan. *Organic Geochemistry*, *33*(4), 477–488. https://doi.org/10.1016/S0146-6380(01)00171-1

Luther, G. W. (1991). Pyrite synthesis via polysulfide compounds. *Geochimica et Cosmochimica Acta*, *55*(10), 2839–2849. https://doi.org/10.1016/0016-7037(91)90449-F

Schoonen, M. A. A. & Barnes, H. L. (1991). Reactions forming pyrite and marcasite from solution: II. Via FeS precursors below 100°C. *Geochimica et Cosmochimica Acta*, *55*, 1505–1514.

Mann, K. H., & Lazier, J. R. N. (2013). Dynamics of Marine Ecosystems: Biological-Physical Interactions in the Oceans: Third Edition. In *Dynamics of Marine Ecosystems: Biological-Physical Interactions in the Oceans: Third Edition*. https://doi.org/10.1002/9781118687901

McCarren, J., Becker, J. W., Repeta, D. J., Shi, Y., Young, C. R., Malmstrom, R. R., Chisholm, S. W., & DeLong, E. F. (2010). Microbial community transcriptomes reveal microbes and metabolic pathways associated with dissolved organic matter turnover in the sea. *Proceedings of the National Academy of Sciences of the United States of America*, *107*(38), 16420–16427. https://doi.org/10.1073/pnas.1010732107

Morgan, B., Burton, E. D., & Rate, A. W. (2012). Iron monosulfide enrichment and the presence of organosulfur in eutrophic estuarine sediments. *Chemical Geology*, *296–297*, 119–130. https://doi.org/10.1016/j.chemgeo.2011.12.005

Naeher, S., Smittenberg, R. H., Gilli, A., Kirilova, E. P., Lotter, A. F., & Schubert, C. J. (2012). Impact of recent lake eutrophication on microbial community changes as revealed by high resolution lipid biomarkers in Rotsee (Switzerland). *Organic Geochemistry*, *49*, 86–95. https://doi.org/10.1016/j.orggeochem.2012.05.014

Nelson, B. C., Eglinton I., T., Seewald, J. S., Vairavamurthy, M. A., & Miknis, F. P. (1995). Transformations in Organic Sulfur Speciation During Maturation of Monterey Shale: Constraints from Laboratory Experiments. *Geochemical Transformations of Sedimentary Sulfur*, *612*(April), 138–166. https://doi.org/10.1021/bk-1995-0612.ch008

Norton, J. T. (2015). Uses and limitations of X-ray diffraction method. *Journal of Applied Physics 8*, 307.

Oni, O. E., Schmidt, F., Miyatake, T., Kasten, S., Witt, M., Hinrichs, K. U., & Friedrich, M. W. (2015). Microbial communities and organic matter composition in surface and subsurface sediments of the Helgoland mud area, North Sea. *Frontiers in Microbiology*, *6*. https://doi.org/10.3389/fmicb.2015.01290

Orr, W. L. (1978). Sulfur in heavy oils, oil sands and oil shales. *Oil Sand and Oil Shale Chemistry: New York, Verlag Chemie*, 223--243.

Orr, W. L. (1986). Kerogen/asphaltene/sulfur relationships in sulfur-rich Monterey oils. *Organic Geochemistry*, *10*(1–3), 499–516. https://doi.org/10.1016/0146-6380(86)90049-5

Ouverney, C. C., & Fuhrman, J. A. (2000). Marine planktonic archaea take up amino acids. *Applied and Environmental Microbiology*, *66*(11), 4829–4833. https://doi.org/10.1128/AEM.66.11.4829-4833.2000

Pekov, I. V., Sereda, E. V., Polekhovsky, Y. S., Britvin, S. N., Chukanov, N. V., Yapaskurt, V. O., & Bryzgalov, I. A. (2013). Ferrotochilinite, 6FeS · 5Fe(OH)2, a new mineral from the Oktyabr'sky deposit, Noril'sk district, Siberia, Russia. In *Geology of Ore Deposits* (Vol. 55, Issue 7, pp. 567–574). https://doi.org/10.1134/S1075701513070106

Pratt, L. M. (1984). Influence of paleoenvironmental factors on preservation of organic matter in middle cretaceous greenhorn formation, pueblo, colorado. In *American Association of Petroleum Geologists Bulletin* (Vol. 68, Issue 9, pp. 1146–1159). https://doi.org/10.1306/AD4616E7-16F7-11D7-8645000102C1865D

Pratt, L. M., & King, J. D. (1986). Variable marine productivity and high eolian input recorded by rhythmic black shales in Mid-Cretaceous pelagic deposits from central Italy. *Paleoceanography*, *1*(4), 507–522. https://doi.org/10.1029/PA001i004p00507

Ravel, B., & Newville, M. (2005). ATHENA, ARTEMIS, HEPHAESTUS: data analysis for X-ray absorption spectroscopy using IFEFFIT. *Journal of Synchrotron Radiation*, *12*(4), 537–541. https://doi.org/10.1107/S0909049505012719

Read, R. A. (1968). Deformation and metamorphism of the San Dionisio pyritic ore body, Rio Tinto, Spain [PhD thesis, Imperial College London]. http://hdl.handle.net/10044/1/16056

Rickard, D. (2019). How long does it take a pyrite framboid to form? *Earth and Planetary Science Letters*, *513*, 64–68. https://doi.org/10.1016/j.epsl.2019.02.019

Rickard, D., & Luther, G. W. (2007). Chemistry of iron sulfides. In *Chemical Reviews* (Vol. 107, Issue 2). https://doi.org/10.1021/cr0503658

Rickard, D. T. (1975). Kinetics and mechanism of pyrite formation at low temperatures. *American Journal of Science*, *275*, 636–652.

Ruíz-Baltazar, A., Esparza, R., Rosas, G., & Pérez, R. (2015). Effect of the Surfactant on the Growth and Oxidation of Iron Nanoparticles. *Journal of Nanomaterials*, *2015*(July). https://doi.org/10.1155/2015/240948

Schneckenburger, P., Adam, P., Albrecht, P., Organique, L. D. G., Cnrs, L., Chimie, I. De, & Pasteur, U. L. (1998). *Thioketones as key intermediates in the reduction of ketones to thiols by HS− in natural environments* (Vol. 39, pp. 447–450).

Schouten, S., van Driel, G. B., Sinninghe Damsté, J. S., & de Leeuw, J. W. (1993). Natural sulphurization of ketones and aldehydes: A key reaction in the formation of organic sulphur compounds. *Geochimica et Cosmochimica Acta*, *57*(23–24), 5111–5116. https://doi.org/10.1016/0016-7037(93)90613-2

Schunck, H., Lavik, G., Desai, D. K., Großkopf, T., Kalvelage, T., Löscher, C. R., Paulmier, A., Contreras, S., Siegel, H., Holtappels, M., Rosenstiel, P., Schilhabel, M. B., Graco, M., Schmitz, R. A., Kuypers, M. M. M., & LaRoche, J. (2013). Giant Hydrogen Sulfide Plume in the Oxygen Minimum Zone off Peru Supports Chemolithoautotrophy. *PLoS ONE*, *8*(8). https://doi.org/10.1371/journal.pone.0068661

Sinninghe Damsté, J. S., & de Leeuw, J. W. (1990). Analysis, structure and geochemical significance of organically-bound sulphur in the geosphere: State of the art and future research. *Organic Geochemistry*, *16*(4–6), 1077–1101. https://doi.org/10.1016/0146-6380(90)90145-P

Sinninghe Damsté, J. S., Kock-Van Dalen, A. C., de Leeuw, J. W., & Schenck, P. A. (1988). Identification of homologous series of alkylated thiophenes, thiolanes, thianes and benzothiophenes present in pyrolysates of sulphur-rich kerogens. *Journal of Chromatography A*, *435*(C), 435–452. https://doi.org/10.1016/S0021-9673(01)82208-1

Sinninghe Damsté, J. S., Kok, M. D., Köster, J., & Schouten, S. (1998). Sulfurized carbohydrates: An important sedimentary sink for organic carbon? *Earth and Planetary Science Letters*, *164*(1–2), 7–13. https://doi.org/10.1016/S0012-821X(98)00234-9

Solé, V. A., Papillon, E., Cotte, M., Walter, P., & Susini, J. (2007). A multiplatform code for the analysis of energy-dispersive X-ray fluorescence spectra. *Spectrochimica Acta Part B: Atomic Spectroscopy*, *62*(1), 63–68. https://doi.org/https://doi.org/10.1016/j.sab.2006.12.002

Sweeney, R. E., & Kaplan, I. R. (1973). Pyrite framboid formation: Laboratory synthesis and marine sediments. *Economic Geology*, *68*(5), 618–634. https://doi.org/10.2113/gsecongeo.68.5.618

Turchyn, A. V., Antler, G., Byrne, D., Miller, M., & Hodell, D. A. (2015). Microbial sulfur metabolism evidenced from pore fluid isotope geochemistry at Site U1385. *Global and Planetary Change*, *141*, 82–90. https://doi.org/10.1016/j.gloplacha.2016.03.004

Vairavamurthy, A., Zhou, W., Eglinton, T., & Manowitz, B. (1994). Sulfonates: A novel class of organic sulfur compounds in marine sediments. *Geochimica et Cosmochimica Acta*, *58*(21), 4681–4687. https://doi.org/10.1016/0016-7037(94)90200-3

Vairavamurthy, M. a, Maletic, D., Wang, S. K., Manowitz, B., Eglinton, T. I., & Lyons, T. (1997). Characterization of sulfur-containing functional groups in sedimentary humic substances by X-ray absorption near-edge structure spectroscopy. *Energy & Fuels*, *11*(3), 546–553. https://doi.org/10.1021/ef960212a

van Dongen, B. E., Schouten, S., Baas, M., Geenevasen, J. A. J., & Sinninghe Damsté, J. S. (2003). An experimental study of the low-temperature sulfurization of carbohydrates. *Organic Geochemistry*, *34*(8), 1129–1144. https://doi.org/10.1016/S0146-6380(03)00060-3

van Dongen, B. E., Schouten, S., Baas, M., Geenevasen, J. A. J., Sinninghe Damsté, J. S., McNamara, M. E., van Dongen, B. E., Lockyer, N. P., Bull, I. D., Orr, P. J., Roberts, A. P., Schouten, S., Jiang, W. T., Florindo, F., Pancost, R. D., & Sinninghe Damsté, J. S. (2003). An experimental study of the low-temperature sulfurization of carbohydrates. *Organic Geochemistry*, *37*(4), 1109–1118. https://doi.org/10.1021/ef0202283

van Dongen, B. E., Schouten, S., & Sinninghe Damsté, J. S. (2006). Preservation of carbohydrates through sulfurization in a Jurassic euxinic shelf sea: Examination of the Blackstone Band TOC cycle in the Kimmeridge Clay Formation, UK. *Organic Geochemistry*, *37*(9), 1052–1073. https://doi.org/10.1016/j.orggeochem.2006.05.007

van Kaam-Peters, H. M. E., Schouten, S., De Leeuw, J. W., & Sinninghe Damsté, J. S. (1997). A molecular and carbon isotope biogeochemical study of biomarkers and kerogen pyrolysates of the Kimmeridge Clay Facies: Palaeoenvironmental implications. *Organic Geochemistry*, *27*(7–8), 399–422. https://doi.org/10.1016/S0146-6380(97)00084-3

van Kaam-Peters, H. M. E., Schouten, S., Köster, J., & Damstè, J. S. S. (1998). Controls on the molecular and carbon isotopic composition of organic matter deposited in a Kimmeridgian euxinic shelf sea: Evidence for preservation of carbohydrates through sulfurisation. *Geochimica et Cosmochimica Acta*, *62*(19–20), 3259–3283. https://doi.org/10.1016/S0016-7037(98)00231-2

Wagreich, M., Hu, X., & Sageman, B. (2011). Causes of oxic-anoxic changes in Cretaceous marine environments and their implications for Earth systems-An introduction. *Sedimentary Geology*, *235*(1–2), 1–4. https://doi.org/10.1016/j.sedgeo.2010.10.012

Waldo, G. S., Carlson, R. M. K., Moldowan, J. M., Peters, K. E., & Penner-hahn, J. E. (1991). Sulfur speciation in heavy petroleums: Information from X-ray absorption near-edge structure. *Geochimica et Cosmochimica Acta*, *55*(3), 801–814. https://doi.org/10.1016/0016-7037(91)90343-4

Walker, J. C. G. (1986). Global geochemical cycles of carbon, sulfur and oxygen. *Marine Geology*, *70*(1–2), 159–174. https://doi.org/10.1016/0025-3227(86)90093-9

Werne, J. P., Hollander, D. J., Lyons, T. W., & Sinninghe Damsté, J. S. (2004). Organic sulfur biogeochemistry : Recent advances and future research directions. *Geological Society of America 4, 135–150.*

Werne, J. P., Lyons, T. W., Hollander, D. J., Formolo, M. J., & Sinninghe Damsté, J. S. (2003). Reduced sulfur in euxinic sediments of the Cariaco Basin: Sulfur isotope constraints on organic sulfur formation. *Chemical Geology*, *195*(1–4), 159–179. https://doi.org/10.1016/S0009-2541(02)00393-5

Wilkin, R. T., & Barnes, H. L. (1997). Formation processes of framboidal pyrite. *Geochimica et Cosmochimica Acta*, *61*(2), 323–339. https://doi.org/10.1016/S0016-7037(96)00320-1

Yusoff, N. F. M., Idris, N. H., Din, M. F. M., Majid, S. R., Harun, N. A., & Rahman, M. M. (2020). Investigation on the Electrochemical Performances of Mn2O3 as a Potential Anode for Na-Ion Batteries. *Scientific Reports*, *10*(1), 1–10. https://doi.org/10.1038/s41598-020-66148-w

Zaback, D. A., & Pratt, L. M. (1992). Isotopic composition and speciation of sulfur in the Miocene Monterey Formation: Reevaluation of sulfur reactions during early diagenesis in marine environments. *Geochimica et Cosmochimica Acta*, *56*(2), 763–774. https://doi.org/10.1016/0016-7037(92)90096-2

Zhbankov, R. G., Andrianov, V. M., Ratajczak, H., & Marchewka, M. (1995). Vibrational spectra and stereochemistry of mono- and polysaccharides - 1. D-glucose anomers. In *Journal of Structural Chemistry* (Vol. 36, Issue 2, pp. 287–294). https://doi.org/10.1007/BF02578069

Supplementary Information

Appendix 4.1: Calculation for the experiments

Mass Number of Elements/Compounds

Fe: 55.85 u, S: 32.07 u, FeS_2: 119.98 g/mol, $H_8N_2S_3$: 132.26 g/mols, $FeCl_2 \cdot 4H_2O$: 198.81 g/mol

Amounts

- **Sulfur**

- **Sulfurized D-glucose**

  1 g of sulfurized D-glucose has **87.3 mg (i.e. 0.0873 g)** S based on CHNS analysis

  $\therefore 1\text{M} = \frac{32.07\ g}{0.0873\ g} \rightarrow \frac{1000\ ml}{x\ ml}$

  Making x the formula subject, 1M of 0.0873 g of S in 1g of sulfurized D-glucose is

  = 2.7 ml

- **Ammonium Polysulfide ($H_8N_2S_3$) --------- 100%**

  1 g of $H_8N_2S_3$ = 0.727 g of S in 100% solution.

  $\therefore 1\text{M} = \frac{132.3\ g}{0.727\ g} \rightarrow \frac{1000\ ml}{x\ ml}$

  Making x the formula subject, 1M of 0.727 g of S in 1g of $H_8N_2S_3$ is

  = 5.5 ml

- **Ammonium Polysulfide ($H_8N_2S_3$) --------- 6.2%**

  Work out for the amount of sulfur in 6.2% of $H_8N_2S_3$ in 500 ml;

  $\frac{1.07}{1}$ x $500 = 535$ g

  535 g x $\frac{6.2\%}{100}$ $= \mathbf{33.17\ g}$

  33.17 g x $\frac{1}{132.2}$ $= 0.25$ mol

  $\frac{0.25}{0.5} = 0.5\ mol/dm3$

  Since $H_8N_2S_3$ has 3 molecules of S thus, 1M = 96.21 g S

  ∴ in 0.5M the expression is given by;

  $\therefore 1\text{M} = \frac{48.12\ g}{0.0873\ g} \rightarrow \frac{1000\ ml}{x\ ml}$

  Making x the formula subject, 1M of 0.0873 g of S in 0.5M of 48.12 g of $H_8N_2S_3$

  = 1.8 ml

- **Iron**

- **Amount of Fe for the experiment**

  Pyrite is FeS_2 however, literature reports that laboratory pyrite synthesis requires S in excess hence, the ratio 1:4 for Fe and S is proposed.

  Therefore, the amount Fe in mol and g in relation to the amount of sulfurized D-glucose (0.0873 g) presented above will be given by;

  0.0873 g S / 32.07 = 0.00272 mol S

  Assuming the ratio 1:4 for pyrite synthesis, amount of Fe needed in mol is;

  0.00272 mol S / 4 = 0.00068 mol Fe

  Hence, amount of Fe in g is;

  0.00068 x 55.85

  = **0.038 g**

  Obtaining 0.038 g of Fe in $FeCl_2 \cdot 4H_2O$;

  Correction factor (CF) of Fe in $FeCl_2 \cdot 4H_2O$;

  $$\mathrm{CF} = \frac{\mathrm{Fe}}{\mathrm{FeCl2 \ \cdot \ 4H2O}}$$

  $$\mathrm{CF} = \frac{55.845}{198.81}$$

  CF = **0.28**

  ∴ the CF is used to work out the amount of $FeCl_2 \cdot 4H_2O$ which would have 0.038 g of Fe by the following expression;

  x x 0.28 = 0.038

  Making x the formula subject, 0.1357 g of $FeCl_2 \cdot 4H_2O$ would have 0.038 g of Fe;

  = 0.1357 g of $FeCl_2 \cdot 4H_2O$ = 0.038 g of Fe

  Hence, 1M of 0.1357 g of $FeCl_2$ is given by;

  $$1\mathrm{M} = \frac{198.81\ g}{0.1357\ g} \rightarrow \frac{1000\ ml}{x\ ml}$$

1M = 0.6825 ml

Stock:

0.1357 g of $FeCl_2 \cdot 4H_2O$ x 48 (No. of exp. (12) x 4) = 6.5136 g $FeCl_2 \cdot 4H_2O$

$$1M = \frac{198.81\ g}{6.5136\ g} \rightarrow \frac{1000\ ml}{x\ ml}$$

1M = 32.76 ml

Chapter 5

5. Overall Conclusions and Future Work

5.1 Conclusions

The principal aim of this project was to investigate the critical factors influencing the formation and stability of organic sulfur compounds (OSCs) in the sedimentary record with a particular focus on the competition between iron (Fe) sulfide [mainly pyrite (FeS_2)] formation and the sulfurisation of organic matter (OM). The project robustly analysed samples from model organic and sulfur (S)-rich basins, e.g. the Kimmeridge Clay (KCF), Monterey (MF) and Whitby Mudstone Formations (WMF), as well as laboratory synthesised sulfurised glucose reacted with Fe(II) chloride, using a wide range of organic/inorganic geochemical, petrographic and state-of-the-art synchrotron-based techniques [e.g. X-ray fluorescence imaging and X-ray absorption near edge structure (XANES)]. The outcomes of these analyses improved our understanding of sulfurisation and Fe sulfides formation processes. The project is subdivided into three sub-projects based on the overall objectives of the project highlighted in section 1.7.2.

i) Project 1 (Chapter 2) – Investigated the critical factors controlling the distribution of S, Fe and Fe sulfides (mainly FeS_2) in sediments from model organic and S-rich basins, e.g. the Blackstone band of the KCF, Upper Calcareous-Siliceous member of the MF and Grey Shale (GS) and Jet Rock (JR) members of the WMF. These mudstones were deposited with a similar suite of oxidants and reductants but differ significantly in their post diagenetic characteristics such as OM and organic S contents, Fe sulfides and other minerals (Howarth, 1962; Orr, 1986; Zaback & Pratt, 1992; Raiswell et al., 1993; Boussafir et al., 1995; Schouten et al., 1995; van Kaam-Peters et al., 1998; Sælen et al., 2000; Morgans-Bell et al., 2001; Bowden et al., 2006; van Dongen et al., 2006; Ghadeer & Macquaker, 2011; Ghadeer & Macquaker, 2012; Salem, 2013; Macquaker et al., 2014; Houben et al., 2016). Multiple high resolution geochemical and petrographic analyses showed that S in the KCF and MF is mostly bound to OM as indicated by the relative abundance of organic S, mainly thiophenic compounds, compared to other hydrocarbons in their pyrolysates (Fig. 2.3; Table 2.4 & 2.6). For the KCF, this is consistent with previous studies (van Dongen et al., 2006; van Kaam-Peters et al., 1998). The relatively low amounts of Fe (which would have served as sink for inorganic S) in both the KCF and MF subdued the formation of FeS_2, thus were low/limited in both settings. Therefore, extensive reaction of S and OM in both KCF and MF occurred

which ensured the preservation of high amounts of S-rich kerogen measured in these settings (Table 2.1 & 2.6). Electron microprobe (EMPA) mapping of total S and Fe in the studied organic and S-rich mudstones was feasible for the first time and provided information/insight about the distribution and nature of S and Fe. S signals in the KCF and MF were almost evenly (not discretely) spread across the whole imaged area, except for carbonate/phosphate-rich regions and Fe signals were relatively very low (Fig. 2.4). This indicate S in the KCF and MF is most likely bound to organics or in solution, in the case of this study organics as supported by the multiple geochemical analyses (Fig. 2.3, Table 2.4 & 2.6).

Contrary to the KCF and MF, S in the GS and JR, were not mostly organically bound as indicated by the relatively low/absence of thiophenic compounds and predominance of other hydrocarbons in their pyrolysates (Fig. 2.3, Table 2.4 & 2.6). The relatively high amounts of Fe in both the GS and JR sequestered S as FeS_2, resulting in the diminution of reaction between S and OM thus, preservation through sulfurisation in these setting was less significant compared to the KCF and MF and this reflected in their measured kerogen compositions (Table 2.1 & 2.6). Furthermore, S signals in the EMPA images of the GS and JR exhibit a different distribution pattern. Although widespread, S exist in discrete shapes/units ranging in geometry and size (from few nm up to 15 μm) and in most cases correlated with Fe when compared with their corresponding Fe EMPA images (Fig. 2.4) thus, indicating that the S in the GS and JR is not mostly in solution or bound to organic compounds/complexes rather, it exists in discrete authigenic mineral phases, in the case of this study FeS_2 as supported by petrographic and geochemical analyses (Fig. 2.2, Table 2.2). In summary, this study reported, for the first time, detailed distribution of OSCs in the MF, GS and JR, and compared/contrasted them with those observed in the KCF (this study; van Dongen et al., 2006; van Kaam-Peters et al., 1998). This study further shows that state-of-the-art EMPA elemental mapping of total S and Fe in organic and S-rich mudstones is feasible.

Overall, the results in this study (Project 1) indicate that the incorporation of S into OM enhances preservation even in low primary productivity environments in line with previous studies (Tegelaar et al., 1989; Koopmans et al., 1996; Sinninghe Damsté et al., 1998; Grice et al., 2003; van Dongen et al., 2006). However, the presence of oxidants such as sesquioxides of Fe could significantly hinder this process (Raiswell,

1982; Berner, 1984; Raiswell & Berner, 1985; Taylor & Macquaker, 2000; Jiang et al., 2017; Shawar et al., 2018; Raven et al., 2019), for example, in the case GS and JR were the presence of high amounts of Fe sequestered much of S as FeS_2, impeding reactions between OM and S that could have led to formation of enormous amounts of S-rich kerogen in GS and JR. In the contrary, the dearth of Fe in KCF and MF permitted OM and S reactions to occur efficiently leading to the formation massive amounts of S-rich kerogens in them. This study (Project 1) showed Fe could have a dominant control on preservation through sulfurisation. However, there is still a need to study S and Fe species (oxidation states) both at low and high resolutions to fully comprehend sulfurisation and FeS_2 formation processes and to arrive at a full bound conclusions. For this, research in Project 2 was carried out.

ii) Project 2 (Chapter 3) – Investigated the mudstone studied in Project 1 using novel state-of-the-art synchrotron-based techniques (X-ray fluorescence imaging and XANES). Detailed analyses at low (mm - cm scale; hand specimen) and high resolution (µm - mm scales; thin sections) showed that X-ray fluorescence imaging and XANES can be used to non-destructively spatially-resolve S and Fe oxidation states in organic and S-rich mudstones. Results reveal a dominance of organic S compared to other S species including sulfate type S in the KCF and MF while sulfate type S dominates the GS compared to organic S and other S species (Fig. 3.3 & 3.6; Table 3.2). Fe was found to be abundant in GS, mostly bound to S and predominantly in the form of FeS_2 with few present as other types of Fe sulfides. In contrast, Fe is much lower in both the KCF and MF and most of the Fe in the KCF is largely bound to S whereas in the MF, S and Fe correlation was less significant (Fig. 3.7 & 3.8). Overall, analyses indicate that the presence of sulfurised OM in the KCF is widespread, in line with the presence of stable euxinic conditions in the water column (van Dongen et al., 2006; van Kaam-Peters et al., 1998), over a relatively long period of time and a relatively low influx of reactive Fe, promoting the preservation of substantial amounts of OM through sulfurisation. In contrast, the presence of sulfurised OM was transitional in the MF, in line with fluctuating redox conditions in the water column over time, likely due to profuse biological production (Isaacs & Rullkötter, 2001; Piper & Isaacs, 2001; Macquaker et al., 2014), and less significant in the GS likely due to the abundance of reactive Fe outcompeting the formation of sulfurised OM. Project 2 showed that even at higher resolutions sulfurisation of OM appears to be promoted in settings/succession starved

of Fe species while it is hindered in settings/successions with high influx of Fe species, supporting work done in Project 1. Although, it is now documented that the abundance of Fe during diagenesis seems to control preservation through sulfurisation, there is a dearth of understanding of the stability of already sulfurised OM, especially during influx of fresh reactive Fe species. This led to the study in Project 3.

iii) Project 3 (Chapter 4) – Investigated the stability of OSCs in the presence of Fe. This was completed by reacting sulfurised glucose with Fe (II) chloride. Results indicate, for the first time, that some S in the sulfurised glucose was utilised by Fe to form metastable FeS materials, which were subsequently converted to minerals with co-ordination of S and Fe that is similar to the co-ordination environment and oxidation state of S and Fe in S^{-2} Fe sulfide minerals (likely pyrrhotite or troilite). Some of these S^{-2} minerals further converted to form traces of a more stable S^{-1} iron sulfides likely FeS_2. However, there was still sulfurised glucose in the product after Fe treatment. This suggest that potentially (specific) parts of the S originally bound to the glucose were lost during the experiments. The metastable FeS materials were likely either formed from that part of the OSCs with weak S-S bonds, while the stronger C-S bonds were stable, and could be preserved for millions of years. However, it cannot be excluded that it is a matter of time before all S in the sulfurised glucose would be stripped off to form iron sulfides. Overall, reaction between OM and S could be said to be partially reversible in the presence of reactive Fe species as proposed in Fig 5.1.

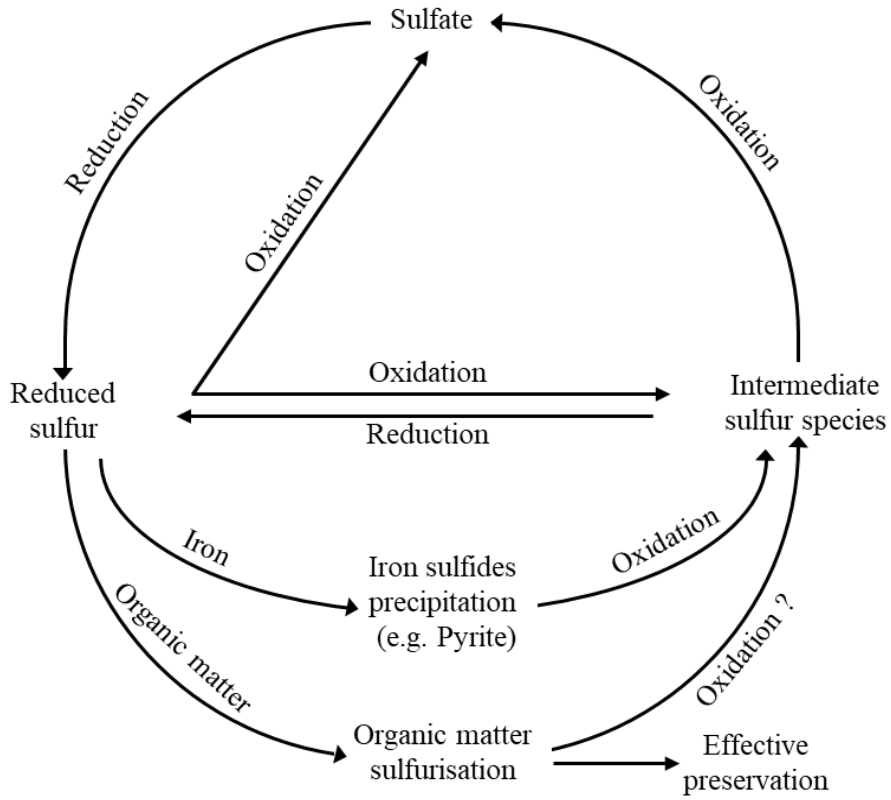

Figure 5.1: Pathways through which sulfur is sequestered either as sulfurised organic matter or iron sulfides in the sedimentary record.

5.2 Future Work

Detailed, multiple high resolution organic/inorganic geochemical, petrographic and synchrotron-based analyses on model organic and S-rich mudstones, e.g. KCF, MF and WMF [Project 1 (Chapter 2) & 2 (Chapter 3)] was completed. These mudstones were selected as extreme endmembers according to the presence, absence and/or distribution of S, Fe, OSCs, and FeS_2 in them. The KCF with high S (mostly organic) but low Fe and FeS_2 was the first endmember, WMF with high S (mostly inorganic) and high Fe and FeS_2 was the second endmember and MF with high S (combination of organic and inorganic) but low Fe and limited FeS_2 although, has same amount of Fe as KCF was the third endmember. Analyses on these endmember mudstones showed Fe could have a dominant control on preservation through sulfurisation where, if abundant, sequesters reduced S as FeS_2 thus limiting preservation through sulfurisation. Since this outcome is based on analysis completed on endmembers as highlighted above, more work is required to improve our understating of sulfurisation and FeS_2 formation processes as suggested below;

i) Organic/inorganic geochemical, petrographic and synchrotron-based analyses where completed on endmembers, as such, analyses on mudstones with similar proportions of

S and Fe is required to investigate if Fe actually has a dominant control on preservation through sulfurisation or OM sulfurisation and FeS_2 formation processes could occur simultaneously.

ii) Synchrotron-based analyses can be extended to map and study the oxidation states of S, Fe and other elements from other depositional settings such as, for example, ancient and recent oxic and dysoxic environments. The techniques could also be potentially used to study cores from sea surface sediments and in sinking flocs and biofilms (OM) in modern water columns to improve our understanding of the timing of sulfurisation. Analyses of FeS_2 forming at sea surface sediments and in water columns could also improve our understanding of the competition between OM sulfurisation and FeS_2 formation processes. All of the above could be achieved by collecting the materials (e.g. sea surface sediments, flocs and biofilms) anaerobically (where possible) to avoid possible oxidation/chemical change, smeared/mounted on glass slides, air-dried anaerobically and analysed directly without prior sample preparation.

The stability of OSCs was tested by reacting sulfurised glucose with Fe (II) chloride [Project 3 (Chapter 4)]. Results showed iron sulfides were formed but there was still sulfurised glucose in the product after Fe treatment. It cannot be concluded whether the iron sulfides were formed from that part of the OSCs with weak S-S bonds, while the stronger C-S bonds were stable, and could be preserved for millions of years or that it is a matter of time before more/all S in the sulfurised glucose would be stripped off to form iron sulfides. Therefore, the following experiments could be done to improve our understanding;

i) Further experiments, for example; (a) reacting S in sulfurised glucose and Fe in equal proportions (b) reacting S in sulfurised glucose with Fe in excess (c) completing such experiments at slightly elevated temperatures (d) completing such experiments at mild temperatures but for a longer period of time than reported in this project are required to fully understand the stability of C-S bonds in OSCs.

ii) Sulfurisation of other types of OM such as phytol, phytadiene, humic and fulvic acids could be completed which could potentially provide information about the different reaction kinetics these OM could exhibit when reacted with S. OSCs formed from these materials could also be reacted with Fe to study their stabilities and be compared with what was reported in this study.

Reference

Berner, R. A. (1984). Sedimentary pyrite formation: An update. *Geochimica et Cosmochimica Acta*, *48*(4), 605–615. https://doi.org/10.1016/0016-7037(84)90089-9

Boussafir, M., Gelin, F., Lallier-Vergès, E., Derenne, S., Bertrand, P., & Largeau, C. (1995). Electron microscopy and pyrolysis of kerogens from the Kimmeridge Clay Formation, UK: Source organisms, preservation processes, and origin of microcycles. *Geochimica et Cosmochimica Acta*, *59*(18), 3731–3747. https://doi.org/10.1016/0016-7037(95)00273-3

Bowden, S. A., Farrimond, P., Snape, C. E., & Love, G. D. (2006). Compositional differences in biomarker constituents of the hydrocarbon, resin, asphaltene and kerogen fractions: An example from the Jet Rock (Yorkshire, UK). *Organic Geochemistry*, *37*(3), 369–383. https://doi.org/10.1016/j.orggeochem.2005.08.024

Ghadeer, S. G., & Macquaker, J. H. S. (2012). The role of event beds in the preservation of organic carbon in fine-grained sediments: Analyses of the sedimentological processes operating during deposition of the Whitby Mudstone Formation (Toarcian, Lower Jurassic) preserved in northeast England. *Marine and Petroleum Geology*, *35*(1), 309–320. https://doi.org/10.1016/j.marpetgeo.2012.01.001

Ghadeer, S. G., & Macquaker, J. H. S. (2011). Sediment transport processes in an ancient mud-dominated succession: A comparison of processes operating in marine offshore settings and anoxic basinal environments. *Journal of the Geological Society*, *168*(5), 1121–1132. https://doi.org/10.1144/0016-76492010-016

Grice, K., Schouten, S., Blokker, P., Derenne, S., Largeau, C., Nissenbaum, A., & Sinninghe Damsté, J. S. (2003). Structural and isotopic analysis of kerogens in sediments rich in free sulfurised Botryococcus braunii biomarkers. *Organic Geochemistry*, *34*(3), 471–482. https://doi.org/10.1016/S0146-6380(02)00187-0

Houben, M. E., Barnhoorn, A., Lie-A-Fat, J., Ravestein, T., Peach, C. J., & Drury, M. R. (2016). Microstructural characteristics of the Whitby Mudstone Formation (UK). *Marine and Petroleum Geology*, *70*, 185–200. https://doi.org/10.1016/j.marpetgeo.2015.11.011

Howarth, M. K. (1962). The Jet Rock Series and Alum Shale Series of the Yorkshire Coast. *Proceedings of the Yorkshire Geological Society*, *33*(18), 381–422.

Isaacs, C. M., & Rullkötter, J. (2001). *The Monterey Formation : from rocks to molecules*. Columbia University Press.

Jiang, S., Mokhtari, M., & Borrok, D. M. (2017). Incorporating the effect of pyrite on total organic carbon estimation in eagle ford shale. *Society of Petroleum Engineers - SPE Liquids - Rich Basins Conference - North America 2017*. https://doi.org/10.2118/187484-ms

Koopmans, M. P., Köster, J., Van Kaam-Peters, H. M. E., Kenig, F., Schouten, S., Hartgers, W. A., De Leeuw, J. W., & Sinninghe Damsté, J. S. (1996). Diagenetic and catagenetic products of isorenieratene: Molecular indicators for photic zone anoxia. *Geochimica et Cosmochimica Acta*, *60*(22), 4467–4496. https://doi.org/10.1016/S0016-7037(96)00238-4

Macquaker, J. H. S., Taylor, K. G., Keller, M., & Polya, D. (2014). Compositional controls on early diagenetic pathways in fine-grained sedimentary rocks: Implications for predicting unconventional reservoir attributes of mudstones. *AAPG Bulletin*, *98*(3), 587–603. https://doi.org/10.1306/08201311176

Morgans-Bell, H. S., Coe, A. L., Hesselbo, S. P., Jenkyns, H. C., Weedon, G. P., Marshall, J. E. A., Tyson, R. V, & Williams, C. J. (2001). Integrated stratigraphy of the Kimmeridge Clay Formation (Upper Jurassic) based on exposures and boreholes in south Dorset, UK. *Geological Magazine*, *138*(05), 511–539. https://doi.org/10.1017/s0016756801005738

Orr, W. L. (1986). Kerogen/asphaltene/sulfur relationships in sulfur-rich Monterey oils. *Organic Geochemistry*, *10*(1–3), 499–516. https://doi.org/10.1016/0146-6380(86)90049-5

Piper, D., & Isaacs, C. (2001). The Monterey Formation: bottom-water redox conditions and photic-zone primary productivity. In *Monterey Formation from Rocks to Molecules.* (pp. 31–58). Columbia University Press.

Raiswell, R. (1982). Pyrite texture, isotopic composition and the availability of iron. In *American Journal of Science* (Vol. 282, Issue 8, pp. 1244–1263). https://doi.org/10.2475/ajs.282.8.1244

Raiswell, R., & Berner, R. A. (1985). Pyrite formation in euxinic and semi-euxinic sediments. In *American Journal of Science* (Vol. 285, Issue 8, pp. 710–724). https://doi.org/10.2475/ajs.285.8.710

Raiswell, R., Bottrell, S. H., Al-Biatty, H. J., & Tan, M. M. (1993). The influence of bottom water oxygenation and reactive iron content on sulfur incorporation into bitumens from Jurassic marine shales. In *American Journal of Science* (Vol. 293, Issue 6, pp. 569–596). https://doi.org/10.2475/ajs.293.6.569

Raven, M. R., Fike, D. A., Bradley, A. S., Gomes, M. L., Owens, J. D., & Webb, S. A. (2019). Paired organic matter and pyrite δ 34 S records reveal mechanisms of carbon, sulfur, and iron cycle disruption during Ocean Anoxic Event 2. *Earth and Planetary Science Letters*, *512*, 27–38. https://doi.org/10.1016/j.epsl.2019.01.048

Sælen, G., Tyson, R. V., Telnæs, N., & Talbot, M. R. (2000). Contrasting watermass conditions during deposition of the Whitby Mudstone (Lower Jurassic) and Kimmeridge Clay (Upper Jurassic) formations, UK. *Palaeogeography, Palaeoclimatology, Palaeoecology*, *163*(3–4), 163–196. https://doi.org/10.1016/S0031-0182(00)00150-4

Salem, N. (2013). *Geochemical characterisation of the Pliensbachian -Toarcian boundary during the onset of the Toarcian Oceanic Anoxic Event. North Yorkshire, UK* (Issue February). Newcastle University, UK.

Schouten, S., Damsté, J. S. S., Baas, M., Kock-van Dalen, A. C., Kohnen, M. E. L., & de Leeuw, J. W. (1995). Quantitative assessment of mono- and polysulphide-linked carbon skeletons in sulphur-rich macromolecular aggregates present in bitumens and oils. *Organic Geochemistry*, *23*(8), 765–775. https://doi.org/10.1016/0146-6380(95)00055-J

Shawar, L., Halevy, I., Said-Ahmad, W., Feinstein, S., Boyko, V., Kamyshny, A., & Amrani, A. (2018). Dynamics of pyrite formation and organic matter sulfurization in organic-rich carbonate sediments. *Geochimica et Cosmochimica Acta*, *241*, 219–239. https://doi.org/10.1016/j.gca.2018.08.048

Sinninghe Damsté, J. S., Kok, M. D., Köster, J., & Schouten, S. (1998). Sulfurized carbohydrates: An important sedimentary sink for organic carbon? *Earth and Planetary Science Letters*, *164*(1–2), 7–13. https://doi.org/10.1016/S0012-821X(98)00234-9

Taylor, K. G., & Macquaker, J. H. S. (2000). Early diagenetic pyrite morphology in a mudstone-dominated succession: The Lower Jurassic Cleveland Ironstone Formation, eastern England. *Sedimentary Geology*, *131*(1–2), 77–86. https://doi.org/10.1016/S0037-0738(00)00002-6

Tegelaar, E. W., de Leeuw, J. W., Derenne, S., & Largeau, C. (1989). A reappraisal of kerogen formation. *Geochimica et Cosmochimica Acta*, *53*(11), 3103–3106. https://doi.org/10.1016/0016-7037(89)90191-9

van Dongen, B. E., Schouten, S., & Sinninghe Damsté, J. S. (2006). Preservation of carbohydrates through sulfurization in a Jurassic euxinic shelf sea: Examination of the Blackstone Band TOC cycle in the Kimmeridge Clay Formation, UK. *Organic Geochemistry*, *37*(9), 1052–1073. https://doi.org/10.1016/j.orggeochem.2006.05.007

van Kaam-Peters, H. M. E., Schouten, S., Köster, J., & Damstè, J. S. S. (1998). Controls on the molecular and carbon isotopic composition of organic matter deposited in a Kimmeridgian euxinic shelf sea: Evidence for preservation of carbohydrates through sulfurisation. *Geochimica et Cosmochimica Acta*, *62*(19–20), 3259–3283. https://doi.org/10.1016/S0016-7037(98)00231-2

Zaback, D. A., & Pratt, L. M. (1992). Isotopic composition and speciation of sulfur in the Miocene Monterey Formation: Reevaluation of sulfur reactions during early diagenesis in marine environments. *Geochimica et Cosmochimica Acta*, *56*(2), 763–774. https://doi.org/10.1016/0016-7037(92)90096-2